75-28,383

LEVI, Shaul, 1942-
SOME MAGNETIC PROPERTIES OF MAGNETITE AS A
FUNCTION OF GRAIN SIZE AND THEIR IMPLICATIONS
FOR PALEOMAGNETISM.

University of Washington, Ph.D., 1974
Geophysics

SOME MAGNETIC PROPERTIES OF MAGNETITE

AS A FUNCTION OF GRAIN SIZE

AND

THEIR IMPLICATIONS FOR PALEOMAGNETISM

by

SHAUL LEVI

A dissertation submitted in partial fulfillment

of the requirements for the degree of

DOCTOR OF PHILOSOPHY

UNIVERSITY OF WASHINGTON

1974

Approved by _Ronald T. Merill_____

(Chairman of Supervisory Committee)

Department__ Geophysics Program _____

(Departmental Faculty sponsoring Candidate)

Date__ **Dec 4, 1974**_____

UNIVERSITY OF WASHINGTON

Date: __August 19, 1974__

We have carefully read the dissertation entitled __Some Magnetic Properties of__ __Magnetite as a Function of Grain Size and Their Implications for__ __Paleomagnetism__ _____submitted by _____in partial fulfillment of the requirements of the degree of_____ __Shaul Levi__ _____ and recommend its acceptance. In support of this recommendation we present the following joint statement of evaluation to be filed with the dissertation.

Most earth scientists concerned with geomagnetism are interested in the stability of magnetization in rocks, since components of magnetization that have not changed with time provide valuable information concerning paleotectonics, the history of the earth's magnetic field, etc. However, because one is dealing with rocks that are commonly millions of years old, this stability must be inferred from various laboratory measurements that deal with stability with respect to temperature, external field, etc. This thesis makes a significant contribution by providing carefully obtained experimental data on how various magnetic properties vary with grain size in pure magnetite samples. Numerous data are provided on how grain size affects the acquisition and stability of anhysteretic remanent magnetization and thermal remanent magnetization in rocks. The latter chapters of this thesis deal with methods to obtain reliable intensity estimates for the earth's magnetic field in the past and with the stability of remanence in magnetite with respect to thermal and alternating field demagnetization.

This independent work represents an important and original contribution in Geophysics.

DISSERTATION READING COMMITTEE: _Ronald T. Merrill_

John Booker

Kenneth C. Clark

Doctoral Dissertation

TABLE OF CONTENTS

List of Abbreviations

NRM	Natural remanent magnetization.
PNRM	Partial NRM.
TRM	Thermoremanent magnetization.
PTRM	Partial TRM.
ARM	Anhysteretic remanent magnetization.
PARM	Partial ARM.
CRM	Chemical remanent magnetization.
VRM	Viscous remanent magnetization.
IRM	Isothermal remanent magnetization.
A. F.	Alternating field.
MDF	Median demagnetizing field.
OE, oe	Oersted.
VSM	Vibrating sample magnetometer.
IAGA	International Association of Geomagnetism and Aeronomy.
SI	Standard international.

List and Definition of Symbols

h   Intensity of steady magnetic field (oersted) such as TRM and ARM biasing field.

Common subscripts:
- ex = external
- L = laboratory
- int = interaction
- eff = effective
- c = critical

H   Intensity of strong magnetic field usually in excess of 10^3 oersted.

H_C Bulk coercivity; reversed field for which the sample magnetization vanishes.

H_{CR} Coercivity of the remanence; that reversed field which upon removal leaves the sample unmagnetized.

H_{ci} Microscopic coercivity.

$\tilde{H}$ Peak value of alternating field.

Common subscripts:
- U = upper
- L = lower
- SAT = saturation

$\tilde{H}_{\frac{1}{2}} \equiv MDF$ Peak alternating field that demagnetizes the remanence to $\frac{1}{2}$ its original value.

J   Magnetization.

Common subscripts:
- S = saturation magnetization
- SP = spontaneous magnetization
- RS = remanence after saturation

$\vec{J}_{TRM} = \vec{J}_T = \vec{TRM}$ Thermoremanent magnetization.

$\vec{J}_{NRM} = \vec{NRM}$ Natural remanent magnetization.

$\vec{J}_{ARM} = \vec{ARM}$ Anhysteretic remanent magnetization.

T   Temperature (^{O}C or ^{O}K).

     Common subscripts: C = Curie point
     R = room
     I = intermediate
     B = blocking

$<T_B>$ Mean blocking temperature of sample. That temperature to which the sample must be heated in zero field such that its room temperature remanence drops to ½ its original value.

A   Exchange interaction parameter.

K   Magnetocrystalline anisotropy constant.

     Common subscripts: 1, 2, order of approximating series

     u = uniaxial

λ Magnetostriction constant.

     Common subscripts: 111, 110 referring to crystallographic axes.

E   Magnetic energy.

     Common subscripts: M = magnetostatic
     W = wall
     EX = exchange
     λ = magnetostrictive
     K = magnetocrystalline

N   Number of particles.

D   Shape demagnetizing factor.

G   Shear modulus.

m,s,M   Exponents.

M_o Electron mass.

e   Electron charge.

k   Boltzmann's constant.

v   Particle volume.

µm   Micron.

W   Domain wall energy density, erg/cm^2.

δ Domain wall width.

σ Stress.

ρ Compaction parameter of magnetic material $o \leqslant \rho \leqslant 1$.

X, χ Susceptibility, low field.

Common subscripts: ARM, TRM.

List of Figures

List of Tables

Acknowledgements

CHAPTER 1

INTRODUCTION

Thermoremanent magnetization, TRM, is acquired by cooling a ferromagnetic or ferrimagnetic substance in the presence of a magnetic field. $\vec{J}_{TRM}(T_j, T_i, h)$ denotes the specimen's TRM, measured at room temperature ($\sim 25°C$), acquired when the specimen is cooled from T_j (°C) to T_i in the presence of field $\vec{h}$. The first temperature in the argument, T_j, always denotes the higher temperature. If the specimen is cooled from above the Curie point (Néel point for a ferrimagnetic substance) to room temperature, T_R, in the continuous presence of a constant field, $\vec{h}$, the remanence is a total-TRM. (Where no ambiguity is likely to arise, the prefix 'total' is often omitted.) In our earlier notation we write $\vec{J}_{TRM}(T_C, T_R, \vec{h})$ or sometimes $TRM(T_C, T_R, \vec{h})$. If $\vec{h}$ is applied during only part of the cooling, say between T_1 and T_2 where $T_R < T_1 < T_2 < T_C$, the remanence is a partial-TRM, PTRM, $\vec{J}_{PTRM}(T_2, T_1, \vec{h})$, or sometimes $\vec{PTRM}(T_2, T_1, \vec{h})$.

Igneous rocks usually have minor fractions of ferrimagnetic minerals—commonly of the order of one percent by weight and almost always less than ten percent—which usually acquire TRM as they cool below their Curie point to room temperature. TRM is also found in baked clays, kilns, baked bricks, and baked artifacts such as vases and jars.

Specific TRM properties are different for each magnetic mineral and are usually sensitive to small fractions of impurities that may be present. Within a certain mineral, TRM properties vary widely depending on the magnetic grains' sizes and shapes and the grains' internal and external states of stress. Although highly variable, TRM has some peculiar and wonderful properties that make paleomagnetism a viable field of study and have enabled

paleomagnetists to extract reliable magnetic information from as far back as a thousand million (10^9) years. Because of its importance in archeomagnetism and paleomagnetism, TRM has been studied extensively by numerous authors, mostly during the last forty years, and some of its important and interesting properties are listed below:

(1) TRM is almost always parallel to the external field, $\vec{h}$, in which it was induced. $\qquad \vec{J}_{TRM}(T_C, T_R, \vec{h}) \, // \, \vec{h}.$

(2) TRM acquired in a weak external field is more intense than isothermal remanent magnetization, IRM, acquired in the same external field

$$\vec{J}_{TRM}(T_C, T_R, \vec{h}) > \vec{J}_{IRM}(T_R, \vec{h}).$$

(3) TRM acquired in a weak external field is generally more stable than IRM acquired in the same external field, such that: (i) TRM is more resistant than IRM to spontaneous time decay in null field; (ii) TRM is more resistant than IRM to demagnetization by direct and alternating fields; and (iii) TRM is more resistant than IRM to thermal demagnetization.

The contrast between TRM and IRM outlined in properties 2 and 3 diminishes with increasing external field or, equivalently, with approach to saturation remanent magnetization such that:

(a) $\quad \lim_{\substack{J_{TRM} \to \text{saturation} \\ \text{remanence}}} [\vec{J}_{TRM}(T_C, T_R, \vec{h})] = \vec{J}_{IRM}(T_R, \vec{h})$

(b) $\quad \lim_{\substack{\vec{J}_{TRM} \to \text{saturation} \\ \text{remanence}}} [\tau(\vec{J}_{TRM})] = \tau(\vec{J}_{IRM})$,

where τ is the relaxation time of the magnetization.

(4) The intensity of TRM acquired in weak external fields ($h \sim 1$ oe) is directly proportional to the inducing fields: $\vec{J}_{TRM}(T_C, T_R, \vec{h}) \propto \vec{h}.$ At higher fields TRM deviates from linearity and approaches saturation.

(5) In his extensive studies of TRM of baked clays and bricks from

archeological sites E. Thellier (1938) discovered one of the more funda-

mental properties of TRM, summarized in Thellier (1946):

> "To any temperature interval T_1, T_2 ($T_R < T_1 < T_2 < T_C$)
> there corresponds for a given specimen and a given
> magnetic field h, a particular magnetic moment which
> is acquired by the specimen when cooled from T_2 to T_1
> in this field h and is unaffected by any heating to
> temperatures less than T_1 but disappears completely
> by heating to T_2. Further, it is quite independent
> of other thermoremanent moments acquired in temperature
> intervals outside T_1 and T_2 even though they be due to
> field h that are different in magnitude and direction.
> All these moments are added geometrically but, para-
> doxical as it may seem, each is quite independent and
> preserves a sort of exact memory of the temperatures
> and field which produced it."

This translation of Thellier's words was taken from Néel (1955, page 212-

213). Nagata (1943) discovered the independence of partial thermoremanent

magnetization (PTRM) for volcanic rocks. The independence of PTRMs acquired

over different temperature intervals can be generalized to what is commonly

known as the additivity law of PTRM, which can be written as follows:

1. $\vec{TRM}(T_C, T_R) = \vec{PTRM}(T_C, T_N, \vec{h}_{N+1}) + \vec{PTRM}(T_N, T_{N-1}, \vec{h}_N) + \vec{PTRM}(T_{N-1}, T_{N-2}, \vec{h}_{N-1})$
$+ \ldots + \vec{PTRM}(T_2, T_1, \vec{h}_2) + \vec{PTRM}(T_1, T_R, \vec{h}_1)$

1'. $\vec{TRM}(T_C, T_R) = \sum_{\substack{T_1 < T_j \leq T_C \\ T_R \leq T_1}} PTRM(T_j, T_1, \vec{h}_j)\, \hat{n}_j$

where $T_C \geq T_N \geq T_{N-1} \geq T_{N-2} \geq \ldots \geq T_2 \geq T_1 \geq T_R$

The values of the argument of $\vec{PTRM}(T_j, T_1, \vec{h}_j)$ denote the temperature

interval T_j, T_1 over which the PTRM is acquired and the external field

$\vec{h}_j$, active in that temperature interval; $\hat{n}_j$, in equation 1' is a unit vector

parallel to $\vec{h}_j$. In the acquisition of TRM by volcanic rocks where cooling

is relatively rapid, and in laboratory experiments, $\vec{h}$ can be usually approx-

imated by a constant vector for the entire interval T_C to T_R so that the

vector sum becomes an arithmetic sum and the above equation can be simplified to:

2.
$$TRM(T_C, T_R, h) = \sum_{\substack{T_i \leq T_j \leq T_C \\ T_R \leq T_i}} |PTRM(T_j, T_i, h)|$$

where $\hat{n}$ is a unit vector in the direction of $\vec{h}$.) If the sample's blocking temperatures are distributed over the entire temperature range T_C to T_R, and if $\vec{h}$ is applied throughout the entire TRM acquisition process between T_C and T_R, then for 2 to hold,

3.
$$T_C - T_R = \sum_{\substack{T_i \leq T_j \leq T_C \\ T_R \leq T_i}} (T_j - T_i)$$

Néel (1949, 1955) was able to theoretically explain many of the properties of TRM by considering an assemblage of identical non-interacting single domain grains of volume v. Single domain particles are defined to be homogeneously magnetized throughout their volume such that their spontaneous magnetization, J_{SP}, equals the saturation magnetization, J_S. Each grain thus has a magnetic moment vJ_S. If such an assemblage is given TRM, $\vec{J}_{TRM}(t=0) \equiv \vec{J}_0$, and the field is subsequently removed, the magnetization, $\vec{J}$, at a time t later will have decayed towards its new equilibrium condition in null field, which is $\vec{J} = 0$, according to:

4.
$$\vec{J}(t) = \vec{J}_0 \exp[- t/\tau]$$

This spontaneous decay of the magnetization is accomplished by thermal fluctuations of the magnetic moment over the potential energy barriers. The decay rate is determined by relaxation time, τ.

The incremental probability dP that in the time increment dt, through

the effect of thermal energy, kT, a magnetic moment might 'relax' toward equilibrium by overcoming the magnetic potential energy barrier, E, (E is most commonly known as the activation energy) is given by

$$5. \qquad dP = C \exp\left[-\frac{E}{kT}\right]dt$$

where C is a constant, k is the Boltzmann Constant, and T is the absolute temperature.

$$6. \qquad \frac{1}{\tau} = \frac{dP}{dt} = C \exp\left[-\frac{E}{kT}\right]$$

where C is of the order of 10^9 sec^{-1} (Nagata, 1961, p. 24). The precise value of C is not so important here, but it should be noted that for $E \approx kT$ the relaxation is essentially instantaneous. If the above value for C is used, then for $E/kT = 20.72$, $\tau = 1$ sec whereas for $E/kT = 60.32$, $\tau = 5 \times 10^9$ years. An increase in E/kT by a factor of three leads to a corresponding increase in τ of seventeen orders of magnitude. This dependence of τ on the exponential leads immediately to the concept of magnetization 'blocking'.

To develop an expression for τ for his single domain grains, Néel further assumed that the grains had only one axis of easy magnetization and that these axes are all aligned parallel to the applied field. Thus for each grain there are two stable orientations (positions of minimum total energy) of the magnetic moments, parallel and antiparallel to the external field, which are separated by an energy barrier. Using the above scheme, Néel derived the following expressions for the relaxation time, τ:

$$7. \qquad \frac{1}{\tau(0,\pi)} = a_0 (1+h/H_{ci})(1-h^2/H_{ci}^2)^{1/2} \exp\left[-\frac{vJ_{SP}(H_{ci}+h)^2}{2kTH_{ci}}\right]$$

8.
$$\frac{1}{\tau(\pi,0)} = a_0 (1-h/H_{ci})(1-h^2/H_{ci}^2)^{1/2} \exp\left[-\frac{vJ_{SP}(H_{ci}-h)^2}{2kTH_{ci}}\right]$$

where 0 and π are the two stable orientations of the magnetization parallel

and antiparallel to the external field, $\vec{h}$, respectively. v is the grain

volume in cubic centimeters, k is the Boltzmann constant, $J_{SP}(T)$ and $H_{ci}(T)$

are the spontaneous magnetization (gauss) and the microscopic coercivity

(oersted) at the temperature $T(°K)$, respectively. In the absence of an

external field these equations reduce to

9.
$$\frac{1}{\tau} = a_0 \exp\left[-\frac{vJ_{SP}H_{ci}}{2kT}\right].$$

Néel derived an expression for a_0 which is expressed by

$$a_0 = \frac{eH_{ci}}{2m_0} [3G\lambda + DJ_S^2][\frac{2v}{\pi GkT}]^{1/2}$$

where G is the shear modulus, λ, the longitudinal saturation magnetostric-

tion, D is related to the shape demagnetizing constant, and m_0 and e are

the mass and charge of an electron. $a_0(1\pm h/H_{ci})(1-h^2/H_{ci}^2)^{1/2}$ is a frequency

factor whose value is of the order of 10^9 sec^{-1} and whose variation with

temperature is mild compared with that of the exponential, which largely

determines τ's temperature dependence. Brown (1959) disagrees with Néel's

derivation of the frequency factor and develops a different expression.

Although Brown's criticisms seem justified, numerical values of the two

frequency factors do not differ significantly. Since we shall never depend

on the specific expression for the frequency factor, we remain faithful to

Néel.

$$\frac{J_{SP}(T)[H_{ci}(T) \pm h]^2}{2H_{ci}} \text{ and } \frac{J_{SP}(T)H_{ci}(T)}{2} \quad \text{represent the grains' energy barriers}$$

(per unit volume) in an external field $\vec{h}$ and in zero field, respectively,

against the rotation of the grain magnetization by the action of thermal

fluctuation due to thermal energy, kT. Both $H_{ci}(T)$ and $J_{SP}(T)$ are sensi-

tive functions of temperature and their values decrease with increasing

temperature and vanish as T approaches T_c.

It can be shown (by substituting realistic values for the parameters

in the equations for the relaxation time) that for a sample containing

noninteracting single domain grains, there is for each grain a temperature

T where $0°K \leqslant T < T_c$ is such that $\tau(T) \ll 1$ sec but $\tau(T-\Delta T) \gg 1$ sec. That is,

at T and higher temperatures the magnetic moment of the grain in question

is free and able to adjust and be in a state of thermal equilibrium with

respect to its surroundings and the field $\vec{h}$. However, at $T-\Delta T$ the magnetic

moment is frozen, blocked in its equilibrium state of temperature T and is

unable to readjust to new thermal equilibrium states of lower temperatures.

Since ΔT is usually small, T, centered in ΔT, is called the blocking tem-

perature, T_B, of the particular grain, and it is determined by the grain

parameters (v, J_{SP}, H_{ci}) and by the external field. T_B represents the

transition temperature for each grain where E/kT, the _ratio_ of the magnetic

energy barrier due to the collective behavior of the magnetic anisotropies

(shape, magnetocrystalline, magnetostrictive, and in seldom cases exchange

anisotropies) _to_ the randomizing effects of the thermal fluctuations, is

such that

10. $$\tau(T_B-\Delta T) \gg 1 \text{ sec} \overset{\sim}{>} \tau(T_B + \Delta T)$$

Thus each grain has a rather well-defined blocking temperature for a given

external field $\vec{h}$. When cooling a sample from T_2 to T_1 in $\vec{h}$, only those

grains with blocking temperatures, T_B, in this interval will be blocked with a net magnetization parallel to $\vec{h}$. Grains with $T_B > T_2$ will have already been blocked and grains with $T_B < T_1$ remain unblocked and in thermal equilibrium with respect to $\vec{h}$ at T_1.

Theller's and Nagata's observations of the independence and additivity of PTRMs are naturally explained by Néel's theory for single domain grains, as is the great stability of TRM against various types of demagnetization.

Consider N independent single domain grains each having one axis of easy magnetization all of which are parallel to the external field. If $T_B < T < T_C$, the grains are unblocked (superparamagnetic), but each possesses spontaneous magnetization, $J_{SP}(T) = J_S(T)$. The ensemble obeys Boltzmann statistics and the magnetic moments are partitioned in the two allowed states parallel and antiparallel to the external field according to:

11.
$$\frac{N_+}{N} = \frac{\exp[vJ_Sh/kT]}{\exp[vJ_Sh/kT] + \exp[-v\,J_Sh/kT]}$$

12.
$$\frac{N_-}{N} = \frac{\exp[-v\,J_Sh/kT]}{\exp[vJ_Sh/kT] + \exp[-v\,J_Sh/kT]}$$

13. $\quad N = N_+ + N_-$

where +(−) denote magnetic moments parallel (antiparallel) to the inducing field, $\vec{h}$. The configuration that is frozen in at $T = T_B$ is the configuration of the remanence.

14. $\quad J_{TRM}(T_B) = NJ_S(T_B)v[\frac{N_+}{N} - \frac{N_-}{N}] = NJ_S(T_B)v \tanh (\frac{vJ_Sh}{kT})_{T = T_B}$

As the temperature decreases below T_B, the remanence increases as J_S. For small values of the argument, $[\dfrac{vJ_S h}{kT}]_{T=T_B} \ll 1$,

15. $\qquad \vec{J}_{TRM}(T) = NvJ_S(T)\dfrac{vJ_S(T_B)\vec{h}}{kT_B} = [\dfrac{Nv^2 J_S(T)J_S(T_B)}{kT_B}]\vec{h}$

for which case $\vec{J}_{TRM}$ is not only parallel to h but also is linearly related to its intensity. At higher fields $\vec{J}_{TRM}$ approaches saturation according to the hyperbolic tangent law.

Néel's theory for single domain grains has been so successful in explaining the most important features of TRM that one might wonder whether further study is necessary. Because of hematite's low saturation magnetization, $J_S < .5$ emu/g (Chevallier and Mathieu, 1943, in Fuller, 1970), hematite's critical diameter, d_c, for the single domain to multidomain transition for spherical grains has been estimated to be of the order of 1 mm (Stacey, 1963). Thus, most naturally occurring hematites in igneous and sedimentary rocks and in baked clays are probably single domain. In addition, the work of Chevallier and Mathieu (1943) shows that for some natural hematites the bulk coercivity, H_C peaks at a grain size of about 15 μm with a value of approximately 1500 oe, suggesting that for these hematites the bulk coercivity, H_C, peaks within the single domain size range.

In igneous rocks where the remanence is often in titanomagnetites, it is much less convincing to argue that the remanence carriers are single domain. The transition diameter, d_c, for the single domain to multidomain transition is obtained by comparing the magnetic energies (magnetostatic, exchange, magnetocrystalline, and wall energies) of the different possible magnetic states of the system. For example, one can compare the state of homogeneous magnetization (single domain) with that of a two-domain

configuration separated by a 180° domain wall. It is assumed that the system will be in the state of minimum energy. Such energy balance calculations lead to values for d_c at room temperature of the order of .05 μm (Morrish and Yu, 1955; Stacey, 1963; Evans, 1972). Stable remanence has been observed in natural and synthetic magnetite grains larger than d_c and in excess of 1 μm (Roquet, 1954; Morrish and Yu, 1955; Rimbert, 1959; Parry, 1965; Dunlop, 1973; present study). In addition, Soffel (1971) observed domain walls in titanomagnetite grains(of composition .55Fe$_2$TiO$_4$.45Fe$_3$O$_4$) as small as 1.3 μm in diameter. This suggests that in Ti-free magnetite, domain walls can exist in even smaller grains. These results suggest that stable remanence exists in grains of diameters larger than d_c; that is, in particles larger than single domain. Indeed, stable remanence may reside in multidomain grains. Titanomagnetite grains in excess of 1μm are very common in igneous rocks. Optical microscopy, which is most commonly used to observe and count the opaque grains in rocks, is strongly biased to viewing grains larger than the wavelength of the light used ($\lambda \approx .5$μm). Hence, grains smaller than .5 μm are extremely difficult to resolve, identify and count. The above reasons have given rise to the development of several multidomain and pseudo single domain theories to explain the stable remanence of rocks.

Néel (1955), Stacey (1958), Everitt (1962) recognize the importance of self-demagnetization in multidomain remanence, which determines the grain's magnetization above T_B. Néel (1955) assumes that $\dfrac{H_C(T)}{H_C(T_0)} = \left[\dfrac{J_S(T)}{J_S(T_0)} \right]^{m=2}$ which in conjunction with the mean self-demagnetizing factor, D, effects blocking. Néel's model can be conceptualized for any m>1, although alternate choices for m will affect the equation for the remanence. Stacey (1958) assumes that at T_B a configuration of minimum energy is maintained

such that $h_{ex} - DJ = 0 \Rightarrow J = h_{ex}D$. For $T<T_B$ the remanence increases as the spontaneous magnetization. Everitt (1962) extended Stacey's approach and obtained an explicit expression for the T_B.

Verhoogen (1959) and Kobayashi and Fuller (1968) seek to explain multidomain remanence in terms of small single domain behaving regions in large grains. These single domain regions are pinned by the uniaxial stress fields associated with dislocations (Verhoogen, 1959) or dislocation pileups (Kobayashi and Fuller, 1968). Ozima and Ozima (1965) visualize single domain behaving regions isolated within large grains by numerous microfractures.

Lowrie and Fuller (1969) and Shive (1969) demonstrate the importance of internal stresses in affecting multidomain remanence, TRM in particular.

To explain the stable remanence found in small multidomain grains up to 15-20 μm in diameter Stacey (1958) considers the Barkhausen discreteness effect. Pseudo-single domain is a term invented by Stacey to describe magnetically stable particles with diameters greater than d_c. Barkhausen discreteness is due to energy barriers to the wall movement. Thus as the external field is removed, the wall is pinned before reaching the fully demagnetized position and leaving the grain with net remanence parallel to the inducing field. Recently, Stacey and Banerjee (1974) propose a new model for pseudo-single domain remanence which attributes their relatively high stability to surface domains that result from the intersection of domain walls with the grain's surfaces. Dunlop (1973) proposes 'wall-like' domain structure in submicron grains to explain some of his experimental results.

Our understanding of remanence in larger-than-single domain particles is only qualitative at present, and it might be naive to expect that one

theory could successfully explain the magnetic behavior of all such particles. Each of the above models has been criticized, and each is usually dependent for its success on inadequately known parameters. The reason for this uncertain state of the science has to do with the complexity of the problem and difficulties of direct observation and determination of the intrinsic properties. Information relating to stress fields associated with different kinds of crystal imperfections and their temperature dependences, and data about actual domain and domain wall structure and their respective temperature dependences in larger than single domain particles would be extremely valuable in establishing constraints for multidomain models.

There is, on the other hand, accumulating experimental evidence suggesting that stable remanence in rocks originates in submicroscopic grains, whose high stabilities suggest single domain behavior (Evans and McElhinny, 1966; Watkins and Haggerty, 1967; Hargraves and Young, 1969). In addition, these studies suggest that the stable remanence in these rocks is associated with the oxidation of silicate minerals: pyroxene, olivine, and plagioclase. This hypothesis is supported by the electron microscope observations of Evans and Wayman (1970).

In this study we investigate, mostly experimentally, some remanence properties in magnetite that are important in paleomagnetism. Titanium free magnetite, Fe_3O_4, was chosen for this study because it is probably the most common remanence carrying mineral in igneous rocks, and both natural and synthetic specimens are readily available and easily prepared in the laboratory. In addition, magnetite is mineralogically stable at T_R. We study a host of magnetic properties for a variety of magnetite particles of differing shapes and sizes and interpret the results in terms of these differences.

In the next chapter we describe the physical and chemical properties of the various magnetites studied in this dissertation, concentrating particularly on the grain-size distribution of the particles. We also examine the effect of heating to above 600°C on the bulk magnetic properties of the synthetic magnetite powders. In the following chapter we describe the method for sample preparation, and in chapter 4 we discuss the stability of weak field TRM of the prepared samples. In Chapter 5 we present experimental data and discuss the field dependence of TRM stability against alternating fields (and thermal) demagnetization for large crystals and fine particles. In Chapter 6 we discuss our experiments on the temperature dependence of A.F. demagnetization of TRM in large crystals and fine particles and the temperature dependence of various hysteresis properties of a submicron magnetite powder. In Chapter 7 we discuss our experiments on the additivity low of partial TRM in magnetite as a function of grain size. In Chapter 8 we discuss experiments on the use of magnetites for paleointensity determinations as a function of grain size. In Chapter 9 and 10 properties of anhysteretic remanent magnetization, ARM, are compared with TRM and an attempt is made to gain a better understanding of the role of magnetic interactions in ARM and TRM.

CHAPTER 2

DESCRIPTION OF THE MAGNETITES

A large fraction of this dissertation is devoted to a systematic and comparative study of some of the magnetic properties of magnetites which are of particular importance for paleomagnetism. The chief variable in these experiments is the characteristic size and shape of the magnetite particles of the different samples, both of natural and synthetic origin. In this chapter we describe the magnetites that will be used in subsequent experiments of this study. We shall elaborate on the particles' physical and chemical properties, their origin, and their shapes and size distributions as obtained from electron microscope photographs. We shall also discuss the synthetic magnetites' bulk magnetic properties.

2.1 PHYSICAL AND CHEMICAL PROPERTIES OF THE NATURAL MAGNETITES

Several magnetite crystals from the same ore body were obtained. One of these crystals was analyzed by an electron microprobe (Johnson and Merrill, 1972), which "indicates that the natural magnetite contains less than 0.03% by weight of V, Cr, Mn, Ni, and Mg, a Ti content less than 0.05% and an Al content less than 0.23%." One crystal was ground and sieved to obtain several size ranges of magnetite particles. Two large chips several millimeters in diameter were used to determine the magnetite's saturation magnetization in a field of 7.9 koe. Values of 94.2 ± 2 emu/g and 92.0 ± 2 emu/g were obtained, in good agreement with the accepted value for pure magnetite of about 92.5 emu/g. This strongly suggests that the natural magnetite is essentially stoichiometric. Curie points were determined using one of the above chips and particles of one of the smaller particle sizes (powder 3). Heating was conducted in a slightly reducing environment

to prevent oxidation of the magnetite, using carbon as a reducing agent and a residual nitrogen atmosphere at low pressure ($\approx$.2 mm of Hg). To accentuate the Curie point determination only moderate external fields were applied. The two J versus T curves were obtained in fields of 560 oe and 720 oe, respectively, yielding single, well defined Curie points of 580° ± 10°C and 582° ± 10°C, respectively. In addition, Johnson and Merrill (1972) report that X-ray diffraction patterns of the natural magnetite powder show no hematite or maghemite lines, but only those spinel lines associated with magnetite. All these pieces of evidence suggest that we are dealing with essentially pure and stoichiometric magnetite, $Fe^{3+}[Fe^{2+}Fe^{3+}]O_4$.

Four massive magnetite crystals, MSC-0, MSC-1, MSC-2, MSC-3 are studied in our experiments. It is very important to note that samples MSC-0 and MSC-1 are identical with 0 and 1, respectively, of subsequent chapters. Samples MSC-0 and MSC-3 are euhedral crystals weighing 6.378 gm and 9.583 gm, respectively. Samples MSC-1 and MSC-2 are chips of the same crystal. MSC-1 weighs 3.569 gm and MSC-2 weighd about 3 tm. The density of magnetite is 5.18 gm/cc. Figure 1 shows MSC-0, MSC-1. MSC-3 resting on one of their (111) surfaces. Sample MSC-2 was pulverized to prepare sized powders before it was weighed and before figure 1 was taken. MSC-2 had about the same base area as MSC-1, but was considerably flatter. The crystals are apparently deformationally twinned (N.I. Christensen, private communications, 1971).

MSC-2 and an additional crystal were pulverized to prepare sized particle fractions. The magnetite was manually dry ground in a porcelain mortar and pestle and mechanically sieved, and the particle fractions are discriminated by the sieves which bracketed them. The particle size

fractions that are later dispersed in a non-magnetic matrix to simulate paleomagnetic specimens were photographed by a scanning electron micro-scope (JEOL JSM-U3) and their shapes and particle size distributions will be discussed in some detail. The particle size fractions will be numbered according to the sample number with which they will be later associated. For example, particle size fractions 2, 3, 4 correspond to samples 2, 3, 4, respectively. Samples 2 and 3 are distinct from samples MSC-2 and MSC-3!

The particle size fraction of the ground natural magnetite crystals bracketed by sieve size of 105 μm and 44 μm is called powder 2. From the sieve sizes one expects that the mean diameter or characteristic length of these particles should be in the range 44 μm<d<105 μm. Figures 2a and b show the electron microscope pictures of powder 2. Photograph 2a is X 200; that is, 1 cm = 50 μm. We see several large particles among many much smaller particles. The particle shapes are quite irregular, and the largest particle has a characteristic length of about 150 μm. The characteristic lengths (or mean diameters) are measured directly off the photograph and their values are approximated such that a circle of that diameter (or characteristic length) should have the same area as that of the measured particle. Photograph 2b focuses on some of the specks of figure 2a. The magnification is X 1000, such that each centimeter on the photograph is equivalent to 10 μm. Figures 5a-c represent the labor of particle counting. Figure 5a is the particle size distribution of powder 2. Because of the broad range of particle sizes, the abscissa is a contracted logarithmic scale while the ordinate represents the particle number. 25 particles were measured off figure 2a and 39 particles off figure 2b. The mean particle diameter for each figure is designated by an arrow on figure 5a. For

Figure 1

Photograph (x 1) of the large magnetite crystals, resting on one of their respective (111) surfaces. From left to right: MSC-0, MSC-1, MSC-3. MSC-0 and MSC-1 are also identified as samples 0 and 1, respectively, in later chapters.

Figure 2

a. Electron microscope picture (x 200) of magnetite powder 2, corresponding to sample 2. These particles were retained between 44 µm and 105 µm sieves. Note the large variation in particle sizes.

b. Electron microscope picture (x 1000), focussing on some of the smaller particles of figure 2a.

1 cm
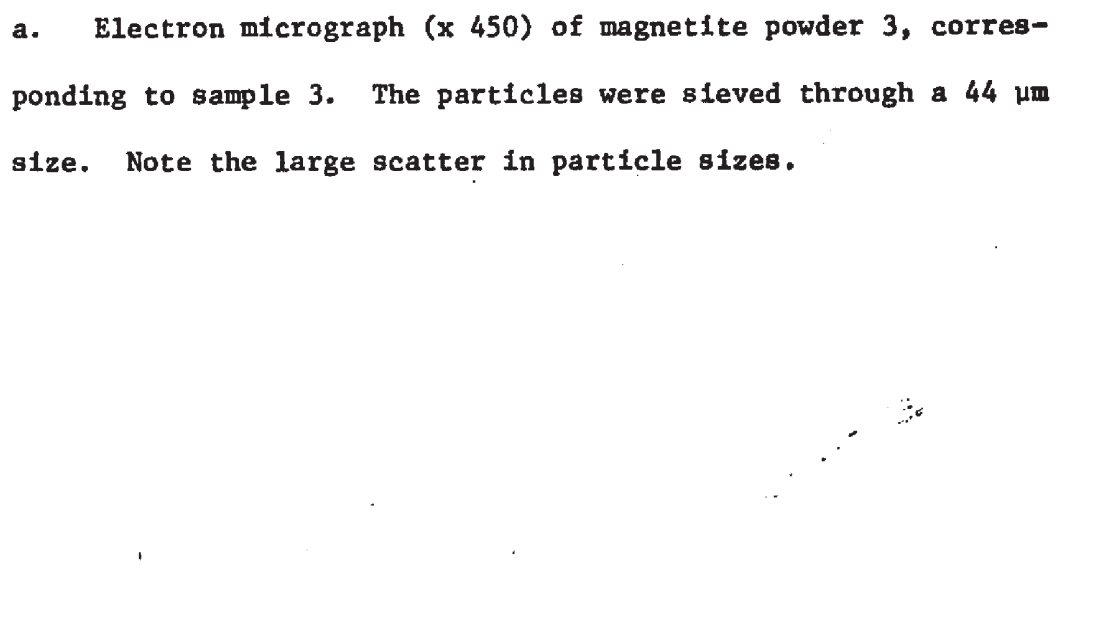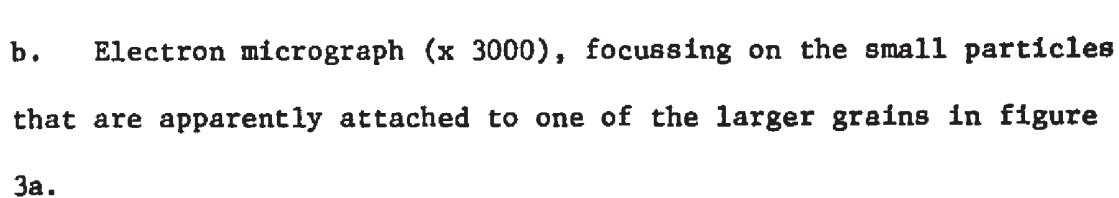
100 μm

20 μm

Figure 3

a.   Electron micrograph (x 450) of magnetite powder 3, corres-
ponding to sample 3. The particles were sieved through a 44 μm
size. Note the large scatter in particle sizes.

b.   Electron micrograph (x 3000), focussing on the small particles
that are apparently attached to one of the larger grains in figure
3a.

50 μm
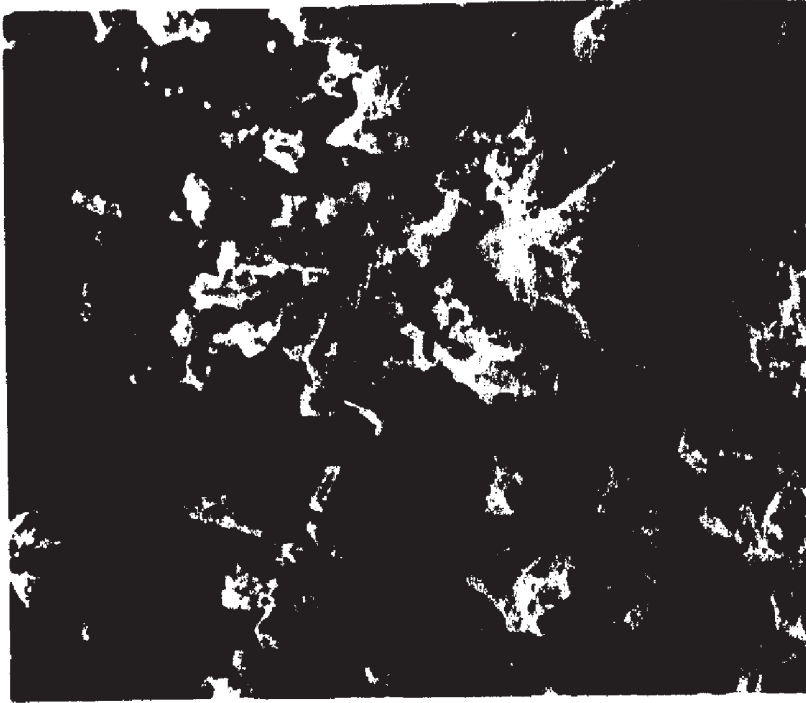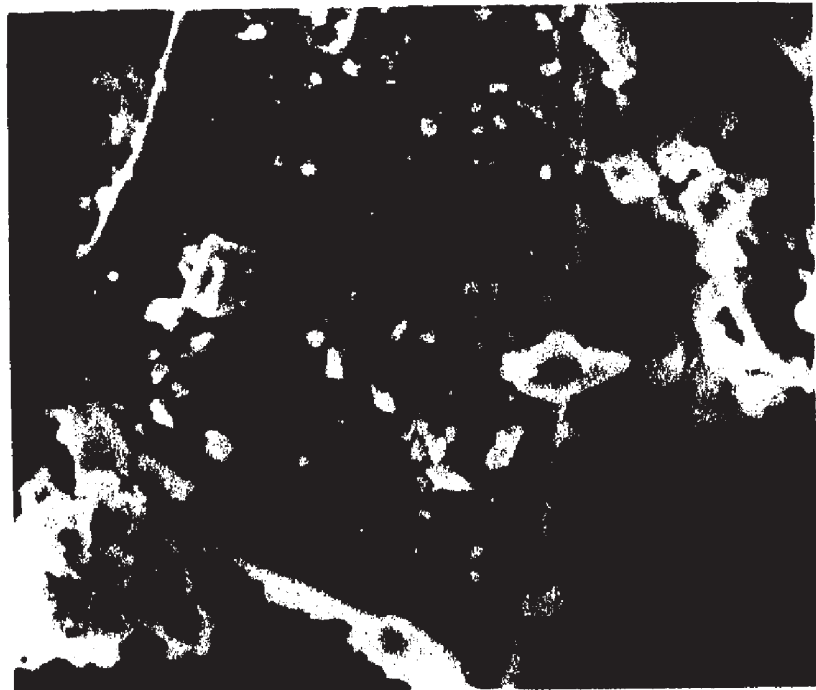
10 μm

figures 2a and 2b the mean diameters are 5.2 and 2.1 μm, respectively. Although a different number of particles is counted in each photograph, each mean diameter is given equal weight. To obtain the overall mean particle diameter we normalize with respect to the magnification; higher magnification is given proportionally greater weight. Thus the over-all mean particle diameter is:

$$<d> = (1/5) (5.2 \ μm) + 4/5 (2.1 \ μm) = 2.7 \ μm$$

This value should be compared with the minimum sieve size of 44 μm.

Powder 3 was also manually ground and sieved through the 44 μm sieve. From the patience required to sieve these particles, one would guess that they are all between 40 μm and 44 μm in size, and certainly none was expected to be smaller than 10 μm. Figures 3a, b are X 450 and X 3000 electron microscope pictures of powder 3, respectively, and each 1 cm of figures 3a and 3b represents 22.2 μm and 3.3 μm, respectively. The particle shapes are irregular and the largest grains have a mean diameter of about 50 μm. Many small particles are attached to the large ones; this is very clear in figure 3b which focuses on one of the larger particles in the center of figure 3a. The abscissa of the particle size distribution, figure 5b, is a contracted logarithmic scale representing the particle diameters. 46 particles were counted in figure 3a and 88 in figure 3b. The mean diameter for each figure is designated by an arrow on the particle size distribution. For figures 3a and 3b the mean particle diameters are 6.4 μm and .64 μm, respectively. As for powder 2, we assign equal weight to the mean diameters obtained from the two photographs of powder 3 and normalize with respect to the magnification, giving proportionately greater weight to the larger magnification. Thus the over-all mean particle diameter of powder 3 is:

$$\langle d \rangle = (450/3000)\ 6.4\ \mu m + (1 - \frac{450}{3000})\ .64\ \mu m = 1.5\ \mu m$$

It appears that one of the major differences between powders 2 and 3 is in the fraction of particles greater than 50 μm, which is essentially absent from powder 3. Both powders have abundant small particles of the order of 1 μm.

Powder 4 was obtained by ball-milling. To prevent heating and possible adverse oxidation effects, ball-milling was carried out in 8 25-minute time segments separated by approximately 30-minute intervals for cooling. The powder was then sieved through a 44 μm sieve. Figure 4 is one of the electron microscope pictures. The particle shapes are more regular and their sizes more uniform than for powders 2 and 3. 79 particles were counted off figure 2.4 and their particle size distribution appears in figure 5c, where both axes are linearly scaled. The distribution can be described by a single mean diameter of .31 μm, and none of the particles is greater than 2 μm.

The particle size distributions in figures 5a-c are not as smooth as might be expected. Rather, there are sometimes rapid fluctuations in the particle numbers counted at successive characteristic diameters. Characteristic particle diameters were measured off the photographs to the nearest 1/2 millimeter, and the jaggedness in the particle size distributions is due to the experimental bias favoring integral millimeter values.

The physical description of the natural magnetites is summarized in table 1. (It is important to note that the sample numbers of column 1 will be followed and maintained throughout the dissertation.) Column 2 lists the sieve sizes that bracket the powder size fractions; column 3 lists the mass of the single crystal samples and mean particle diameter, $\langle d \rangle$, of the powders; column 4 lists the maximum particle sizes observed in

Figure 4

Electron micrograph (x 12000) of magnetite powder 4, corresponding to sample 4. The particles were first ball-milled and then sieved through a 44 μm sieve. Note the smaller particle sizes and the smaller scatter in the particle size distribution in comparison with powder 3, figure 3.

Figure 6

Electron micrograph (x 20,000) of heated, synthetic, Toda magnetite powder, corresponding to sample 11. Note the elongated shapes of the particles whose mean axial ratio is 8:1.

2 μm

1 μm

Figure 5

a.   Particle size distribution for magnetite powder 2 obtained

from   grain counts of figure 2a (open circles) and figure 2b

(solid circles). Note the logarithmic contraction of the

abscissa due to the broad range of particle sizes. The arrows

indicate the mean particle diameter of each figure <d> = 2.7 μm.

b.   Particle size distribution for magnetite powder 3 obtained

from grain counts of figure 3a (open circles) and figure 3b

(solid circles). The arrows indicate the mean particle diameter

of each figure. Note the logarithmic contraction of the

abscissa. <d> = 1.5 μm.

c.   Particle size distribution of magnetite powder 4 determined

from particle counts of several electron micrographs including

figure 4. Note that the abscissa is linear, and the arrow

designates the mean particle diameter. <d> = .31 μm.

SAMPLE 2

No. of PARTICLES

CHARACTERISTIC DIAMETER, μm

SAMPLE 3

No. of PARTICLES

CHARACTERISTIC DIAMETER, μm

SAMPLE 4

No. of PARTICLES

CHARACTERISTIC DIAMETER, μm
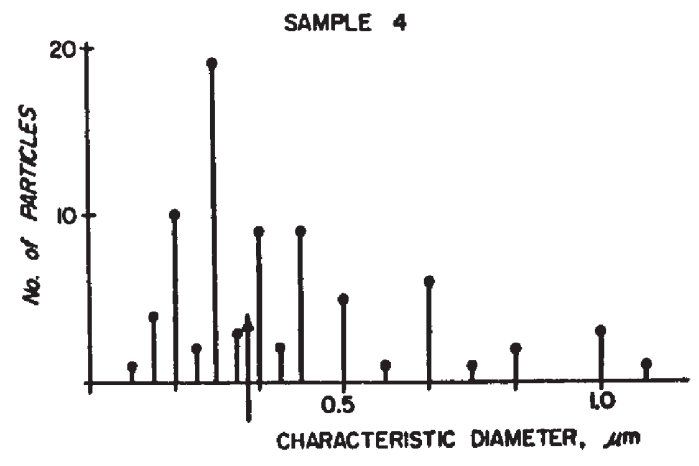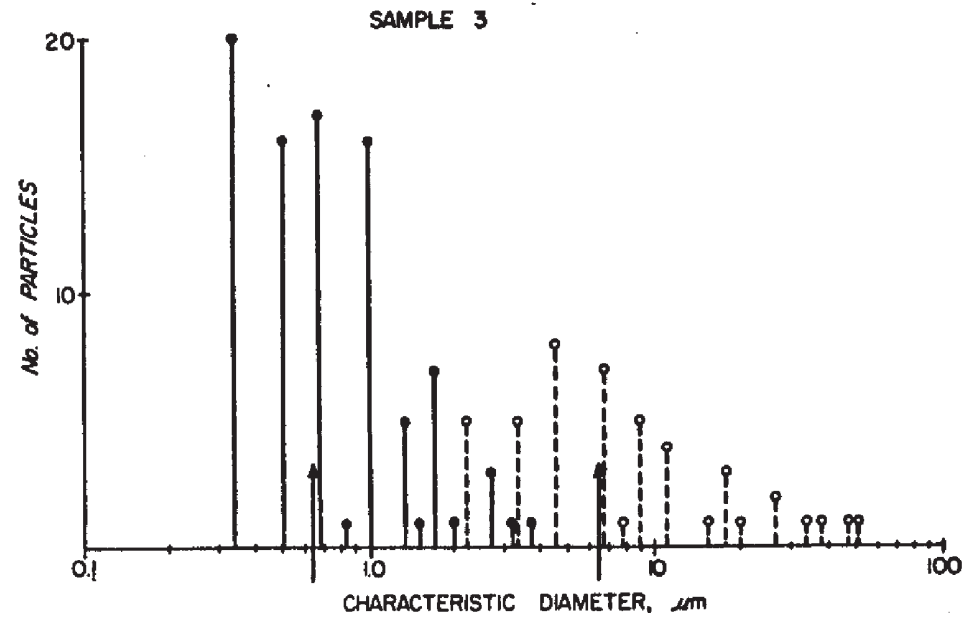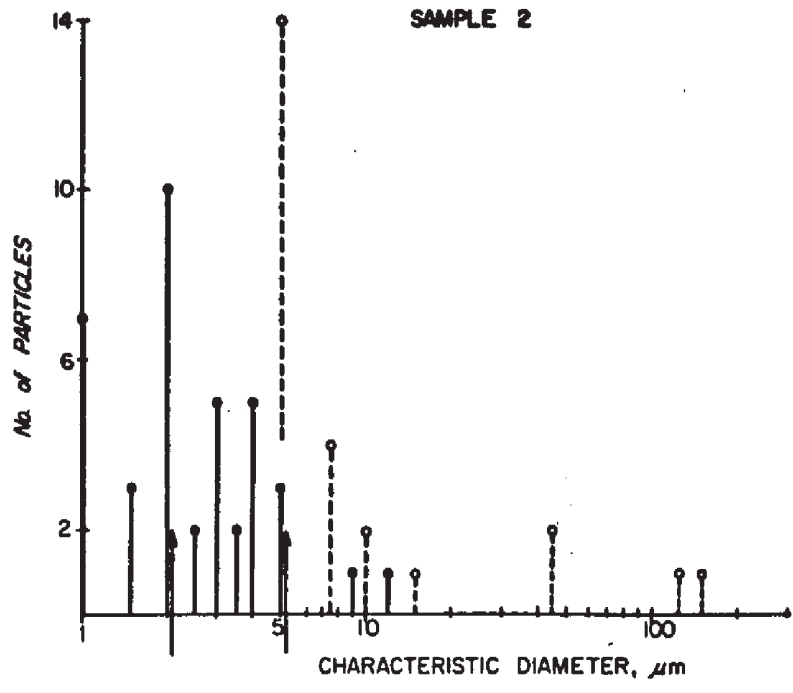
TABLE 1

PHYSICAL DESCRIPTION OF THE NATURAL MAGNETITES

Sample and/or Powder No.	Sieve Size, μm	$<d>$, μm (gm)	d_{max}, μm	Predominant Shape
MSC-0 ≡ 0		6.378 gm		Euhedral Crystal
MSC-0 ≡ 0		3.569 gm		Crystal Chip
MSC-2		~3 gm		Crystal Chip, Flat
MSC-3		9.583 gm		Euhdral Crystal
2	44<d<105	2.7	150	Irregular
3	d<44	1.5	50	Irregular
4	d<44	0.31	2	Regular Polygons

each powder; and column 5 describes the shapes of the particles.

2.2 PHYSICAL AND CHEMICAL PROPERTIES OF THE SYNTHETIC MAGNETITES

In addition to the natural magnetites, several synthetic magnetite powders were obtained and studied. Two species of equidimensional magnetite powder were received, one from the Columbian Carbon Company (C.C.C.) and one from the Pfizer Company (BK-5099). These magnetite powders are prepared by direct precipitation from an aqueous solution. An additional species of equidimensional magnetite was prepared in the laboratory according to a recipe of Elmore (1938) by its direct precipitation from an appropriate solution of ferric and ferrous chloride in the presence of sodium hydroxide. An acicular, needle-shaped magnetite powder was obtained from Toda Industries, Inc. All the synthetic magnetite powders have impurity contents less than 1%.

Magnetites prepared at room temperature by precipitation in an aqueous solution are usually slightly oxidized (Gallagher et al., 1968), and their FeO/Fe_2O_3 ratio is usually 20%-24% by weight rather than the 31% for stoichiometric magnetite. Gallagher et al. (1968) showed that the X-ray diffraction pattern of the oxidized magnetite is identical in its structure to that of stoichiometric magnetite down to an FeO/Fe_2O_3 ratio of 22% by weight. There is, however, a steady shift of the diffraction peaks to higher 2θ angles, representing a decrease in the lattice spacings. In addition, Gallacher (1968) also noted a broadening in the diffraction peaks of the oxidized magnetites with respect to the unoxidized material. As the oxidation nears completion (pure maghemite in their case), the peaks become narrower again. In addition to changes in the mineralogy, the magnetic properties also are affected by oxidation (Johnson and Merrill, 1972). For example, the saturation magnetization, J_S, of oxidized

magnetites is always less than that of stoichiometric magnetite.

In our subsequent experiments we shall be particularly interested in various TRM and PTRM properties of prepared samples containing dilute concentrations of the various magnetite powders. That is, the powders will be heated above their Curie points before they are studied. Heating may drastically affect the magnetic properties of the powders through their oxidation or reduction, through annealing of some of the strains introduced in the precipitation process, and through sintering and grain growth. In order that the characterization of the powders be applicable to the magnetites in the samples, the powders are first heated above their Curie points before they are further studied. Since we would like to study the properties of unoxidized magnetites similar to those found in many unaltered igneous rocks, the magnetite powders are heated above 600°C in a slightly reducing chemical environment, using carbon as a reducing agent and a residual nitrogen atmosphere at 0.1 - 0.3 mm of Hg. The temperature is maintained above 600°C for 6.5 hours before cooling back to T_R. X-ray diffraction patterns of the heated and unheated C.C.C. magnetite show only magnetite peaks. No maghemite or hematite peaks are observed. Although they are never observed in any of our experiments, it is still possible that small fractions of hematite and/or maghemite (<5%) are present but hiding. There is a systematic shift of the peaks of the heated powder to lower 2θ angles and higher lattice spacings with respect to the unheated powder. The cell parameter of the heated powder is 8.39 ± .01 A°, which is indistinguishable from stoichiometric magnetite. Johnson (1973, private communication) has made similar observations for this and other precipitated magnetites. He also noted a decrease in the line broadening of the heated powders, which he interpreted as grain growth; however, in view of the work of Gallagher

et al. (1968) such a decrease in line width would also be consistent with the reduction to stoichiometry of the oxidized magnetite powder.

Electron microscope pictures were taken of the heated powders. Representative pictures of the Toda MRM B-450, C.C.C. magnetite, Pfizer BK-5099, and Elmore magnetite powders are shown in figures 6 - 9, respectively. Figure 6 of Toda (MRM B-450) magnetite shows that the particles are predominantly acicular (needle-shaped). However, only a few of the particles (25) could be completely measured and their mean dimensions, both length and width, are nearly double the values reported by Toda Industries, although their mean length to width ratio is close to the reported value of 8:1. This suggests that the particles that we were able to measure are near the maximum end of the particle sizes. Because data obtained by us, such as the bulk coercivity, H_C (Table 3), and the saturation magnetization, $J_S(T_R)$, to characterize the Toda magnetite powder are in close agreement with similar data provided by Toda Industries, we shall assume that the true mean particle dimensions are those reported by Toda Industries which are 0.35 µm x .04 µm and whose approximate axial ratio is 8:1.

Characteristic particle diameters were measured off figures 7, 8, and 9a and other similar pictures to obtain the particle size distributions plotted in figures 10a - c, where both axes in each of these figures is linearly scaled. A total of 232 particles in two photographs were measured for the C.C.C. magnetite. 111 particles were measured off two photographs for the Pfizer BK-5099 powder, and 249 particles off three photographs were measured for the Elmore magnetite. The mean particle diameter for each powder is designated by an arrow in the particle size distributions. The mean diameters are .12µm, .21µm, and .24µm for Elmore, C.C.C., and Pfizer BK-5099 magnetite powders, respectively, with maximum observed

Figure 7

Electron micrograph (x 20,000) of heated, synthetic, Columbian

Carbon magnetite powder, corresponding to sample 6 and 7. Note

the relatively small dispersion in the particle size distribution

and the rather uniform and polygonal shapes of the particles.

Figure 8

Electron micrograph (x 20,000) of heated, synthetic, Pfizer

BK-5099 magnetite powder, corresponding to sample 5. Note the

similarity of these particles to those of figure 7.

1 μm
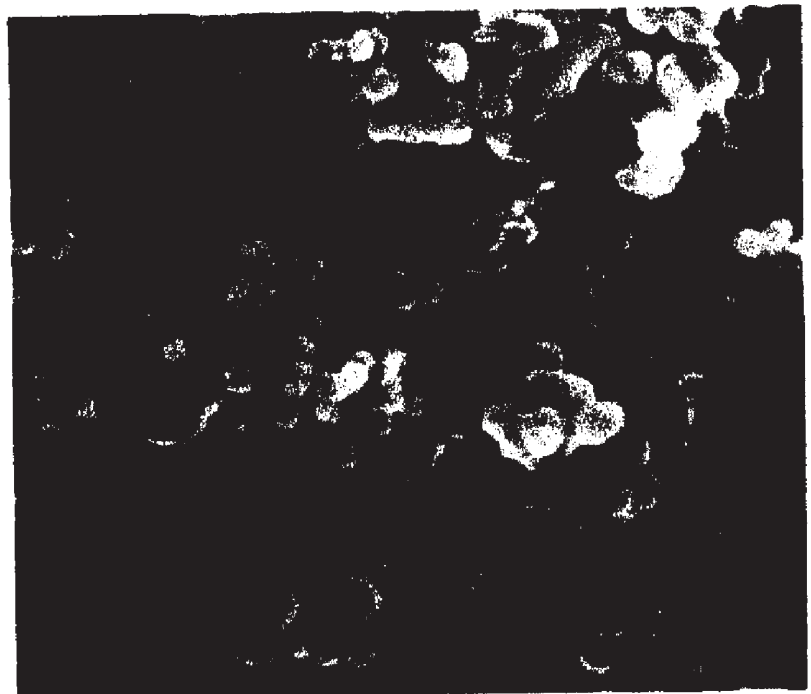
1 μm

Figure 9

a. Electron micrograph (x 20,000) of heated, synthetic, 'Elmore' magnetite powder, corresponding to samples 8 and 9. Note the small dispersion in the particle size distribution and the rather uniform and polygonal shapes of the particles.

b. Electron micrograph (x 40,000) of unheated, synthetic, 'Elmore' magnetite powder. Note the dramatic increase in the particle sizes upon heating seen by comparing figure 9b with 9a.
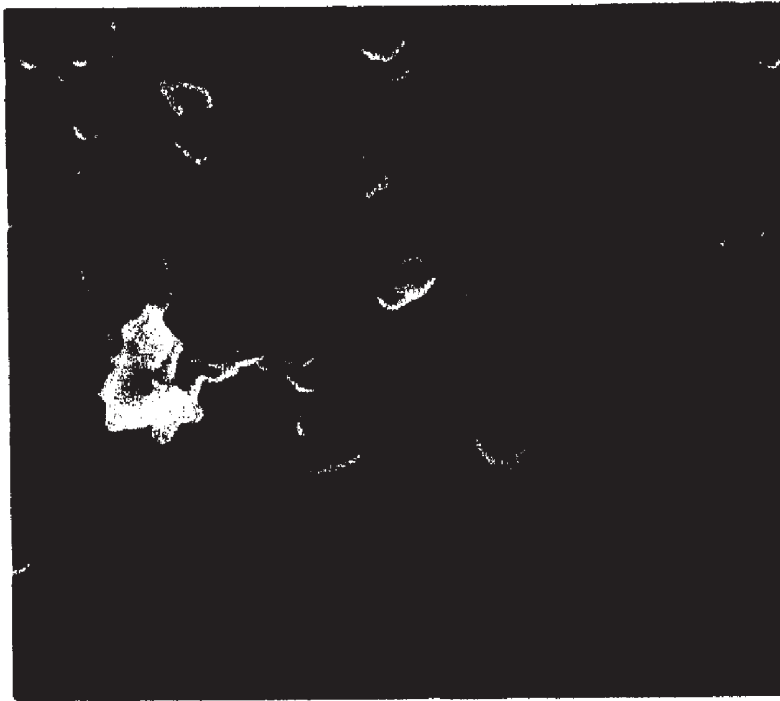
1 μm

.5 μm

Figure 10

Particle size distributions of the heated, synthetic,
magnetite powders obtained from **diameter** measurements and par-
ticle counts off electron micrographs such as figures 7,8, and 9.
The arrows indicate the distributions' mean particle diameters.

a.   Sample 5   Pfizer BK-5099 magnetite powder, <d> = .24 μm.

b.   Samples 6 and 7   Columbian Carbon magnetite powder, <d> = .21 μm.

c.   Samples 8 and 9   'Elmore' magnetite powder, <d> = .12 μm.

SAMPLE 5

No. of PARTICLES / CHARACTERISTIC DIAMETER, μm

SAMPLES 6 AND 7

No. of PARTICLES / CHARACTERISTIC DIAMETER, μm

SAMPLES 8 AND 9

No. of PARTICLES / CHARACTERISTIC DIAMETER, μm
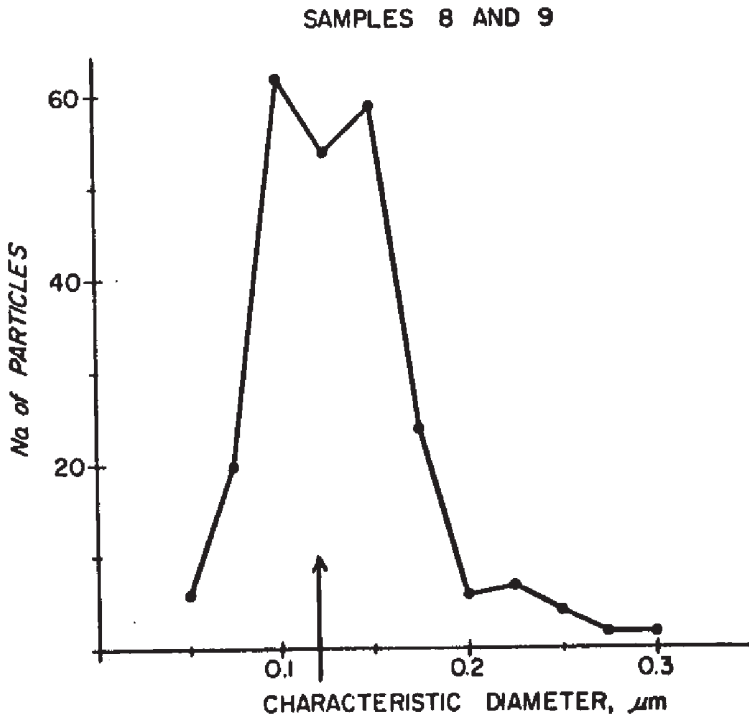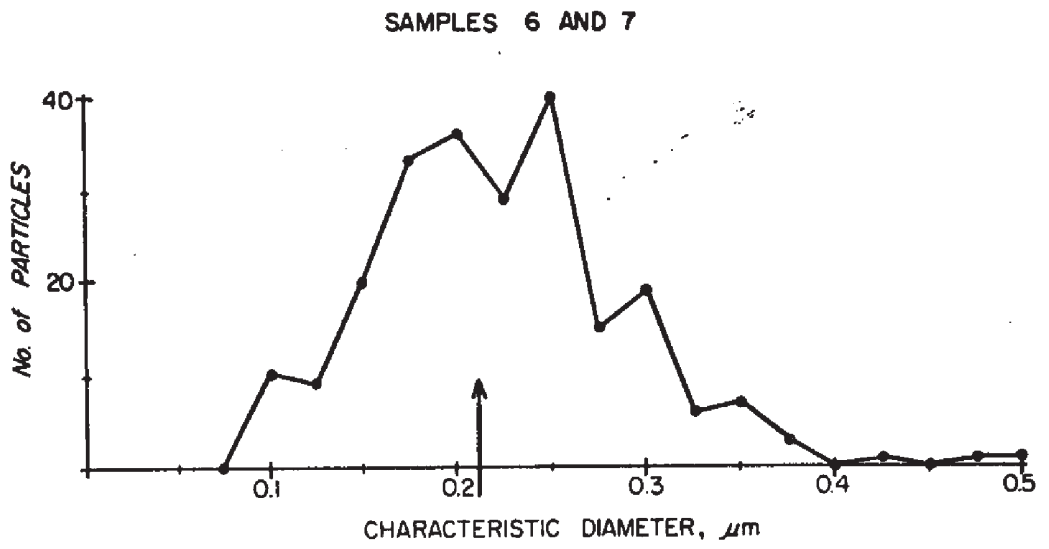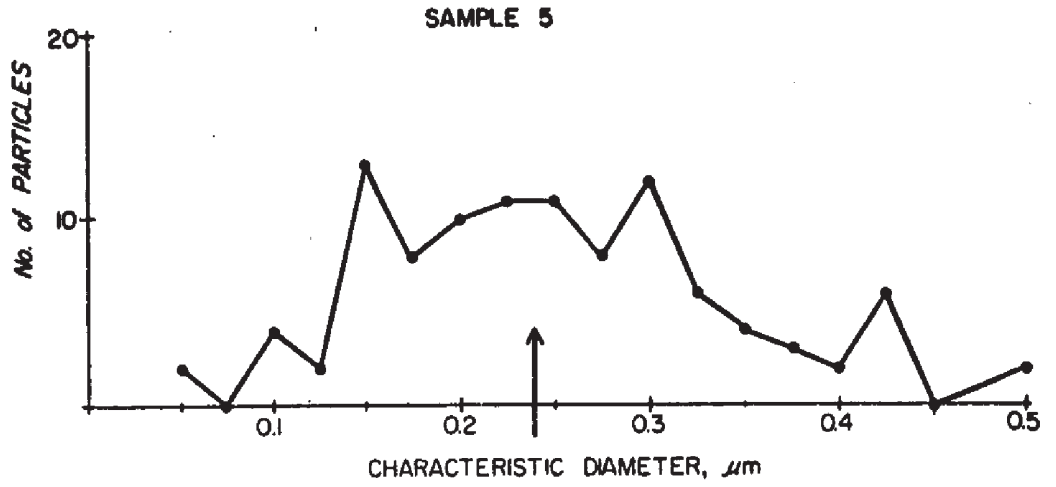
TABLE 2

PHYSICAL DESCRIPTION OF THE SYNTHETIC MAGNETITE POWDERS

Magnetite Powder	Sample Number	$\langle d \rangle$ (µm)	d_{max} (µm)	Predominant Particle Shape
Pfizer BK-5099	5	0.24	0.9	Reg. Polyg. Cubes → Spheres
C.C.C.	6, 6A 6B, 6C 7	0.21	0.5	Reg. Polyg. Cubes → Spheres
Elmore	8, 9	0.12	0.3	Reg. Polyg. Cubes → Spheres
Toda MRM B-450	11	0.35 x 0.04	1.2 x 0.13	Acicular Axial Ratio 8:1

diameters for particles of these powders of 0.3 μm, 0.5 μm, and 0.9 μm, respectively. It should be pointed out that the observed mean particle diameters of both C.C.C. and Pfizer BK-5099 magnetite powders are less than those reported by their makers: 0.2μm - 0.8μm and 0.3μm - 0.4μm, respectively.

Table 2 summarizes the physical description of the heated synthetic magnetite powders. Column 2 gives the sample numbers corresponding to the particular magnetite powders present in that sample. These sample numbers will be maintained throughout the remainder of this study. Columns 3 and 4 list the mean particle diameter, $<d>$, and the maximum observed particle diameter, d_{max}, respectively, for each of the powders. In column 5 the particle shapes are listed.

2.3 COMPARISON OF THE BULK MAGNETIC PROPERTIES OF THE UNHEATED AND HEATED SYNTHETIC MAGNETITE POWDERS

Table 3 describes the effect of heating on the bulk magnetic properties of the synthetic magnetite powders. All the data in table 3, as well as the values for T_C in tables 1 and 2, and the values of J_S for the natural magnetites, were obtained using a vibrating sample magnetometer (VSM) manufactured by the Princeton Applied Research Company. H_C, the bulk coercivity, is the reverse field for which the sample magnetization is zero. H_{CR}, the coercivity of the remanence, is that reversed field which upon removal leaves the sample unmagnetized. J_S is the saturation magnetization and J_{RS} is the remanence remaining after the saturating field is removed. Heating above 600°C is conducted in a slightly reducing evironment to prevent the oxidation of the magnetite, as described earlier in this chapter. That this is indeed the case was strongly suggested by the fact that, after heating, J_S is always greater than or equal to its value prior to heating.

TABLE 3

THE EFFECT OF HEATING ON THE BULK MAGNETIC PROPERTIES OF THE SYNTHETIC MAGNETITE POWDERS

Magnetite Powder	T_C, °C ±10°	$H_C(T_R)$, OERSTED ± < 3 OE		$H_{CR}(T_R)$, OERSTED ± < 7 OE		$H_{CR}/H_C\vert_{T_R}$ ± < .10		$J_{RS}/J_S\vert_{T_R}$ ± .005	
		Unheated	Heated	Unheated	Heated	Unheated	Heated	Unheated	Heated
Pfizer BK-5099	565	98	100	270	278	2.76	2.78	.103	.103
C.C.C.	570	148	105	400	279	2.70	2.66	.144	.121
Elmore	575	26.5	112	175	315	6.60	2.81	.004	.116
Toda MRM B-450	591	440	438	600	582	1.36	1.33	.440	.448

(Reduction of the iron oxide beyond magnetite is highly unlikely in our experiments.)

Comparison of electron micrographs of heated and unheated C.C.C. and Pfizer BK-5099 magnetite powders shows no measurable difference in the mean particle diameters or particle shapes, where we have assumed throughout that the particles that we observe and measure are indeed representative of the entire powder. This observation suggests that the observed changes upon heating of the magnetic properties of these magnetite powders are not caused by grain growth. The effects of heating on the magnetic properties of the Toda and Pfizer magnetite powders are small and probably not significant. The effects of heating on C.C.C. magnetite is probably caused by the reduction of the iron oxide to magnetite and/or by annealing. It is not possible to distinguish among these two mechanisms because both are present in our experiments with the synthetic powders. The annealing effect is expected to reduce the coercivities and the J_{RS}/J_S values as observed for the C.C.C. powder, while the trend of the effect of oxidation and reduction is more difficult to assess. Figures 9a and 9b are electron microscope pictures of heated and unheated Elmore magnetite powder, respectively. Figure 9a is X 20,000 and figure 9b is X 40,000. It is clear that the mean particle diameter of the heated powder in figure 9a is substantially greater than that of the unheated powder. The relatively large effect of heating on the magnetic properties of the Elmore magnetite is, therefore, at least in part due to grain growth of some of the superparamagnetic grains into the stable single domain size range. The observed trends of the coercivities, H_C and H_{CR}, and the J_{RS}/J_S values are consistent with this interpretation. Equations 7, 8, and 9 show that for Néel-type single domain grains, if all other parameters are held constant, τ increases with

increasing grain volume—from superparamagnetic ($\tau \ll t$) to single domain ($\tau \gg t$). That is, the observed magnetic behavior before and after heating of the magnetite powder in question could be explained by Néel's theory for single domain grains as being due to grain growth. It is very interesting that after heating the bulk magnetic properties of all three equidimensional magnetite powders are rather similar. It will be seen later, in Chapter 4, that the bulk magnetic properties of these equidimensional magnetites are much more similar than their TRM properties. Specifically, it will be seen that samples containing Elmore magnetite are less stable than corresponding samples of C.C.C. and Pfizer magnetite powders.

CHAPTER 3

SAMPLE PREPARATION

The content of magnetic minerals in rocks is highly variable, but is usually between a fraction of one percent and several percent, and it is rare that the magnetic mineral content exceeds ten percent. Usually the magnetic minerals are uniformly distributed throughout the rock. To simulate rocks it is necessary to dilutely disperse the various magnetite powders in a suitable matrix.

The matrix chosen in which to disperse the magnetites is Alcoa's high purity alumina powder, A-16, bonded by Alcoa's calcium aluminate cement, CA-25. The advantage of this matrix is its strength, durability, and resistance to high temperatures. Typical chemical properties and size characteristics for these powders are presented in Table 4. The data in this table was obtained from Alcoa's product data: Alcoa Reactive Aluminas (1972) and Calcium Aluminate Cement CA-25 (1970).

TABLE 4

PHYSICAL PROPERTIES OF THE SAMPLE MATRIX

	Alumina A-16	Calcium Aluminate CA-25
% Al_2O_3	99.5+	79.0
% Na_2O	.06 - .10	.5
% SiO_2	.01 - .02	.15
% Fe_2O_3	.01 - .02	.3
% CaO		18.0
% MgO		.4
% through 100 mesh		99
% through 200 mesh		97
% through 325 mesh (<44 μm)	99.5	90

Approximately 20% CA-25 cement is thoroughly mixed with 80% alumina. To the matrix mixture small amounts of magnetite powder are added (from .15% to 5% by weight). The mixture is thoroughly mixed, and sieved through a 250 μm sieve to break up small clumps and improve the sample homogeneity. Water should be added dropwise (the difference between too little water and too much water is amazingly small), and when the mixture becomes a thick paste, it is ready to be molded into a sample-size cylinder, approximately 22 mm in diameter and 22 mm high. CA-25 cement has a typical setting time of less than one hour, and, normally, full development of its bonding strength takes place within twenty-four hours. The sample should be dried at about 100°C for several hours before it is subjected to higher temperatures.

Because of magnetite's high saturation magnetization and the resulting attractive forces between the magnetic moments, magnetite powders tend to flocculate, and despite careful mixing the sieving small scale magnetite clusters surely remain. To avoid flocculation one could start out with hematite which is much less magnetic than magnetite. The room temperature saturation magnetization, $J_S(T_R)$, of hematite depends on its origin, mode of preparation, and grain size, but is usually less than 0.5 emu/gm (Chevallier and Matthieu, 1943 in Fuller, 1970). The flocculating tendency greatly reduced, hematite can be uniformly and dilutely dispersed in the matrix. The resulting hematite samples can then be reduced to magnetite. The difficulty one then encounters is making sure that all the hematite has been reduced. However, it will be shown that the possible existence of small scale magnetite clusters seems to have no measurable influence on the experiments reported here.

Before commencing with the experiments of interest, the prepared

samples were placed in an evacuated (.1 -.3 mm of Hg) quartz tube, and were outgassed at room temperature for about 24 hours. Nitrogen is the residual gas in the quartz tube, and granulated carbon is used as a reducing agent. To reduce the magnetic minerals to pure magnetite and to stabilize their magnetic properties, the samples were dried for an additional 24 hours at about 110°C, and then they were heated to 650°C where the temperature was maintained for 5 hours. On cooling, the samples were given TRM in the laboratory field. Subsequent heatings used similar procedure with elimination of the drying step and a much shortened outgassing time. The samples were subjected to repeated TRM, until their alternating field (A.F.) demagnetization spectra and their TRM values were reproducible within a few per cent. For specific examples of the reproducibility of the TRM values for the various samples see Table 6, and for the reproducibility of the A.F. demagnetization spectra refer to Table 8 and to figures 43 to 54. When these conditions were satisfied, the samples were declared stable and ready for further experiments.

Initial experiments with the matrix material suggested that, as far as our experiments were concerned, it was non-magnetic. Several blank (magnetite free) sample slugs were prepared, and one was heated with the other samples and given TRM. It was then discovered that the 'blank' sample carried measurable and stable remanence. The TRM of the 'blank' sample increased during subsequent heatings in the constant laboratory field until reaching a stable and reproducible plateau, about 1.6 times its first TRM value. In addition, the IRM of the 'blank' at the TRM plateau is 2.4 times as intense as the IRM of the unheated slub (2.24×10^{-2} emu as compared with $.95 \times 10^{-2}$ emu; both IRMs were induced in a field of 7.2 koe.) The TRM of the 'blank' sample is about 1/9 as intense as the

as the TRM of the next most feeble sample and less than 1/40 as intense as the TRM of the third most feeble sample (see Table 5). The specific magnetization (in emu/gm of sample) of the 'blank' slug diminishes yet further relative to subsequent samples reaching a minimum value of approximately 1/440 for the most intensely magnetized sample. Further experiments with the 'blank' sample revealed that more than 97 percent of the blocking temperatures are below 580°C, although the Curie point of hematite is near 695°C (Chevallier, 1951) and despite the fact that the TRM was given between 650°C and room temperature.

The Fe in the original unheated matrix material is probably partly in iron oxides and partly as paramagnetic impurities in some of the other matrix minerals such as alumina. The presence of an oxidized iron oxide mineral with low J_S such as hematite in the unheated matrix is suggested by the large increase in both IRM and TRM when the sample is heated in a reducing environment. Presumably, some of the original iron oxide is reduced to magnetite upon heating. Due to the small grain size of the matrix material and hematite's low room temperature saturation magnetization, $J_S(T_R)$, a substantial fraction of the native iron oxide may be superparamagnetic, whereas upon reduction to magnetite with its much larger $J_S(T_R)$, some of these grains may have been transformed into carriers of stable remanence. Part of the original magnetization of the matrix can be due to the presence of minor fractions of other magnetic minerals such as magnetite and maghemite with varying degrees of Mg and Al impurities. The reduction of maghemite could possibly account for some, though only a minor fraction, of the 'thermogenic' magnetite generated by reduction upon heating. The large increase in the IRM of the heated 'blank' relative to its unheated value suggests that about 70 percent of the stabilized magnetization of the

'blank' resides in this 'thermogenic' magnetite. The remaining 30 percen-
of the magnetization could reside in magnetite, hematite, and/or maghemite.
The thermal demagnetization spectrum of figure 11 shows that about 97 per-
cent of the magnetization is blocked below 580°C. There is no evidence in
the demagnetization curve for more than one magnetic phase. On the other
hand, hematites, too, have blocking temperatures below 580°C, and mineralo-
gically stable maghemites are known to exist whose Curie point is very
similar to magnetite's (Everitt, 1961). We prefer the interpretation that
the 'blank's' magnetization is dominated by magnetite, and further experi-
ments to be discussed later suggest that its TRM resides in single domain
remanence carriers.

We decided to run a 'blank' sample along in all our experiments for
two primary reasons: one, it is important to know the magnetic behaviour
of the matrix material to be able to assess whether and to what extent the
magnetic properties of the matrix affect and interfere with the study of
the magnetite grains embedded in it; two, since the magnetic minerals of
the 'blank; are naturally dilute and probably well dispersed and since a
substantial fraction of the magnetite is probably generated by the reduction
of hematite, it alone among the prepared samples avoids the previously dis-
cussed flocculation problem. Since its magnetic grains are the most dilute
and most uniformly distributed of all the prepared samples, the 'blank'
sample is least affected by the sample demagnetizing field. If, as is
strongly suggested by the experiments, the remanence carriers of the 'blank'
sample are indeed single domain, the 'blank' sample is, ironically, ideal
to examine single domain theories. On the other hand, due to the very nature
of the 'blank' sample certain of its properties remain unknown. Thus, for
example, the distribution of the particle sizes and shapes remains a matter

Figure 11

Stepwise thermal demagnetization of weak field TRMs (0.37 oe $<h_{ex} < .49$ oe) of sample 10. Different symbols imply independent demagnetization experiments. The initial TRM was given between 650°C and T_R, and subsequent TRMs were induced between 600°C and T_R. Heatings were done in a slightly reducing environment and at low ambient pressures (0.1 - 0.3 mm of Hg).

'BLANK', SAMPLE 10
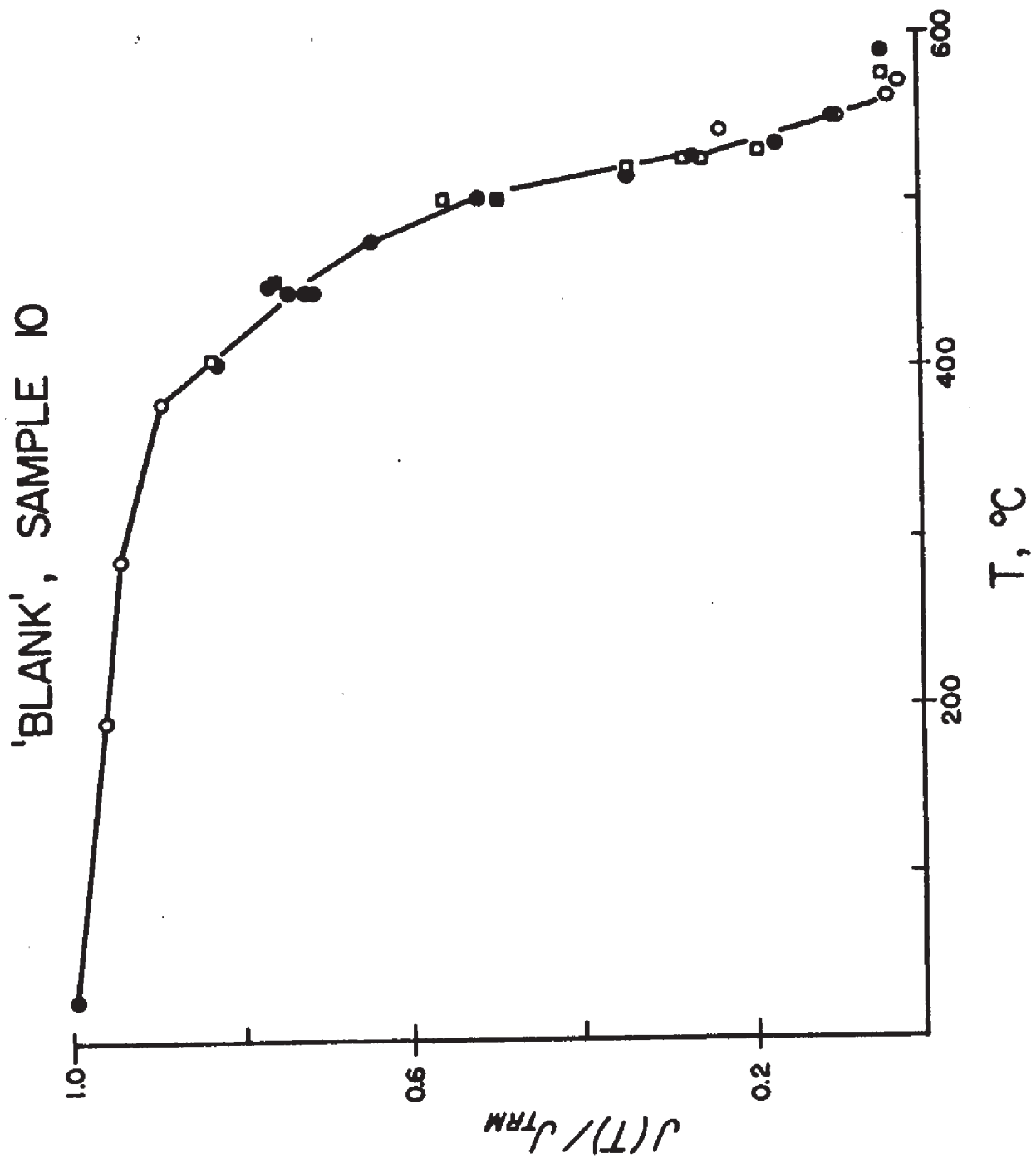
for conjecture, as does the precise mineralogical and chemical nature of the magnetic particles. It should be stated here, and it will be abundantly clear from the experimental evidence, that the effect of the matrix magnetization nowhere seems to interact with or disguise the magnetic properties of the magnetite particles it hosts. The magnetic effect of the matrix appears to be directly and simply related to its magnetic mineral concentration and has no further effect on the experimental results.

CHAPTER 4

SAMPLE DESCRIPTION AND TRM PROPERTIES OF PREPARED SAMPLES

4.1 SUMMARY

In this chapter we discuss experiments conducted to study various
of the TRM stability parameters of the prepared magnetite samples. In
particular we discuss the stability with respect to alternating field
(A.F.) demagnetization, stability with respect to spontaneous decay in
zero field, stability with respect to thermal demagnetization, and
stability with respect to low temperature cycles in zero field to below
magnetite's magnetocrystalline anisotropy transition temperature near 130°K.
It is observed that in general TRM stability is high for small, single
domain particles and decreases for multidomain remanence carriers and is
minimum for large crystals of magnetite. This trend is obeyed most closely
by the stability against low temperature cycles.

4.2 EXPERIMENTS AND RESULTS

The TRM in these experiments was induced by a field of .467 ± .002 oe.
The magnetization of the prepared samples (and rock specimens) in this
chapter and throughout this dissertation are measured by a Schonstedt Slow
Spinner magnetometer with a maximum sensitivity of about 10^{-7} emu which is
at least three orders of magnitude more sensitive than required for our
experiments. The TRM properties are listed in table 5. The first column
lists the samples according to their anticipated magnetic behavior from
sample 0, which should be most multidomain, to sample 11, which should be
the most single domain in its behavior. The sample order is determined
from the measured or inferred sizes and shapes of their magnetite grains.
Placing sample 10 into the sequence, some of the stability characteristics

are considered as well. The second column lists the origin and average grain sizes and shapes of the magnetite powders. In the third solumn we list the samples' mean TRM per grams of sample, obtained from the arithmetic mean of the TRM values in table 6 for each sample. Column 4 gives the mean destructive, peak, alternating field, $\tilde{H}_{1/2}$(oe), defined as that alternating field which demagnetizes the sample's TRM to 1/2 its original room temperature value. Column 5 gives the mean blocking temperature, $<T_B>$, defined as that temperature to which a sample must be heated in null field so that its room temperature magnetization drops to 1/2 its original value. Column 6 represents the TRM decay when subjected to temperature cycles in zero field to below the magnetite magnetocrystalline anisotropy transition temperature. This transition temperature is also called the isotropic point, because at that temperature the sum of the magnetocrystalline anisotropy constants vanishes: $K_1 + K_2 = 0$. For pure magnetite the isotropic point is near 130°K (Bickford et al., 1956; Syono and Ishikawa, 1963). The decay characteristics are a measure of the relative fraction of the remanence controlled by the magnetocrystalline anisotropy. Kobayashi et al. (1965) observed that the relative low temperature decay of the magnetization decreases with decreasing grain size and is essentially absent for single domain grains. The values for each sample represent the fraction of the magnetization remaining after each of three successive low temperature cycles. Column 7 describes the spontaneous decay of the TRM when the samples were placed in zero field for 24 hours.

The uncertainty brackets of columns 4, 5, and 7 are conservative, but subjective estimates obtained from: (1) the uncertainty in deducing a particular value from the demagnetization curves, including uncertainties in $\tilde{H}$ and the absolute values of T; and (2) uncertainty estimated from repeated

independent determinations. All measurements of remanence that appear in table 5 are made at room temperature.

The last four columns are different measures of TRM stability for the various samples. The data within each of the last four columns is ranked, with respect to the other samples, by an integer between 0 and 11 appearing to the right of each datum in these columns. The larger the integer, the greater is the sample's TRM stability under the particular treatment. The integer ranking system is somewhat subjective and may, when used by itself, lead to misinterpretations. It should only be used as a guide, and the actual data should be used for specific comparisons.

One striking observation is the poor correlation between T_B and $\tilde{H}_{1/2}$. This is especially apparent in samples 2, 3, 4, 8, and 9. It is often assumed in paleomagnetism that there is a one-to-one correlation between TRM stability against temperatures and the stability against alternating fields for samples of a given mineral. Equivalently, it is assumed that samples having a certain sequence of relaxation times, τ, at room temperature will have the same sequence of relaxation times at other temperatures. Thus higher values for τ at T_R, associated with higher stability, imply higher values for T_B. We restrict our discussion to single domain grains of a particular mineral whose relaxation time is given by equations 7 and 8 and where the microscopic coercivity, H_{ci}, is a function of the various magnetic anisotropy energies. If we suppose that $J_S(T)$ and the spontaneous magnetization are the same for all single domain grains of the same material, then differences in the temperature dependence of τ for different particles are largely a function of the temperature dependence of the different functions that make up H_{ci}.

For example, consider two samples A and B whose remanence is carried

TABLE 5

TRM PROPERTIES OF THE SAMPLES

Sample Number	Description of Magnetite Particles	Mean TRM emu/gm of Sample h = .47 OE	$\tilde{H}_{1/2}$ (Oersted)	$<T_B>$ (°C)	Low Temp. Cycles $J(LN_2, h=0)$ / J_{TRM}	Spontaneous Decay $J(h=0; t=24 \text{ hours})$ / J_{TRM}
0	Natural Crystal Euhedral 6.379 gm	$.75 \times 10^{-3}$	12±4	300°±40°	.136 (1) .110 (1) .106 (1)	.926±.013
1	Chip of Natural Crystal 3.569 gm	1.63×10^{-3}	17±2	380°±80°	-.091 (0) -.092 (0) -.101 (0)	.924±.012
2	Natur., Irreg. $<d>=2.7$ μm $d_{max}=150$ μm	1.45×10^{-4}	77±5	475°±15°	.590 (2) .465 (2) .476 (2)	.938±.002
3	Natur., Irreg. $<d>=1.5$ μm $d_{max}=50$ μm	1.32×10^{-3}	138±10	493°±10°	.593 (3) .521 (3) .497 (3)	.970±.005
4	Natur. Regular $<d>=.31$ μm $d_{max}=2$ μm	0.573×10^{-3}	380±15	444°±10°	.936 (4) .889 (4) .822 (4)	.990±.002
5	Synthetic, Cubes→Spheres $<d>=.24$ μm $d_{max}=.9$ μm	1.78×10^{-3}	351±15	492°±10°	.945 (5) .935 (6) .929 (6)	.992±.002

TABLE 5
(cont'd)

TRM PROPERTIES OF THE SAMPLES

Sample Number	Description of Magnetite Particles	Mean TRM emu/gm of Sample h = .47 OE	$\tilde{H}_{1/2}$ (Oersted)	$<T_B>$ (°C)	Low Temp. Cycles $J(LN_2, h=0)$ / J_{TRM}	Spontaneous Decay $J(h=0; t=24 \text{ hours})$ / J_{TRM}
6	Synthetic, Cubes→spheres <d> = .21 μm, d_{max} = .5 μm	.729x10^{-3}	338±15 6	507°±10° 9	.976 (7) .951 (7) .945 (7) 7	.995±.004 9
7	Synthetic, Cubes→spheres <d> = .21 μm, d_{max} = .5 μm	7.68x10^{-3}	360±15 8	508°±10° 10	.965 (6) .961 (8) .955 (8) 8	.998±.002 10
8	Synthetic, Cubes→spheres <d> = .12 μm, d_{max} = .3 μm	.707x10^{-3}	295±15 4	400°±15° 2	.990 (10) .971 (9) .965 (10) 10	.967±.002 4
9	Synthetic Cubes→spheres <d> = .12 μm, d_{max} = .3 μm	.657x10^{-3}	300±15 5	418°±10° 3	.986 (9) .910 (5) .907 (5) 6	.958±.002 3
10	Magnetite Unknown Size and Shape	.158x10^{-4}	430±20 10	503°±10° 8	.982 (8) .974 (10) .960 (9) 9	.994±.012 8
11	Synth., Acicular Ax. Ratio 8:1 .35 μm x .04 μm	1.95x10^{-3}	571±20 11	519°±10° 11	1.003 (11) .995 (11) .994 (11) 11	.998±.002 11

by similar single domain grains whose coercivities are controlled by uniaxial magnetocrystalline and shape anisotropy energies, respectively, such that

$$H_{ci}^A = W \frac{K(T)}{J_{SP}(T)} \qquad H_{ci}^B = M\, J_{SP}(T)$$

where $K(T)$ is the magnetocrystalline anisotropy constant and $J_{SP}(T)$ is the grains' spontaneous magnetization. W is a constant referring to the orientation of the magnetic easy axes with respect to the inducing field and M is a constant describing the demagnetizing factors along the grains' major and minor axes. According to Fletcher (1971),

$$\frac{K(T)}{K(T_R)} = \left[\frac{J_S(T)}{J_S(T_R)}\right]^m$$

where $m = 8$ for magnetite. Therefore,

$$\frac{H_{ci}^A(T)}{H_{ci}^A(T_R)} \propto \left[\frac{J_S(T)}{J_S(T_R)}\right]^7$$

whereas

$$\frac{H_{ci}^B(T)}{H_{ci}^B(T_R)} \propto \left[\frac{J_S(T)}{J_S(T_R)}\right]^1$$

Hence, although it is possible for $H_{ci}^A(T_R) > H_{ci}^B(T_R)$, there will be a temperature $T_R < T < T_C$ such that $H_{ci}^B(T) > H_{ci}^A(T)$. Similarly, it is possible for $\tau_A(T_R) > \tau_B(T_R)$, however, at some temperature $T_R < T < T_C$ this order will reverse such that $\tau_A(T) < \tau_B(T)$. Therefore, even for single domain particles, similar relaxation times (and similar stabilities) at one temperature do not imply similar relaxation times (and similar stabilities) at other temperatures but are critically dependent on the temperature variation of H_{ci}. For samples 2, 3, and 4, whose particle size distributions (see Chapter 2) suggest that a substantial fraction of the remanence is in

multidomain particles, the above analysis does not apply. However, the
fact that sample 4 is so much more stable against A.F. demagnetization than
samples 2 and 3, while having a lower value for $<T_B>$, should suggest some
caution against the generalization that higher A.F. demagnetization stabili-
ties imply higher blocking temperatures.

It should be pointed out that the values for $<T_B>$ in column 5 are not
unique. In our experiments the remanence is always measured at room temper-
ature; therefore, our definition for $<T_B>$ specifies that temperature above
which 1/2 the room temperature magnetization is blocked. If one uses the
above definition for $<T_B>$ but measures the demagnetized remanence at ele-
vated temperatures, one will obtain lower values for $<T_B>$ than in column 5,
because $\frac{\partial J_S(T)}{\partial T} < 0$, which decreases the magnetization regardless of
whether any unblocking has occurred. Thus the condition where 1/2 the room
temperature TRM is thermally demagnetized is reached at a lower temperature.
Although the measurement of the remanence at elevated temperatures will
yield lower values for $<T_B>$, the sequence of $<T_B>$ values for the different
samples is expected to remain unaffected as are the conclusions drawn there-
from. When the thermally demagnetized remanence is measured at elevated
temperatures, a better measure for the stability of TRM with respect to
temperature might be the temperature corresponding to the maximum slope
in the demagnetization curve. In our experiments, however, where the former
method is used to obtain $<T_B>$ for the samples, the demagnetization curves
are often so abrupt that it is impossible to distinguish between the point
of maximum slope and the point where 1/2 the room temperature TRM is
thermally demagnetized.

The TRM decay after a low temperature cycle is the only stability
measure that follows the grain size and 'domainness' pattern of column 1.

The relative decay decreases proceeding from large, multidomain grains to smaller and to single domain grains, when the behavior of samples with the same species of magnetite powder--samples 6 and 7 and samples 8 and 9--is averaged. This data is in agreement with the work of Kobayashi et al. (1965) and Merrill (1970). As the ratio of a grain's volume to surface area decreases with diminishing particle size the relative importance of the magnetocrystalline anisotropy energy diminishes with respect to the surface energies, and so does its role in domain wall formation in magnetite. As the grain sizes decrease, the magnetocrystalline anisotropy energy controls a relatively smaller fraction of the magnetization, because of the decreasing number of domain walls per grain. Therefore, with diminishing particle size, a lesser fraction of the magnetization is affected by temperature cycles to below the magnetocrystalline anisotropy transition temperatures.

The low temperature reversal of the magnetization of sample 1 is not considered significant due to the unstable nature of the magnetization. Even after total thermal demagnetization above the Curie point, a residual magnetization of about 10 percent is not uncommon in samples 0 and 1, but such a residual magnetization is so soft that it can be reversed by fifteen minutes' viscous magnetization in the earth's field. What is significant is that the bulk of the TRM of samples 0 and 1 seems to be controlled by magnetocrystalline anisotropy.

The trends of $\tilde{H}_{1/2}$ and of the spontaneous decay also generally follow that of column 1. The exceptions are samples 8 and 9, which are relatively unstable with respect to alternating fields and spontaneous decay. In addition, these samples have the lowest blocking temperatures, except the large crystals. The relatively low stability of samples 8 and 9 suggests the

presence in the particle assemblage of a considerable fraction of grains near the superparamagnetic-single domain transition region, having relatively low values for the relaxation time. It is interesting that magnetization of samples 8 and 9 is stable to low temperature cycles, as expected from the small average grain size of their magnetite.

Sample 4 is also anomalous in its magnetic behavior, having high value of $\tilde{H}_{1/2}$ despite its relatively large grain size and low $<T_B>$. Sample 11 lives up to expectations in being more single domain in character than any of the samples studied in all the stability categories.

4.3 CONCLUSIONS

It is comforting to note that samples of like magnetite powder--samples 6 and 7, and samples 8 and 9--behave more similarly to one another than to samples of different magnetites. Comparison of the data for the pairs of like samples may provide a realistic appraisal for within-species uncertainties. Such comparisons also indicate some of the problems that can occur when two laboratories try to reproduce each other's results by using magnetite particles of slightly different origin or of slightly different characterization.

We have seen in this chapter that in general the TRM stability is relatively low for large multidomain magnetite particles and it increases for smaller and single domain particles. This trend is followed most faithfully by the stability with respect to temperature cycles below magnetite's isotropic point. However, the differences are small in the low temperature behavior of the small, equidimensional, synthetic particles, and it may be questioned whether differences in the low temperature behavior of samples 5 through 10 are significant. The total spread in the data for spontaneous decay is 7.6%, and the total spread in the spontaneous decay data for

samples 4, 5, 6, 7, 10, 11 is 1%. The range in the values for $\langle T_B \rangle$ is relatively narrow as compared with the spread in $\hat{H}_{1/2}$. It is also seen in table 5 that the samples queue slightly differently for each stability test, although sample 11 is always the most stable while samples 0 and 1 are always least stable. Whereas it appears that the particle sizes and shapes are primary in determining TRM stability, it seems that the different stability tests see the samples slightly differently; that is, the different stability tests emphasize different aspects of the samples' particle distributions. For example, sample 4 is more stable than samples 5, 6, and 7 with respect to A.F. demagnetization, while being less stable with respect to low temperature cycles and having lower $\langle T_B \rangle$. Although the magnetite particles of sample 4 are of more regular shapes than those of samples 2 and 3, their shapes are considerably more angular and less regular than the particles of samples 5, 6, and 7. It is possible that stability with respect to temperature—high and low—is more sensitive to the particle volumes, while stability with respect to alternating fields is more sensitive to the particle shapes. On the other hand, samples 8 and 9 are relatively stable with respect to low temperature cycles, while being relatively unstable with respect to temperatures above T_R. This behavior of samples 8 and 9, however, can be explained in terms of particles which carry stable remanence at T_R, but are near the superparamagnetic-single domain transition diameter.

CHAPTER 5

THE FIELD DEPENDENCE OF TRM STABILITY AGAINST
ALTERNATING FIELD, A. F., (AND THERMAL) DEMAGNETIZATION

5.1 SUMMARY

In this chapter we investigate the field dependence of TRM stability against alternating field, A. F., (and thermal) demagnetization in some magnetite samples.

For multidomain crystals of magnetite we find that the stability with respect to A. F. and thermal demagnetization increases with increasing TRM fields. This trend can be explained by the fact that there are statistically fewer domains and domain walls in the crystal when magnetized by higher fields, such that demagnetization by domain wall movement requires larger paths of wall movement. In addition, relatively more energy is consumed in the demagnetization of the crystal when magnetized by higher fields due to the energy input required to nucleate reversed domains.

For a sample whose magnetization resides in single domain magnetite the stability with respect to alternating fields decreases smoothly with increasing TRM fields. This behavior can be explained in terms of Néel's single domain theory. For fine grain magnetite ($<d> = .21$ μm) of diameters greater than the single domain critical size, the stability with respect to alternating fields decreases smoothly increasing TRM fields greater than .5 oe, as for the single domain particles. There is, however, a maximum in the stability between 0.1 and 0.5 oe. For TRM fields less than that corresponding to the maximum stability, there fine grain magnetites behave more like the multidomain crystals. This behavior is not yet fully understood, although one possible mechanism is suggested in the text.

5.2 MULTIDOMAIN CRYSTALS

Lowrie and Fuller (1971) showed experimentally that the 'hardness' of multidomain TRM sgainst A. F. demagnetization increases with increasing TRM inducing field. Figures 12a and 12b illustrate the A. F. demagnetization curves of a 0.5 oe and 9.5 oe TRMs for samples MSC-0 and MSC-1. The A. F. demagnetization method is described in Appendix B-1. The same field dependence of the stability of the TRM is observed as reported by Lowrie and Fuller (1971): The higher field TRM is more stable with respect to A. F. demagnetization than the lower field TRM for multidomain particles. The reversal of the magnetization of sample MSC-0 is not understood, but it is thought to be real, because it was observed in two separate demagnetization runs. The reversal is not ARM induced, because the magnetization at each A. F. value is the average of two demagnetizations--one where the ARM is parallel and one where it is antiparallel to the remanence. See also Appendix B-1. In figures 13a and 13b the thermal demagnetization spectra of 0.5 oe and 9.1 oe TRMs of samples MSC-0 and MSC-1 are shown. The squares and triangles are data obtained during separate 'Thellier' experiments, and the circles are data obtained by heating untreated TRMs in zero field to the designated temperatures. Despite considerable scatter in the data, the 9.5 oe TRM of both samples is clearly more resistant to thermal demagnetization than the 0.5 oe TRM. This trend is precisely opposite to that observed by Roquet (1954) in whose sample, composed of a dilute dispersion of magnetite powder approximately .1 μm in diameter, thermal stability decreased with increasing TRM fields of .42 oe, 17 oe, 86 oe, and 570 oe, respectively. The same trend as observed by Roquet (1954) was also seen by Dunlop and West (1969) in their six samples containing single domain grains, including two samples containing magnetite.

In large multidomain crystals, as in the present sequence of experiments,

Figure 12

a.   Normalized A.F. demagnetization curves of .5 oe and 9.5 oe
TRM for sample MSC-0. Note that the 9.5 oe TRM is more stable.
The magnetization reversal is not understood, but it is reproducible
and apparently real.

b.   Normalized A. F. demagnetization curves of .5 oe and 9.5 oe
TRM for sample MSC-1. The 9.5 oe TRM is consistently and signifi-
cantly more stable than the   .5 oe TRM.
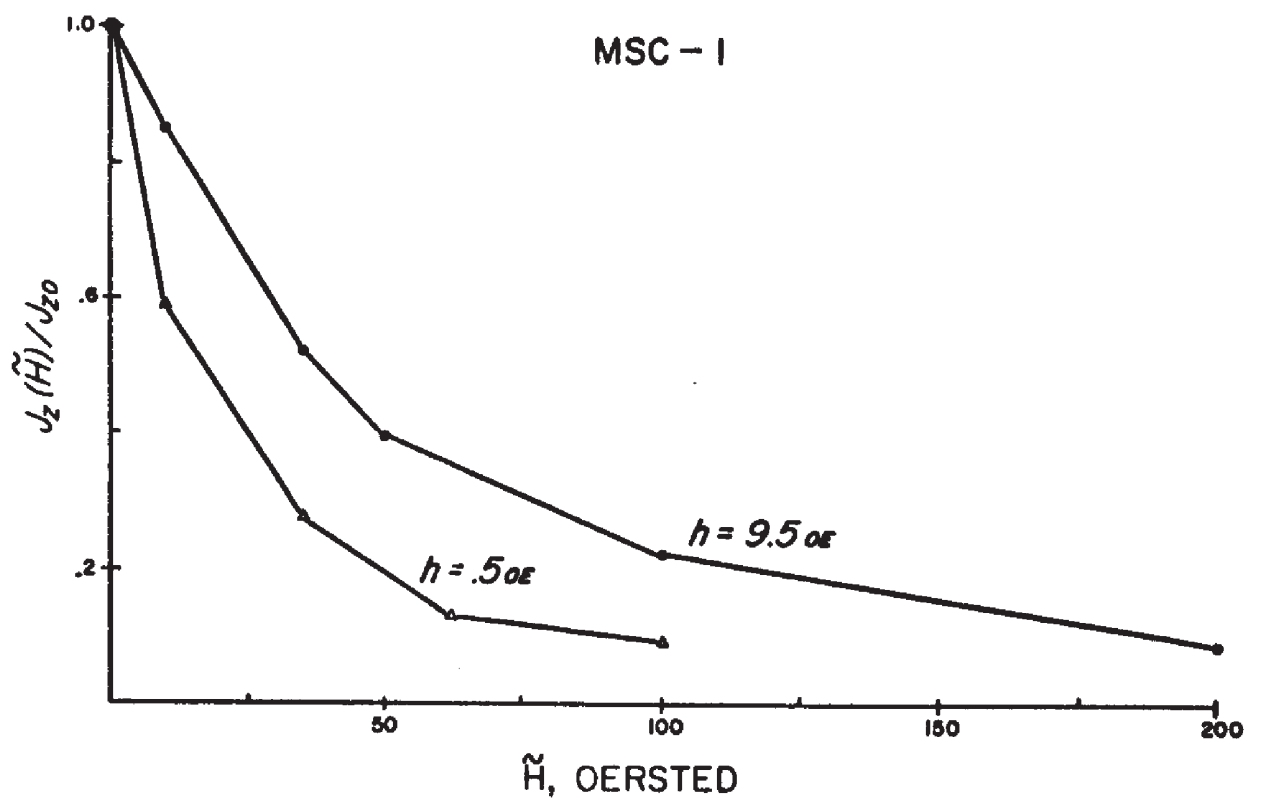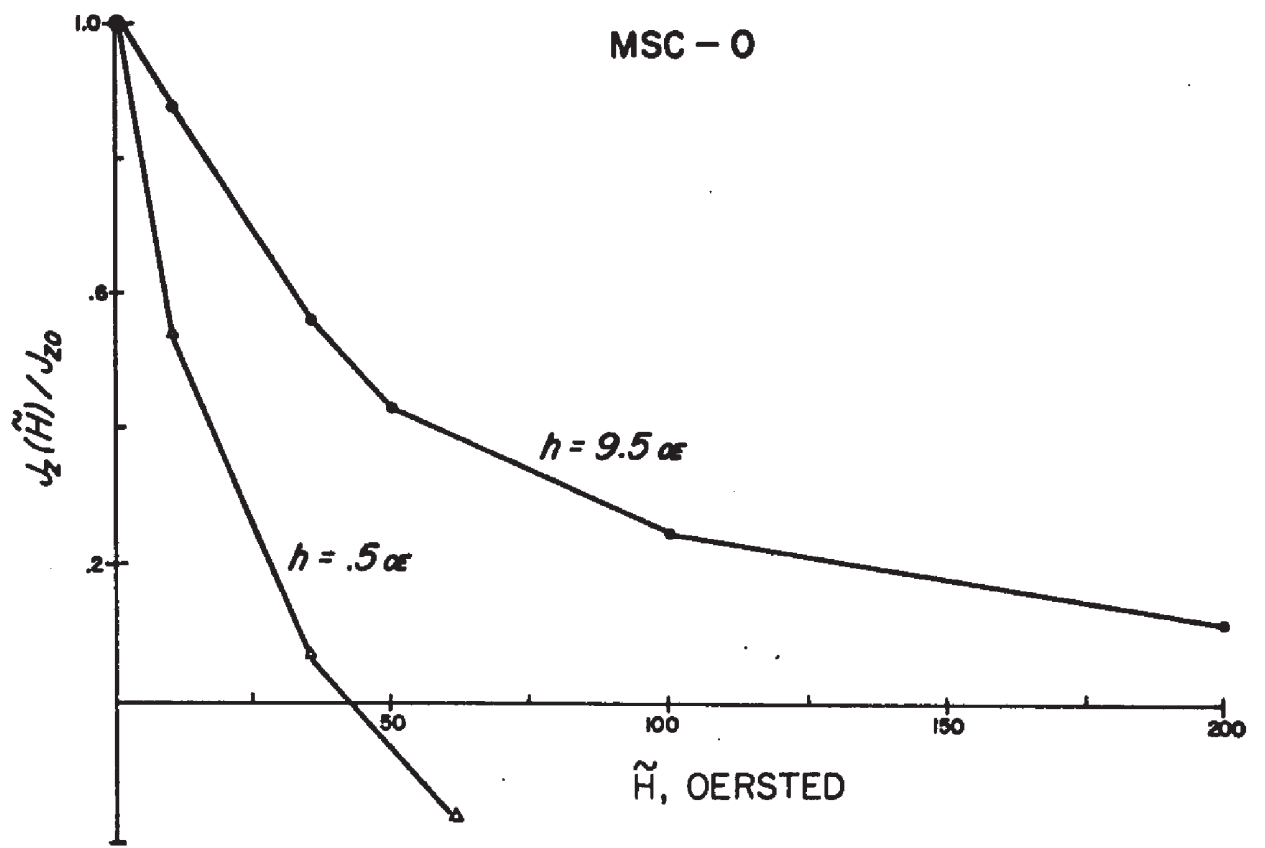
Figure 13

Stepwise thermal demagnetization of .5 oe and 9.1 oe TRMs. The different types of open symbols denote independent thermal demagnetization experiments. Note that despite the large scatter in the .5 oe demagnetization curves, the .5 oe TRM is consistently and significantly 'softer' with respect to thermal demagnetization than the 9.5 oe TRM.

a.   Sample MSC-0.

b.   Sample MSC-1.
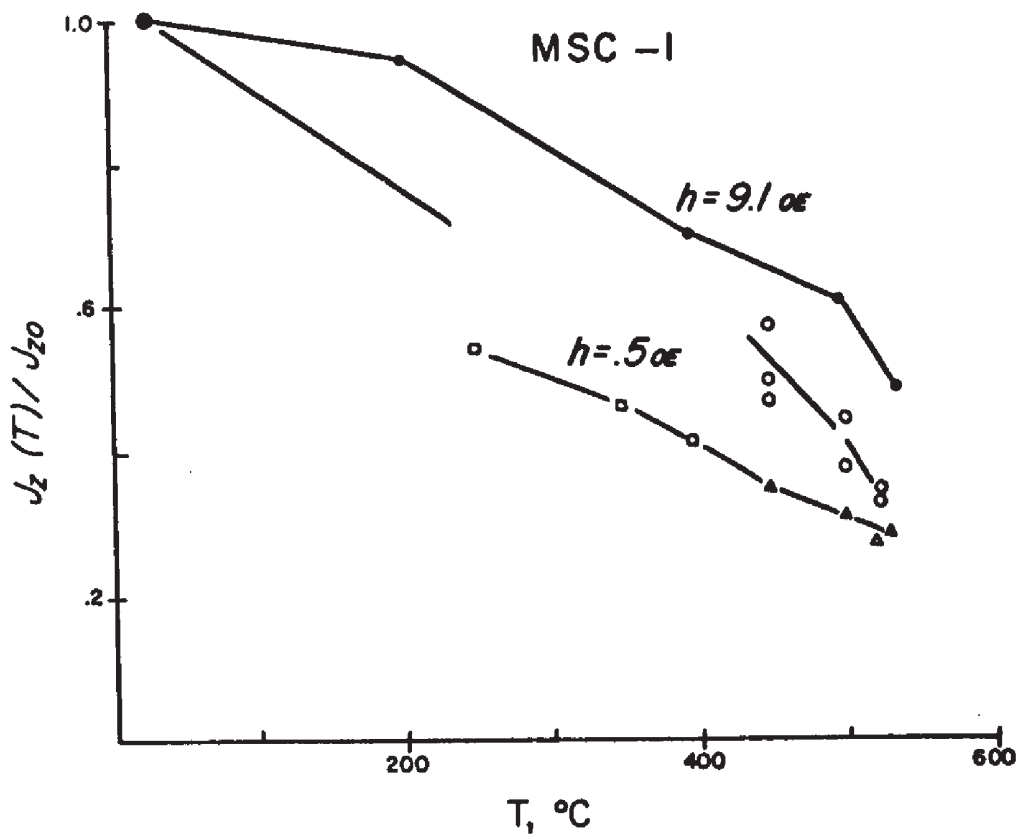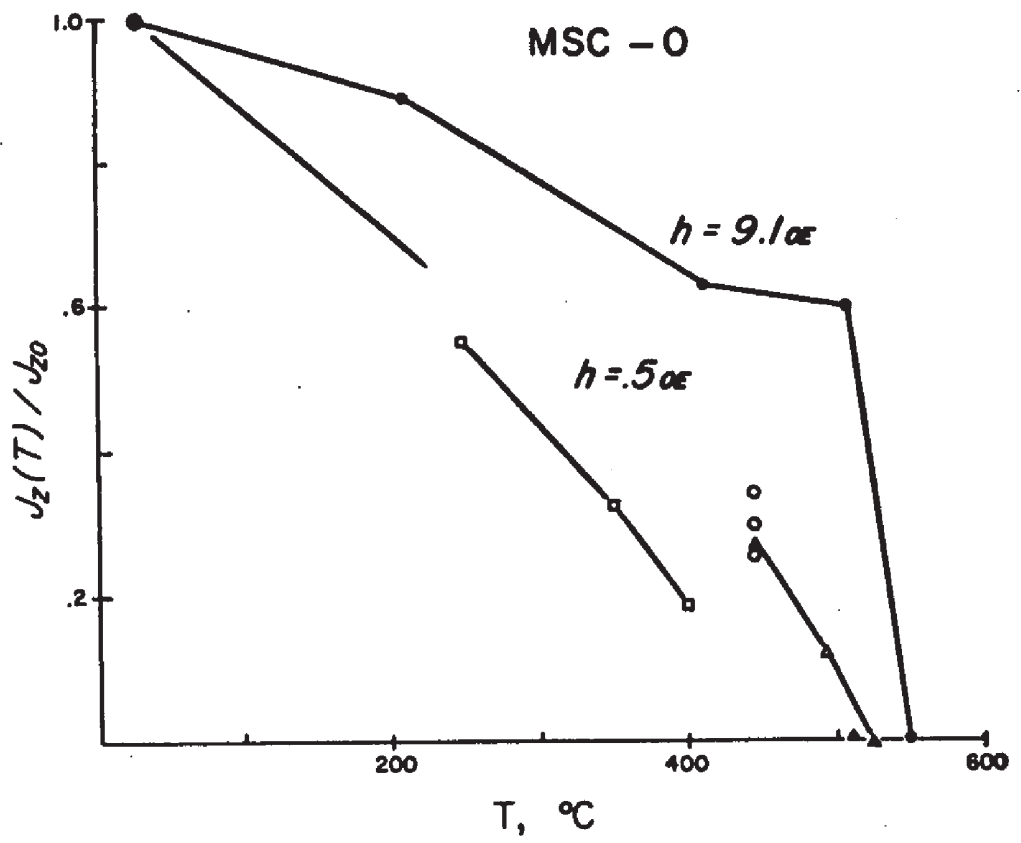
the response of the grain's magnetization to external fields that are well below those required for saturation is to a large extent through domain-wall movement. The wall movement in the presence of an external field is such as to increase the grain's magnetization component in the field direction. The wall movement is impeded by the local demagnetizing fields and by energy barriers, caused by internal stresses associated with crystal imperfections, that the wall must overcome. As the field increases, the number of domains decreases (as does the number of the domain walls) until the final state is reached, where the grain is homogeneously magnetized to saturation along the applied field. As the field is removed the energy minimization principle is responsible for the renucleation of oppositely magnetized domains (to minimize the magnetostatic energy), and the sample demagnetizing fields act to return the grain to a demagnetized state. A domain wall is 'pinned' when the restoring torques due to the demagnetizing field cannot move the wall beyond a particular energy barrier.

The intensity of the remanent magnetization of multidomain crystals is a measure of how far from a demagnetized configuration the walls are 'pinned' when the external field is removed. It is reasonable to expect that the farther from a demagnetized configuration the walls are 'pinned' the greater are the demagnetizing torques that try to drive the walls over energy barriers towards a more demagnetized state. To explain the increased stability with increasing biasing fields, we assume that each point in the crystal has approximately the same distribution of energy barriers and that the distribution is field independent. We recall that the greater the remanence of the crystal the smaller is the number of the domains and domain walls within it. It follows, therefore, that there are statistically fewer domains and domain walls in the crystal subject to a 9.5 oe TRM than in the same crystal having

a 0.5 oe TRM. If demagnetization occurs purely by domain wall movement, then the multidomain particle having a higher-field-TRM behaves more as if it were a smaller multidomain particle compared to the same crystal having lower-field TRM, and their A. F. demagnetization is accomplished by the movement of the domain walls over statistically longer paths, thus possessing greater stability. We assume above that longer demagnetization paths of fewer domain walls imply greater stability than shorter demagnetization paths of a relatively greater number of domain walls. Neglected above are the possible effects of interaction between domains and domain walls and between several domain walls, which may depend on their number density. However, it is also possible that such an effect is statistically cancelled.

Demagnetization in multidomain crystals is probably affected by a combination of both domain wall movement and the nucleation of new domains with reversed magnetization. To initiate the nucleation process a certain activation energy must be available to the crystal. Therefore part of the energy of the demagnetization process, whether in the form of alternating fields or thermal energy, is used in wall nucleation. Since a relatively greater amount of energy is needed for domain nucleation of the higher-field-TRM, more energy will be required to demagnetize higher-field remanence. It follows that the stability of multidomain crystals increases with increasing remanence-inducing fields, as is shown in figures 12a, b and 13 a, b for both A. F. and thermal demagnetization. (The relative stability of the crystal having the higher-field-TRM will, however, be lower than that of a geometrically similar but smaller crystal with an identical domain and domain wall configuration, because the former is farther from equilibrium in zero field and a relatively smaller activation energy is required to nucleate additional reversed domains and domain walls.)

5.3 FINE PARTICLES

As was described and discussed in the previous paragraphs, the stability against thermal A. F. demagnetization of large magnetite crystals increases with increasing TRM field. This behavior is a sharp contrast to the data obtained by Dunlop and West (1969) in their study of single domain particles. In their samples the A. F. demagnetization curves become progressively 'softer' with increasing TRM fields for five of their six samples. Dunlop and West (1969) also observed that the thermal stability decreases for increasing TRM fields in all six samples.

Rimbert (1959) studied the A. F. demagnetization characteristics of a sample containing approximately 1% synthetic magnetite powder approximately .1 μm in size. TRMs in fields of .192 oe, 30 oe, and 50 oe were A. F. demagnetized, the stability of the TRMs becoming progressively 'softer' with increasing fields. Rimbert (1959), Dunlop and West (1969), and Lowrie and Fuller (1971), noted for the particular samples that they studied, that the stability of TRM fields (sufficient for saturation remanence) approaches the stability of saturation IRM. Lowrie and Fuller (1971) first discovered the fundamental difference between the A. F. demagnetization behavior of large multidomain grains and fine particles. They devised a method to test whether remanence is carried by single or multidomain particles: normalized A. F. demagnetization curves of weak field TRM and saturation IRM for the same sample are compared. If the saturation IRM is more stable, the remanence is in multidomain particles, and, if the weak field TRM is more stable, it is in single domain carriers.

The stability with respect to A. F. demagnetization for five distinct TRM fields was determined for samples 6A, 7, and Olby 269A. Samples 6A and 7 contain Columbian Carbon magnetite powder previously described in Chapter 2

Figure 14

Stepwise A.F. demagnetization curves of TRMs induced in different magnetic fields in basalt sample Olby 269A. Note that the TRM stability increases monotonically with decreasing inducing fields, as is expected for single domain particles.

OLBY 269 A

Legend:
- ▼ J.O OE TRM
- ○ .25 OE
- ● .49 OE
- □ 39 OE
- △ 145 OE

$\tilde{H}$, OERSTED

$J(\tilde{H})/J_o$
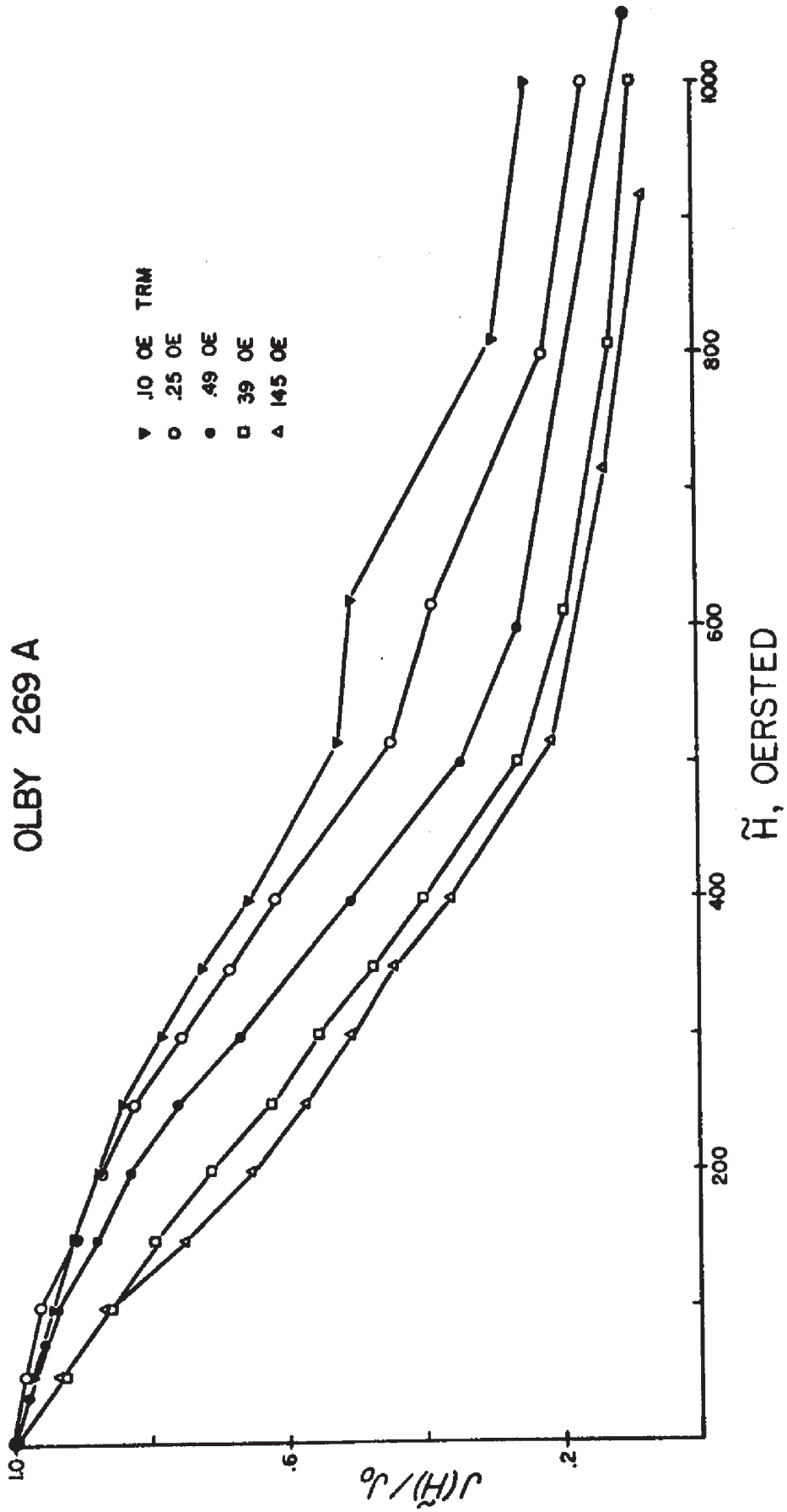
Figure 15a

Stepwise A. F. demagnetization curves of TRMs induced in different magnetic fields in sample 6A, which contains synthetic, equidimensional, magnetite particles whose mean diameter is about .21 μm. Note that the most stable demagnetization curve corresponds to the .25 oe TRM and not to the .10 oe TRM, which is the lowest inducing field used.

SAMPLE 6A

TRM

▼ .10 OE
○ .25 OE
● .49 OE
□ 41.5 OE
△ 153 OE

$J(\tilde{H})/J_0$

$\tilde{H}$, OERSTED
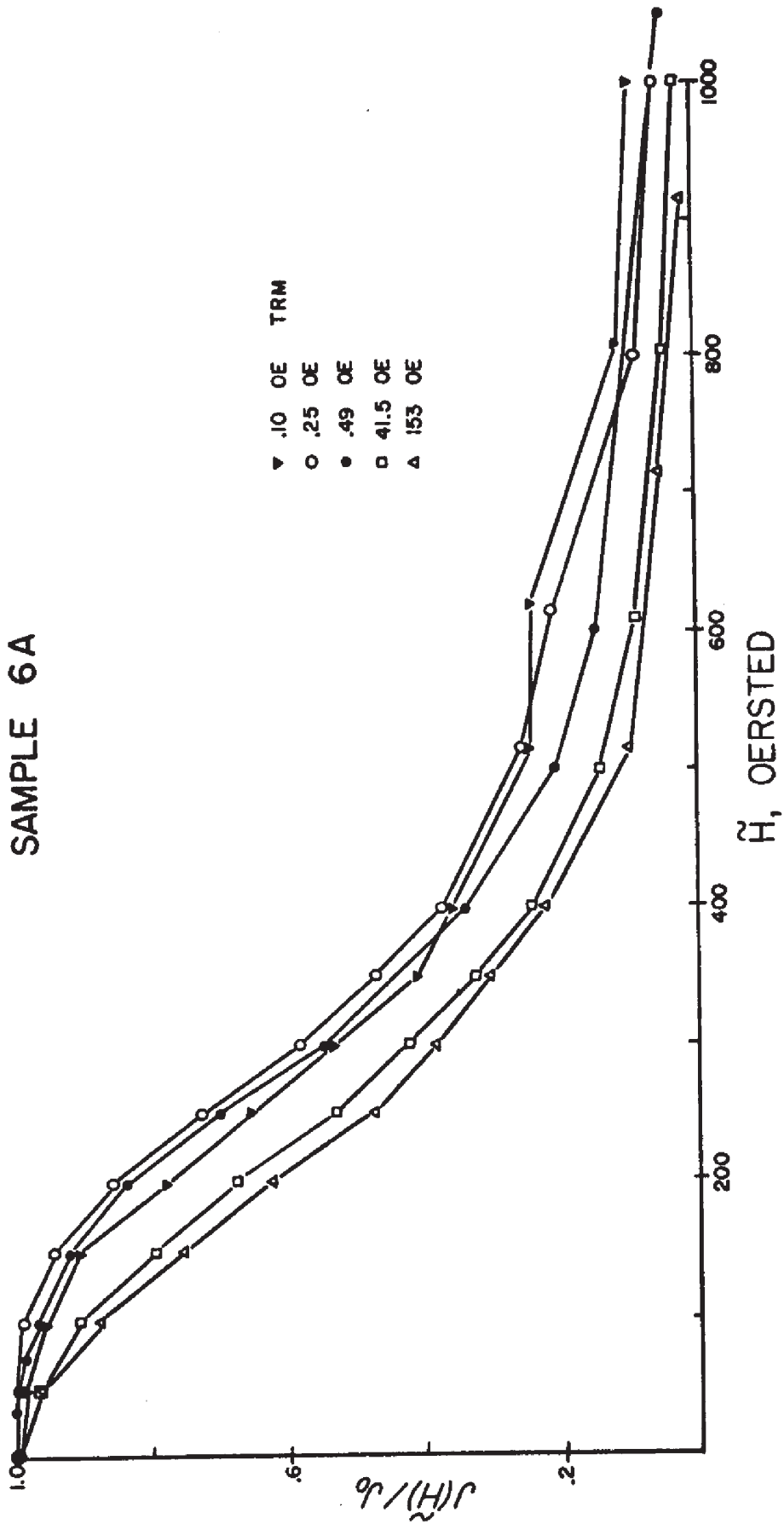
Figure 15b

Stepwise A.F. demagnetization curves of TRMs induced in different magnetic fields in sample 7, which contains identical magnetite particles as figure 15a. Note again that the most stable demagnetization curve corresponds to the .25 oe TRM and not to the .10 oe TRM, which is the lowest inducing field used. Both in figure 15a and 15b the .49 oe TRM is also more stable than the .10 oe TRM.

SAMPLE 7

J(H̃)/J₀

H̃, OERSTED

▼ .10 OE TRM
○ .25 OE
● .49 OE
□ 41 OE
△ 153 OE
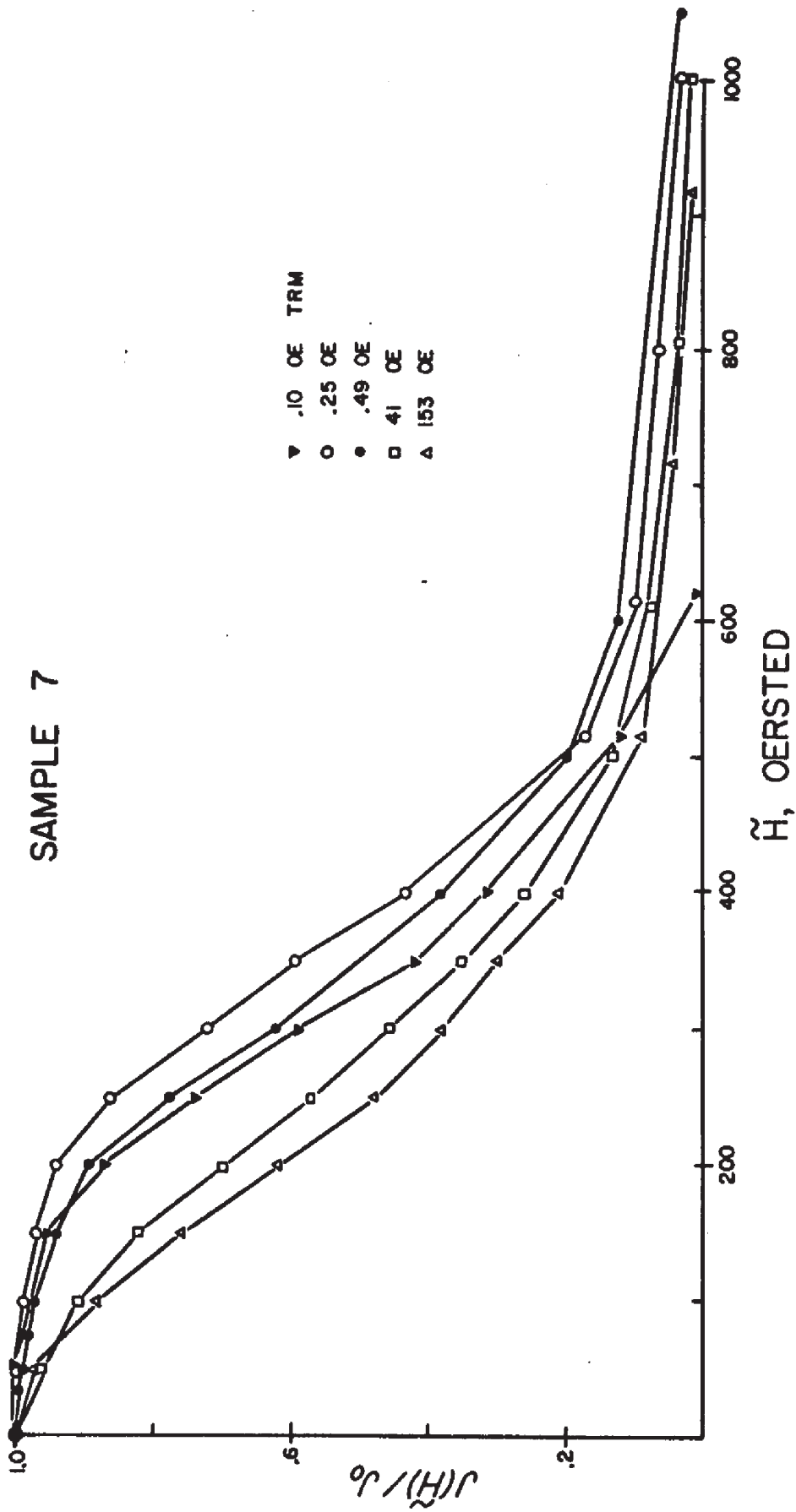
and summarized in Table 2 and whose bulk magnetic properties are summarized in Chapter 2 Table 3. Sample 7 of this chapter is the same as sample 7 of Chapter 4, and samples 6A, B, and C are made in the same way as sample 6 of Chapter 4, where the various TRM properties are described and discussed. Sample Olby 269-A is a basalt specimen (cylindrical; about 1 inch in diameter and 1 inch long) from the Olby flow, France. The paleomagnetism and some rock magnetic aspects of this flow were described by Bonhommet and Zähringer (1969) and Bonhommet (1970). Using various mineralogical and rock magnetic clues, Whitney et al. (1971) concluded that the remanence of the Olby flow probably resides in single domain magnetite grains. The TRM field strengths chronology according to which the demagnetization experiments were performed is: .49 oe, .25 oe, 0.10 oe, 150 oe, and 40 oe, respectively. The TRM fields are listed chronologically to show that the particular sequence of the demagnetization curves in figures 14 and 15a, b cannot be explained by the order in which they were executed. That is, the particular sequence of the demagnetization curves is not due to chemical, mineralogical, or annealing effects on the samples. The demagnetization spectra are drafted in figures 14 and 15 a, b for samples Olby 269A, 6A and 7, respectively.

For the Olby sample, whose remanence carriers have been previously judged to be single domain magnetite particles, the stability decreases with increasing TRM field, consistent with the observations of Rimbert and Dunlop and West. Lowrie and Fuller (1971, p. 6342-6343) convincingly explain this behavior in terms of Néel's equations (equations 7 and 8 of the introduction). It is seen that the ARM effect becomes visible only for the .10 oe TRM when the alternating field is near 600 oe, but it has no substantive effect on the result. (The ARM acts parallel to the initial remanence.) Clearly, the

Olby sample is single domain according to the 'Lowrie-Fuller' test for all the TRM fields that were studied.

The TRM stability of samples 6A and 7 is drafted in figures 15a and 15b. In both samples a slight ARM component is observed in the .25 oe demagnetization curves for alternating fields above 500 oe. A more noticeable ARM component appears in the .10 oe curve at alternating fields above 400 oe. For alternating fields less than 400 oe, the sequence of the demagnetization curves is identical for both samples. For alternating fields greater than 400 oe the ARM distorts the sequence of the demagnetization curves. Due to the opposite orientations of the remanence of the two samples with respect to the axis of the demagnetizing coil, the ARM in sample 6A is parallel to the TRM, while in sample 7 the ARM is antiparallel to the TRM. It is seen in figures 15a and 15b that the two curves affected by ARM are shifted upwards for sample 6A and downwards for sample 7.

Dunlop (1973) showed experimentally, using TRM fields of 1 oe or greater, that the transition from single domain to multidomain behavior under the 'Lowrie-Fuller' test occurs at particle diameters much larger than the theoretically predicted single domain to multidomain critical diameter, d_c. Equidimensional magnetite particles up to .22 μm were shown to behave as single domain particles under the 'Lowrie-Fuller' test.

Looking across the Abscissa of figures 15a and 15b at $J(\tilde{H})/J_o = 1/2$ the TRM fields in order of their increasing stabilities are: 153 oe, 41 oe, .10 oe, .49 oe, and .25 oe. This sequence is identical for both samples. Apparently there is a maximum in the field dependence of the TRM stability for these samples between .10 oe and .49 oe. That is, for sufficiently low TRM fields, the stability pattern is that characteristic of multidomain grains, whereas at higher TRM fields, h > .5 oe, it is characteristic of single domain

behavior. This interesting phenomenon which causes the stability sequence of samples 6A and 7 to reverse with increasing TRM fields is not yet fully understood. It might be possible that a grain's domain structure is field dependent, such that for TRM fields, h, greater than a certain critical value, h_c, the nucleation of domain walls is inhibited, but for values $h < h_c$ domain walls might be able to nucleate. For Columbian Carbon magnetite the critical field might be 0.1 oe $< h_c <$ .49 oe. For $h > h_c$ the samples would behave more as single domain particles, and for $h < h_c$ their behavior might more closely resemble multidomain particles. It would be very instructive to study the field dependence of other stability parameters of these samples, such as the stability with respect to temperature cycles below magnetite's isotropic point and the stability with respect to elevated temperatures between T_R and T_C. It would also be instructive to study the effect of an external field on the critical diameter, d_c, for the single domain to two domain transition. Under a 'Lowrie-Fuller' test, however, both samples 6A and 7 behave as if their remanence is carried by single domain crystals, although the average diameter of their magnetite crystals, .21 μm, is much greater than d_c. Further experiments with truly single domain particles (highly acicular or of diameters smaller than d_c) and with magnetite particles that have diameters greater than d_c yet exhibit single domain behavior when subjected to a 'Lowrie-Fuller' test are required to test whether the peculiar field dependence of TRM stabilities for biasing fields less than .5 oe, observed for samples 6A and 7, is a general phenomenon that might be used to distinguish amongst these two types of particles.

5.4 DISCUSSIONS

In the previous section we saw that the results of the 'Lowrie-Fuller' test are not as simple to interpret as was originally conceived. We saw that

some particles whose diameters are much greater than d_c behave as single

domain particles under the 'Lowrie-Fuller' test, although a more detailed

analysis of their demagnetization curves shows that the characteristic single

domain stability pattern breaks down for TRM fields less than 0.49 oe and

becomes similar to that of multidomain particles. More experimental and

theoretical work is needed to substantiate and to improve the understanding

of these findings.

The 'Lowrie-Fuller' test loses its simplicity when more than one magnetic

species is present in a sample and when the sizes of the particles wherein

the remanence resides span the gamut from single to multidomain. For dis-

cussion's sake we shall assume the presence in our sample of an equal number

of both 'single domain' and 'multidomain' particles. The quotation marks are

present because the particles are declared 'single domain' or 'multidomain'

according to their behavior in the 'Lowrie-Fuller' test. Both the contribu-

tion of the particles to the remanence and their respective stabilities must

be considered. Two extreme examples will be discussed. In the first the

active grains are single domain; and in the second the active grains are

multidomain.

Table 3 of Chapter 2 gives values of J_{RS}/J_S for the synthetic submicron

particles varying from .11 to .44. Although a 'Lowrie-Fuller' test was

performed only for the Columbia Carbon variety, probably all the synthetic

submicron particles listed in table 3 are 'single domain' in the 'Lowrie-

Fuller' sense. In multidomain particles J_{RS}/J_S is usually much lower than

for submicron particles. For example, a chip of a natural crystal, weighing

.0261 gm, has a J_{RS}/J_S value of .008. Ground magnetite powder trapped between

two sieves such that 250 μm < d < 500 μm has a J_{RS}/J_S value of .005.

The first example can be visualized to result from the lower relaxation

times of the 'multidomain' particles such that when the rock measured in the laboratory the NRM resides primarily in 'single domain' particles. Saturation IRM will reactivate the 'multidomain' remanence, but because the J_{RS}/J_S of 'multidomain' particles is much lower than that of 'single domain' particles, a much greater total volume of 'multidomain' grains is required so that their remanence will be of the order of the intensity of the 'single domain' particles. Remagnetization of the 'multidomain' particles may also affect the demagnetization curve. In particular, the presence of the multidomain particles will either not affect or depress the demagnetization curve of the saturation IRM relative to the hypothetical demagnetization curve of saturation IRM of only the 'single domain' particles. The correct result is obtained by 'Lowrie-Fuller' tests: namely, that the remanence is carried by 'single domain' particles. The difference between the demagnetization curves of the NRM and the saturation IRM in our example may be greater than if the sample contained only 'single domain' particles. Thus the difference between the demagnetization curves cannot by itself be used to make statements about the degree of 'single domain' versus 'multidomain' remanence.

The second example might be visualized to occur in an intrusive rock whose magnetic grains are generally 'multidomain' and the remanence blocked upon cooling through T_C is largely in these particles. At lower temperatures, say 300°-400°C, new 'single domain' grains are created by possible oxidation of the silicate minerals or by possible mineralogical changes of the Fe-Ti minerals. It is assumed that these newly generated grains carry no net remanence. The NRM is thus carried by 'multidomain' particles. Saturation IRM magnetizes both 'multidomain' and 'single domain' particles. The effect on the total remanence of the 'single domain' particles depends on their J_{RS}/J_S value and on their relative total volume. The newly magnetized 'single domain'

particles will either have no effect or increase the stability of the demagnetization curve of the saturation IRM relative to the hypothetical saturation IRM curve of only the 'multidomain' particles. The 'Lowrie-Fuller' test predicts the correct result that the remanence is in 'multidomain particles. As in the first example, the difference between the NRM and the saturation IRM curves may be greater than if the sample contained only 'multidomain' particles, so that the spread between the two demagnetization curves cannot by itself be used to make statements regarding the degree of 'multidomain' versus 'single domain' remanence.

If half the NRM is in 'single domain' particles and half in 'multidomain' particles and if the same partition of remanence is maintained when the sample is given a saturation IRM, then the normalized NRM and saturation IRM demagnetization curves will display similar behavior and will be close together. Thus even for samples having both 'single domain' and 'multidomain' particles, the 'Lowrie-Fuller' test predicts the correct remanence carriers (within their definition).

CHAPTER 6

THE TEMPERATURE DEPENDENCE OF SOME STABILITY PARAMETERS IN MAGNETITES

6.1 SUMMARY

In this chapter we study some stability parameters of magnetite as a function of temperature between T_R and T_C.

A. F. demagnetization of large crystals of magnetite at elevated temperatures shows that for these multidomain particles there is a maximum in the $\tilde{H}_{1/2}$ versus T curve. This behavior can be explained by the competing effects on H_{ci} of $<\lambda>$ and J_S, both of which decrease monotonically between T_R and T_C. The possibility of fewer domains in the crystal at elevated temperatures might also explain the maximum in the $\tilde{H}_{1/2}$ versus T. curve.

Hot A. F. demagnetization of fine particles yields a linear decrease in the $\tilde{H}_{1/2}$ versus T curve until just below the blocking temperatures.

In studying hysteresis properties as a function of temperature for equidimensional, synthetic magnetite powder whose mean diameter is .21 μm, the following relationships are observed:

a.
$$\frac{\tilde{H}_{1/2}(T)}{\tilde{H}_{1/2}(T_R)} \approx \left[\frac{J_S(T)}{J_S(T_R)}\right]^{5/2}$$

b.
$$\frac{\tilde{H}_{1/2}(T)}{\tilde{H}_{1/2}(T_R)} \approx \left[\frac{J_{RS}(T)}{J_{RS}(T_R)}\right]^{3/2 \to 2}$$

c.
$$\frac{H_C(T)}{H_C(T_R)} \approx \frac{H_{CR}(T)}{H_{CR}(T_R)} \approx \left[\frac{J_S(T)}{J_S(T_R)}\right]^{3/2}$$

d. $$\frac{H_C(T)}{H_C(T_R)} \, \underset{\sim}{\chi} \, \frac{H_{CR}(T)}{H_{CR}(T_R)} \, \underset{\sim}{\chi} \, \left[\frac{J_{RS}(T)}{J_{RS}(T_R)}\right]^1$$

6.2 INTRODUCTION

From equation 7 and 8 of chapter 1 it is seen that the microscopic coercivity, $H_{ci}(T)$, and the spontaneous magnetization, $J_{SP}(T)$, are two temperature sensitive parameters that are prominent in influencing the relaxation time, τ, and hence the blocking of TRM. For ideal single domain particles $J_{SP}(T) = J_S(T)$. Where the grain magnetization is not uniform and homogeneous, $J_{SP}(T)$ can be estimated from the remanence of saturation IRM, $J_{RS}(T)$, at each temperature. $H_{ci}(T)$ is determined by a combination of the relevant magnetic anisoptropies (magnetocrystalline, magnetostatic, magnetoelastic and exchange) that are active at each temperature. To know the relative importance of the various magnetic anisotropies in the blocking of TRM and in determining its stability with respect to time and in fixing the grain's magnetic configuration, the temperature dependences of the magnetic parameters and anisotropy constants must be known, especially in the vicinity of T_B. In addition, the relative contribution of the various anisotropies to H_{ci} is intrinsically dependent on the size and shape of the magnetic particle.

One fruitful approach is to study the temperature dependence of the anisotropy constants. Thus Bickford et al. (1956) and Syono and Ishikawa (1963a) and Syono (1965) measured the magnetocrystalline anisotropy constants for magnetite and titanomagnetites between 78°K and T_R. Fletcher (1971) extended the measurements of K_1 for magnetite from T_R to T_C. Bickford et al. (1955) determined the magnetostriction constants for

magnetite between $\sim 120^{\circ}$K and T_R, and Ishikawa and Syono (1963b) and

Syono (1965) measured λ_{111} and λ_{100} for titanomagnetites between 78°K

and T_R. Klapel and Shive (1974) extended measurements of λ_{111} and λ_{100}

for magnetite between T_R and T_C. Measurements of the anisotropy constants

require single crystals whose crystallographic axes are known such that

the crystal can be oriented as needed. Dealing with samples containing

a large number of randomly oriented fine particles, the above approach

cannot be used; rather, one can study the temperature dependence of the

various stability parameters which are determined by the influence of

the magnetic anisotropies. Although this procedure is one step removed

from the individual anisotropies, it is hoped that additional independent

knowledge of the character of the magnetic particles and the anisotropy

constants will help us understand which anisotropies are dominant near

T_B, and to observe differences in behavior due to differences in grain

sizes and shapes. It is hoped that such data will improve our understand-

ing of how TRM is blocked in different types of magnetite particles.

Several investigators have studied stability parameters of magnetite

and other magnetic substances as a function of temperature, setting the

stage for our experiments. Morrish and Watt (1958) studied the tempera-

ture dependence of the bulk coercivity, H_C, between 77°K and 300°K for

several samples containing different species of magnetite powders. They

observed minima in H_C near magnetite's isotropic temperature; the rela-

tive decrease in the H_C was observed to diminish with decreasing particle

sizes. Dunlop (1969) measured the remanence coercivity, H_{CR}, as a function

of temperature between T_R and 600°C for several samples containing single

domain particles to determine which magnetic anisotropy is dominant in controlling their coercivity. Dunlop (1970) A. F. demagnetized high temperature IRM both at T_R and at the temperature where the IRM was induced and noted the drastic decrease in the IRM stability with increasing temperature. Rathenau (1953) measured the temperature dependence of the coercive force of Ba-ferrite powder between $-196^{\circ}C$ and its Curie point near $460^{\circ}C$. A maximum in the coercivity near $280^{\circ}C$ was observed and interpreted as a decrease in the number of domains with increasing temperature.

The approach in this chapter is to study the stability with respect to A. F. demagnetization at temperatures between T_R and T_B, and it is hoped and assumed that the A. F. demagnetization characteristic are directly related to the temperature dependence of the microscopic coercivities, H_{ci}. Hot A. F. demagnetization experiments are done for large crystals of magnetite, for a rock containing single domain magnetite particles, and for samples containing a species of equidimensional, synthetic magnetite pwoder whose mean particle diameter is .21 μm. For the later samples we also determine the hysteresis parameters as a function of temperature. In addition to possibly providing a functional form for H_{ci}, such data might provide certain constraints for TRM theories.

6.3 HOT A. F. DEMAGNETIZATION OF MULTIDOMAIN CRYSTALS

Figures 16 a-d show A. F. demagnetization curves of samples MSC-0,1, 2,3, taken at various temperatures. TRM was induced in an external field of 9.1 oe, because for a 0.5 oe TRM $\tilde{H}_{\frac{1}{2}}$ was only about 20 oe. After inducing TRM of about 9.1 oe, the samples were thermally demagnetized at

Figure 16

Normalized A. F. demagnetization curves at elevated temperatures of $9.1 \pm .5$ oe TRMs of the large magnetite crystals. The remanence is measured at T_R, and the initial points represent the thermally demagnetized remanence at the temperature where the demagnetization was subsequently executed. Although the induced ARM direction in the $T = 25^{\circ}C$ demagnetization curves is opposite to the ARM sense of the higher temperature demagnetization curves, it is seen that the $200^{\circ}C$ and $400^{\circ}C$ curves are more stable or as stable as the $25^{\circ}C$ demagnetization curves for values of $J_z(\hat{H})/J_{zo} > .4$, where the ARM effect is relatively minor.

     a.   Sample   MSC-0

     b.   Sample   MSC-1

MSC − O

MSC − I

Figure 16

Normalized A. F. demagnetization curves at elevated tempera-
tures of 9.1 ± .5 oe TRMs of the large magnetite crystals. The
remanence is measured at T_R, and the initial points represent the
thermally demagnetized remanence at the temperature where the
demagnetization was subsequently executed. Although the induced
ARM direction in the T = 25°C demagnetization curves is opposite
to the ARM sense of the higher temperature demagnetization
curves, it is seen that the 200°C and 400°C curves are more
stable or as stable as the 25°C demangetization curves for
values of $J_z(\hat{H})/J_{zo}$ > .4, where the ARM effect is relatively
minor.

c.   Sample   MSC-2

d.   Sample   MSC-3

MSC – 2

$J_z(\tilde{H})/J_{zo}$

$\tilde{H}$, OERSTED

	T = 25°C
o	200°C
△	400°C
□	500°C

MSC – 3

$J_z(\tilde{H})/J_{zo}$

$\tilde{H}$, OERSTED

	T = 25°C
o	200°C
△	400°C
□	500°C
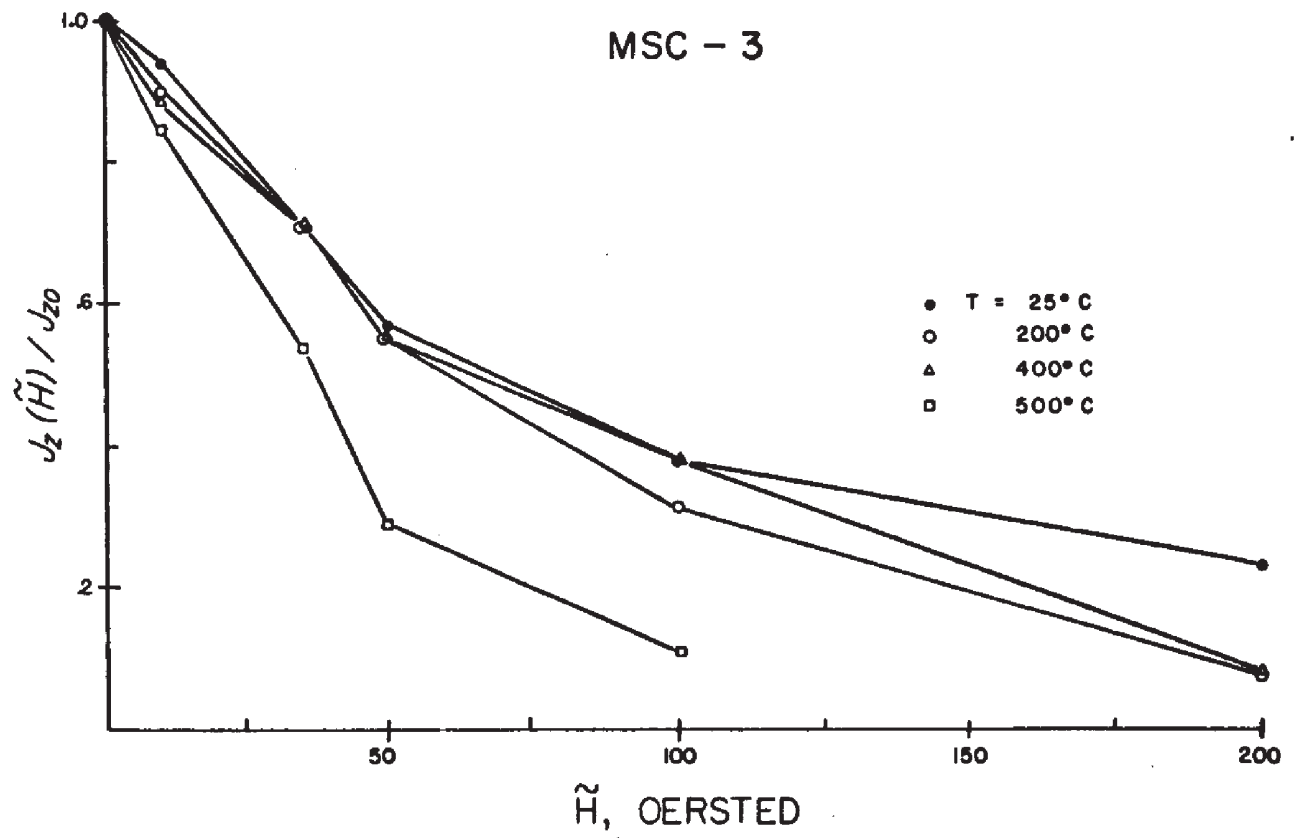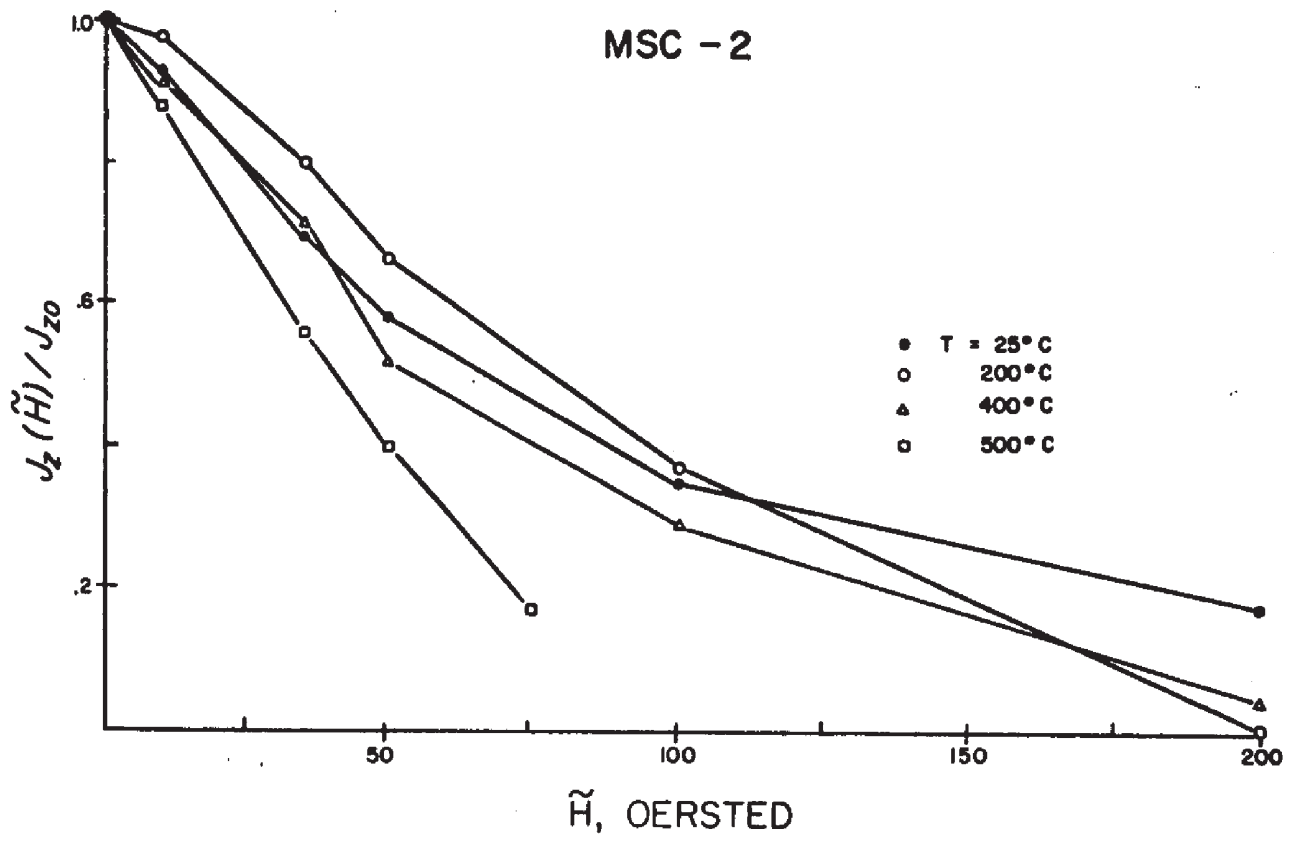
the elevated temperature where they were subsequently A. F. demagnetized.
The remanences were always measured at room temperature, and the demag-
netization curves at each temperature were obtained by normalizing the
remanence with respect to the magnetization remaining after the thermal
demagnetization step. The room temperature stability curves were taken
more than a month before those at elevated temperatures. Due to an
interchange in the polarity of the leads connecting the demagnetizing
coil to the inductrol, it is seen that the sense of the ARM for the room
temperature spectra is opposite to the ARM sense in elevated temperature
curves. (See appendix B-1). There is hardly any doubt that this is
the reason that in all four samples studied the room temperature demag-
netization curves cut across the hitherto more stable curves at relatively
higher alternating field, when the ARM becomes more noticeable. (See
figure 16).

Focussing our attention on the region of the demagnetization curves
where the ARM effect is relatively small ($J_z(H)/J_{z0} > .4$), we see that for
all samples the stabilities at $200^{\circ}C$ and $400^{\circ}C$ are either greater than or
similar to those at $25^{\circ}C$. The $500^{\circ}C$ curves are 'softest' for all samples.
In figure 17,$\tilde{H}_{\frac{1}{2}}$ versus T is plotted for the various crystals. Clearly, $\tilde{H}_{\frac{1}{2}}$
is not a fundamental quantity, and similar curves can be drawn using
other criteria such as fixing the level of magnetization (e.g. $J_z(H)/J_{z0}$
= .9, .8, ..., .4, .3 ....) or by fixing the A. F. demagnetization level
(e.g. $\tilde{H}_{\frac{1}{2}}$= 10 oe, 25 oe, ...). This was done using the latter criterion
and the resulting curves (not reproduced here) have the same features
as in figure 17, as long as the ARM effect is relatively minor. As seen

Figure 17

A plot of the median demagnetizing field, MDF, versus temperature for the large
crystals of magnetite; the data are obtained from figure 16. The MDF values are
either flat up to about 400°C (MSC-3) or display a broad maximum between T_R and
400°C. Note the relatively large scatter in the MDF values of the different samples.
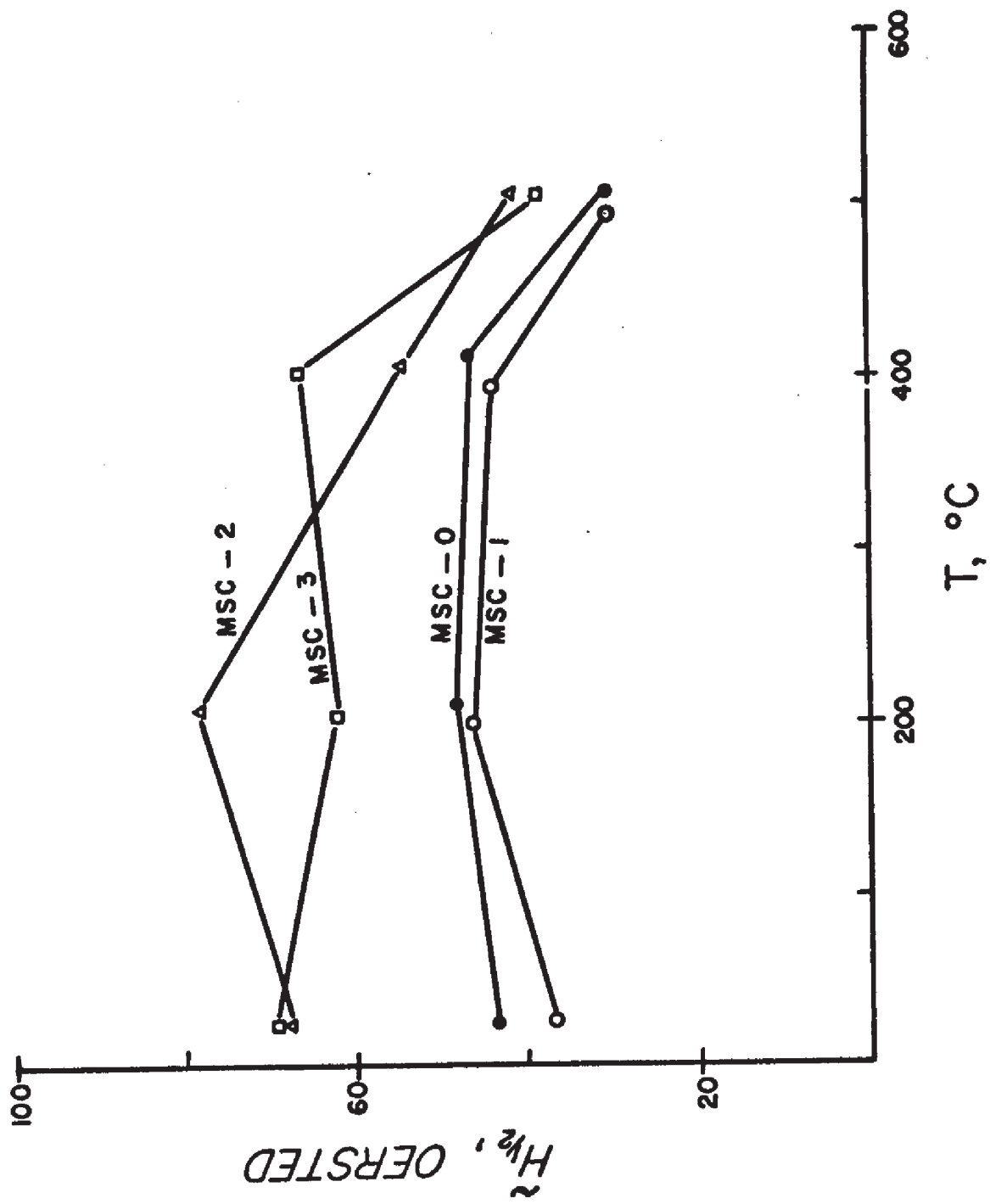
Figure 18

Normalized thermal demagnetization of 9.1 ± .5 oe TRMs of the large crystals of magnetite. Note the relatively high thermal stability of these TRMs and the relative similarity of the curves of the different crystals.

$h = 9.1 \pm .5$ OE

MSC — 0
— 1
— 2
— 3

$J_z(T)/J_{z0}$

1.0

.6

.2

T, °C

200   400   600
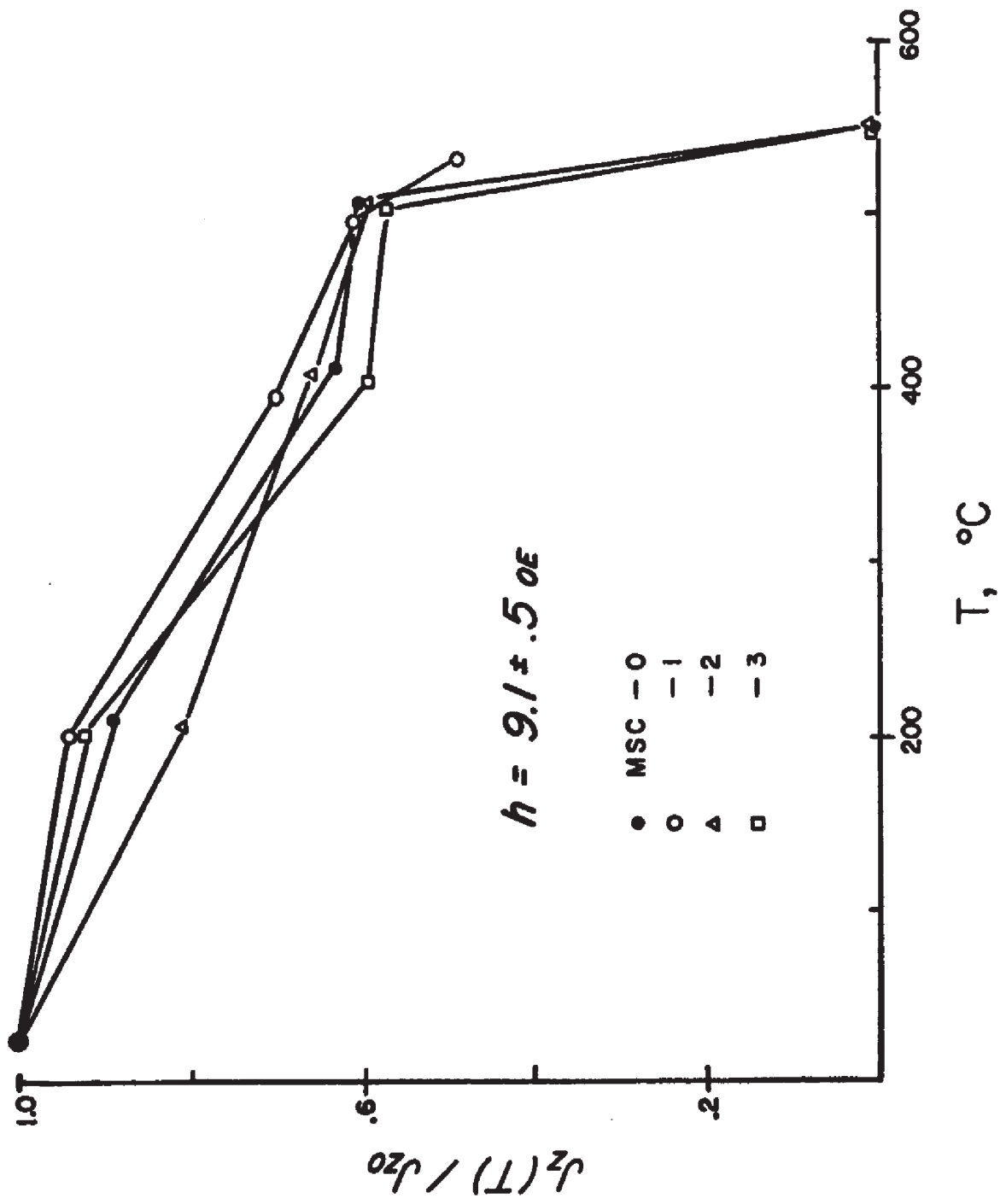
in figure 17, three of the samples display a borad maximum in their stabilities between 200° and 400°C. For the fourth sample the stability curve is essentially flat out to 400°C. Figure 18 depicts the similarity of the TRM thermal demagnetization curves of samples MSC-0,1,2,3.

For bulk magnetic material, where changes in magnetization are largely caused by domain wall movement, the microscopic coercivity is related to

16. $$H_{ci}\Big|_{MAX} = \frac{\pi \lambda \sigma}{J_S}$$

where λ is the relevant magnetostrictive constant, σ denotes the magnitude of the internal stress, and J_S is the saturation magnetization. (See Chikazumi, 1964, p. 285-287 or Morrish, 1965, p. 385-387.) H_{ci} is the maximum field required to drive a single domain wall across all the energy barriers in the crystal, where the energy barriers are due to a sinusoidal internal stress distribution, associated with crystal imperfections such as dislocations and dislocation pileups. In our crystals some of the stresses may be a result of deformational twinning. Substituting the appropriate value for λ ($\lambda_{111} = 7.8 \times 10^{-5}$) and for J_S (480 gauss) for magnetite and assuming that $H_{ci}\big|_{MAX} \approx H_{\frac{1}{2}}(=20$ oe), we obtain, using equation 16, a value for the internal stress in our crystals, $\sigma \approx .4$ kg/mm^2.

Klapel and Shive (1974) have shown that λ_{111} decreases linearly between T_R and 500°C. Their data for λ_{100} is less conclusive, but the overall magnetostrictive effect decreases with increasing temperature. At T_R λ_{111} is the dominant magnetostriction constant (at T_R, $\lambda_{111} = 78 \times 10^{-6}$ and $\lambda_{100} = -20 \times 10^{-6}$); however, at temperatures approaching T_C the relative effect of λ_{100} seems to increase. This possibility suggested

by the data of Klapel and Shive and also by the data of Syono (1965), who studied the magnetostriction constants of the $xFe_2TiO_4(1-x)Fe_3O_4$ solid solution. The data show that for increasing values of x and corresponding decreasing values of T_C λ_{100} becomes relatively more visible and even exceeds λ_{111} for x = .56 in the temperature interval that was examined. Although Syono's data may not be directly applicable to pure magnetite, because both the chemistry and the Curie points are variables of the solid solution series, it seems from the data of Klapel and Shive and that of Syono that, as the temperature approaches T_C, λ_{100} (which is apparently always negative, while λ_{111} is always positive) becomes relatively more important in pure magnetite (x = 0).

The temperature dependence of the stress field is not known. However, as the temperature rises, the apparent height of the energy barriers decreases, and wall movement is more easily implemented, causing a decrease in H_{ci} and $\tilde{H}_{\frac{1}{2}}$. In addition, J_S decreases with temperature. These two effects have an opposite effect on the H_{ci} and may cause the observed maximum in the $\tilde{H}_{\frac{1}{2}}$ curves. This implies that at moderate temperatures above T_R, up to 300° or $400^\circ C$, $\tilde{H}_{\frac{1}{2}}$ is dominated by the decrease in J_S causing the initial increase in $\tilde{H}_{\frac{1}{2}}$. We have assumed in the above paragraph that H_{ci} and $\tilde{H}_{\frac{1}{2}}$ have similar temperature dependences.

Alternatively, the observed temperature dependence of $\tilde{H}_{\frac{1}{2}}$ of the large crystals can be explained using an argument similar to that proposed by Rathenau (1953). Caused by the rapid decrease with temperature of the magnetocrystalline constant, K, there is a corresponding thickening of the domain walls, $\delta \sim J_S/\sqrt{K}$, with temperature. Using Fletcher's (1971) data

for the decay of K_1 with temperature,

$$\frac{K_1(T)}{K_1(T_R)} = \left[\frac{J_S(T)}{J_S(T_R)}\right]^8$$

one obtains for the relative domain wall thickness, δ.

$$\frac{\delta(T)}{\delta(T_R)} = \left[\frac{J_S(T_R)}{J_S(T)}\right]^3 .$$

Thus at elevated temperatures the domain walls occupy a larger fraction of the volume of the magnetic particles. As the temperature increases, the crystal is composed of fewer domains and domain walls, and demagnetization requires longer paths of domain wall movement, implying higher demagetizing fields and greater stability. On the other hand, rising T decreasing the barriers to domain wall movement thus decreasing the stability. Again, these two effects affect $\tilde{H}_{\frac{1}{2}}$ in opposite sense, possibly giving rise to the observed maximum in $\tilde{H}_{\frac{1}{2}}$.

6.4 HOT A.F. DEMAGNETIZATION OF FINE PARTICLES OF MAGNETITE

Hot A. F. demagnetization was also done on Olby 269-A and samples 6B and 6C. The demagnetization curves of the three samples are displayed in figures 19a, 20a, and 21a, respectively. It is seen that the spectra become less stable with increasing temperatures. In figures 19b, 20b, and 21b, $\tilde{H}_{\frac{1}{2}}$ and the TRM thermal demagnetization spectra are plotted against temperature on the left and right ordinate, respectively, for the samples. Despite (or because of) the small number of data points, the temperature dependence of $\tilde{H}_{\frac{1}{2}}$ can be approximated reasonably by a line. The experiments

Figure 19

a.   Normalized A. F. demagnetization curves at elevated tempera-
tures of .49 oe TRM of basalt sample Olby 269A, whose magnetic
carriers are single domain magnetite particles. The remanence is
measured at T_R and the initial points represent the thermally
demagnetized remanence at the temperatures where the demagneti-
zation is subsequently performed.   The demagnetization curves
become monotonically 'softer' with increasing temperature.

b.   Solid circles, left hand ordinate, represent the MDF versus
temperature curve, which are well approximated by a linearly
decreasing function with increasing temperature.

Open circles, right hand ordinate, represent the sample's
normalized demagnetization curve.

OLBY – 269A

T = 25°C
△ 400°C
■,□ 500°C
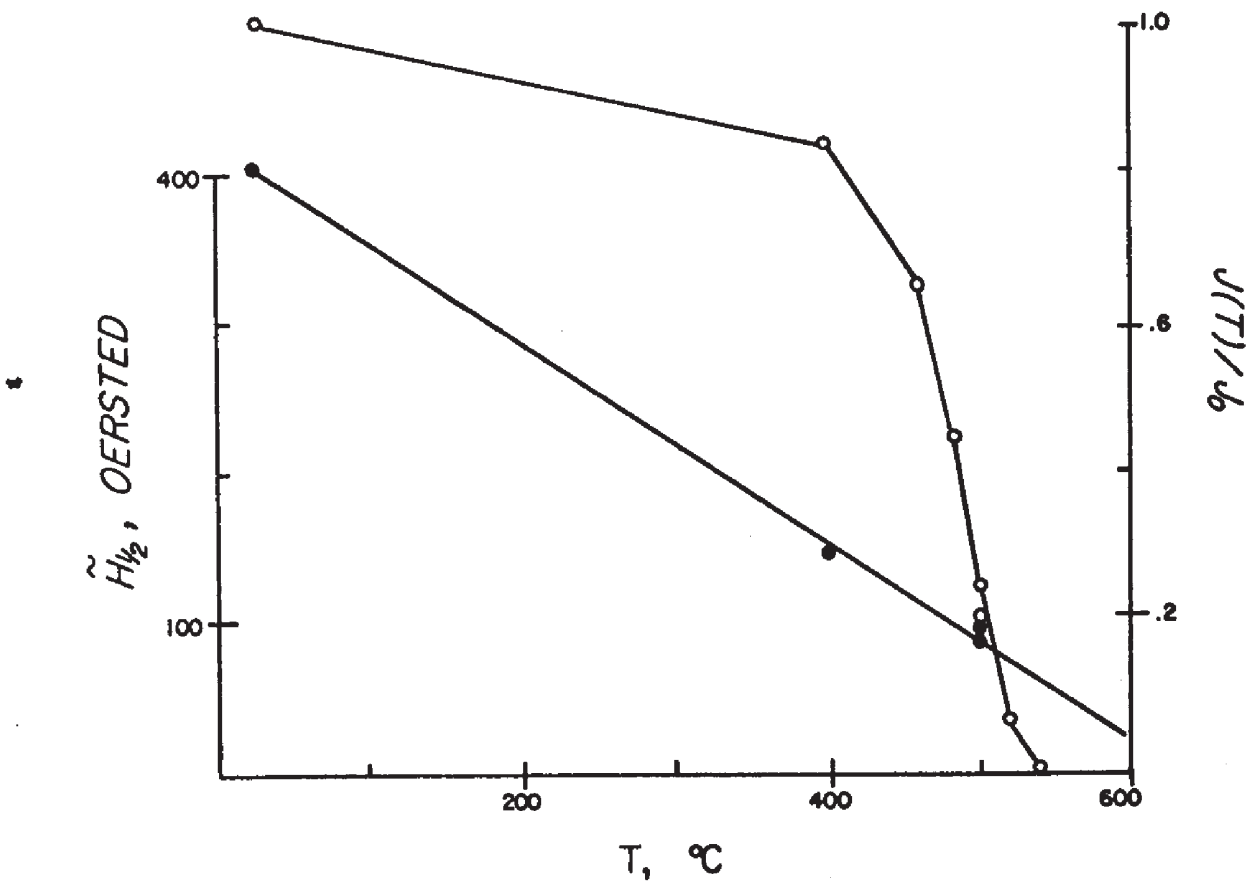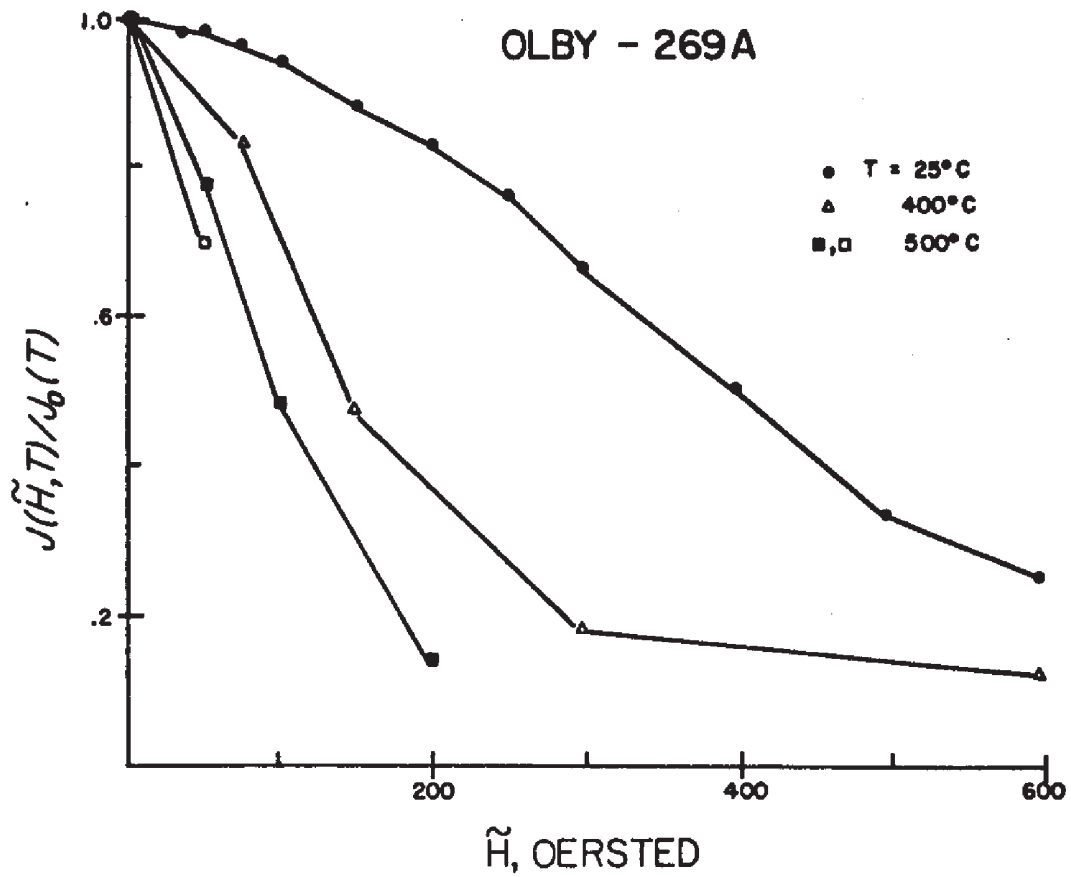
Figure 20

a.   Normalized A. F. demagnetization curves at elevated tempera-
tures of .49 oe TRM of sample 6B, whose magnetite carriers are
synthetic, equidimensional magnetite particles whose mean diameter
is .21 μm. The remanence is measured at T_R and the initial points
represent the thermally demagnetized remanence at the temperatures
where demagnetization is subsequently performed. The demagneti-
zation curves become monotonically less stable with increasing
temperature.

b.   Solid circles, left hand ordinate,represent the MDF versus
temperature curve, which is well approximated by a linearly
decreasing function with increasing temperature.

Open circles, right hand ordinate, represent the sample's
normalized thermal demagnetization curve.

SAMPLE 6B
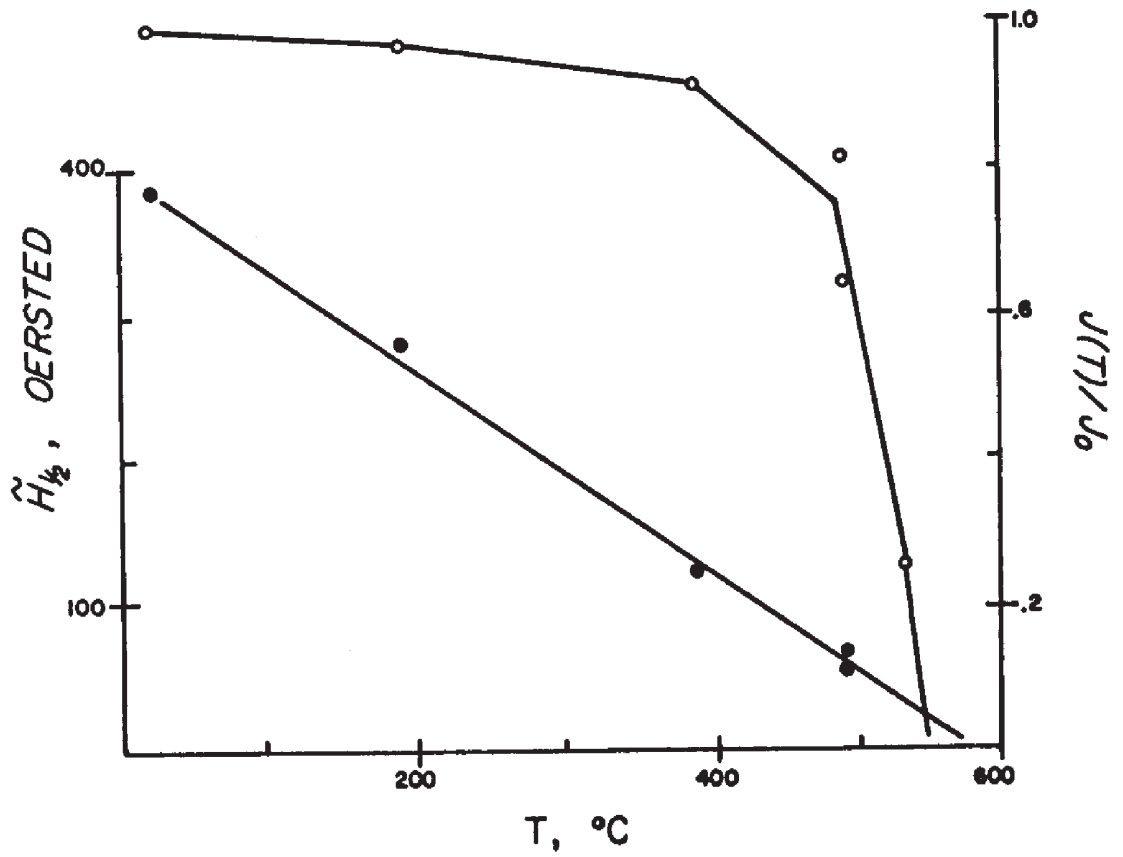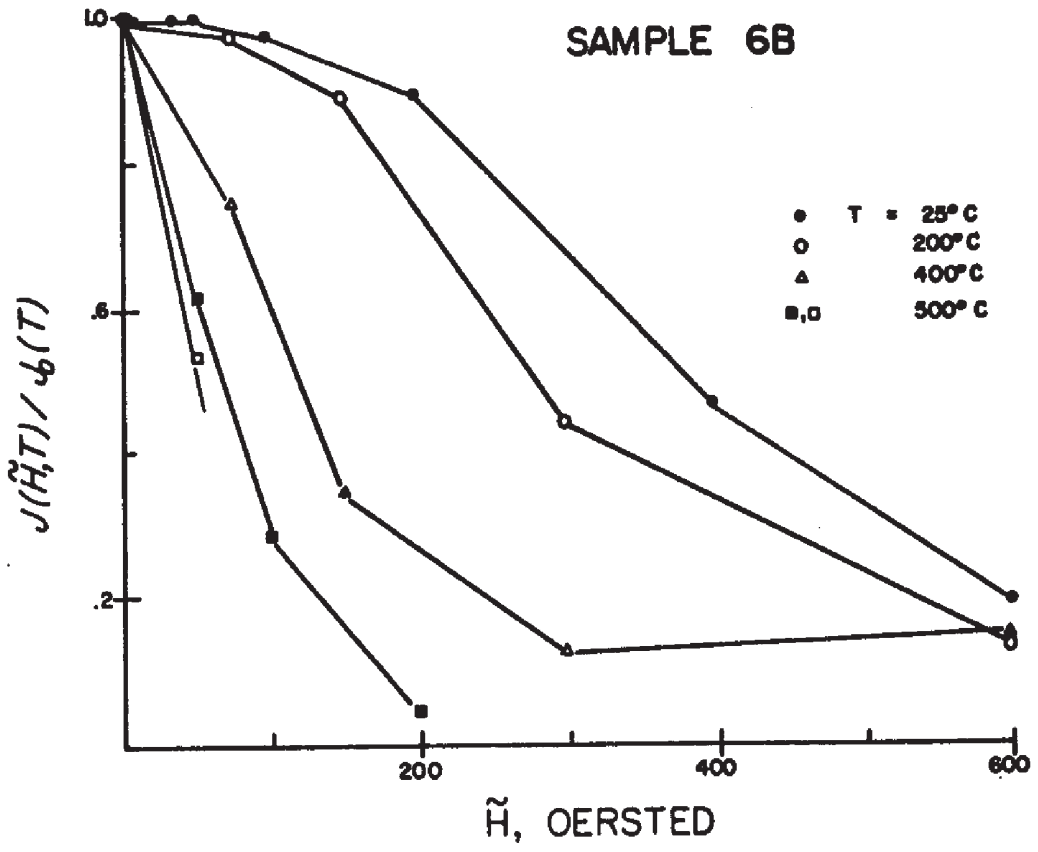
Figure 21

a.   Normalized A.F. demagnetization curves at elevated temperatures of .49 oe TRMs of sample 6C, whose magnetic carriers are synthetic, equidimensional magnetite particles whose mean diameter is .21 µm. The remanence is measured at T_R and the initial points represent the thermally demagnetized remanence at the temperatures where demagnetization is subsequently performed. The demagnetization curves become monotonically less stable with increasing temperature.

b.   Solid circles, left hand ordinate, represent the MDF versus temperature curve, which is well approximated by a linearly decreasing function with increasing temperature.

Open circles, right hand ordinate, represent the sample's normalized thermal demagnetization curve.

SAMPLE 6C
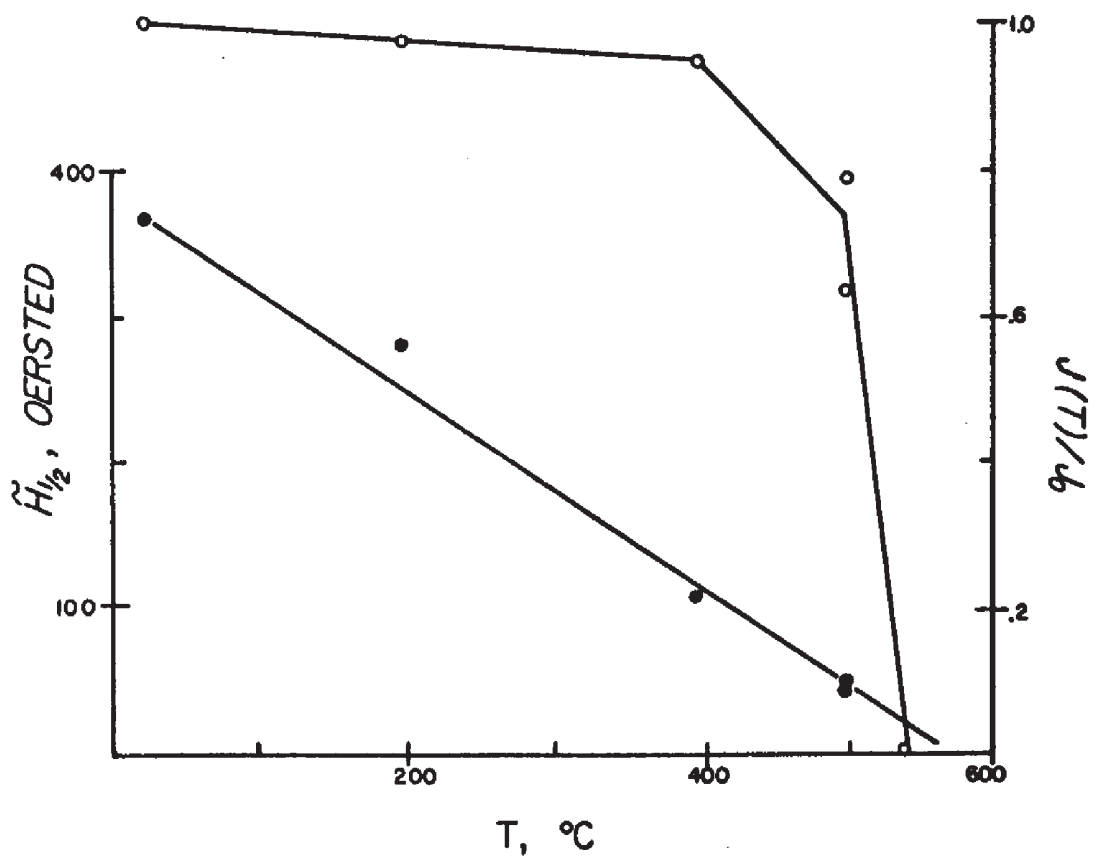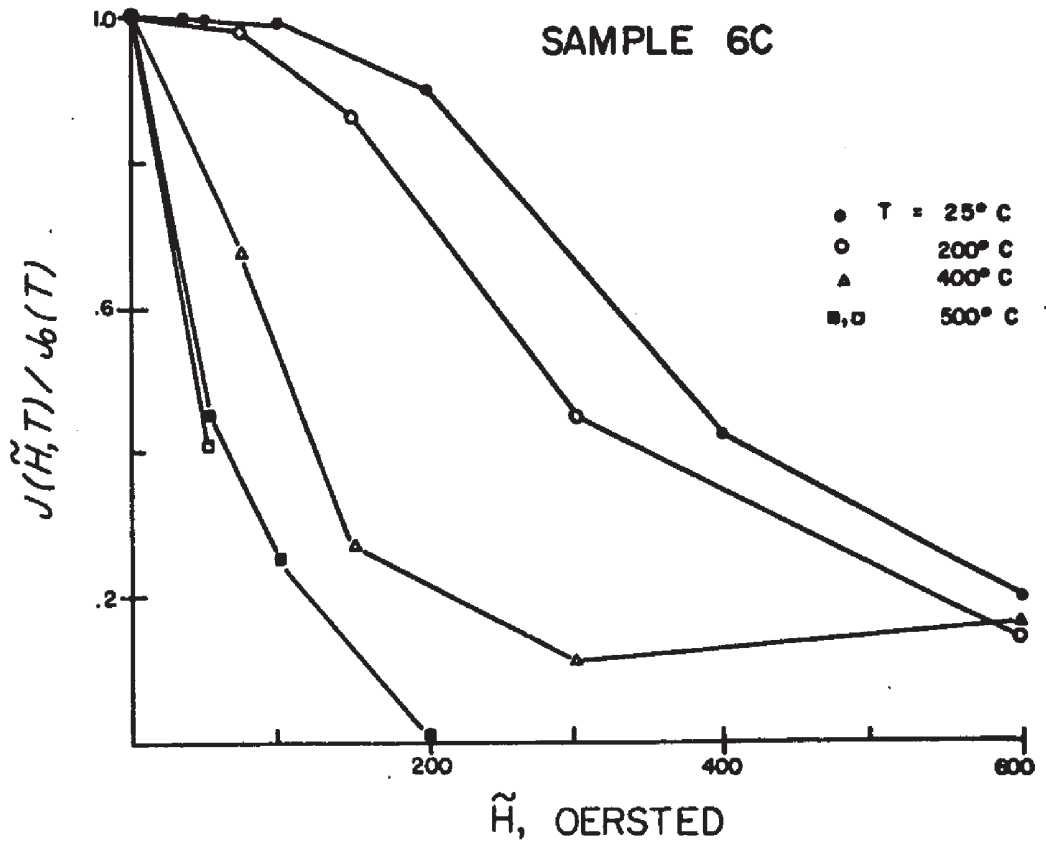
at 500°C were repeated thus giving some measure of the reproductibility of the results. The temperature values are thought to be known to ±10°C, and the values of $\tilde{H}_{\frac{1}{2}}$ to ±5%. If the lines for the temperature dependence of $\tilde{H}_{\frac{1}{2}}$ are extended to intersect the temperature axes, the points of intersection are about 630°C, 580°C, and 570°C, for samples Olby 269A, 6B and 6C, respectively. In reality one would expect $\tilde{H}_{\frac{1}{2}}$ to vanish with the TRM as in the thermal demagnetization curves. For samples 6B and 6C the intersection is peculiarly close to T_C, although for Olby 269A the intersection is substantially above T_C (T_C = 565°±10°C, Whitney et al., 1971). For the samples studied, to a reasonable approximation, stability decreases linearly with temperature up to near the blocking temperature, where a more rapid decay of the stability is inferred. This behavior is markedly different from that of the large magnetite crystals.

That $\tilde{H}_{\frac{1}{2}}$ of the samples containing fine particles of magnetite decays linearly with temperature implies that its temperature decay is more rapid than would be expected if $\tilde{H}_{\frac{1}{2}}$ were determined by shape anisotropy, but that the decay of $\tilde{H}_{\frac{1}{2}}$ is less rapid than would be expected if it were completely determined by magnetocrystalline anisotropy. Although we now have numbers detailing the temperature variations of λ_{111} and λ_{100}, the magnetoelastic effects on $\tilde{H}_{\frac{1}{2}}$ are difficult to assess because we lack knowledge on how the internal stresses, σ, vary with temperature. In the next section we shall pursue further the effects of the magnetic anisotropies on controlling the stability.

6.5 TEMPERATURE DEPENDENCE OF HYSTERESIS PROPERTIES

For purposes of comparison we also investigated the temperature dependence of the high-field hysteresis properties of the Columbian Carbon

magnetite powder, which is the magnetite species of samples 6, 6A, 6B, 6C, and 7. The experiments were performed on a Princeton Applied Research (P.A.R.) Vibrating Sample Magnetometer (V.S.M.). The experiments were performed with previously heated and stabilized powders. One set of experiments was performed with undiluted powder ($J_S(T_R)$ = 85 emu/g). In the second set of experiments we diluted the powder to the sample concentration ($J_S(T_R)$ = 1.20 emu/g).

In figure 22 the open and solid circles represent the temperature dependence of the saturation magnetization, $J_S(T)$, (with H = 7.3 koe) of the undiluted and diluted powders, respectively. The difference in the two sets of data is not thought to be significant. The squares and triangles represent the bulk coercivity, H_C, of the undiluted and diluted powders, respectively. At lower temperatures the two sets of data are quite divergent, but they converge at higher temperatures. It should be noted that the room temperature coercivity of both diluted and undiluted powders is the same, 105±3 oe, which suggests that interaction effects due to different powder concentrations are not the determining factors causing the differences in the lower-temperature H_C data. The curves represent an average of the two sets of data. The temperature dependence of H_C is seen to be similar to that of J_S though its decay is generally more rapidly.

For comparison (the right hand ordinate) the dash curve is drawn to represent $(T_C - T)^M$, where M = .50 and T_C is taken to be $580^\circ C$. We see that for $J_S(T)/J_S(T_R)$, M > .50 (M $\approx$ .53); for $H_C(T)/H_C(T_R)$, M < .50 for high temperatures, T > $300^\circ C$, and M > .50 for T < $300^\circ C$.

Figure 22

Hysteresis parameters as a function of temperature for Columbian Carbon magnetite powder whose equidimensional particles have a mean diameter of .21 μm. Open symbols represent the undiluted powder, and solid symbols represent powder diluted to a concentration of about 1.5% by wieght.

Circles represent the normalized J_S versus T dependence.

Squares represent the normalized H_C versus T dependence.

Dash line, right hand ordinate, represents the curve $(T_C-T)^{\frac{1}{2}}$.
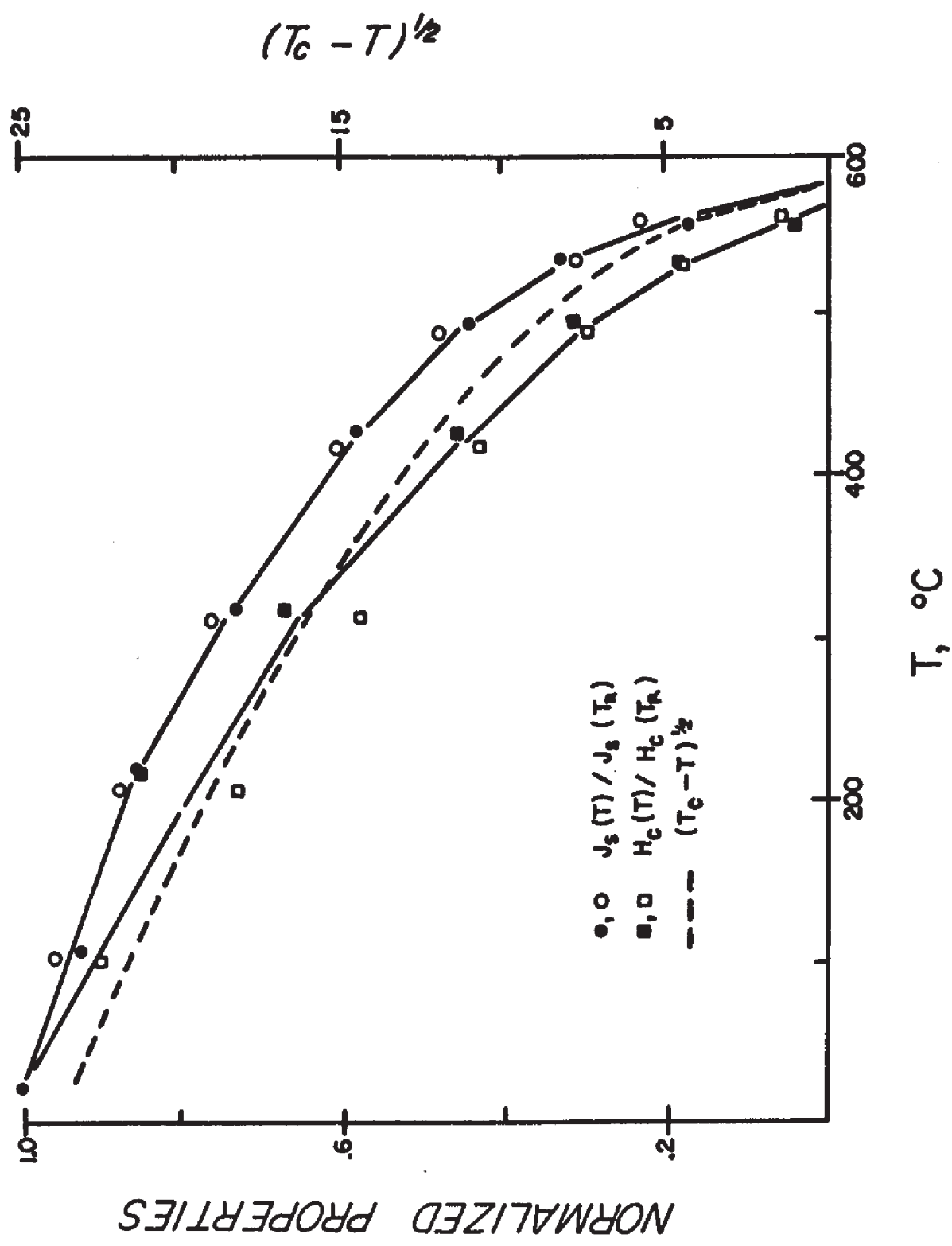
In figure 23 the value of $\tilde{H}_{\frac{1}{2}}$ for samples 6B and 6C taken from figures 20b and 21b are normalized with respect to their room temperature values and plotted along the ordinate versus $J_S(T)/J_S(T_R)$. The curves drawn for reference are obtained from the equation $[J_S(T)/J_S(T_R)]^M$ where M = 2, 5/2, 3 for the upper, middle, and lower curves, respectively. It is seen that

17.
$$H_{\frac{1}{2}}(T)/H_{\frac{1}{2}}(T_R) = [J_S(T)/J_S(T_R)]^{5/2}$$

approximates the data quite well.

In figure 24 we plot $H_C(T)/H_C(T_R)$ versus $J_{RS}(T)/J_{RS}(T_R)$. J_{RS} is the remanence after the application and subsequent removal of an external field sufficient to saturate the sample. J_{RS} is a measure of the average spontaneous magnetization of the grains. Despite the fact that some of the H_C data of the two powders are rather divergent (see figure 22), the data plotted in figure 24 can be approximated by a line whose slope is unity. It is again to be noted that the approximation is improved for the higher temperature points. This is an interesting result, showing that for this particular type of magnetite powder the hysteresis loop contracts linearly at elevated temperatures.

18.
$$H_C(T)/H_C(T_R) = [J_{RS}(T)/J_{RS}(T_R)]^1$$

The representation of figure 24 has an advantage in that the determinations of H_C and J_{RS} are essentially simultaneous so the temperature is known to be identical (within $1°$ or $2°C$), whereas in figure 22

Figure 23

Normalized MDF values from figure 20 (open triangles) and figure 21 (solid triangles) are plotted versus normalized J_S values from figure 22, extrapolated to the appropriate temperatures. The solid curves represent $[J_S(T)/J_S(T_R)]^M$ where $M = 2$, $5/2$, 3, for the upper, middle, lower curves respectively. It is seen that $M = 5/2$ approximates the data quite well.

SAMPLE 6B △

SAMPLE 6C ▲

$J_s(T)/J_s(T_0)$

$\tilde{H}_{l_2}(T)/\tilde{H}_{l_2}(T_0)$
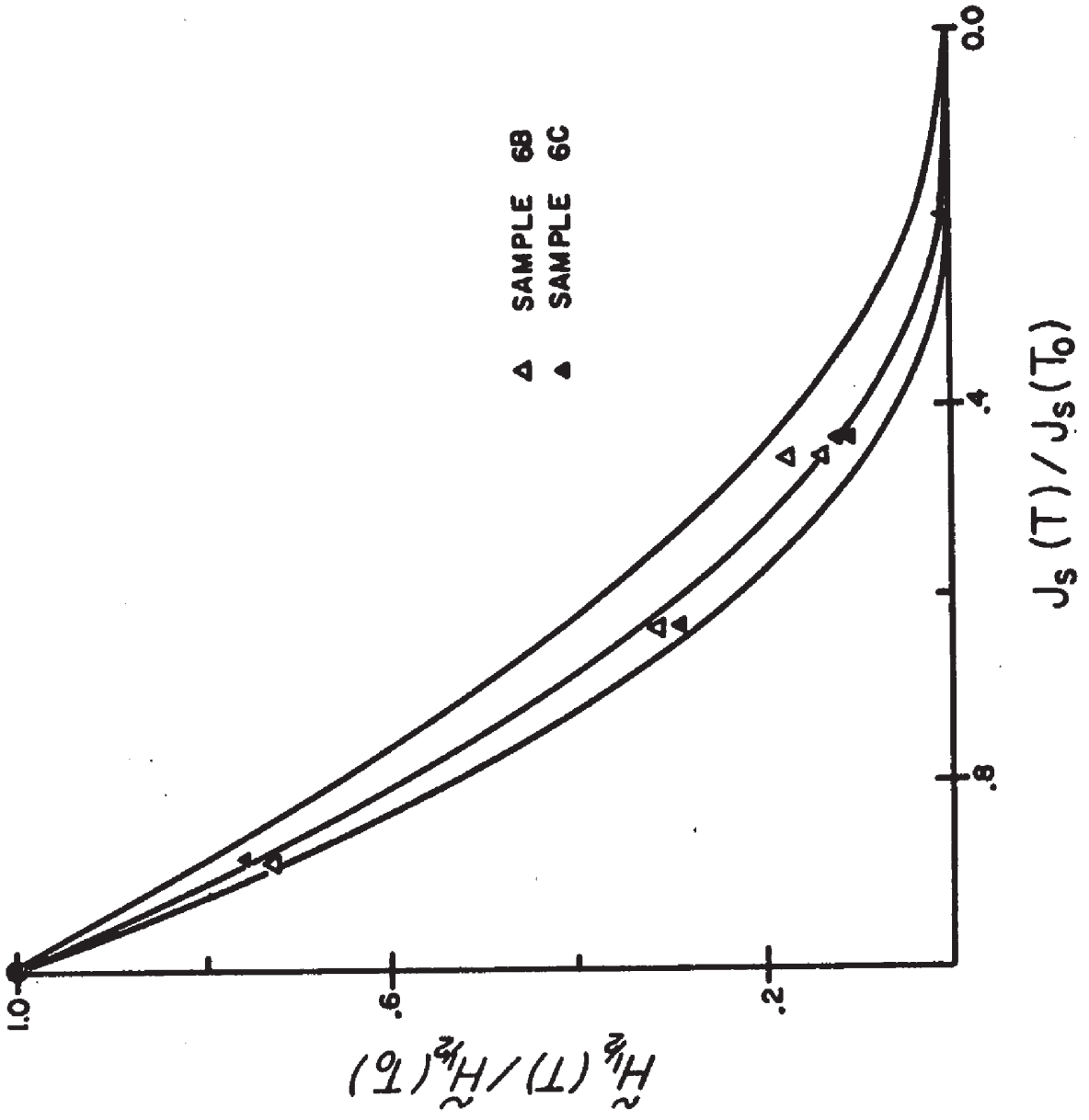
Figure 24

The normalized bulk coercivity, H_C, is plotted versus the normalized saturation remanence, J_{RS}, for different temperatures, for Columbian Carbon magnetite powders. It is argued in the text that J_{RS} is a measure of the spontaneous magnetization, J_{SP}. The data are essentially linear, and this approximation improves at higher temperatures.

UNDILUTED MAGNETITE POWDER

DILUTED TO SAMPLE CONCENTRATION

$J_{RS}(T) / J_{RS}(T_0)$

$H_c(T) / H_c(T_0)$
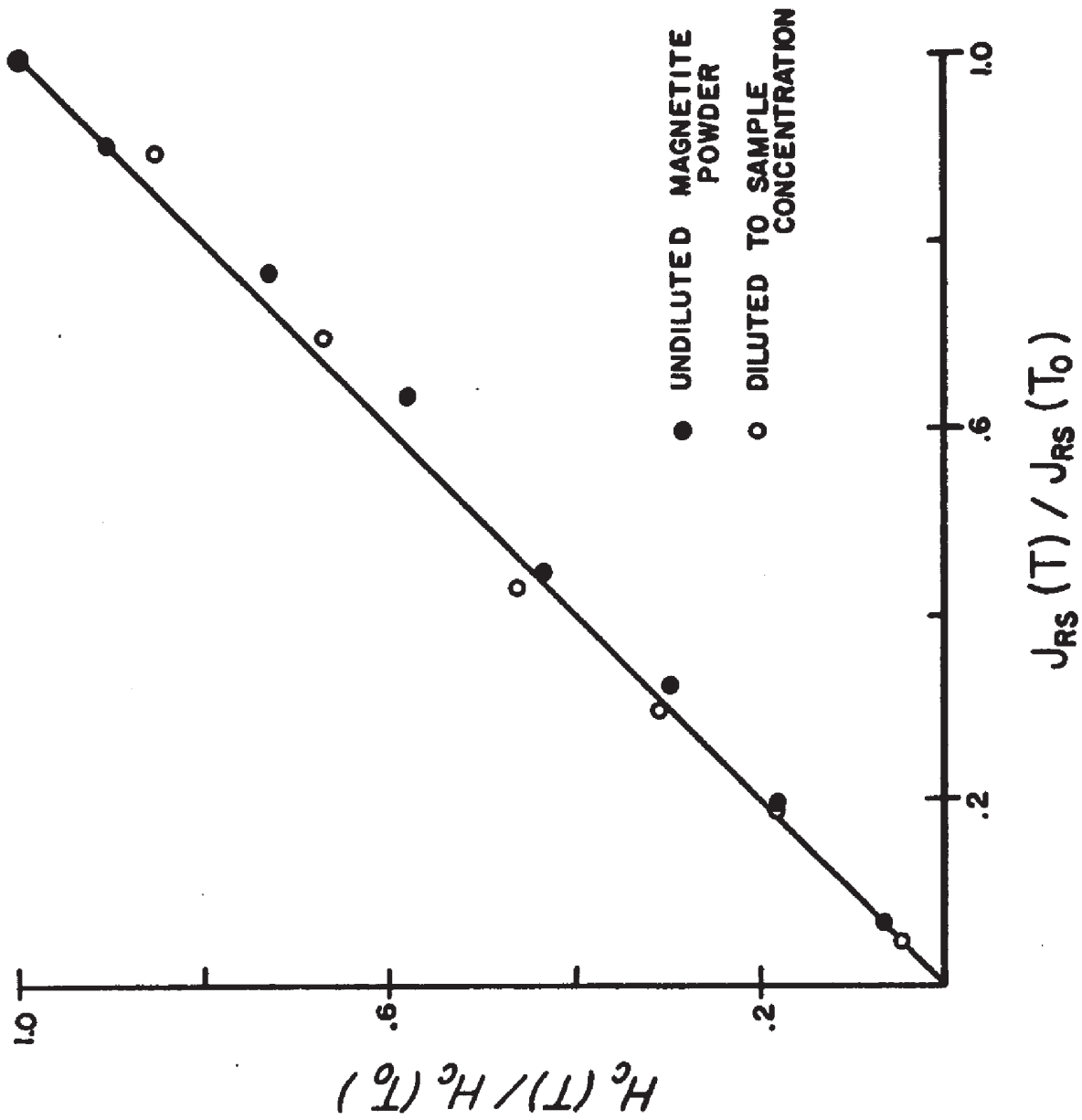
the temperature cannot be ascertained to better than $\pm 10^{\circ}C$.

For a single domain particle of uniaxial anisotropy the intrinsic coercivity, H_{ci}, is the intensity of the reverse (critical) field needed to reverse the grain's magnetization. For solid rotation of the magnetization (rotation in unison) H_{ci} is linearly proportional to K_u/J_{SP} where K_u is the dominant anisotropy and J_{SP} the spontaneous magnetization. For single domain particles that are homogeneously magnetized, $J_{SP} = J_S$. For magnetite particles, when magnetocrystalline anisotropy is dominant,

$$K_u \approx <K> \quad \text{and} \quad H_{ci} \propto <K>/J_{SP}.$$

When shape anisotropy is dominant,

$$K_u = \tfrac{1}{2}DJ_{SP}^2 \quad \text{and} \quad H_{ci} \propto DJ_{SP}$$

where D is a shape factor which can vary from 0 to 4π. When the uniaxial anisotropy is magnetoelastic in origin,

$$K_u \propto <\lambda>\sigma \quad \text{and} \quad H_{ci} \propto <\lambda>\sigma/J_{SP},$$

where $<\lambda>$ is the relevant combination of λ_{111} and λ_{100} and σ is the internal stress. The total intrinsic coercivity is a combination of the contributing anisotropies.

The two coercivities obtained from hysteresis loops are the bulk coercivity, H_c, the reverse field for which the sample magnetization is zero, and the coercivity of the remanence, H_{CR}, the reverse field required such that when it is removed (H = 0), the magnetization vanishes ($H_{CR} > H_C$).

The precise relation between H_{ci} and H_c and H_{CR} is difficult to ascertain. Although the process of obtaining H_c is similar to the procedure followed in calculating H_{ci}, in practice, the sample whose hysteresis is measured contains a distribution of particles with a distribution of H_{ci}, and H_c is therefore a weighted average of all the particles of the sample including those that are superparamagnetic and multidomain. The presence of superparamagnetic grains is particularly disturbing because their contribution is felt when H_c is measured, although they do not contribute to the remanence. Thus H_c is always lower than the appropriate average value of H_{ci} for the grains actually responsible for the remanence.

In the measurement of H_{CR} the final external field is zero, so that its value is not affected by contributions of superparamagnetic particles, so that its value is higher than H_c and more closely related to an average value of H_{ci}, corresponding to the remanence carrying particles. In addition, H_{CR} is numerically more closely related to $\tilde{H}_{\frac{1}{2}}$. Wohlfarth (1958) calculated that for an assembly of identical uniaxial single domain particles $H_{CR}/H_c = 1.09$ this ratio is increased to 1.29 when allowing for a distribution in H_{ci} values. It is expected that the H_{CR}/H_c ratio will increase markedly, due to an increase in the induced magnetization, with an increasing superparamagnetic fraction and with an increasing fraction of multidomain particles.

The dominant anisotropy controlling H_{ci} near the blocking temperature can be determined from the functional form of its temperature dependence. For better visualization one can plot H_{ci}/J_{SP} versus T (or T/T_c). Then for shape anisotropy $H_{ci}/J_{SP} \propto D = $ Constant; for magnetocrystalline

anisotropy $H_{ci}/J_{SP} \propto <K>/J_{SP}^2 \propto J_{SP}^6$; for magnetoelastic anisotropy $H_{ci}/J_{SP} \propto <\lambda>\sigma/J_{SP}^2$. If we take $<\lambda> \approx \lambda_{111}$ and if we use the data of Klapel and Shive (1974) and assume further that λ_{111} decreases linearly with increasing temperature between T_R and $T_C = 580^\circ C$, then $<\lambda> \propto 1 - T/T_C$. Assuming that σ is constant with T (where ignorance is bliss) and taking $J_{SP} \propto J_{RS} \propto (1 - T/T_C)^{.5}$, one obtains $H_{ci}/J_{SP} =$ Constant. Therefore, H_{ci}/J_{SP} should be constant with temperature for shape controlled coercivity and possibly for magnetoelastic controlled coercivity and should decay with temperature as J_{SP}^6 for magnetocrystalline controlled coercivity.

For a sample containing only homogeneously magnetized, blocked, single domain grains, where for each particle $J_{SP} = J_S$, the variation of J_S with T is a good measure of the dependence of J_{SP} on T (Dunlop, 1969). For a sample whose particles range in size from superparamagnetic upwards the temperature dependence of J_S is no longer a good measure of the temperature decay of J_{SP}. J_S in this latter case is artificially inflated because it includes the magnetization of many particles that do not contribute to the remanence. A better measure of J_{SP} versus T is obtained from J_{RS} versus T values, whose decay rate with increasing T is more rapid than that of J_S.

In figure 25a H_{CR}/J_S and H_C/J_S are plotted against T. Despite differences in H_{CR} and H_C, their temperature dependences are similar. The curves of the diluted samples are slightly more resistant to thermal decay. The approximate mean of all these curves can be approximated by $H_{CR}/J_S \approx H_C/J_S \propto J_S^{1/2}$. The temperature dependence in figure 25a is certainly not determined by the magnetocrystalline anisotropy. Rather, the observed

Figure 25

a.   Circles represent H_{CR}/J_S versus T data,

Squares represent H_C/J_S versus T data

for Columbian Carbon magnetite powder. Open (solid) symbols

correspond to undilute (dilute) powder. The relative flatness

of the curves suggests that shape anisotropy is the predominant

anisotropy determining the coercivity.

b. H_C/J_{RS} versus T left hand ordinate,

H_{CR}/J_{RS} versus T right hand ordinate

for Columbian Carbon magnetite particles. Open (solid) symbols

correspond to undiluted (diluted) powder. The flatness of the

curves suggests that shape anisotropy and magnetostatic energy

are dominant in determining the coercivity.
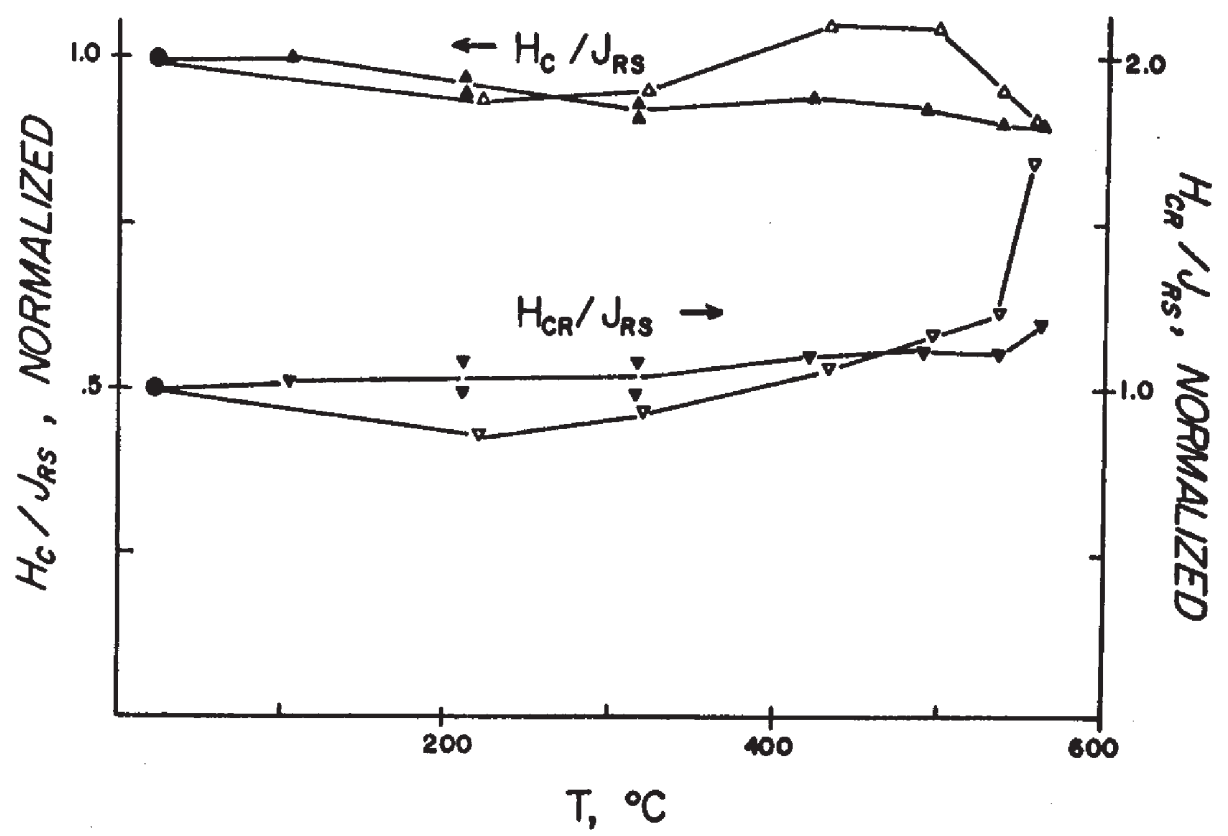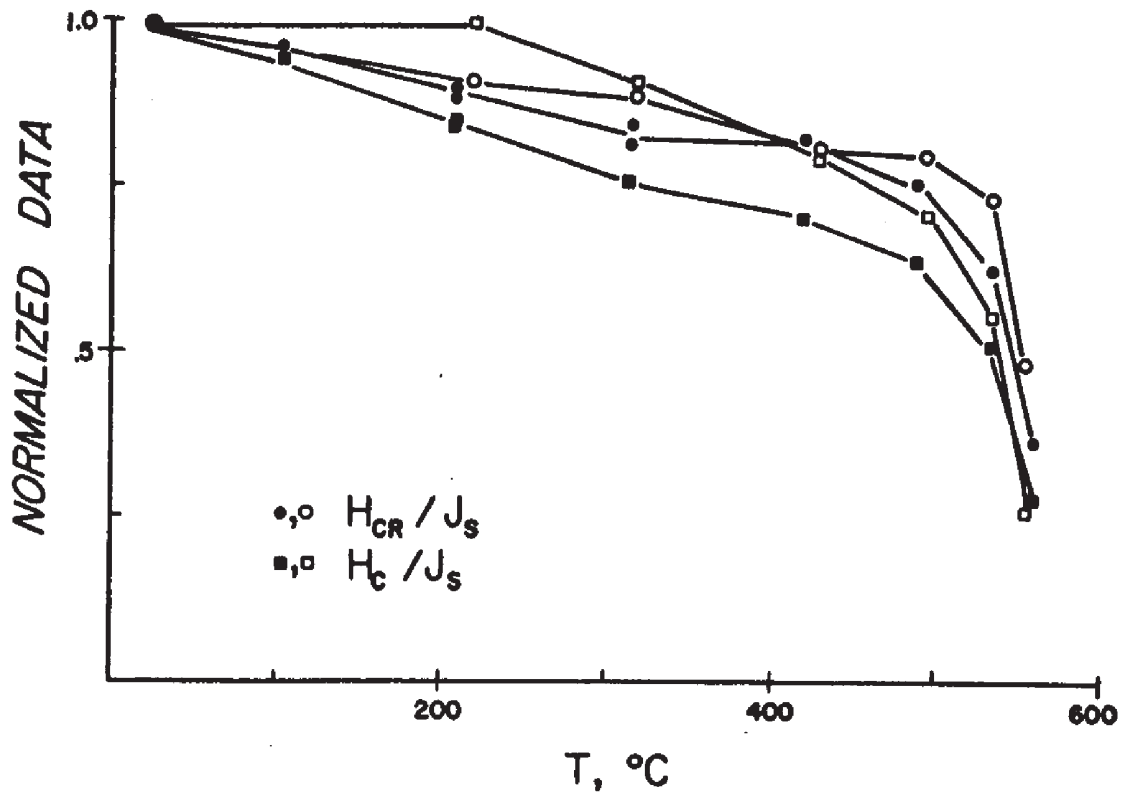
decay is believed to be caused by a relative inflation of J_S as compared to J_{SP} due to the contribution of the superparamagnetic fraction which increases with the temperature.

In figure 25b we plot H_{CR}/J_{RS} and H_C/J_{RS} versus T, and the curves are essentially flat up to about $300^{\circ}C$. Above this temperature a gradual increase is observed in H_{CR}/J_{RS} curves. This behavior is not understood. Neither can we explain the datum at $555^{\circ}C$ where $H_{CR}/J_{RS} = 1.7$. Due to the similarity in the temperature dependence of H_{CR} and H_C observed in figure 25a, greater confidence is placed in the H_C data; experimentally, it is much easier and quicker to obtain H_C than H_{CR}, and this fact becomes more true at higher temperatures.

From the data of figure 25, and mostly from the data of figure 25b, we conclude that magnetocrystalline anisotropy plays only a minor role in controlling the coercivity of the Columbian Carbon magnetite powder. This conclusion is consistent with the observations of chapter 4 where it was discovered that only about 6% of the magnetization decays after cycles in zero field to below magnetite's isotropic temperature. The data suggest that the coercivity depends linearly on J_{SP}, implying that the coercivity is largely controlled by magnetostatic anisotropy due to the shape effect and/or, possibly, by magnetoelastic anisotropy due to magnetostriction.

6.6 CONCLUSIONS AND DISCUSSION

In this chapter we have seen that there is a fundmental difference between the temperature dependence of the A. F. demagnetization charac-teristics of fine particles and large crystals of magnetite. For the

large crystals there is a maximum in the $\tilde{H}_{\frac{1}{2}}$ versus T curve, whereas for the fine magnetite particles the $\tilde{H}_{\frac{1}{2}}$ versus T curve decreases linearly until just below the blocking temperatures.

The temperature dependence of the microscopic coercivity is the key to Néel's (1955) theory for TRM in multidomain particles. Néel assumes that

$$\frac{H_C(T)}{H_C(T_R)} = \left[\frac{J_S(T)}{J_S(T_R)}\right]^{s=2}$$

The coercivity in the above expression is that obtained from hysteresis loops; in addition, it is assumed that each particle has a square hysteresis loop. Schmidt (1973) has shown that Néel's multidomain theory would work for any s > 1; that is, the only requirement is that the height of the hysteresis loop, J_S, should contract more rapidly with temperature than its width, H_C. However, real multidomain particles do not have square hysteresis loops; that is, for multidomain particles $J_{SP} \neq J_S$, such that it is not clear whether J_S or J_{SP} is appropriate in Néel's expression given above. In addition, hysteresis loops are usually not measured for single particles (especially in situations that are of interest in rock magnetism), so that it is not clear which of the various representations for the stability, $H_C \cdot H_{CR}$, of $\tilde{H}_{\frac{1}{2}}$ (or some other stability parameter) is the best measure for the intrinsic coercivity. Using equidimensional, synthetic magnetite powder whose mean particle diameter is .21 μm, we made a comparative study of the above 'coercivities' and their temperature dependences. Although the particles studied are too large to be classical

single domain grains, they are thought to be small to accommodate 'truly' multidomain behavior. (That is, due to previously presented magnetic data it is believed that magnetization and demagnetization processes are not primarily controlled by domain wall movement.) Although the particles we studied may not be ideal to test multidomain theories, the results are interesting and offer direction for future work. We saw in figure 25a that

19.
$$\frac{H_C(T)}{H_C(T_R)} \sim \frac{H_{CR}(T)}{H_{CR}(T_R)} \sim \left[\frac{J_S(T)}{J_S(T_R)}\right]^{3/2}$$

From figure 23 we have that

20.
$$\frac{\tilde{H}_{\frac{1}{2}}(T)}{\tilde{H}_{\frac{1}{2}}(T_R)} \sim \left[\frac{J_S(T)}{J_S(T_R)}\right]^{5/2}$$

Although H_C and H_{CR} are numerically very different, their temperature dependences are very similar. This observation is not so surprising in retrospect because both H_C and H_{CR} are obtained from the same hysteresis loop and its contraction with temperature affects them similarly. $\tilde{H}_{\frac{1}{2}}$, on the other hand, is determined in a totally independent manner, as is its temperature dependence. If the above values of the exponent are used in Schmidt's (1973) expressions for TRM, one obtains:

$$s = 3/2 \implies J_{TRM} \alpha h^{0.33}$$

$$s = 5/2 \implies J_{TRM} \alpha h^{0.6}$$

Neither of these values is particularly satisfying in view of the observed linear dependence of TRM on applied fields for small fields. Other objections to Néel's multidomain theory are discussed in Verhogen (1959) and Stacey (1963).

In addition to J_S, we also use the previously discussed approximation $J_{SP} \sim J_{RS}$, thus obtaining from figure 25b

$$\frac{H_C(T)}{H_C(T_R)} \sim \frac{H_{CR}(T)}{H_{CR}(T_R)} \sim \left[\frac{J_{RS}(T)}{J_{RS}(T_R)}\right]^1$$

and

$$\frac{\tilde{H}_{\frac{1}{2}}(T)}{\tilde{H}_{\frac{1}{2}}(T_R)} \sim \left[\frac{J_{RS}(T)}{J_{RS}(T_R)}\right]^{3/2 \to 2}$$

If nothing else, we have shown that hysteresis-obtained coercivities and the stability with respect to A.F. demagnetization are intrinsically different and have different temperature dependence. In addition, we see that although H_{CR} and $\tilde{H}_{\frac{1}{2}}$ appear to be similar due to their similar absolute values, experiments on their temperature dependencies show that they are intrinsically quite different. H_{CR} is rather more similar to H_C, although they are quite distinct in their absolute values. It is not obvious which type of stability parameter best describes the microscopic coercivity; however, it appears to us that neither the bulk coercivity, H_C, nor the coercivity of the remanence, H_{CR}, is probably the best description for H_{ci} of particles possessing weak-field remanence. Hysteresis loops and the

resulting H_c and H_{CR} deal with the saturation IRM due to all the magnetic particles, thus different ensembles of magnetic particles and different regions of magnetization are sampled during bulk measurements than are affected by weak-field remanence such as TRM or ARM. It therefore seems to us that stability parameters describing the actual remanence are better measures for the intrinsic coercivity of the particles and regions of magnetization participating in a particular remanence. Whether stability with respect to alternating fields is the best measure for H_{ci} is not known, but it should be a better measure than the bulk coercivities. Rather surprising and yet unexplained is the fact that the temperature decay of $\tilde{H}_{\frac{1}{2}}$ is more rapid than that of the bulk coercivities H_c and H_{CR}.

CHAPTER 7

ON THE ADDITIVITY OF PARTIAL THERMOREMANENCE (PTRM)

7.1 SUMMARY

In this chapter we shall test the additivity law of partial-TRMs for our prepared samples each containing magnetites of different mean particle size, spanning the single domain to multidomain size range. The experiments compare the sum of two PTRMs, $PTRM_1 + PTRM_2$, with that of the total-TRM. It is found that, statistically, $\Sigma PTRM \gtrsim TRM$. This tendency is true to the same degree for all samples, regardless of their mean particle size. Thus, it appears that the additivity law is obeyed to the same degree by multidomain magnetite particles as by single domain particles.

7.2 BACKGROUND

In the introduction we saw that Néel's theory for single domain grains is successful in explaining Thellier's and Nagata's observations of the independence and additivity of PTRMs. In addition, we argued from the magnetic properties of hematite (αFe_2O_3) that most hematite found in rocks and clays is probably single domain, such that Néel's (1949) single domain theory applies directly. In volcanic rock, where the remanence usually resides in titanomagnetites, a substantial fraction of the magnetic grains is larger than 1 μm. Thus it appears likely that remanence in multidomain particles may contribute substantially to the TRM of volcanic rocks.

Current theories for multidomain TRM do not possess the generality and elegance of Néel's (1949) single domain theory, and do not provide a definitive statement regarding the additivity and independence of PTRMs. However, Néel (1955) argues that additivity should hold for two domain grains whose different states of magnetization are determined by wall displacements over

two types of potential barriers ('high' and 'low' barrier) which do not interact and whose distribution is temperature independent. Stacey (1963) also argues that multidomain particles should act in accordance with the additivity law. Above all, Nagata's (1943) experiments remain! the additivity law and the independence of PTRM are obeyed by volcanic rocks.

Ozima and Ozima (1965) argued that the additivity law should be strictly satisfied only where the high temperature IRM is negligible in comparison to the PTRM, but in general the sum of the PTRMs should exceed the total-TRM by the sum of the IRMs at the elevated temperatures. In the simplest case, where only one intermediate temperature is used, their prediction leads to:

21. $$\vec{TRM}(T_C,T_R,\vec{h}) + \vec{IRM}(T_1,\vec{h}) = \vec{PTRM}(T_C,T_1,\vec{h}) + \vec{PTRM}(T_1,T_R,\vec{h})$$

They verify their prediction by comparing partial inverse TRMs with total inverse TRM for an assemblage of magnetite grains of approximately 30 μm in size and in an external field of 10 oe.

Dunlop and West (1969) verified equation 21 for samples containing single domain grains of γFe_2O_3 and $CoFe_2O_4$ using external fields of 45 and 90 oe, respectively.

The independence of PTRM and the additivity law are among the more fundamental properties of TRM. Indeed, their validity is crucial for reliable determinations of the intensity of the paleomagnetic field, using samples whose remanence is TRM. In addition, it is of fundamental interest to test the semi-quantitative predictions of Néel and Stacey that additivity should be obeyed by multidomain grains. For these reasons, we study in this chapter the additivity law in magnetites whose magnetic properties are well characterized and whose sizes and magnetic behavior range from single to multidomain. We conduct our study of additivity in fields typical of the earth's.

7.3 PTRM EXPERIMENTS AND RESULTS

To study the additivity of PTRM we conduct experiments according to the following sequence:

(a) The samples are given a total-TRM in the laboratory field, h_L, to obtain $TRM(T_C, T_R, h_L)$.

(b) The samples are reheated above T_C and cooled in <u>null</u> field to a temperature T_I where $T_R < T_I < T_C$. The temperature is maintained at T_I to allow the samples to equilibrate at T_I. (Depending on T_I, the temperature is maintained from between 60 to 90 minutes.) The laboratory field, h_L, is turned <u>on</u> about five minutes before cooling the samples from T_I to T_R to obtain $PTRM_1(T_C, T_I, NULL; T_I, T_R, h_L)$.

(c) Step (a) is repeated to obtain $TRM(T_C, T_R, h_L)$. (Step (c) was added during the experiments, therefore it is absent in slightly over half the experiments.)

(d) The samples are reheated above T_C and cooled in h_L to T_I. The temperature is maintained at T_I until the entirety of each sample is of that temperature. h_L is turned off about five minutes before cooling the samples from T_I to T_R in <u>null</u> field to obtain $PTRM_2(T_C, T_I, h_L; T_I, T_R, NULL)$.

(e) Step (a) is repeated.

The samples are always heated in a slightly reducing chemical environment in the manner described in the chapter on sample preparation. These experiments were performed for three and sometimes four independent values of T_I for each sample. The data is presented in table 6. Column 1 identifies the samples from 1 to 11 in an identical scheme as in table 5. The samples gradually vary from multidomain (sample 1 is a large single crystal) to single domain (sample 11 is composed of needle-shaped (.04 μm x .35 μm) magnetite

crystals). Column 1 also reveals the samples' relative intensity of the total TRM in emu by listing their magnetization multipliers. Column 2 lists the total-TRMs of steps (a), (c), and (e) in chronological order where

$$h_L = .467 \pm .002 \text{ oe}$$

In column 3 the arithmetic means of the total-TRMs are given as well as the variance brackets, where

$$\sigma^2 \equiv [\sum_{i=1}^{n}(x_i - <X>)^2]/n^2$$

n is the total number of independent experiments performed to obtain the mean value, $<X>$. In these experiments n is 2 or 3. X_i is the result of a particular experiment—a particular TRM value. Column 4 lists the various T_I for each sample. Column 5 lists the $PTRM_1(T_C,T_I,NULL;T_I,T_R,h_L)$. Column 6 lists $PTRM_2$ $(T_C,T_I,h_L;T_I,T_R,NULL)$. Column 7 lists the sume of $PTRM_1 + PTRM_2$. The values in the parentheses under each datum in columns 3, 5, 6, and 7 are normalized with respect to the mean TRM for each experiment. In column 8 we note whether or not the difference between the $\Sigma PTRM$ and the mean total-TRM is significant. Significance is defined as:

significant: $\left| \Sigma PTRM - < TRM(T_C,T_R,\vec{h}_L) > \right| > \sigma$

not significant: $\left| \Sigma PTRM - < TRM(T_C,T_R,\vec{h}_L) > \right| \leqslant \sigma$

In column 8 an N.S. implies <u>no</u> significance and an S implies significant difference.

Disregarding for the moment differences between the samples, in 18 experiments out of a total of 38, there is no significant difference between the mean TRM and the $\Sigma PTRM$. Of these 18 experiments there are 9 for which the normalized $\Sigma PTRM < 1$ and 9 for which $\Sigma PTRM > 1$. For 8 of these 18 experiments $\sigma < .01$. In other words, for these 18 experiments the additivity law seems to be obeyed. In the remaining 20 experiments a 'significant difference' is

TABLE 6
THE ADDITIVITY OF PTRM

Sample; Magnet. Multp.	TRM (T_C,T_R) h=.467 oe	<TRM> ±σ	T_I,°C	PTRM$_1$	PTRM$_2$	ΣPTRM	Sig. Diff.
1	.5374 .4625 .4800	.4933±.032 (1.000±.065)	446	.2862 (.580)	.1950 (.395)	.4812 (.975)	N.S.
	.6775 ——— .5600	.6188±.058 (1.000±.094)	501	.3975 (.642)	.2275 (.368)	.6250 (1.010)	N.S.
x 10^{-2} emu	.5925 .5025 .5625	.5525±.037 (1.000±.067)	520	.3700 (.670)	.2062 (.373)	.5762 (1.043)	N.S.
	.5450 ——— .5125	.5288±.016 (1.000±.030)	525	.3512 (.664)	.1888 (.357)	.5400 (1.021)	N.S.
2	2.175 2.188 2.200	2.188±0.010 (1.000±.005)	452	1.234 (.564)	1.012 (.463)	2.246 (1.027)	S.
	2.462 ——— 2.430	2.446±.016 (1.000±.007)	493	1.538 (.629)	.935 (.382)	2.473 (1.011)	S.
x 10^{-3} emu	2.362 2.360 2.340	2.354±.010 (1.000±.004)	511	1.688 (.717)	.7100 (.302)	2.398 (1.019)	S.
	2.335 ——— 2.325	2.330±.005 (1.000±.002)	516	1.681 (.721)	.6875 (.295)	2.369 (1.017)	S.
3	2.062 2.062 2.012	2.045±.024 (1.000±.012)	452	.7825 (.383)	1.281 (.626)	2.064 (1.009)	N.S.
	2.275 ——— 2.238	2.256±.019 (1.000±.008)	493	1.081 (.479)	1.181 (.523)	2.262 (1.003)	N.S.
x 10^{-2} emu	2.150 2.150 2.150	2.150±.000 (1.000±.000	511	1.265 (.588)	.919 (.427)	2.184 (1.016)	S.
	2.212 ——— 2.175	2.194±.019 (1.000±.009)	516	1.275 (.581)	.888 (.405)	2.163 (.986)	S.
4	.894 .894 .881	.890±.006 (1.000±.007)	426	.3220 (.362)	.5725 (.643)	.894 (1.004)	N.S.
x 10^{-2} emu	.900 .900 .900	.900±.000 (1.000±.000)	485	.6800 .756	.2390 (.266)	.919 (1.021)	S.
	.888 ——— .875	.882±.007 (1.000±.008	493	.7700 (.873)	.1050 (.119)	.8750 (.992)	N.S.

TABLE 6
(cont'd)

THE ADDITIVITY OF PTRM

Sample; Magnet. Multp.	$TRM(T_C,T_R)$ h=.467 oe	$<TRM>$ ±σ	T_I,°C	$PTRM_1$	$PTRM_2$	$\Sigma PTRM$	Sig. Diff.
5	2.475 ——— 2.512	2.494±.019 (1.000±.008	468	.4350 (.174)	2.050 (.822)	2.485 (.996)	N.S.
x 10⁻² emu	2.512 ——— 2.688	2.600±.088 (1.000±.034·	490	.6825 (.262)	1.850 (.712)	2.532 (.974)	N.S.
	2.700 2.750 2.800	2.750±.041 (1.000±.015)	512	1.650 (.600)	1.094 (.398)	2.744 (.998)	N.S.
6	1.156 ——— 1.188	1.172±016 (1.000±014)	493	.2688 (.229)	.944 (.805)	1.213 (1.035)	S.
x 10⁻² emu	1.250 1.260 1.298	1.269±.021 (1.000±.017)	512	.5700 (.449)	.7400 (.583)	1.310 (1.032)	S.
	1.150 ——— 1.262	1.206±.056 (1.000±.046)	517	.6575 (.545)	.5825 (.483)	1.238 (1.027)	N.S.
7	1.394 ——— 1.375	1.384±.010 (1.000±.007	493	.1125 (.0813)	1.269 (.917)	1.381 (.998)	N.S.
x 10⁻¹ emu	1.310 1.300 1.331	1.314±.013 (1.000±.010)	512	.4950 (.377)	.7750 (.590)	1.270 (.967)	S
	1.369 ——— 1.400	1.384±.016 (1.000±.012)	517	.5410 (.391)	.906 (.655)	1.447 (1.046)	S
8	1.025 1.031 1.031	1.029±.003 (1.000±.003)	426	.5350 (.520)	.4925 (.479)	1.028 (.999)	N.S.
x 10⁻² emu	1.056 1.055 1.050	1.054±.003 (1.000±.003)	485	.8375 (.795)	.2300 (.218)	1.068 (1.013)	S
	1.119 ——— 1.088	1.104±.016 (1.000±.014)	493	.994 (.900)	.1131 (.102)	1.107 (1.003)	N.S.
	1.081 ——— 1.069	1.075±.006 (1.000±.006)	517	1.055 (.981)	.01875 (.0174)	1.074 (.999)	N.S.

TABLE 6
(cont'd)

THE ADDITIVITY OF PTRM

Sample; Magnet. Multp.	TRM(T_C,T_R) h = .467 oe	<TRM> ±σ	T_I, °C	PTRM$_1$	PTRM$_2$	ΣPTRM	Sig. Diff.
9	.956 ——— .944	.950±.006 (1.000±.006)	468	.5550 (.584)	.3900 (.411)	.945 (.995)	N.S.
x 10^{-2} emu	.938 .925 .938	.934±.006 (1.000±.006)	485	.6575 (.704)	.2920 (.313)	.9495 (1.017)	S.
	.938 ——— .925	.932±.007 (1.000±.008)	490	.6675 (.716)	.2800 (.300)	.9475 (1.017)	S.
10	2.762 2.775 2.775	2.771±.006 (1.000±.002)	447	.7225 (.261)	2.100 (.758)	2.822 (1.018)	S.
x 10^{-4} emu	2.762 ——— 2.775	2.768±.006 (1.000±.002)	501	-1.344 (.486)	-1.469 (.531)	2.813 (1.016)	S.
	2.712 2.710 2.700	2.707±.005 (1.000±.002)	520	-1.875 (.693)	-.919 (.339)	2.794 (1.032)	S.
	2.720 ——— 2.712	2.716±.004 (1.000±.002)	525	1.869 (.688)	.931 (.343)	2.800 (1.031)	S.
11	2.912 ——— 2.925	2.918±.007 (1.000±.002)	468	.3487 (.110)	2.625 (.900)	2.974 (1.019)	S.
x 10^{-2} emu	2.950 ——— 3.250	3.100±.150 (1.000±.048)	490	.5775 (.186)	2.325 (.750)	2.903 (.936)	S.
	3.075 2.962 3.062	3.033±.050 (1.000±.016)	511	.950 (.313)	2.125 (.701)	3.075 (1.014)	N.S.

observed between the mean TRM and the ΣPTRM. In 17 of these experiments the normalized ΣPTRM > 1, and only in 3 experiments is the normalized ΣPTRM < 1. Only for two samples (samples 2 and 10) is there a 'significant difference' for all the experiments. For both of these samples all experiments have ΣPTRM > 1. Wherever a 'significant difference' is observed it varies from unity by an average of 2 to 3 percent. The results of these experiments show that, statistically, regardless of 'domainness' and particle size,

22.
$$\Sigma \ PTRM(T_j, T_i, h) \geqslant TRM(T_C, T_R, h)$$
$$T_i \leqslant T_j \leqslant T_o$$
$$T_R \leqslant T_i$$

A closer look at experiments for the individual samples reveals no grain size or 'domainness' pattern. The behavior of the large grain magnetites is statistically identical with that of the small grain magnetites. That is the degree of adherence to the additivity law does not seem to depend on the grain size and 'domainness' of the magnetite particles.

7.4 DISCUSSION

It is interesting to consider the reasons causing a substantial fraction of the experiments to deviate from the expected 'additivity' and to satisfy in inequality of equation 22.

IRM at elevated temperature, $IRM(T_I, \vec{h}_L)$, as suggested by Ozima and Ozima (1965) and by Dunlop and West (1969), is a possible mechanism, adding remanence in the proper direction. In addition, high temperature viscous remanent magnetization, $VRM(T_I, \vec{h}_L)$, is another possible mechanism behaving similarly to the IRM. VRM implies the presence of an external field for

an extended time interval, while IRM suggests that the magnetization process is of short duration. We arbitrarily define the transition from IRM to VRM as t = 60 sec. That is, particles which become magnetized along $\vec{h}_L$ during the first 60 sec. of the field's application are designated as IRM. Magnetization acquired by grains after exposure to an external field for longer than 60 sec. is defined as VRM. At this point it should be recalled that both IRM and VRM are measured after the external field has been removed. In chapter 6 we presented and discussed the temperature dependence of various hysteresis properties of Columbian Carbon magnetite, which is the magnetite powder of samples 6 and 7. In table 7 some of the relevant hysteresis parameters are listed for both the diluted (i) and undiluted (ii) powders at temperatures near T_I.

TABLE 7

HYSTERESIS PROPERTIES OF COLUMBIAN CARBON MAGNETITE
AS A FUNCTION OF TEMPERATURE

T(°C)	425°		492°		535°	
	i	ii	i	ii	i	ii
H_C(oe)	48	45	33	32	19	19
H_{CR}(oe)	147	140	111	102	75	62
J_{RS}/J_S T	.094	.090	.082	.08	.070	.066
$J_{RS}(T)/J_{RS}(T_R)$	.43	.45	.30	.33	.19	.20

The data in table 7 show that even at 535°C, which is higher than any of the values for T_I, $h_L << H_C$; thus isothermal magnetization in 0.5 oe, even at that temperature, is probably almost entirely in the reversible region, which becomes more true as the temperature drops and the hysteresis loop expands. Assuming that the results for the Columbian Carbon magnetite are typical for the remaining powders, we are tempted to conclude that in our experiments high temperatures IRM could account for only a small fraction of the observed increase in the remanence which averages between 2 and 3 percent. Of course, for higher inducing fields the IRM effect becomes more important. VRM is similar to IRM but its magnetization is due to grains of higher relaxation times such that its contribution to the remanence at T_I may be as important or more important the the IRM, depending upon the duration of the sample's exposure to external fields. As with IRM, the VRM effect becomes more important for increasing fields.

In addition to the IRM and VRM discussed above, the experimental procedure used to test the additivity law is such that a component of magnetization with blocking temperatures above T_I is induced at T_I and is measured as part of both PTRM$_1$ and PTRM$_2$. In step b of the experimental procedure particles with blocking temperatures $T_I < T_B < T_C$ are demagnetized. The field is turned on at T_I and grains with $T_R < T_B < T_I$ acquire remanence upon cooling. $\vec{h}_L$ is turned on approximately 5 to 10 minutes before cooling from T_I to T_R and is kept on until just before the remanence is measured. It seems, therefore, that the demagnetized region with blocking temperatures $T_I < T_B < T_C$ is highly susceptible to induced magnetization as h_L is turned on at T_I. This induced magnetization becomes more stable upon cooling and part of it contributes to the PTRM measured at T_R. Therefore, some

particles with $T_I < T_B < T_C$ contribute to $PTRM_1(T_C, T_I, NULL; T_I, T_R, \vec{h}_L)$. It is apparent that these grains will again be statistically aligned parallel to $\vec{h}_L$ as $PTRM_2(T_C, T_I, \vec{h}_L; T_I, T_R, NULL)$ is induced. The contribution to the remanence of these grains will be counted twice in summing the PTRMs. The relative importance of the induced magnetization effect depends on $h_L/H_{ci}(T_I)$ of the grains with blocking temperatures $T_I < T_B < T_C$ and on their relative concentration. As with the IRM and VRM, the induced magnetization increases with increasing fields. Although it is not possible to say unambiguously which of the three mechanisms that were presented above (IRM, VRM, and induced magnetization) is dominant in our experiments, the hysteresis parameters obtained at elevated temperatures which appear in table 7 lead us to conclude that high temperature IRM is probably not the primary cause for the observed deviations from additivity. In addition, extrapolating the VRM data of Rimbert (1959) and Shimizu (1960) to external fields of the order of .5 oe applied for less than 10 minutes suggests that in our experiments the differences between IRM and VRM are small. On the other hand, it appears that in our experiments induced magnetization provides a much more likely mechanism for the observed deviations from the conditions of pure additivity.

Everitt (1961,1962) and Dunlop and West (1969) thermally demagnetized partial-TRMs given over narrow temperature intervals (T_2, T_1, with $T_C > T_2 > T_1$), and they observed a 'tail' in the magnetization remaining above T_2. It is possible that these 'tails' are due to high temperature induced magnetization in grains whose blocking temperatures are between T_2 and T_C, which were originally blocked with random magnetic orientations at $T > T_2$. This hypothesis is supported by the fact that the 'tails' are relatively

more sustantial the more intense the inducing field.

7.5 CONCLUSIONS

We have demonstrated experimentally in this chapter that, statisti
cally, $\Sigma PTRM > TRM(T_C, T_R)$. Deviations from additivity have been explained
primarily in terms of high temperature induced magnetization. In the limit
of small fields, h, and short exposure times, t, additivity is obeyed.

23.
$$\lim_{\substack{h \to 0 \\ t \to 0}} \Sigma PTRM = TRM(T_C, T_R)$$

It is seen that the tendency to deviate from linearity is true to the
same degree and to the same extent for all samples, regardless of their
mean particle size. In the limit where equation 23 applies, it appears
that the additivity law is obeyed similarly by multidomain as by single
domain magnetites, as anticipated by Néel (1955) and Stacey (1963).

Looking ahead to their behavior in intensity studies, it appears that,
from the point of view of the additivity law, multidomain magnetites can be
used in intensity studies with the same expectations as single domain
magnetites.

CHAPTER 8

THE USE OF MAGNETITES FOR PALEOINTENSITY DETERMINATIONS

8.1 SUMMARY

In this chapter the 'Thellier method' for paleointensity determinations is applied to the prepared magnetite samples, each containing different size particles spanning the gamut from single domain to multidomain, and to several rock specimens. The following are the principal findings:

(1) When a large fraction of the remanence resides in multidomain particles, non-linear (concave up) P'NRM'-PTRM curves are observed such that a linear approximation to the lower blocking temperature data leads to apparent paleointensities that are higher than the actual paleofield. However, the ratio of the end points, 'NRM'/ TRM, yields the corect (laboratory) intensity.

(2) Two mechanisms are developed to explain the observed non-linear behavior; one uses Néel's equations for single domain particles, and the other approach discusses the P'NRM'-PTRM behavior in a two-domain grain separated by 180° wall.

(3) There is a positive correlation between ideal behavior in the Thellier sense and high thermal and A. F. stability.

(4) Paleointensity determinations should be based on data spanning the sample's entire blocking temperature range, and, wherever, non-ideal behavior is observed, further tests should be conducted to determine its cause.

8.2 BACKGROUND

That TRM is linearly proportional to the external field, $\vec{h}$, for small values of $\vec{h}$, say $\vec{h} < 1$ oe, was demonstrated by Thellier (1938) for baked

earths, Nagata (1943) for igneous rocks, and Roquet (1954) for dispersed

magnetite and hematite powders. Assuming that we are in this so-called

'linear region' of the TRM, then

$$\vec{J}_{TRM} = \chi_{TRM}\vec{h},$$

where χ_{TRM} is the TRM susceptibility. It becomes possible to determine the

intensity of the magnetic field in which this TRM was acquired by merely

heating it above its Curie point and cooling it in the presence of a known

field, $\vec{h}_L$. One then has:

24.
$$\frac{J_{NRM}}{J_{TRM}} = \frac{h}{h_L}$$

where $\vec{h}$, the field responsible for the NRM, is the one unknown. The assump-

tions made in obtaining h are:

(1) $\vec{J}_{NRM}$ is a TRM with negligible secondary components of magneti-

zation;

(2) both $\vec{h}$ and $\vec{h}_L$ are in the 'linear region' of the TRM;

(3) $\vec{J}_{TRM}$ and $\vec{J}_{NRM}$ are independent of the cooling rate;

(4) the sample demagnetizing field due to its surroundings (such as

remainder of the lave flow) has a negligible effect on the

induced remanence; and

(5) $\chi_{NRM} = \chi_{TRM}$. This is synonymous with saying that, when the sample

is heated above T_C, it undergoes no chemical or physical changes

that alter in any way its TRM acquisition properties.

The existence of a 'linear region' for TRMs induced in small fields

may have been known much earlier than the above-cited references suggest.

According to Thellier and Thellier (1959), Folgheraiter (1899) tried to

obtain values for the intensity of the earth's magnetic field in the

historical past by comparing NRMs and laboratory TRMs of ancient vases of known ages. Repeated TRMs, however, were not self consistent. Thus no reliable comparisons could be made between the ancient field and that of the 1890s.

Direct observations of the geomagnetic field for the last few centuries, and geomagnetic intensity determinations of archeomagnetic sites (Smith, 1967), and the large majority of the available data of paleomagnetic intensities in the geologic past (Smith, 1967) suggest that the earth's magnetic intensity is usually substantially less than 1 oersted. It therefore appears that the TRM of most samples used in paleomagnetism is in its 'linear region'. Thus the second assumption is usually obeyed, and, if there is a suspicion that it is not, linearity can be tested experimentally (assuming the validity of assumption 5), and the intensity determination duly corrected, Coe (1967).

The original remanence in igneous rocks and baked clays, bricks, and kilns is TRM, but depending on the samples' rock type, their chemistry, their ages, and their field environments, the original TRM may have been modulated by secondary magnetizations such as viscous remanence, VRM, (or spontaneous decay) and/or by chemical remanence, CRM. Some rocks are struck by lightning and some pick up secondary magnetizations between sampling and measuring. Some rocks are subjected to partial reheating to $T < T_C$ and cooling to T_R in a field different from that inducing the original NRM.

To minimize the secondary components in samples to be used for intensity studies the specimens should be chemically unaltered, and the sample magnetization should undergo no significant change upon storage test. For rapidly chilled volcanic rocks, where cooling is of the order of a few hours to a few days, the original TRM (NRM) usually records a single value of the

geomagnetic field (direction and intensity). Therefore, the directions of magnetization in samples of the same lava flow, for example, should record the same field, and the only variations should be due to sampling uncertainties and the presence of surface magnetic anomalies, such that only a small uncertainty should be associated with the samples' mean direction. Large scatter in the directions usually suggests the presence of unwanted secondary components of magnetization. Hence the samples should be chosen from sites whose mean direction is determined with high precision, and the individual samples should have their magnetization vectors close to the site mean values. For intrusive igneous rocks, whose cooling may span a much greater time interval than for extrusive volcanic rocks, scatter in the magnetic directions may reflect actual variations in the geomagnetic field, and the requirement of small scatter in the directions may be too restrictive and should be deemphasized. When a sample is chosen for intensity studies, it is assumed that the first assumption is obeyed.

We are not familiar with any conclusive results on the effects of the rate of cooling on the acquisition of TRM. In our experiments the normal cooling rate near the blocking temperatures is of the order of 3°C/min. In order to test the effects of the rate of cooling on TRM acquisition we quenched the samples in air, thus increasing the cooling rate by at most a factor of two. To prolong cooling we introduced a temperature step at about 525°C, but it is difficult to estimate the resultant effect on the cooling rate. The TRM values did not exhibit a pattern that could be attributed to changes in the cooling rate. Although more controlled experiments are needed, we shall assume that TRM is unaffected by cooling rates less than 5°C/min.

Coe (1973) considered the effect of changes in the sample's environment on the paleomagnetic measurements, by causing a change in the

demagnetizing field acting on the sample. In his calculation Coe considers
the effect of removing a spherical sample from a horizontal lava flow of
infinite extent. He finds that "errors in the estimated paleointensity of
up to 5 percent may be caused by shape anisotropy in specimens which acquire
a total TRM of 0.01 emu/cc in an applied field of 0.5 oe." Since most sub-
aerial igneous rocks acquire a total TRM of less than 0.01 emu/cc in a 0.5 oe
field, the shape demagnetizing factor will little affect intensity determina-
tions in such rocks. Indeed, we are not aware of any paleointensity deter-
minations where the adverse effects of shape anisotropy were unambiguously
demonstrated.

Probably the most common source of adverse effects on paleointensity
determinations is caused by irreversible alterations in the sample's TRM
upon heating in the laboratory (Thellier and Thellier, 1959; Coe, 1967a,b).
Such alterations irreversibly affect the TRM capacity of the magnetic
minerals and their blocking temperatures. These changes usually become
more pronounced with increasing temperature. Often, however, most of the
mineralogical and chemical alterations of the specimen occur upon the first
heating to above T_C, while on subsequent heatings only minor changes occur,
such that a second heating to above T_C to test the consistency and relia-
bility of the result of the first heating may detect only small variations
in the TRM crowning the result with deceptive confidence.

8.3 THE 'THELLIER METHOD'

The 'Thellier method' for paleointensity determination substitutes
several heating steps between T_R and T_C for the single heating above T_C
used for the intensity determination in equation 24. In addition to the
assumptions listed in connection with intensity determinations using
equation 24, the 'Thellier method' rests on the observation that PTRMs

acquired over different temperature intervals are independent and additive. Therefore, if the total TRM is in the 'linear region', then the PTRMs are also linearly proportional to the inducing field. For a given sample, then, the PNRM and PTRM acquired over a particular temperature interval are directly proportional to the inducing fields.

25.
$$\frac{PNRM\ (T_2,\ T_1,\ \vec{h})}{PTRM\ (T_2\ T_1,\ \vec{h}_L)} = \frac{h}{h_L}$$

where T_2, T_1 denote the temperature interval; $\vec{h}_L$ and $\vec{h}$ are the laboratory and unknown fields, respectively. As a sample with NRM is heated to a temperature, T, with $T_R < T < T_C$, the <u>ratio</u> of the PNRM lost upon heating to T in null field <u>to</u> the PTRM acquired by cooling the sample through the identical temperature interval in a known field, h_L, equals the <u>ratio</u> of the ancient. unknown field, h, <u>to</u> that of h_L. This process is repeated at successively higher temperatures until all blocking temperatures are exceeded. The data thus generated consists of PTRM and PNRM pairs between T_R and temperature T, spanning the interval T_R to T_C. Ideal behavior in the Thellier sense implies that equation 25 is obeyed for each temperature interval, $T < T_C$, thus each PNRM-PTRM pair should yield the same h/h_L ratio. The data can be presented graphically by plotting the PNRM versus PTRM for the different temperature steps. This representation was first suggested by Arai (1963; in Coe, 1967) and was first published by Nagata et al. (1963). The initial point is (NRM, PTRM = 0) and the final point is (NRM = 0, TRM); see figures 26-35. Ideally behaving data will be linear connecting initial and final points having a slope of h/h_L. Deviations from linearity suggest that at least one of enumerated assumptions has not been fulfilled, and such deviations have been extensively discussed and analyzed by Coe (1967 a, b).

The chief advantage of the 'Thellier method' is the self consistency checks offered by the various PNRM-PTRM pairs as the sample is gradually heated to its Curie point, and systematic deviations with increasing temperature can be readily recognized. To test for irreversible changes in the sample's TRM capacity, Thellier and Thellier (1959) suggest that, after a PNRM-PTRM pair is obtained at a given temperature, PTRM acquisition at lower temperature intervals should be repeated. As was pointed out by Coe (1967a, b), this test only recognizes changes that occur to regions with blocking temperatures less than T, while possible irreversible alterations to regions of higher blocking temperatures go undetected. Coe and Grommé (1974) studied historical lavas that erupted in known fields, and they show that irreversible TRM changes occur at higher temperatures and irreversibly affect the PNRM-PTRM curves, whereas the lower temperature data provide a good approximation to the unknown field.

8.4 EXPERIMENTAL RESULTS AND DISCUSSION

In our experiments the 'Thellier method' was applied to prepared samples of previously characterized magnetite particles. Since the NRM was a laboratory TRM, assumptions 1 to 4 are immediately satisfied. In addition, we tried to minimize irreversible changes in the TRM properties of the samples by prior stabilization of the samples' magnetic properties and by always trying to heat the samples in a slightly reducing chemical environment (see chapter 3). Our experiments should thus test how different types of magnetite behave in a 'Thellier experiment'.

The 'Thellier method' has been executed three different ways: in the first which is described and used by Thellier and Thellier (1959) and by Kono and Nagata (1968) the sample is always heated in the local geomagnetic field.

(a)   the NRM is measured at T_R.

(b)   the sample is first heated to $T > T_R$ and cooled back to T_R in the
      continuous presence of $\vec{h}_L$; the magnetization is measured at T_R.

(c)   the sample is then carefully rotated 180° about a horizontal axis
      perpendicular to the local geomagnetic meridian.

(d)   The sample is reheated to the same $T > T_R$ and cooled back to T_R
      in the continuous presence of $\vec{h}_L$; the magnetization is measured
      at T_R.

Half the sum of the magnetization vectors obtained after steps (b) and (d)
represents the PNRM remaining after heating to temperature T. Half the
difference of the magnetization vectors obtained in steps (b) and (d)
represents the PTRM acquired between T and T_R. Steps (b), (c), and (d)
are repeated at successively higher temperatures until all the blocking
temperatures are exceeded.

Coe (1967 a, b) and Coe and Grommé (1974) execute a slightly modified
'Thellier method'.

(a)   The NRM is measured at T_R.

(b)   The sample is heated to $T > T_R$ and cooled back to T_R in zero field,
      and the magnetization is measured at T_R representing the PNRM
      acquired between T_C and T.

(c)   The sample is reheated to $T > T_R$ and cooled back to T_R in $\vec{h}_L$, which
      is continuously present throughout the heating and cooling cycle.
      The magnetization is measured at T_R to obtain the PTRM acquired
      between T and T_R.

Steps (b) and (c) are repeated at successively higher temperatures until all
blocking temperatures are exceeded.

A further modification to the above version of the 'Thellier method'

has been used: in order to avoid high temperature VRM, $\vec{h}_L$ in step (c) above is not turned on until just prior to cooling.

Represented in figures 26 to 35 are the results of the three versions of the 'Thellier method' for the prepared samples 2 to 11. Three groups of data are plotted. The upper data correspond to the Thellier and Thellier (1959) version of the 'Thellier method', where both heatings are conducted in the laboratory field and the samples are reoriented between the two heatings; the middle data correspond to the Coe (1967 a, b) version of the 'Thellier method', where the sample orientation is maintained throughout, the first heating is in zero field, and in the second heating the field is on throughout the entire heating; and the bottom sets of data correspond to the 'modified Coe' version, where during the second heating the field is turned on only for the cooling branch. The data is always normalized with respect to the 'NRM'. $\vec{h}_L$ is always between .46 oe and .49 oe, and it is known to better than $\pm$ .5%. In the Coe version of the 'Thellier method' the zero field in which the samples are heated is nulled to within 50γ of zero in the region of the experiment. Although the field associated with some of the more strongly magnetized samples distorts the 'zero' field, many experiments were performed in which the strongly magnetized samples are removed, included, or have their orientation changed to assess the influence of the distorted 'zero' field. No measurable effect was ever present. It seems that in our experiments and with our samples the condition to be satisfied is that $h(residue)/h_L \ll 1$, whereas the absolute zeroing of the field is secondary. The numbers associated with the PNRM-PTRM points correspond to the temperature in °C. The reproducibility of the temperature for a particular position in the oven for the various paired heatings is thought to be within $\pm$ 3°C. This uncertainty is estimated

Figure 26

P'NRM'-PTRM data for sample 2, normalized.

      ●   The Thellier and Thellier version of Thelliers' method.

□,■   The 'Coe' version of Thelliers' method.

▽,▲   The 'modified Coe' version of Thelliers' method.

See text for further explanation.

The numbers in the figure correspond to temperature steps in ^{o}C. The

The lines in the figure represent 'ideal' behavior expected if

equation 25 is satisfied exactly. (Sometimes the lines are drawn to

connect the initial and final data points.)

$$J_{TRM} = 1.4 \times 10^{-4} \text{ emu/gm} \quad \text{for } h_L = .47 \text{ oe.}$$

Note that each of the three sets of data has its own origin and

abscissa.

SAMPLE 2

Figure 27

P'NRM'-PTRM data for sample 3, normalized.

● The Thellier and Thellier version of Thelliers' method.

□,■ The 'Coe' version of Thelliers' method.

△,▲ The 'modified Coe' version of Thelliers' method.

See text for further explanation.

The numbers in the figure correspond to temperature steps in ^{o}C.

The lines in the figure represent 'ideal' behavior expected if

equation 25 is satisfied exactly. (Sometimes the lines are drawn to

connect the initial and final data points.)

$$J_{TRM} = 1.3 \times 10^{-3} \text{ emu/gm} \quad \text{for } h_{L} = .47 \text{ oe.}$$

Note that each of the three sets of data has its own origin and

abscissa.

SAMPLE   3

$\Delta J_{NRM} (T) / J_{NRM}$

$\Delta J_{TRM} (T) / J_{NRM}$

Figure 28

P'NRM'-PTRM data for sample 4, normalized.

●　　　The Thellier and Thellier version of Thelliers' method.

□, ■　The 'Coe' version of Thelliers' method.

△, ▲　The 'modified Coe' version of Thelliers' method.

See text for further explanation.

The numbers in the figure correspond to temperature steps in ^{o}C.

The lines in the figure represent 'ideal' behavior expected if

equation 25 is satisfied exactly. (Sometimes the lines are drawn to

connect the initial and final data points.)

$$J_{TRM} = 5.7 \times 10^{-4} \text{ emu/gm} \quad \text{for } h_L = .47 \text{ emu.}$$

Note that each of the three sets of data has its own origin and

abscissa.

SAMPLE 4

Figure 29

P'NRM'-PTRM data for sample 5, normalized.

    ●   The Thellier and Thellier version of Thelliers' method.

    ■,□   The 'Coe' version of Thelliers' method.

    ▲,△   The 'modified Coe' version of Thelliers' method.

See text for further explanation.

The numbers in the figure correspond to temperature steps in ^{o}C.

The lines in the figure represent 'ideal' behavior expected if

equation 25 is satisfied exactly. (Sometimes the lines are drawn to

connect the initial and final data points.)

$$J_{TRM} = 1.8 \times 10^{-3} \text{ emu/gm} \quad \text{for } h_{L} = .47 \text{ oe.}$$

Note that each of the three sets of data has its own origin and
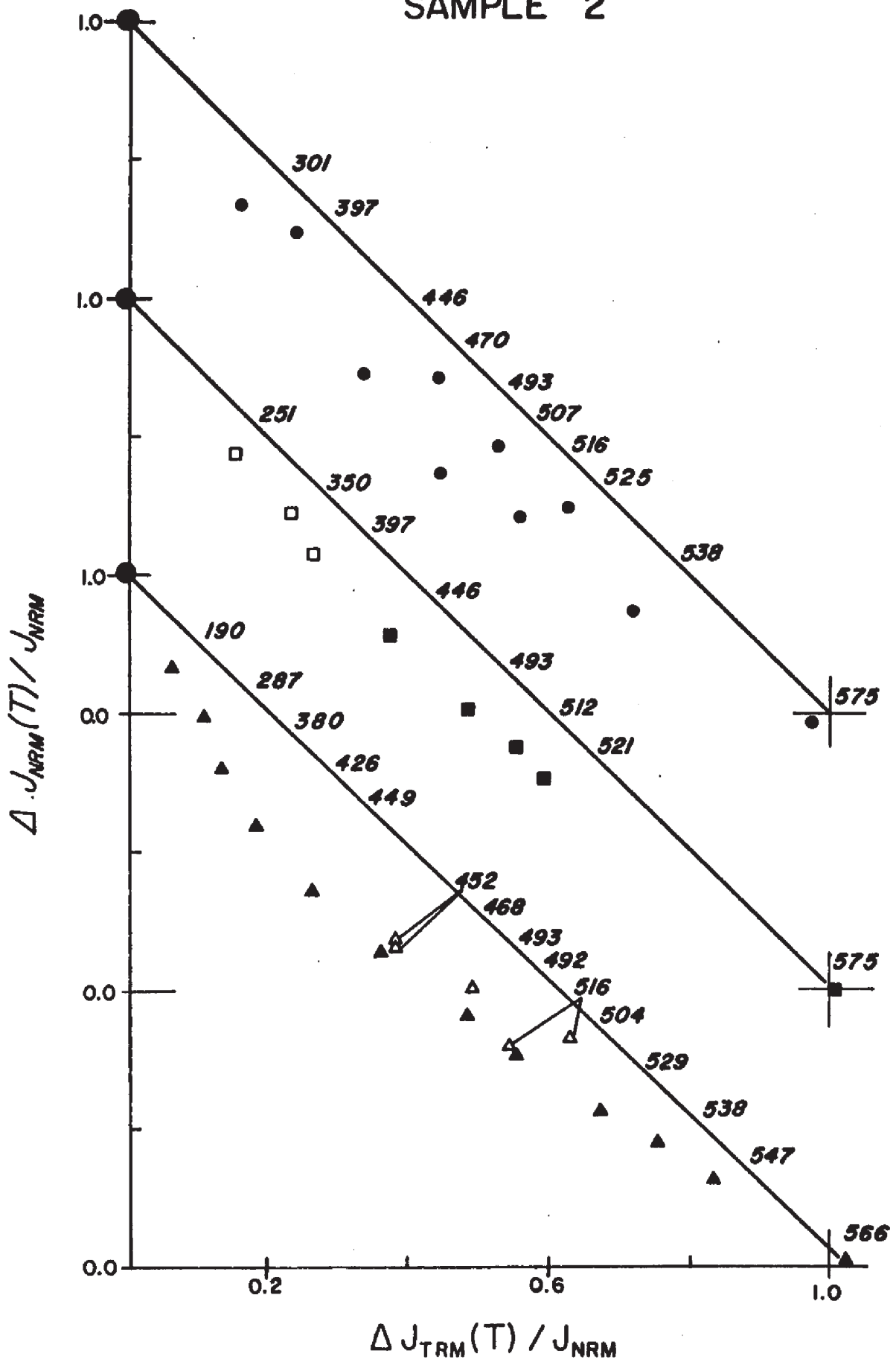
abscissa.

SAMPLE 5

Figure 30

P'NRM'-PTRM data for sample 6, normalized.

●   The Thellier and Thellier version of Thelliers' method.

□,■   The 'Coe' version of Thelliers' method.

△,▲   The 'modified Coe' version of Thelliers' method.

See text for further explanation.

The numbers in the figure correspond to temperature steps in $^{\circ}$C.

The lines in the figure represent 'ideal' behavior expected if

equation 25 is satisfied exactly. (Sometimes the lines are drawn to

connect the initial and final data points.)

$$J_{TRM} = 7.3 \times 10^{-4} \text{ emu/gm} \quad \text{for } h_L = .47 \text{ oe.}$$

Note that each of the three sets of data has its own origin and

abscissa.

SAMPLE 6
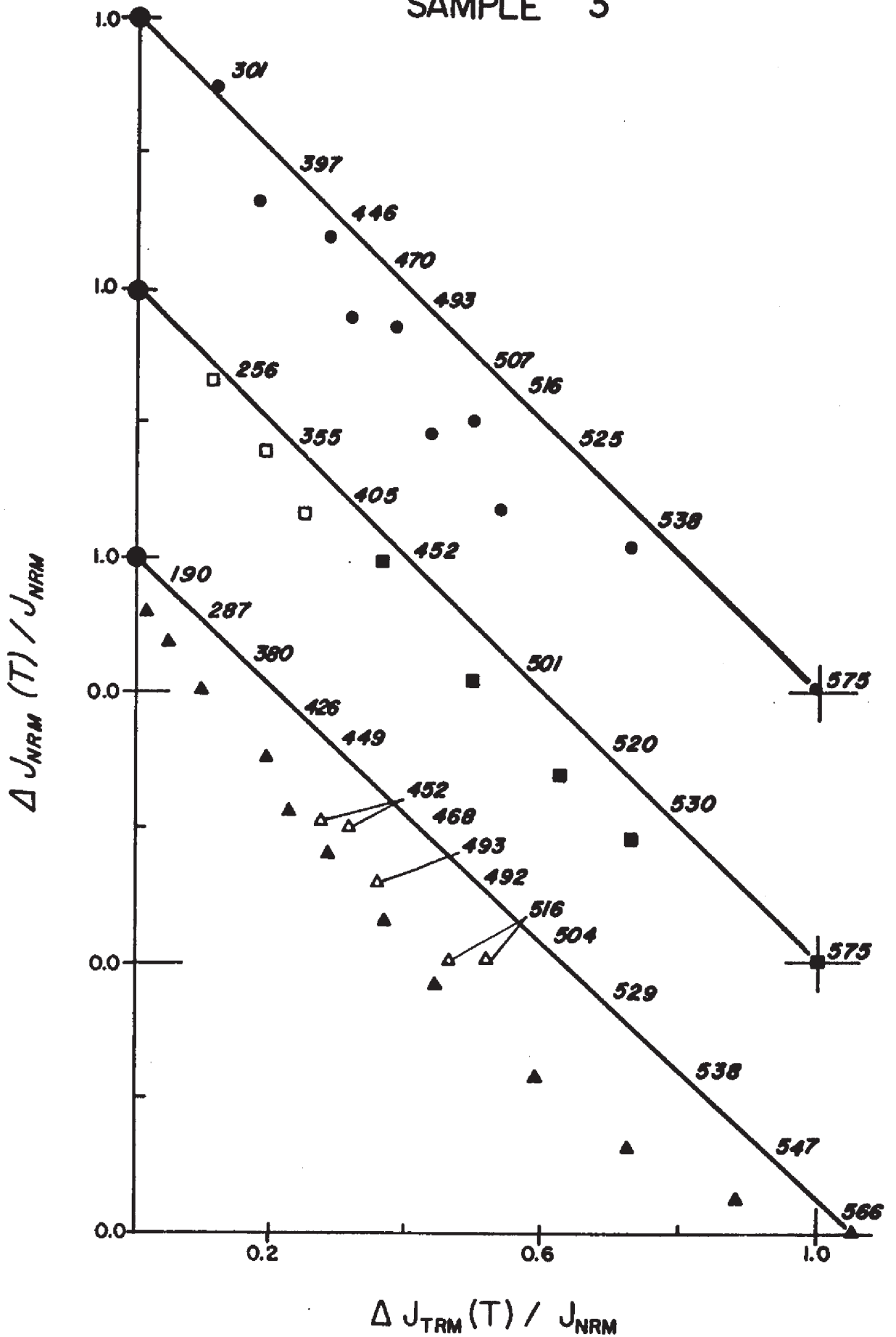
Figure 31

P'NRM'-PTRM data for sample 7, normalized.

●   The Thellier and Thellier version of Thelliers' method.

□ , ■   The 'Coe' version of Thelliers' method.

△ , ▲   The 'modified Coe' version of Thelliers' method.

See text for further explanation.

The numbers in the figure correspond to temperature steps in ^{o}C.

The lines in the figure represent 'ideal' behavior expected if

equation 25 is satisfied exactly. (Sometimes the lines are drawn to

connect the initial and final data points.)

$$J_{TRM} = 7.7 \times 10^{-3} \text{ emu/gm} \quad \text{for } h_L = .47 \text{ oe.}$$

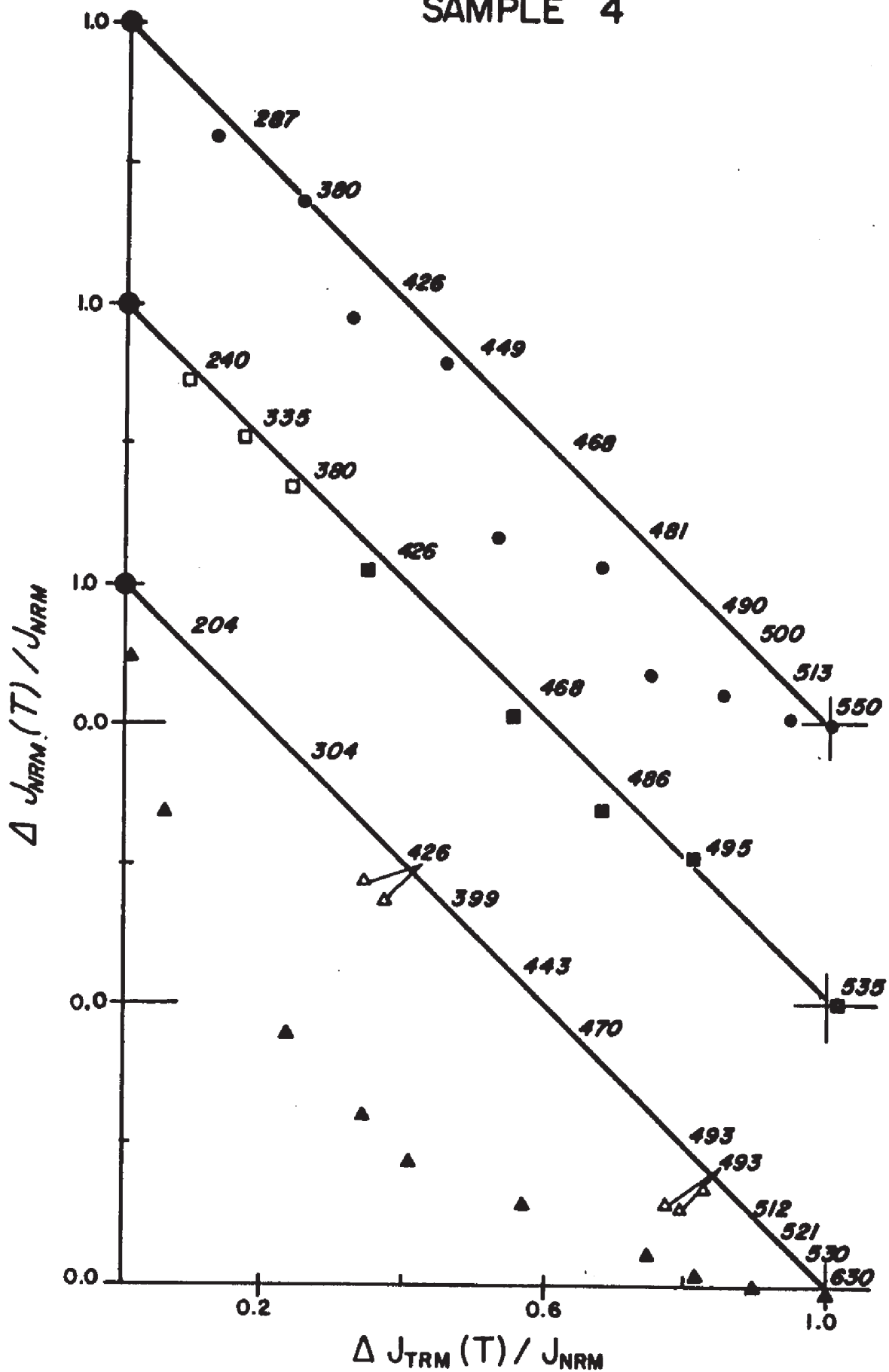Note that each of the three sets of data has its own origin and

abscissa.

SAMPLE 7

Figure 32

P'NRM'-PTRM data for sample 8, normalized.

● The Thellier and Thellier version of Thelliers' method.

□,■ The 'Coe' version of Thelliers' method.

△,▲ The 'modified Coe' version of Thelliers' method.

See text for further explanation.

The numbers in the figures correspond to temperature steps in ^{o}C.

The lines in the figure represent 'ideal' behavior expected if

equation 25 is satisfied exactly. (Sometimes the lines are drawn to

connect the initial and final data points.)

$$J_{TRM} = 7.1 \times 10^{-4} \text{ emu/gm} \quad \text{for } h_L = .47 \text{ oe.}$$

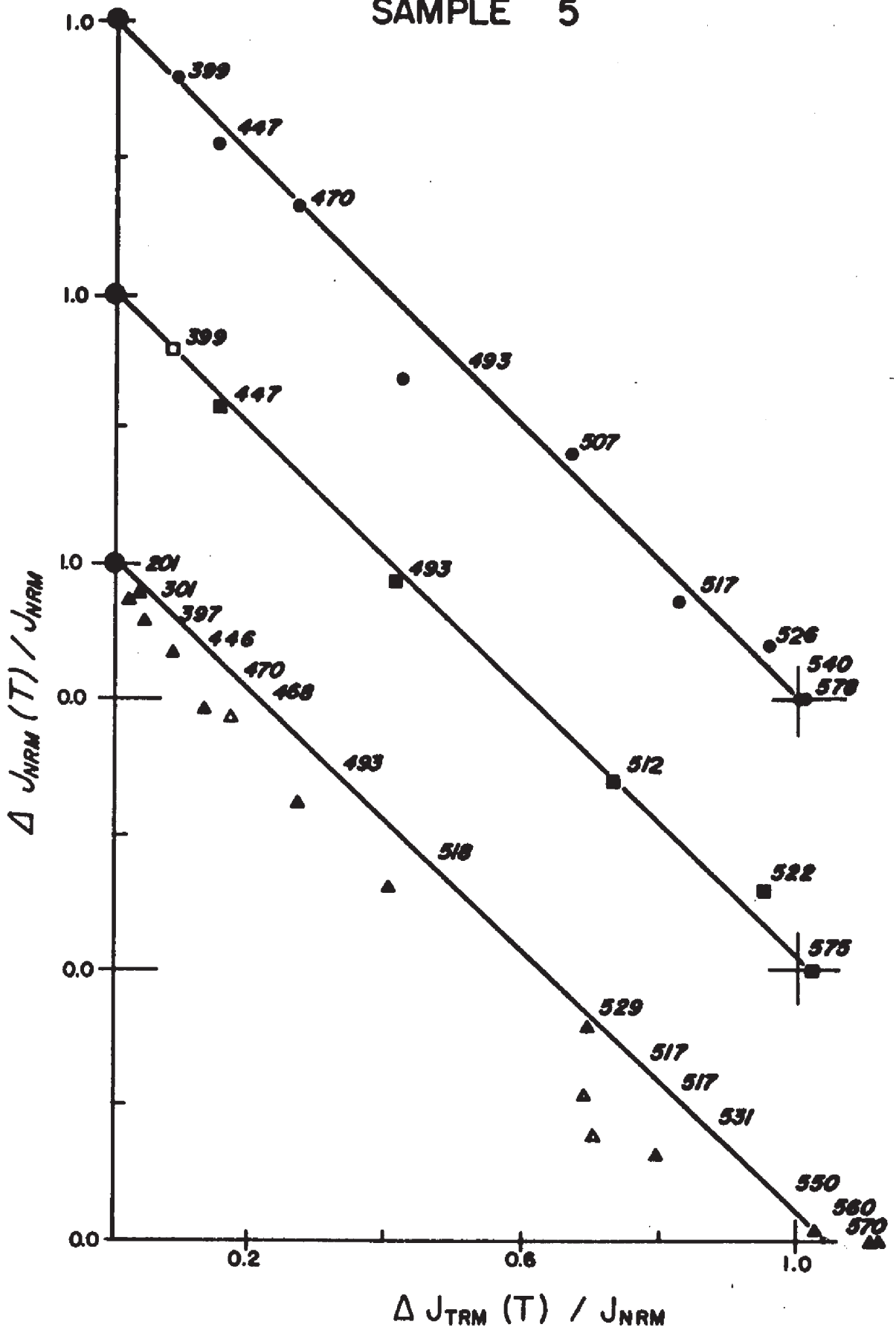Note that each of the three sets of data has its own origin and

abscissa.

SAMPLE 8

Figure 33

P'NRM-PTRM data for sample 9, normalized.

      ●   The Thellier and Thellier version of Thelliers' method.

   □ , ■   The 'Coe' version of Thelliers' method.

   △ , ▲   The 'modified Coe' version of Thelliers' method.

See text for further explanation.

The numbers in the figures correspond to temperature steps in ^{o}C.

The lines in the figure represent 'ideal' behavior expected if

equation 25 is satisfied exactly. (Sometimes the lines are drawn to

connect the initial and final data points.)

$$J_{TRM} = 6.6 \times 10^{-4} \text{ emu/gm} \quad \text{for } h_L = .47 \text{ oe.}$$

Note that each of the three sets of data has its own origin and
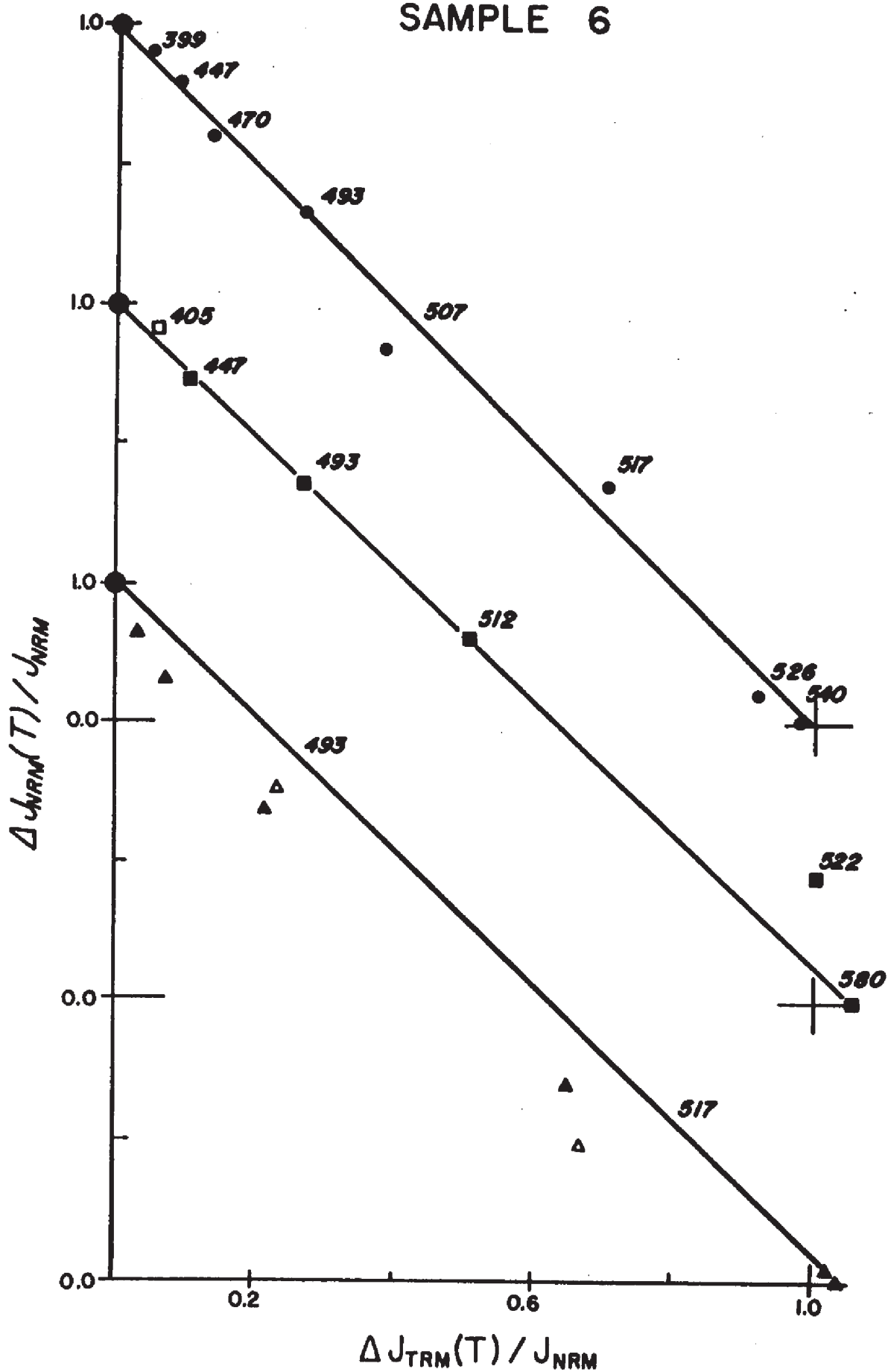
abscissa.

SAMPLE 9
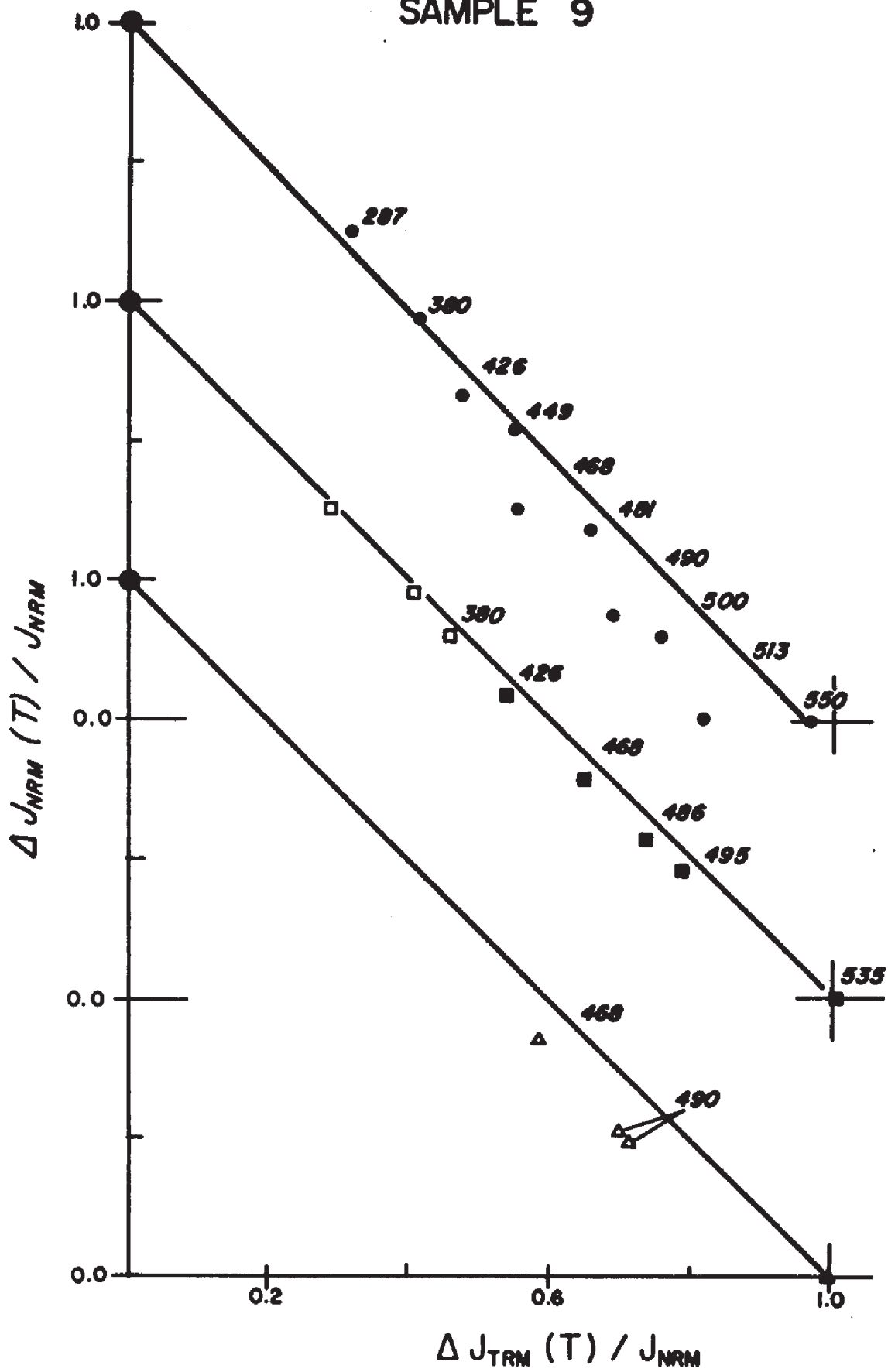
Figure 34

P'NRM'-PTRM data for sample 10, normalized.

●   The Thellier and Thellier version of Thelliers' method.

□ , ■   The 'Coe' version of Thelliers' method.

△ , ▲   The 'modified Coe' version of Thelliers' method.

See text for further explanation.

The numbers in the figures correspond to temperature steps in ^{O}C.

The lines in the figure represent 'ideal' behavior expected if

equation 25 is satisfied exactly. (Sometimes the lines are drawn to

connect the initial and final data points.)

$$J_{TRM} = 1.6 \times 10^{-5} \text{ emu/gm} \quad \text{for } h_L = .47 \text{ oe.}$$

Note that each of the three sets of data has its own origin and
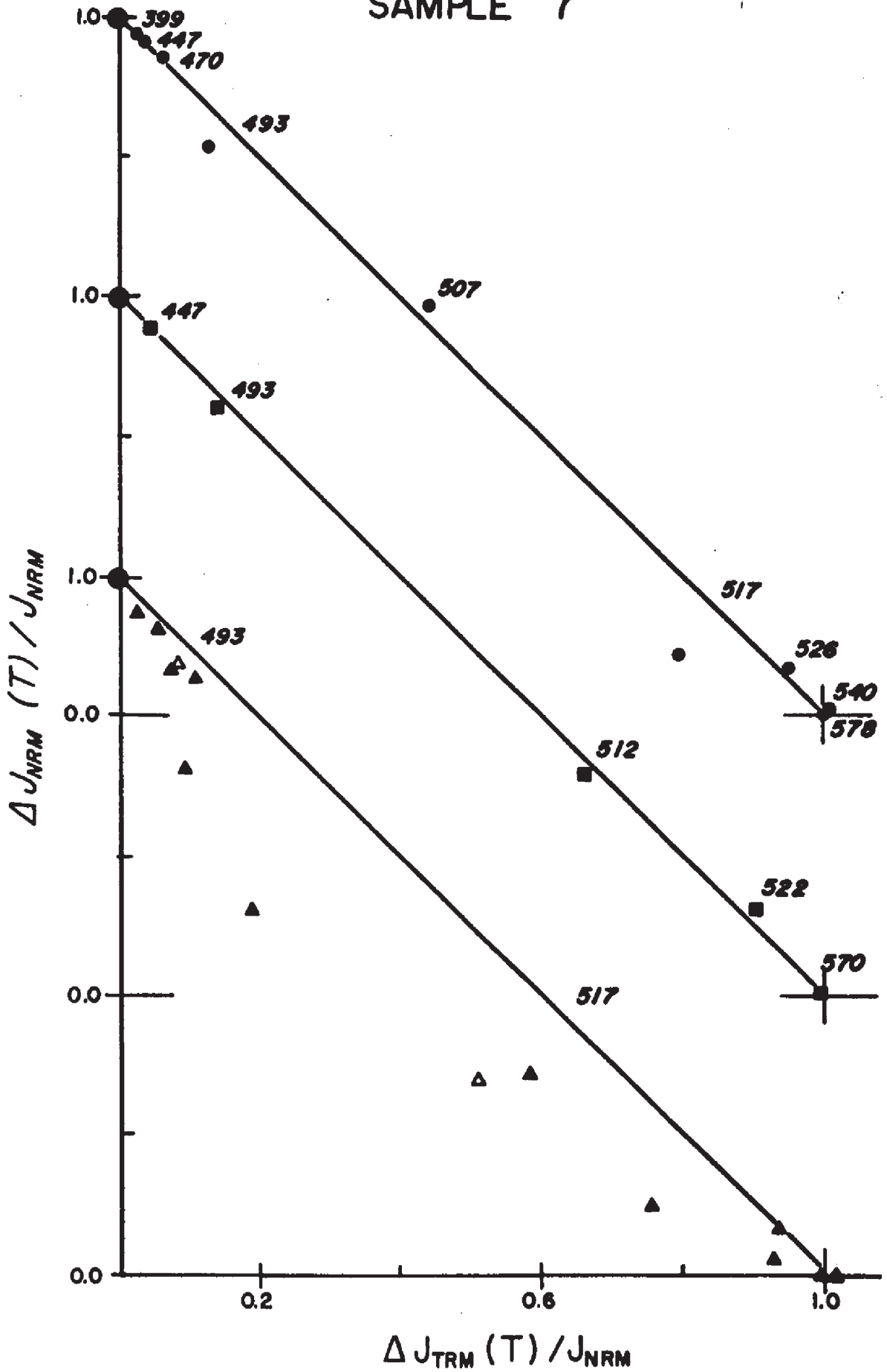
abscissa.

SAMPLE 10
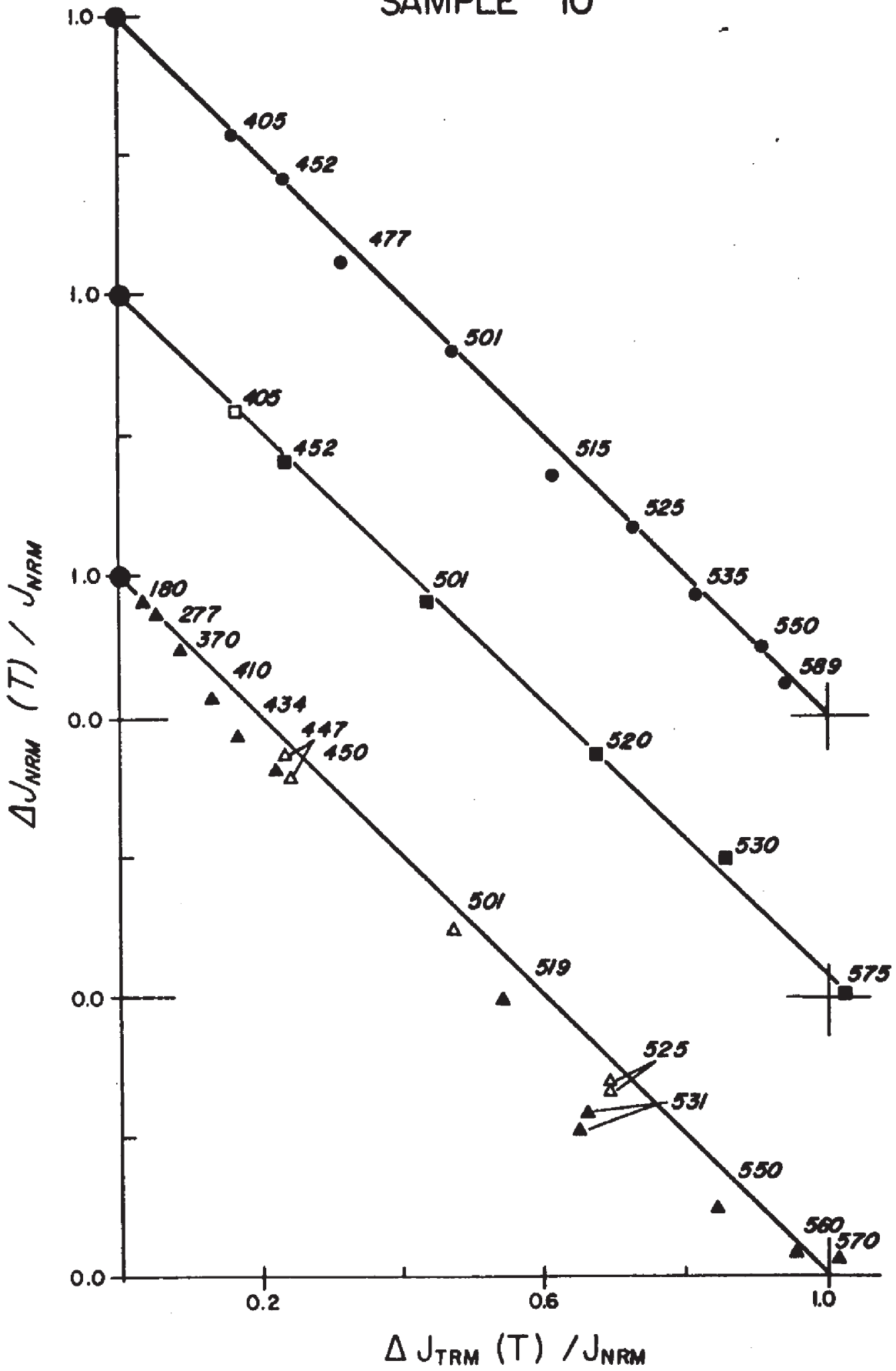
Figure 35

P'NRM'-PTRM data for sample 11, normalized.

●　　The Thellier and Thellier version of Thelliers' method.

□ , ■　The 'Coe' version of Thelliers' method.

△ , ▲　The 'modified Coe' version of Thelliers' method.

See text for further explanation.

The numbers in the figures correspond to temperature steps in $^{\circ}C$.

The lines in the figure represent 'ideal' behavior expected if

equation 25 is satisfied exactly. (Sometimes the lines are drawn to

connect the initial and final data points.)

$$J_{TRM} = 1.9 \times 10^{-3} \text{ emu/gm} \quad \text{for } h_L = .47 \text{ oe.}$$

Note that each of the three sets of data has its own origin and

abscissa.

SAMPLE II
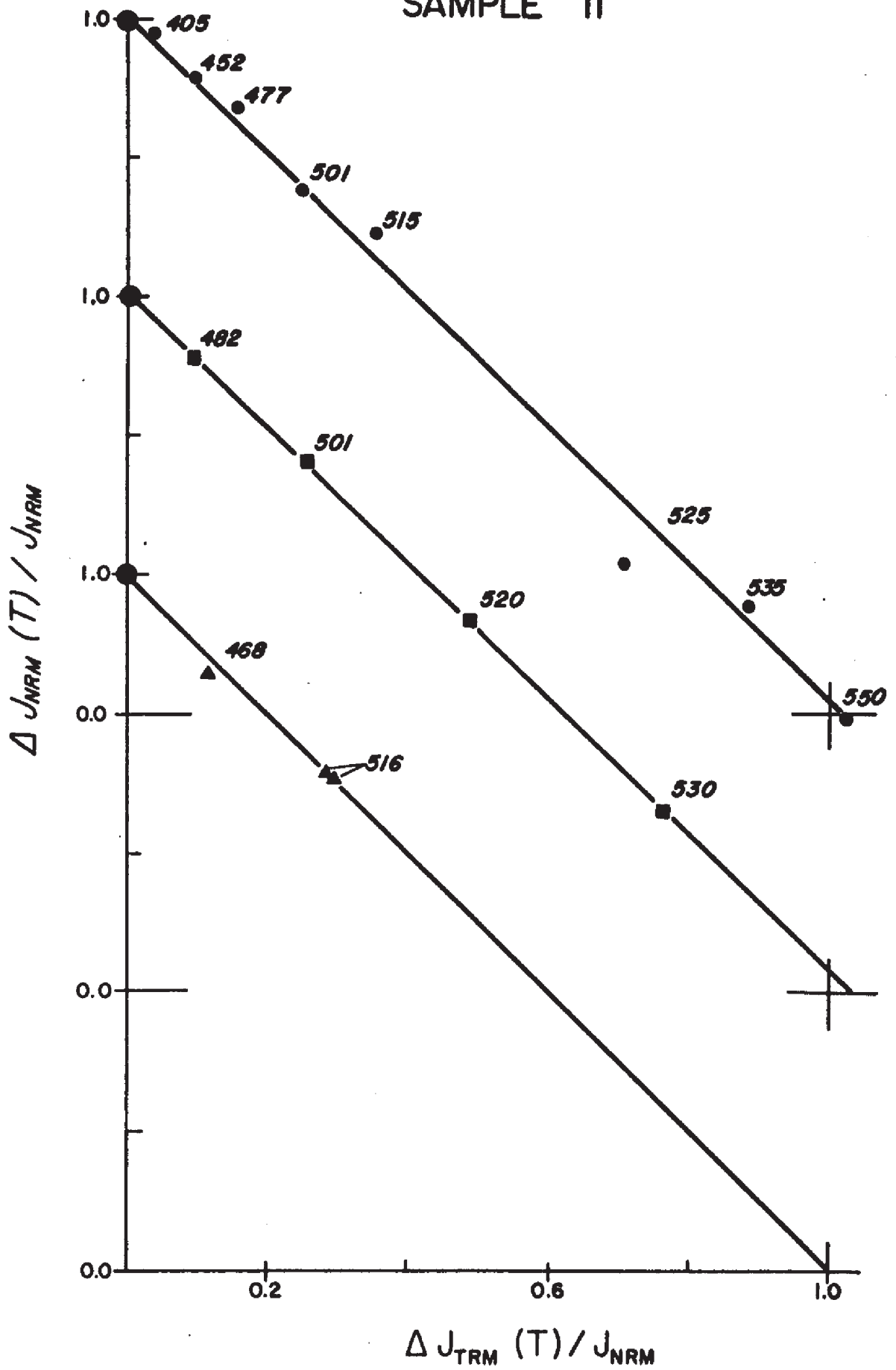
from repeated PNRM-PTRM pairs for a given temperature in figures 26 to 35 and from repeated thermal demagnetization experiments such as in figure 11. The lines usually connect the initial and final points or the points (1.0, 0) and (0, 1.0). The TRMs were always induced in a vertical field along the axes of the cylinders, so that in the Thellier and Thellier version the samples were rotated 180° about any horizontal axis. In the lower two sets of data the samples occupied identical positions and orientation during both heatings at each temperature step.

It is seen in figures 26 to 35 that for the bottom sets of data, represented by triangles and corresponding to the experiments where $\vec{h}_L$ is turned on just prior to cooling from T to T_R, the data for all but one sample lie below the line connecting initial and final points, and their shapes are concave up. For the one exception, sample 11, only three points define its behavior. It appears that while carefully avoiding high temperature VRM, we introduced excessive spontaneous decay. Even for the stable sample 10 the PNRM-PTRM curve is concave up. The degree of curvature or the high temperature spontaneous decay is not simply related to grain size or to the various stability criteria. For example, the curvature of sample 7 is at least comparable to that of sample 2. The maximum deviations from the line for the lower sets of data occur near $<T_B>$, approximately midpoint on the line; this occurs near 508°C for sample 7 and at about 450°C for sample 2. The closed triangles represent a single experiment where the temperature steps increase from T_R to T_C. The open triangles represent a single temperature experiment each.

With the possible exception of sample 11, all the PNRM-PTRM plots are non-linear, concave up. Only when high temperature spontaneous decay can be neglected will this particular experimental procedure yield linear plots.

The middle sets of data were obtained using Coe's version of the 'Thellier method', that is, h_L is active throughout the entire heating and cooling cycle, $T_R \rightarrow T \rightarrow T_R$. In other words, h_L is active at elevated temperatures for the same length of time as was the null field of the previous step. It is seen that the curvature is decreased for all samples. Samples 5, 6, 7, 10, and 11 are linear for all practical purposes throughout their entire spectra of blocking temperatures. For these samples the high temperature VRM precisely nulls the high temperature spontaneous decay of the previous step. In figures 28, 29, 30 for samples 5, 6, and 7 the PNRM-PTRM point at 522°C is consistently above the line for all three samples. This behavior is probably due to a temperature discrepancy in the paired heatings. The phenomenon could be explained if during the thermal demagnetization the temperature was somewhat lower than during the PTRM heating. This explanation is favored over one that invokes chemical change, because the samples occupied adjacent positions in the oven during the heatings such that the similarity in their behavior follows naturally out of the temperature discrepancy explanation. The PNRM-PTRM plots of samples 2, 3, and 4 are still concave up, the curvature decreasing with decreasing mean magnetite particle size from sample 2 to 4. The ratio of initial to final points, however, is within 2% of unity. For samples 8 and 9 the data sag below the line just slightly at higher blocking temperatures. A line through all but the final point, that of the total TRM, has a slope of -1.03 for sample 8 and -1.04 for sample 9. This compares with slopes of -.996 and -.994 for the line connecting the initial and final points, NRM/TRM, of samples 8 and 9, respectively. The open and closed squares represent data obtained in two separate experiments.

The upper sets of data correspond to the Thellier and Thellier version

of the 'Thellier method'. The data for samples 5, 6, 7, 10 and 11 zig-zag
about the line connecting the initial and final points. The zig-zag or
step-like appearance of the data is a result of temperature gradients in
the oven and our particular experimental procedure: If for a given tempera-
ture step $\vec{h}_L$ is parallel (antiparallel) to the remanence during the first
heating, then during the next temperature step $\vec{h}_L$ is antiparallel (parallel)
to the remanence. The data for samples 2, 3, 4, 8, and 9 forms a zig-zag
about an imaginary curve that is concave up. The zig-zag of the data is
much more step-like for these samples because in their position in the
oven the thermal gradients are more pronounced than in the positions of
samples 5, 6, 7, 10, and 11. For more elaborate description of the oven's
thermal environment and temperature gradients, turn to Appendix B-2.
Despite the presence in our oven of thermal gradients, the data of the
Thellier and Thellier version contain essentially the same features as
the data obtained using the Coe version of the 'Thellier method'. In the
case of negligible thermal gradients, the data obtained from the above
two versions of the 'Thellier method' should become increasingly similar.
This statement is supported by the increased similarity of the upper
two sets of data for samples 5, 6, 7, 10, 11 which occupied the oven
positions of minimum temperature gradients. In our subsequent discussion
we shall focus our attention to the middle sets of data obtained using
the Coe version of the 'Thellier method'.

Figures 26 to 35 show that samples 5, 6, 7, 10, and 11 behave ideally
in the Thellier sense, having essentially linear PNRM-PTRM curves. The
average diameter of the magnetite particles in these samples is less than
.25 μm, and the samples possess high stabilities against A. F. demagnet-
ization, $\tilde{H}_{\frac{1}{2}}$ > 340 oe and mean blocking temperatures near or above $500^{\circ}C$,
$<T_B> > 493^{\circ}C$.

The remaining samples display varying degrees of non-ideal behavior, which is always concave up with respect to the line connecting initial and final points. For samples 2, 3, and 4, which contain progressively smaller particles originating from the same parent magnetite crystal, the deviation from linearity diminishes with decreasing particle size. $\tilde{H}_{\frac{1}{2}}$ values for samples 2, 3, and 4 are 77 oe, 138 oe, and 380 oe, respectively, and their values for $<T_B>$ are 475°C, 493°C, and 444 °C, respectively. It seems that the deviation from linearity of samples 2, 3, and 4 is more closely related to their A. F. demagnetization stabilities: increase in non-linearity with decreases in $\tilde{H}_{\frac{1}{2}}$. It is interesting to note that $\tilde{H}_{\frac{1}{2}}$ of sample 4 is higher than that of samples 5, 6, and 7, although its $<T_B>$ is at least 50°C lower. That is, the degree of non-linearity cannot be ascertained from $\tilde{H}_{\frac{1}{2}}$ alone. Samples 8 and 9 display a slight degree of non-linearity. Their values for $\tilde{H}_{\frac{1}{2}}$ are 295 oe and 300 oe, respectively, and their values for $<T_B>$ are 400°C and 418°C, respectively. Both their $\tilde{H}_{\frac{1}{2}}$ and $<T_B>$ values are substantially and consistently lower than the corresponding values for samples 5, 6, 7, 10, and 11.

Non-linear behavior similar to that observed in the prepared samples is also observed in some extrusive igneous rock samples. In particular, we studied a young lava flow on Pagan Island in the northern Mariana Arc, whose mean magnetic direction had high precision parameters with a cone of confidence whose half angle, $\alpha_{95} = 5.95°$. PNRM-PTRM curves of three NRM bearing samples of this lava flow were obtained by H. Kinoshita (1973; private communications). It is not known which version of the "Thellier method' was used in his experiments, however, all three PNRM-PTRM curves are very similar to one another. They are all non-linear and their

Figure 36

Volcanic rock specimen from Pagan Island (flow ϕ, specimen ϕ 8.1).

▲   PNRM-PTRM data (normalized) obtained by the 'modified

Coe' version of Thelliers' method.

●   P'NRM'-PTRM data (normalized) obtained by the Thellier

version of Thelliers' method.

The numbers in the figure correspond to temperature steps in $^{\circ}$C.

The lines are drawn connecting the initial and final data points.

Note that the two sets of data have separate origins and abiscissae.

PAGAN I. FLOW ∅
SAMPLE ∅ 8.1

● TRM, h_L = .465 OE
▲ NRM, h_L = .465 OE
J_{NRM} = 3.30 × 10⁻³ EMU/GM
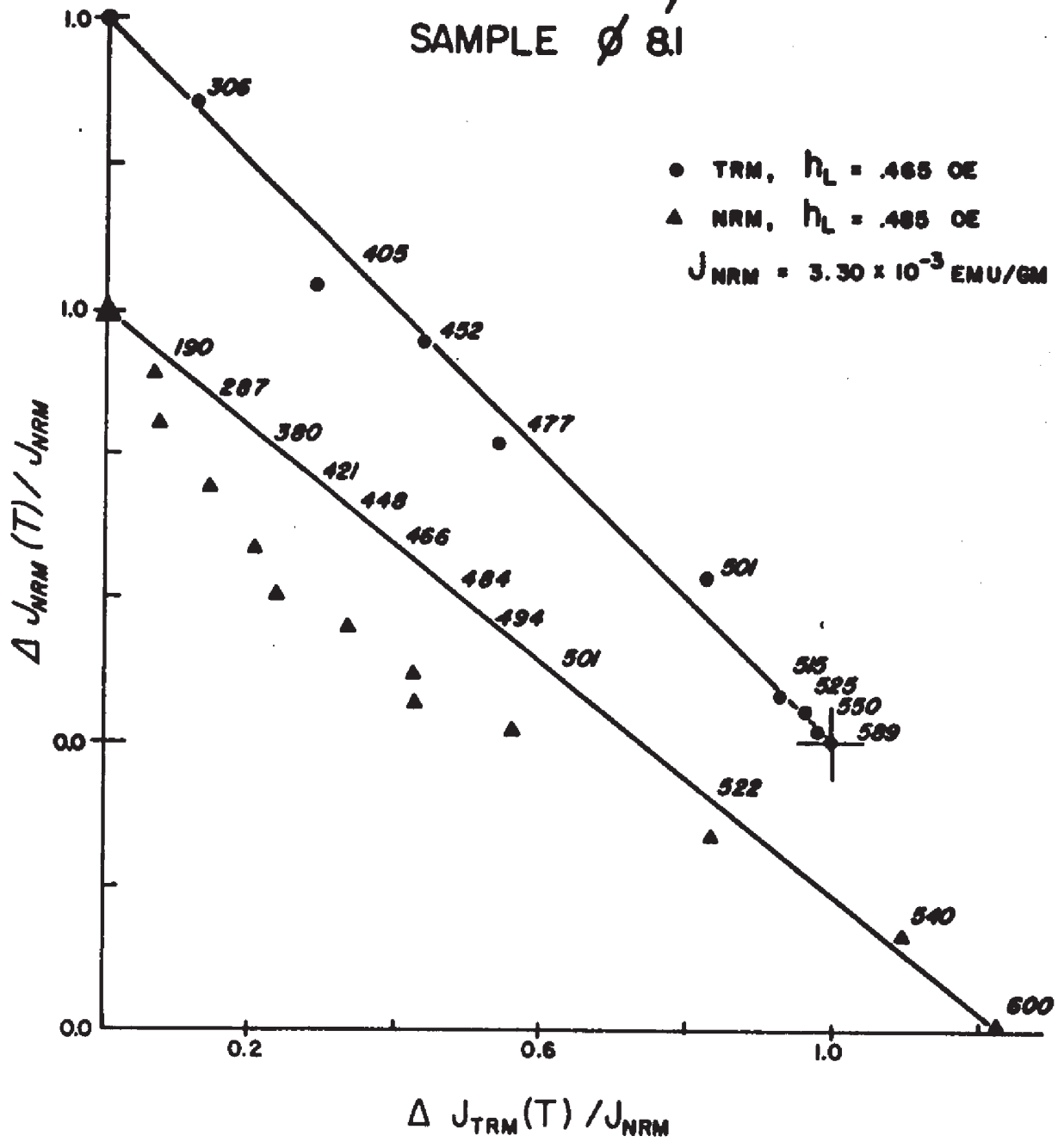
Figure 37

Volcanic rock specimen from Pagan Island (flow ϕ, speciment ϕ 1.1).

▲   P'NRM'-PTRM data (normalized) obtained by the 'modified Coe' version of Thelliers' method.

●   P'NRM'-PTRM data (normalized) obtained by the Thellier version of Thelliers' method.

The numbers in the figure correspond to temperature steps in ^{o}C.

The lines are drawn connecting the initial and final data points.

Note that the two sets of data separate origins and abiscissae.

$$J_{TRM} = 4.96 \times 10^{-3} \text{ emu/gm} \quad \text{for } h_L = .485 \text{ oe.}$$

PAGAN I. FLOW ∅
SAMPLE ∅ 1.1
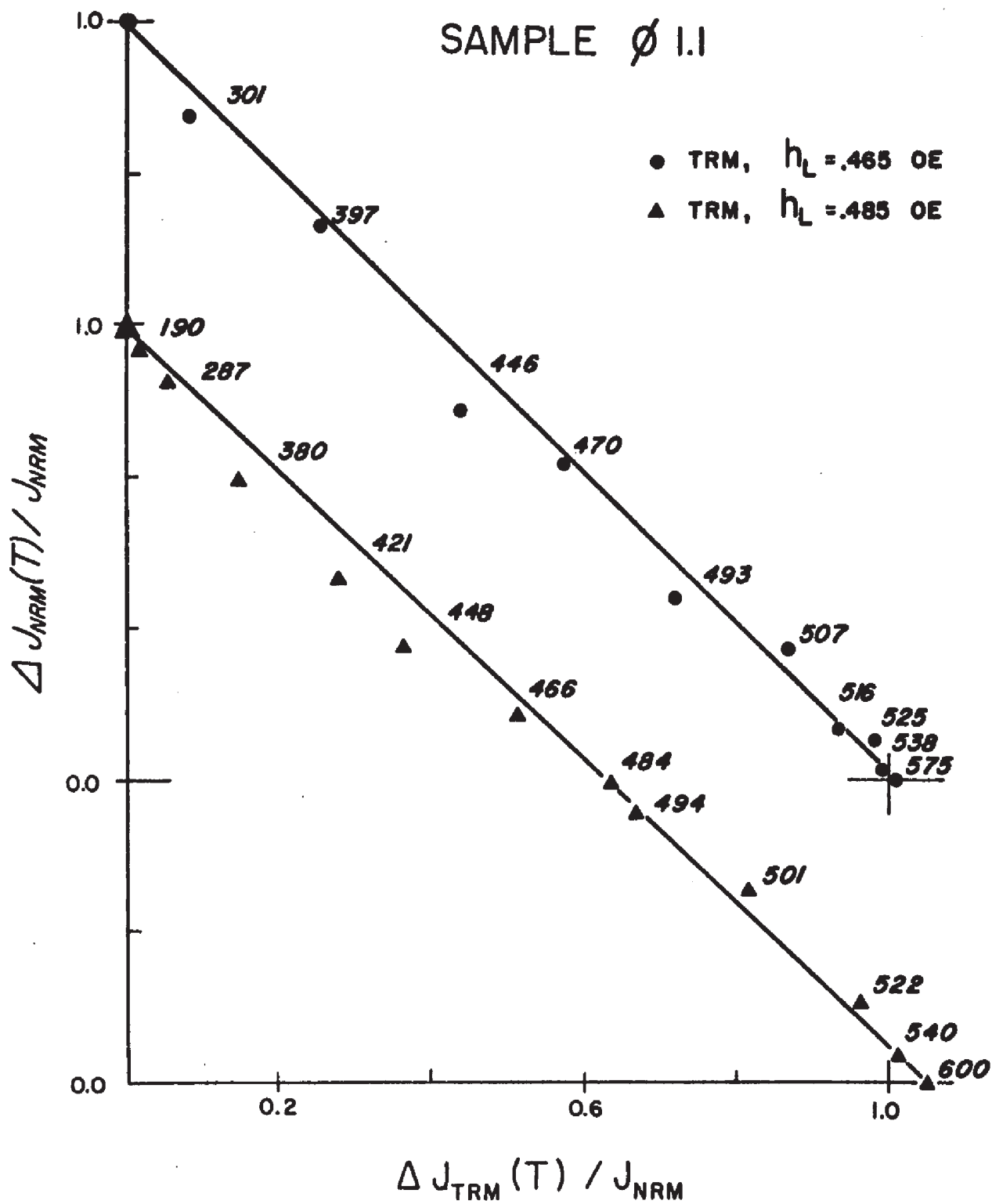
Figure 38

Strong-field magnetization versus temperature (J - T) curves for a chip from flow ϕ, Pagan Island. Both heating and cooling curves were run in a slightly reducing environment ('vacuum' with residual nitrogen gas and carbon) and in an applied field, H, of 7.3 koe. Both heating and cooling curves display a single Curie point of $525^{\circ} \pm 10^{\circ}$C.

PAGAN I. FLOW Ø

$H = 7.3$ koe

J, ARBITRARY UNITS

T, °C
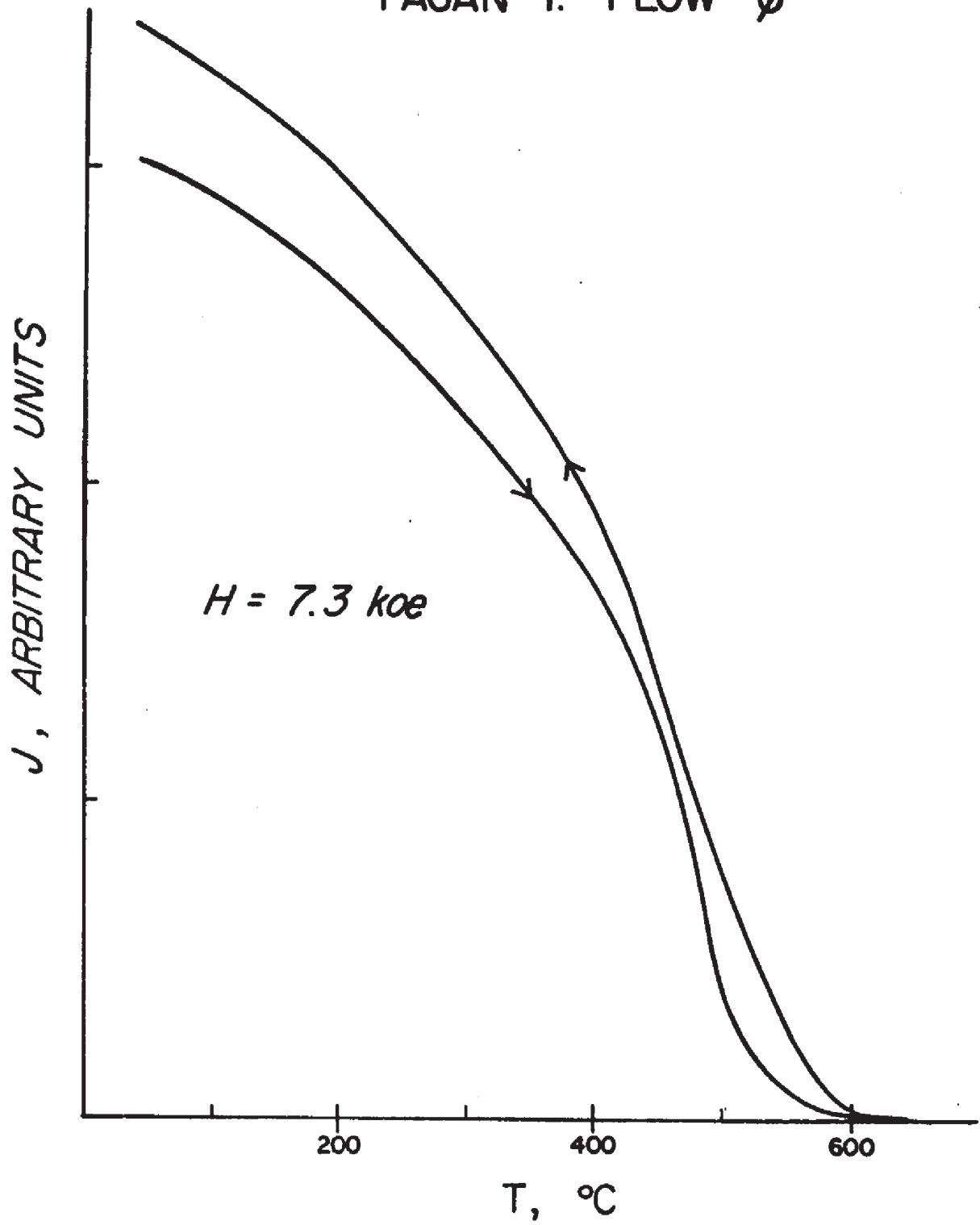
curvature is concave up. Linear approximations through the lower temperature data up to between 400° and 500° yield slopes of 1.68 and 1.79, while the ratios of initial to final points are .79 and .83, respectively, less than half the slopes of the lines through the lower temperature points. The latter values are in far better agreement with the geomagnetic intensity one would expect to be recorded in a recent flow near latitude 18°N.

In our laboratory we obtained PNRM-PTRM curves for two additional samples of this lava and the results are plotted in figures 36 and 37. The lower curves in these figures represent the 'modified Coe' version of the 'Thellier method' for the NRM of sample φ8.1 and for a laboratory TRM of sample φ1.1. The PNRM-PTRM curve of sample φ8.1 is highly non-linear. The slope of the line through the lower temperature data up to 448°C is 1.69, whereas the ratio of the initial to final points is .81; both values are in excellent agreement with Kinoshita's data. The P'NRM'-PTRM curve of sample φ1.1 is also highly non-linear. Although the degree of non-linearity is different for the two samples, the main features are similar. For sample φ1.1 the linear approximation through the lower temperature data up to 448°C yields a slope of 1.28, and the ratio of the initial to final points is .96, which is within about 4% of the known laboratory field. Thus, it appears that the non-linear behavior in these samples is intrinsic to the magnetic minerals and to the particular way in which the 'Thellier method' was carried out. The upper curves represent the Thellier and Thellier version of the 'Thellier method' for laboratory TRM of samples φ8.1 and φ1.1. It is seen that the P'NRM'-PTRM curves are very similar for both samples, displaying a slight non-linearity which is concave up. Figure 38 shows the high field magnetization versus temperature (J-T) curve, performed in a field of 7.3 koe. Oxidation was retarded by using carbon

Figure 39

Pagen Island - 1925 flow: Two samples.

▲   PNRM-PTRM data (normalized) obtained by the 'modified

Coe' version of Thelliers' method. The line is drawn

through the four highest temperature points.

$$J_{NRM} = 1.13 \times 10^{-1} \text{ emu.}$$

△   P'NRM' - PTRM data (normalized) obtained by the

'modified Coe' version of Thelliers' method. The

line is drawn connecting the initial and final

points.

$$J_{TRM} = .70 \times 10^{-1} \text{ emu} \quad \text{for } h_L = .485 \text{ oe.}$$

Note that both sets of data are set in a single coordinate system

and have a common initial point (NRM = 1; PTRM = 0).

PAGAN I. 1925 FLOW
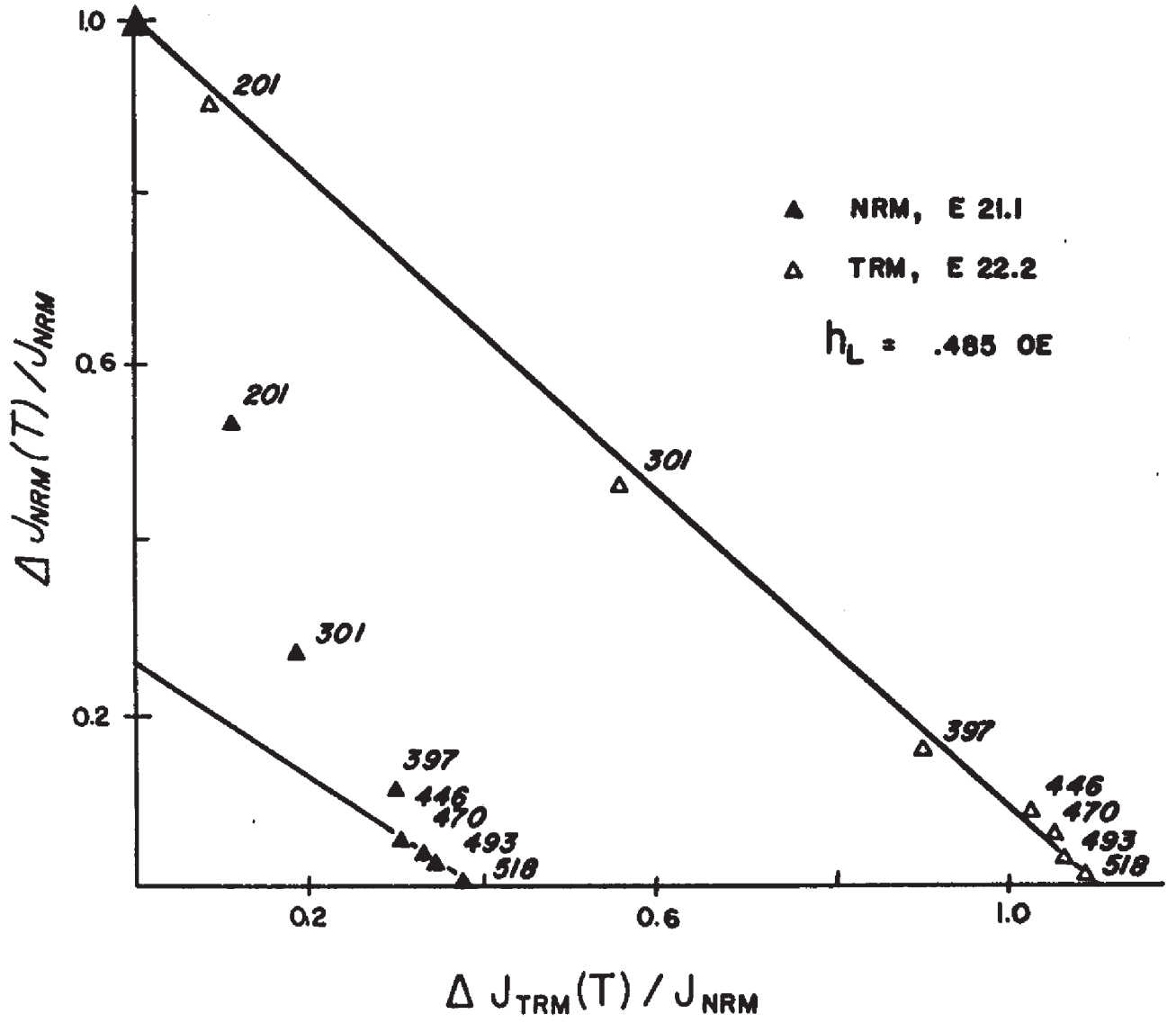
Figure 40

Strong-field magnetization versus temperature (J - T) curves for
a chip from the 1925 flow, Pagan Island. Both heating and cooling curves
were   run in a slightly reducing environment ('vacuum', with residual
nitrogen gas and carbon) and in an applied field, H, of 7.3 koe.
The curves are irreversible and both heating and cooling branches
appear to have two magnetic phases whose Curie points are:

$$T_C = 325° \pm 10°C.$$

$$T_C = 570° \pm 10°C.$$

PAGAN I.   1925 FLOW

J, ARBITRARY UNITS

H = 7.3 koe

T, °C
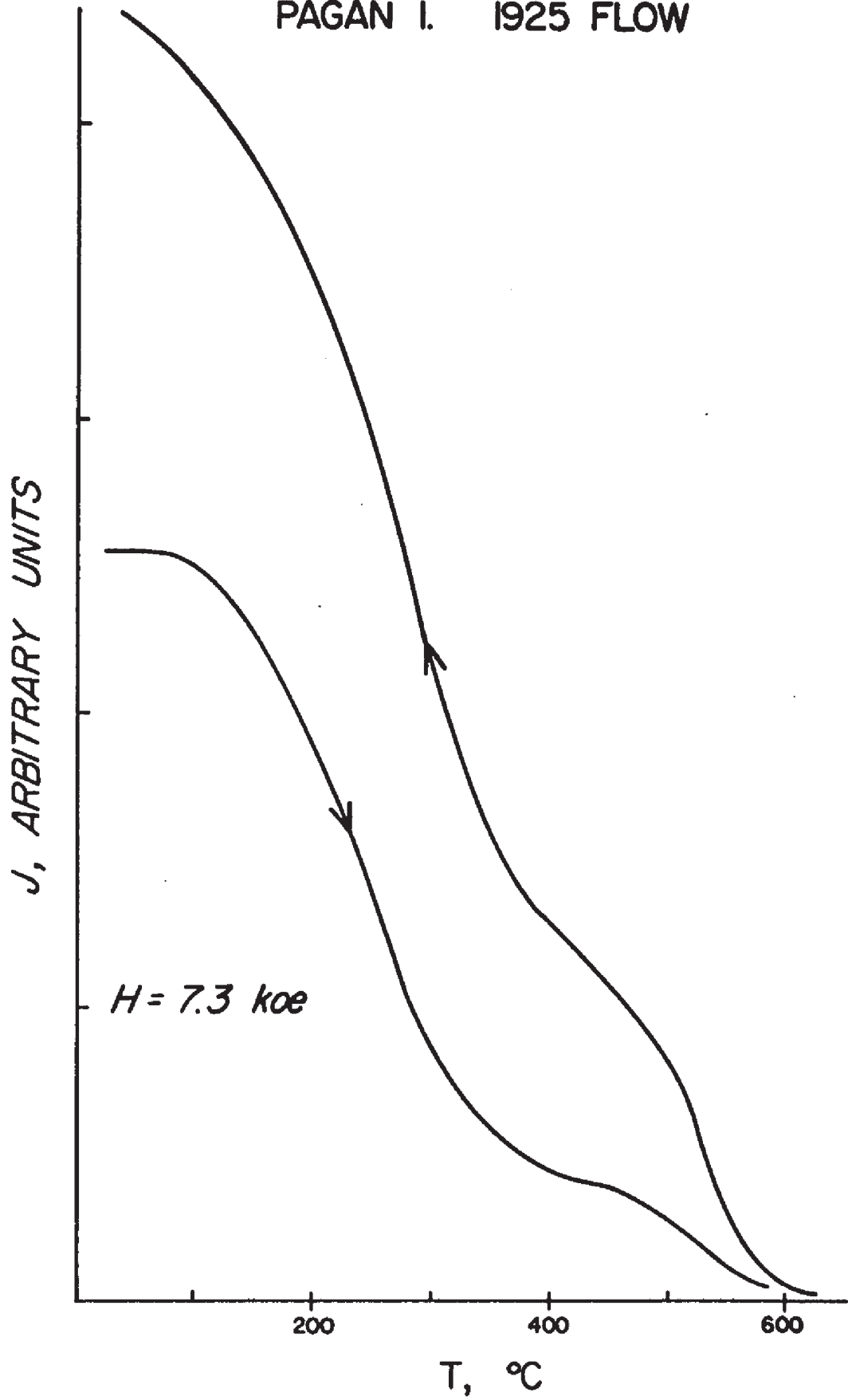
as an oxygen getter and heating under 'vacuum' in a residual nitrogen atmosphere. A single Curie point at 525°C ± 10°C is observed.

Pagan Island is also blessed with two historical lava flows which were sampled as part of another study (Levi et al. to be published). Flow H erupted in 1873 and Flow E is of 1925 vintage. The NRM directions of these flows were highly scattered and it required alternating fields of about 200 oe to sufficiently reduce the secondary components to be able to use the magnetic directions for paleomagnetic purposes. In each of figures 39 and 41 two PNRM-PTRM curves are displayed for lava flows E and H, respectively. The 'modified Coe' version of the 'Thellier method' was used. Two samples are used from each flow, one having NRM and the other a laboratory TRM. The solid and open triangles represent the NRM and TRM bearing samples, respectively. The NRM of sample E21.1 was 1.13×10^{-1} emu, and the TRM of sample E22.2 was $.70 \times 10^{-1}$ emu. The NRM of sample H4.1 was 1.87×10^{-1} emu, and the TRM of sample H3.1 was $.872 \times 10^{-1}$ emu. The TRMs of samples E22.2 and H3.1 were induced in a laboratory field of .485 oe. The NRM of samples E21.1 and H4.1 decays rapidly with temperature and the PNRM-PTRM curves are highly non-linear. For sample E21.1 the data for temperatures above 446°C form a line whose slope is about -.68. For sample H4.1 the data above 306°C form a line whose slope is about -.92. It is noteworthy also that it took higher alternating fields to demagnetize the secondary components of flow E. The P'NRM'-PTRM curves of the laboratory induced TRMs of samples E22.2 and H3.1 have display varying degrees of non-linearity of undetermined causes. There is an increase in the TRM capacity of about 10% and 12% for samples E22.2 and H3.1, respectively, suggesting that chemical and/or mineralogical changes are taking place increasing the samples' TRM capacity. This result is not surprising, in retrospect, in view of the characteristics

Figure 41

Pagan Island – 1873 flow; Two samples.

▲ PNRM-PTRM data (normalized) obtained by the 'modified Coe' version

of Thelliers' method. The line is drawn through the higher tempera-

ture points.

$$J_{NRM} = 1.87 \times 10^{-1} \text{ emu}$$

△ P'NRM'-PTRM data (normalized) obtained by the 'modified Coe' version

of Thelliers' method. The line is drawn connecting the initial and

final points.

$$J_{TRM} = .872 \times 10^{-1} \text{ emu} \qquad \text{for } h_L = .485 \text{ oe.}$$

Note that both sets of data are set in a common coordinate system and have a common

initial point (NRM = 1; PTRM = 0).

PAGAN I. 1873 FLOW

▲ NRM, H 4.1
△ TRM, H 3.1

h_L = .485 OE
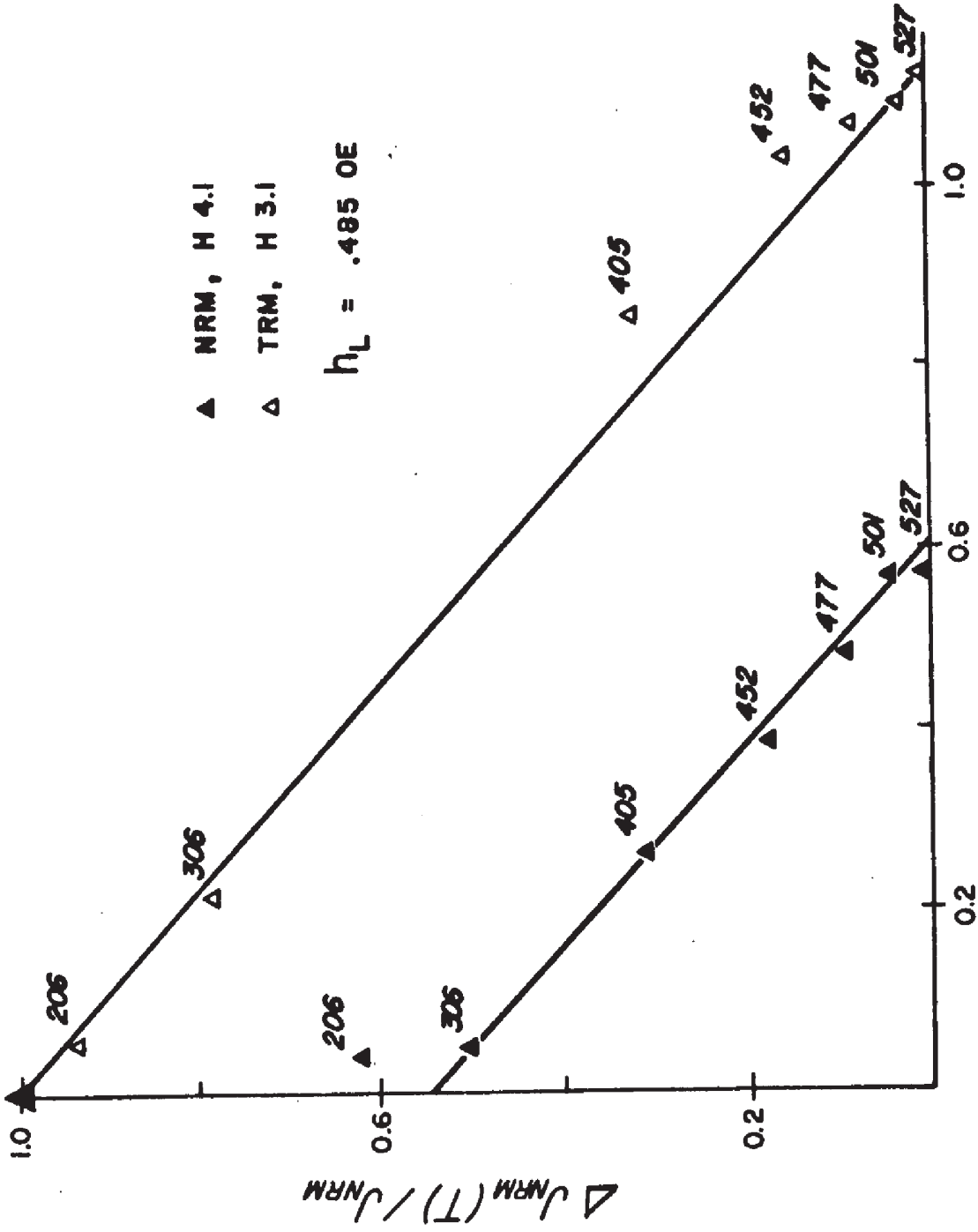
$\Delta J_{TRM}(T) / J_{NRM}$

$\Delta J_{NRM}(T) / J_{NRM}$

Figure 42

Strong-field magnetization versus temperature (J - T) curves from a chip from the 1873 flow, Pagan Island. Both heating and cooling curves were run in a slightly reducing environment ('vacuum' with residual nitrogen gas and carbon) with an applied field, H, of 7.3 koe. The heating and cooling curves are nearly reversible having a single Curie point of $455° \pm 10°C$.

PAGAN I.   1873 FLOW

J, ARBITRARY UNITS

T, °C

H = 7.3 koe
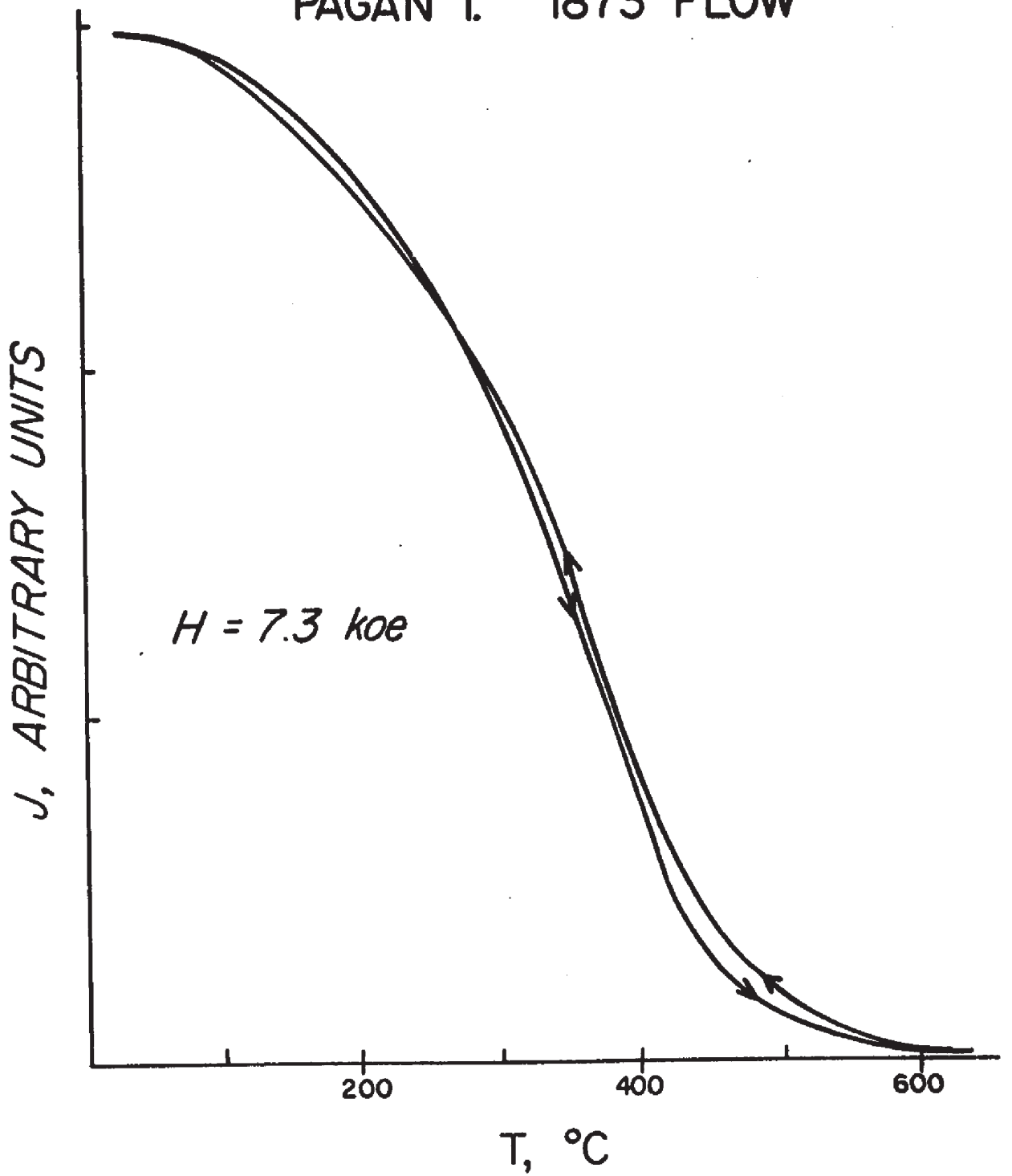
of the high field J-T curves for flows E and H, appearing in figures 40 and 42, respectively. The experimental procedure and heating environment is identical to that used for the J-T of flow ϕ. Flow E has two Curie points, one near $325° \pm 10°C$ and one near $570° \pm 10°C$, and there is a large increase in the magnetization seen during cooling. Although the J-T curve of flow H is reversible, displaying a single Curie point, the Curie point is low, $T_C = 455° \pm 10°C$, characteristic of an intermediate member of the titano-magnetite solid solution with approximately 25% Fe_2TiO_4, which is in metastable equilibrium at T_R. Certainly the short linear segments of the higher blocking temperatures cannot be used by themselves to obtain reliable paleointensities, although it appears that the higher temperature data lead to more realistic paleointensities than the lower temperature data. These experiments are only used to illustrate that sometimes secondary magnetization which adversely affects the PNRM-PTRM curve at lower temperatures can be demagnetized at higher temperatures and may reveal the correct ancient field intensity. In order to obtain more reliable estimates for the field intensity recorded by flows E and H, more PNRM-PTRM curves must be obtained for each flow to check the reliability and self consistency of the results.

8.5 EXPLANATION OF THE NON-IDEAL PNRM-PTRM CURVES

Before attempting to explain the departure from linearity, it is worth recalling that in chapter 7 we found that samples 2 to 11 are similar in obeying the additivity law. No distinction could be made on the basis of particle size. On the other hand, the experimental procedure used to test the additivity law is fundamentally different from that used in the 'Thellier method'.

Although the data presented in chapter 4 suggest that a substantial fraction of the TRM of samples 2 and 3 resides in multidomain particles,

we shall first try to explain the non-linear PNRM-PTRM curves in terms of Néel's single domain theory described by equations 7, 8, and 9. We shall assume that differences between single domain particles and non-single domain particles are due primarily to differences in the energy barriers impeding changes in the particles' magnetization, whereas the functional form of the equations is assumed to remain essentially unaltered.

As the sample acquires its original TRM, the grain's blocking is determined by the height of the potential barrier $\dfrac{v\,J_{SP}(H_{ci} \pm h_L)^2}{2H_{ci}}$ where $+(-)$ refers to moments parallel (antiparallel) to h_L. Upon reheating the samples to $T > T_R$ in zero field, the potential barriers are $\dfrac{v\,J_{SP}H_{ci}}{2}$ That is, the barriers to the rotation of moments parallel to h_L decrease, while the barriers to the rotation of moments antiparallel to h_L increase. Thus some moments originally blocked parallel to h_L at temperatures higher than T are unblocked at T. If there are Q such magnetic moments their contribution to the sample magnetization parallel to h_L is $v\,J_{SP}Q$. After heating the sample to T in zero field and cooling to T_R, these moments are randomized such that Q/2 of the moments are parallel and Q/2 of the moments are antiparallel to the original remanence. On second heating to T, h_L is on throughout, and the values of the energy barriers are as during the original TRM acquisition. Only the Q/2 moments antiparallel to h_L are unblocked and partitioned along h_L according to the hyperbolic tangent law, equation 14. Therefore, at the end of the second heating between .75 Q and Q of the moments will be aligned along h_L. The net result of this effect is that for equal NRM and TRM fields the amount of PNRM lost by heating in zero field to T is greater than or equal to the PTRM gained by cooling in a field from T to T_R, leading to a PNRM-PTRM curve that is concave up. The relative importance of this effect depends on h_L/H_{ci} at the grain's blocking

temperature, becoming less important for larger H_{ci} (T_B). Similar analysis as above shows that the effect is maximum when the PTRM is induced parallel to the remanence, and the effect is minimum when the PTRM is induced anti-parallel to the remanence.

The non-linear behavior can be further reduced by reversing the procedural steps (b) and (c) in the Coe version of the 'Thellier method'. That is, the first heating is executed in h_L and the second in zero field. This statement was verified for samples 2, 3, 4, and 8 for a single temperature experiment at about 440°C. The above mechanism for non-ideal behavior of PNRM-PTRM curves is independent of the particular domain configuration; rather, it is dependent on the value of h_L/H_{ci}(T_B) and on the assumption that τ for non-single domain particles, as for single domain particles, is determined by energy barriers that impede changes in the grain's magnetizations and that Boltzmann's is the appropriate statistics. Although there may not be a simple relationship between H_{ci} and $\tilde{H}_{\frac{1}{2}}$ one usually expects their trends to be similar; that is, an increase (decrease) in $\tilde{H}_{\frac{1}{2}}$ is usually a reflection of an increase (decrease) in H_{ci}. It is interesting to note that amongst the cogenetic magnetite particles of samples 2, 3, and 4, there is a direct correlation between lower values of $\tilde{H}_{\frac{1}{2}}$ and an increase in the deviations from linear PNRM-PTRM curves.

We shall now develop an alternate model to explain the observed non-ideal behavior for multidomain particles. We shall consider particles that are composed of two domains for all temperatures between T_R and T_B. We shall neglect the temperature variations of the domain wall width. We shall further assume that each point within the grain has the same distribution of barriers to wall movement and that the temperature variation of these distributions of the barriers is position independent. Consider such a

particle cooling through T_C in the presence of h_L, where h_L is applied along the grain's easy axis. Just below T_C, J_S is small and the magneto-static energy is dominant, and the grain magnetization is essentially parallel to h_L. As the temperature drops, J_S increases, and the demagnet-izing field becomes more important, driving the wall to a more demagnetized position. Decreasing temperatures also lead to a decrease in the thermal fluctuation energy, kT, and a relative increase in the potential barriers impeding domain wall movement. At each temperature $T > T_B$ the equilibrium wall position in the absence of barriers to wall movement is determined by the magnetostatic and demagnetizing energies. As the temperature is reduced the wall moves towards its new more demagnetized equilibrium positions. The magnetization is blocked when the wall can no longer overcome a particu-lar energy barrier. The magnetization is therefore blocked in configuration such that the TRM is higher or equal to the equilibrium value. In other words, the wall is blocked on the higher TRM side of the potential barrier, causing higher TRM than the equilibrium value. As the sample is heated to T in zero field, the grains whose blocking temperatures are exceeded are demagnetized in a statistical sense when back at T_R. Upon reheating to T in the presence of h_L the grains' walls with $T_B \stackrel{\sim}{<} T$ are blocked such that the remanence is less than or equal to the equilibrium remanence. Thus the PTRM acquired in a certain temperature interval is less than or equal to the PNRM that is lost in that particular interval, giving rise to PNRM-PTRM curves that are concave up.

8.6 CONCLUSIONS

Because considerable temperature gradients exist in our oven, the Coe version of the 'Thellier method' has yielded the best results, since the sample orientation is maintained during both heatings such that each point

in each sample is heated to the same temperature on both heatings, and the temperature gradients do not affect the results. In the limit of no temperature gradients the Coe version and the Thellier and Thellier version should provide essentially identical results. In addition, our experiments show that, during the PTRM acquisition step of the Coe version, the laboratory field must be in effect throughout the entire heating run.

We now summarize our observations. (1) We saw that in our magnetites ideal behavior in the Thellier sense is correlated with high A. F. demagnetization stability $\tilde{H}_{\frac{1}{2}} > 340$ oe, and high mean blocking temperatures, $<T_B> 493°C)$. In our experiments with pure magnetites the linear approximation to the lower blocking temperature data of the PNRM-PTRM curves yield intensities within 10% of the laboratory field whenever $\tilde{H}_{\frac{1}{2}} \geq 300$ oe. (2) We saw that non-ideal behavior can occur in samples with small grains of lower stability and in samples with a substantial fraction of multidomain remanence carriers. (3) The non-ideal behavior in our experiments leads to non-linear PNRM-PTRM curves that are concave up with respect to the line connecting the initial and final points. (4) This non-ideal behavior is reproducible, and it is a function of the magnetite particles and the experimental procedure, and it is not due to irreversible alterations of the particles. (5) Where part of the remanence is in multidomain particles, the non-linear behavior becomes more pronounced with an increase in the mean particle diameter (and with the corresponding decrease in $\tilde{H}_{\frac{1}{2}}$). Whenever the non-linearity of the PNRM-PTRM curve is an intrinsic property of remanence carriers, substantial error can be introduced into the paleointensity determination by using a linear approximation to the lower blocking temperature points. If the non-linear behavior is concave up, as in our experiments, such an approximation leads to anomalously high

paleointensities, although the ratio of the end points may yield the correct paleointensity, as with Coe's (1967 b) Mt. Lassen rocks.

Two mechanisms are developed to explain the observed non-linear behavior; one uses Néel's equations for single domain particles and depends on the variations of τ with h. The second mechanism discusses the PNRM-PTRM characteristics in a two-domain grain separated by a 180° wall.

While systematic non-ideal behavior is observed during intensity studies for samples with multidomain particles and for samples with submicron grains of relatively low stabilities, no such systematic differences are observed among these samples during experiments testing the additivity law of PTRM. The reason is due to the fundamental difference in the experimental procedure. In the experiments on additivity there is a tendency to induce magnetization parallel to $\vec{h}$ in the unmagnetized higher blocking temperature region thus giving rise to the inequality $\Sigma PTRM \geq TRM$. In the intensity experiments there is a tendency for spontaneous decay of the magnetization of the higher blocking temperature regions; this spontaneous decay cannot always be totally reclaimed by the VRM during the subsequent heating, thus leading to the non-linear PNRM-PTRM curves.

Samples for paleointensity determinations should be carefully chosen to minimize their secondary components of magnetization. More than one sample should be chosen to determine paleointensity recorded in a particular rock unit. For each sample the PNRM-PTRM curve must be evaluated over its entire blocking temperature range. For samples whose PNRM-PTRM curve is linear over the entire blocking, temperature range, the paleointensity is determined directly from the slope of the line. If non-ideal behavior is observed further experiments must be conducted to determine its source. It is not sufficient to assume that the non-linear behavior is due to chemical

or mineralogical alterations of the sample. If the Thellier and Thellier

(1959) test for redetermination of PTRM at lower temperatures shows that

irreversible changes have occurred in the sample's TRM spectrum, then a

linear approximation to the lower temperature data might yield a proper

paleointensity, assuming that the sample's NRM is very stable with respect

to A. F. demangetization, $\tilde{H}_{l_2} \geq 350$ oe. If, on the other hand, the

Thelliers' PTRM test suggests no irreversible alteration of the sample,

the non-linear behavior might be intrinsic to the sample's magnetic minerals.

A further test would be to obtain a P'NRM'-PTRM curve for the sample bear-

ing a laboratory TRM and comparing its behavior to that of the NRM. If the

same or similar non-linear features are observed in both curves (which are

assumed to be concave up) and if the end points of the P'NRM'-PTRM curve

reproduce the laboratory field, then the linear approximation to the lower

temperature data will lead to an erroneous paleointensity, while a more

accurate paleointensity might be obtained using the end points only. This

last sentence is not intended to suggest that paleointensities should be

determined from the NRM:TRM ratio. Such a procedure would discard the

consistency checks for which the Thellier method was originally developed.

The point that we wish to emphasize is that non-linear PNRM-PTRM behavior

can occur in samples having no secondary magnetizations and where no

chemical or mineralogical alterations have occurred. The consistency

checks of the 'Thellier method' are of the utmost importance, because

chemical and mineralogical alterations upon heating in the laboratory are

probably the most common source of non-linear PNRM-PTRM curves. Intensity

determination using the ratio of the end points should be resorted to only

when it has been demonstrated that the non-linearity is intrinsic to the

sample's magnetic minerals and where a linear approximation would lead to

a greater error as for the Pagan Island flow ϕ. The only time when great confidence can be placed in an intensity determined using the NRM to TRM ratio is when the geomagnetic field intensity is independently known.

CHAPTER 9

COMPARISON OF ARM AND TRM STABILITIES IN MAGNETITES

9.1 SUMMARY

ARM and TRM stabilities are studied in samples containing different types of magnetite particles ranging from single domain to multidomain. The ARM and TRM stabilities are compared for the very same samples. We find that ARM and TRM are amazingly similar in their stabilities with respect to A. F. demagnetization, in their stabilities with respect to spontaneous decay and in their stabilities with respect to temperature cycles below magnetite's isotropic point, suggesting an intrinsic similarity between ARM and TRM. It appears that ARM and TRM in magnetites are held in similar magnetic regions and their stabilities (relaxation times) are determined by the same anisotropies, such that an ARM model for TRM is a useful first approximation as far as most stability parameters are concerned, and can be used successfully as a rock magnetic and paleomagnetic tool.

9.2 BACKGROUND

Anhysteretic remanent magnetization, ARM, as defined in geophysics, is obtained by superposing an alternating field, $\tilde{H}$, on a usually much smaller direct field, $\vec{h}$, and reducing the amplitude of the alternating field from its peak value, $\tilde{H}_U$, to a lower value, $\tilde{H}_L$, in the presence of $\vec{h}$. The resulting ARM is usually measured after $\vec{h}$ has been removed and is denoted by $\vec{J}_{ARM}(\tilde{H}_U, \tilde{H}_L, \vec{h}) \equiv \vec{ARM}(\tilde{H}_U, \tilde{H}_L, \vec{h})$. If $\tilde{H}_U \gtrsim \tilde{H}_{SAT}$, an alternating field of sufficient amplitude to saturate the sample's ARM for a given $\vec{h}$, and if $\tilde{H}_L = 0$, then one is left with a total-ARM. In analogy with

TRM, if the $\tilde{H}_U \to \tilde{H}_L$ interval is any subset of the $\tilde{H}_{SAT}-0$ interval, then one if left with a partial-ARM, PARM.

The phenomenon of ARM has been known since the beginning of this century and studied as early as 1904 by Ch. Maurain. Further experimental and theoretical studies by Néel et al. (1942), Néel (1942, 1943, 1955), Lliboutry (1950), Thellier and Rimbert (1954) showed that for a given direct field, $\vec{H}$, ARM was much more intense, had substantially greater initial susceptibility, and had greater stability than IRM, isothermal remanent magnetization. For these reasons ARM is sometimes called 'ideal' magnetization. The contrast between ARM and IRM was successfully explained in a qualitative way be the use of Preisach diagrams (Preisach, 1935). Recent work on ARM has been spurred by its similarity and application to magnetic recording. ARM is an idealization of the recording process, where the slowly varying audio signal is recorded by rapidly alternating fields (Woodward and Della Torre, 1960; Daniel and Levine, 1960).

Although it has not been verified, it has been suggested (Nagata,1961) that lightning may provide an alternating field to produce an ARM in the earth's field. On the other hand, it is possible that lightning remanence is an IRM. The two alternatives could be discriminated for an observed lightning strike: an ARM would be parallel to the local geomagnetic field, while an IRM would be concentric with respect to the flowing current. An additional method to distinquish whether lightning produces an IRM or an ARM will be discussed later in light of some experimental evidnece that will be presented. In any case, with the possible exception of lightning remanence, ARM does not occur in nature.

In routine paleomagnetic work, knowledge of ARM is important because of the common use of alternating field (A.F.) demagnetization, where

spurious components of magnetization are often observed when the earth's field is not perfectly cancelled or when the alternating signal is not perfectly symmetric, but contains anharmonic components. In addition to the direct and alternating fields that characterize the process, a sample's capacity to acquire ARM depends on the density of its magnetic grains, their intrinsic magnetization, and their stability. In paleomagnetism, whether ARM is caused by lightning or during A. F. demagnetization, it is to be avoided! And as it has been often documented in human experience, knowledge of the devil helps to ward him off.

In her very extensive and thorough study of ARM in rocks and rock-forming minerals, Rimbert (1959) showed that ARM and TRM have comparable stabilities against alternating fields and thermal demagnetization. In addition, she showed that ARM is linearly related to the direct inducing field, $\vec{h}$, for small values of $\vec{h}$. This was also shown by Patton and Fitch (1962) and Banerjee and Mellema (1974). Patton and Fitch (1962) and Dunlop and West (1969) demonstrated that the additivity law is obeyed for partial-ARMs. Thus ARM has the same characteristics as TRM, outlined in Chapter 1. Because of its similarity to TRM and because ARM is an isothermal process involving neither chemical mor mineralogical alteration of the specimen, ARM is potentially a very powerful rock magnetic tool. For the reasons mentioned, Johnson and Merril (1972,1973) usually used ARM instead of TRM in their oxidation experiments, and Kinoshita, Johnson and Merrill (1974, personal communication) used ARM in an attempt to detect chemical variations in oceanic sediments. It has also been suggested that ARM could provide a non-destructive method for paleointensity

determinations (Banerjee and Mellema, 1974).

In this chapter we wish to see how far the ARM-TRM analogy can be carried and where their properties diverge. The magnetic properties of the magnetite powders, sample preparation, and TRM properties of the samples were discussed in previous chapters, and the samples are numbered as in Chapter 4. In this chapter we compare weak field ARM and TRM stability properties in the same samples. Separating TRM and ARM demagnetization experiments, there was only one heating -- that of a total thermal demagnetization at about 590°C. Comparison of both ARM and TRM properties is made for small inducing fields, similar to the earth's. The ARM of all samples is saturated by an alternating field of 2,000 oe.

9.3 COMPARISON OF THE STABILITY OF ARM AND TRM

A. A. F. DEMAGNETIZATION EXPERIMENTS

Figures 43 to 54 depict the samples' A.F. demagnetization curves for weak field ARM and TRM. The solid symbols represent the TRM data and the open symbols the ARM data. The circles represent stepwise A. F. demagnetization and it is seen that the demagnetization curves of ARM and TRM have similar shapes for all samples. The stabilities of the ARM and TRM are amazingly similar in view of the differences in their modes of acquisition. Because the TRMs and ARMs were induced in slightly different biasing fields, it is not possible to be certain whether the differences in the demagnetization curves are due to differences between ARM and TRM or whether they are caused by differences in the inducing fields. In eight of the twelve samples (samples 2, 3, 4, 5, 7, 8, 9, 10) the TRM is slightly more stable than the ARM. For sample 3 (figure 46; table 8) the differences are

Figure 44

Alternating field demagnetization of ARM (open symbols) and TRM (solid symbols) for sample 1- magnetite single crystal chip weighing 3.57 gm. The squares represent independent demagnetization experiments to test the reproducibility of the curves and the median demagnetizing field. The shapes of the demagnetization curves are very similar, and the inducing fields are indicated on the figure.

Figure 43

Alternating field demagnetization of ARM (open symbols) and TRM (solid symbols) for sample 0- magnetite single crystal weighing 6.38 gm. The squares represent independent demagnetization experiments to test the reproducibility of the curves and the median demagnetizing field. Due to the persistent reversed TRM component, comparison between the ARM and TRM curves is not straight forward. The inducing fields are indicated on the figure.

SAMPLE I

TRM (.467 OE)
ARM (.48 OE)
ARM (.59 OE)

$J(\tilde{H})/J_0$

$\tilde{H}$, OERSTED

SAMPLE O

TRM (.467 OE)
ARM (.54 OE)
ARM (.65 OE)

$J(\tilde{H})/J_0$

$\tilde{H}$, OERSTED

Figure 45

Alternating field demagnetization of ARM (open symbols) and TRM (solid symbols) for sample 2, composed of natural, irregular, magnetite particles whose mean diameter is about 2.7 μm. The squares represent independent demagnetization experiments to test the reproducibility of the curves and to redetermine the MDF value. The shapes of the ARM and TRM demagnetization curves are very similar, and the inducing fields are indicated on the figure.

Figure 46

Alternating field demagnetization of ARM (open symbols) and TRM (solid symbols) for sample 3, containing natural, irregular, magnetite particles whose mean diameter is about 1.5 μm. The squares represent independent demagnetization experiments to test the reproducibility of the curves and to redetermine the MDF value. The shapes of the ARM and TRM demagnetization curves and the MDF values are very similar, and the inducing fields are indicated on the figure.

SAMPLE 3

TRM (.478 OE)
TRM (.375 OE)
ARM (.55 OE)
ARM (.69 OE)

H̃, OERSTED

J(H̃)/J₀

SAMPLE 2

TRM (.478 OE)
TRM (.375 OE)
ARM (.52 OE)
ARM (.72 OE)

H̃, OERSTED

J(H̃)/J₀

156

Figure 48

Alternating field demagnetization of ARM (open symbols) and TRM (solid symbols) for sample 5, containing synthetic, equidimensional, magnetite particles whose mean diameter is about .24 μm. The squares represent independent demagnetization experiments to test the reproducibility of the curves and to redetermine the MDF value. The shapes of the ARM and TRM demagnetization curves are similar, as are the MDF values. The inducing fields are indicated on the figure.
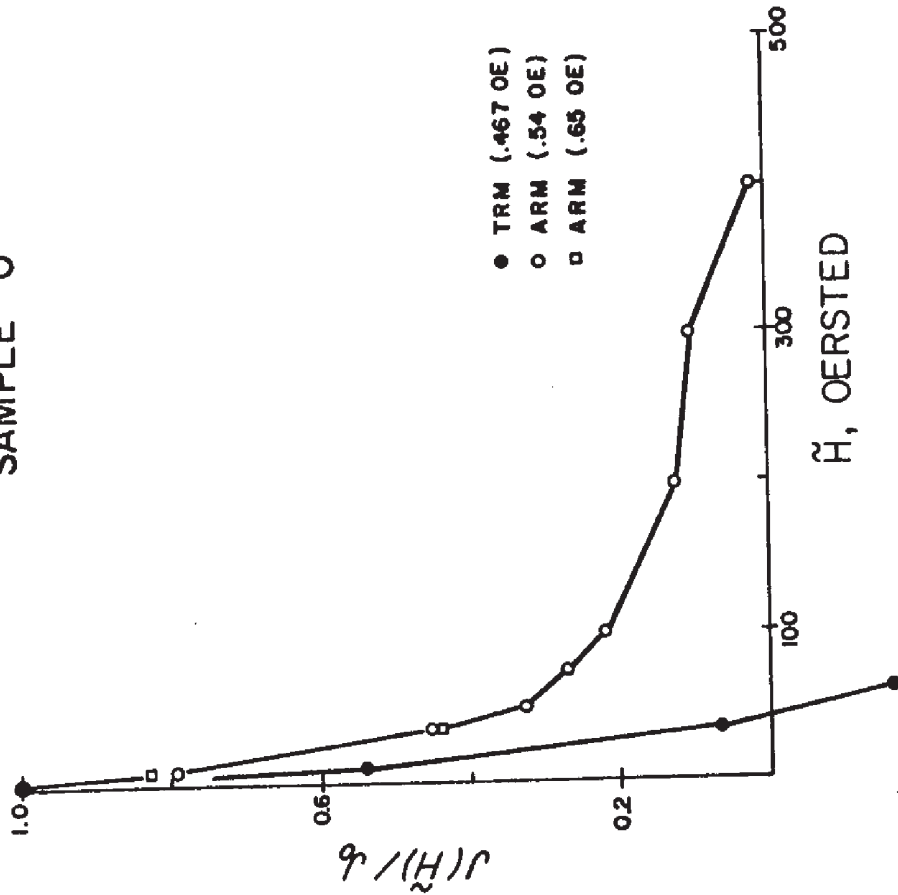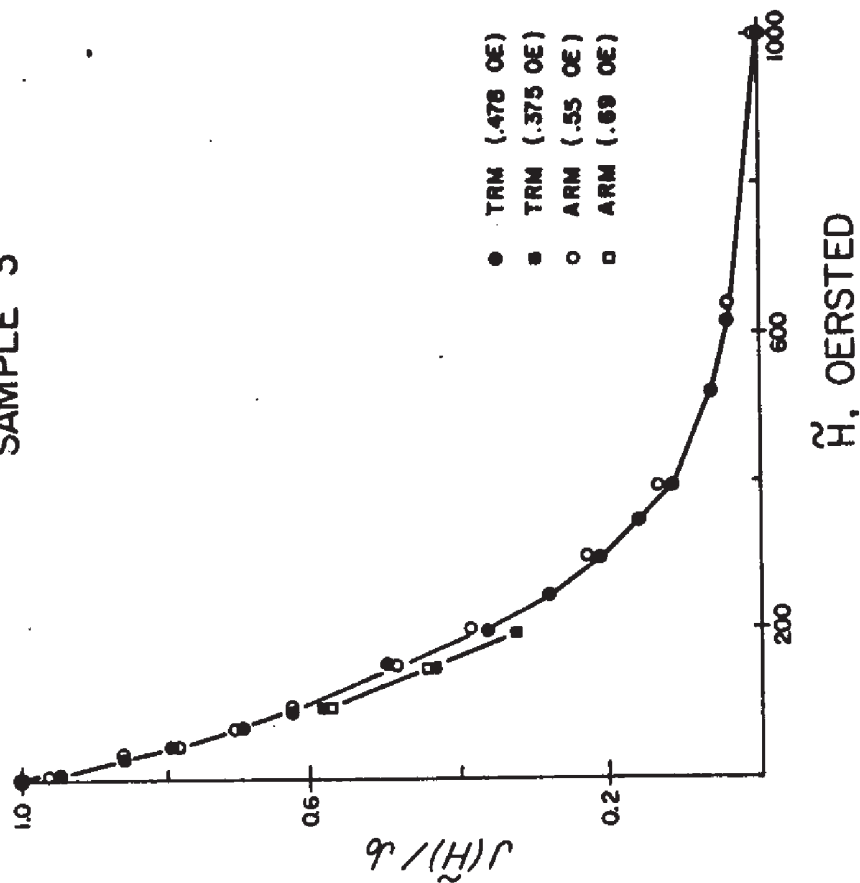
Figure 47

Alternating field demagnetization of ARM (open symbols) and TRM (solid symbols) for sample 4, containing natural, equidimensional, magnetite particles whose mean diameter is about .31 μm. The squares represent independent demagnetization experiments to test the reproducibility of the curves and to redetermine the MDF value. The shapes of the ARM and TRM demagnetization curves are similar, and the inducing fields are indicated on the figure.

SAMPLE 5

TRM (.478 OE)
TRM (.467 OE)
ARM (.68 OE)
ARM (.54 OE)

$\tilde{H}$, OERSTED

$J(\tilde{H})/J_0$

SAMPLE 4

TRM (478 OE)
TRM (.375 OE)
ARM (.62 OE)
ARM (.74 OE)

$\tilde{H}$, OERSTED

$J(\tilde{H})/J_0$

Figure 49

Alternating field demagnetization of ARM (open symbols) and TRM (solid symbols) for sample 6, containing synthetic,equidimensional, magnetite particles whose mean diameter is about .21 um. The squares represent independent demagnetization experiments to test the reproducibility of the curves and to redetermine the MDF value. The shapes of the ARM and TRM demagnetization curves are similar, and the ARM is consistently more stable than the TRM. The inducing fields are indicated on the figure.
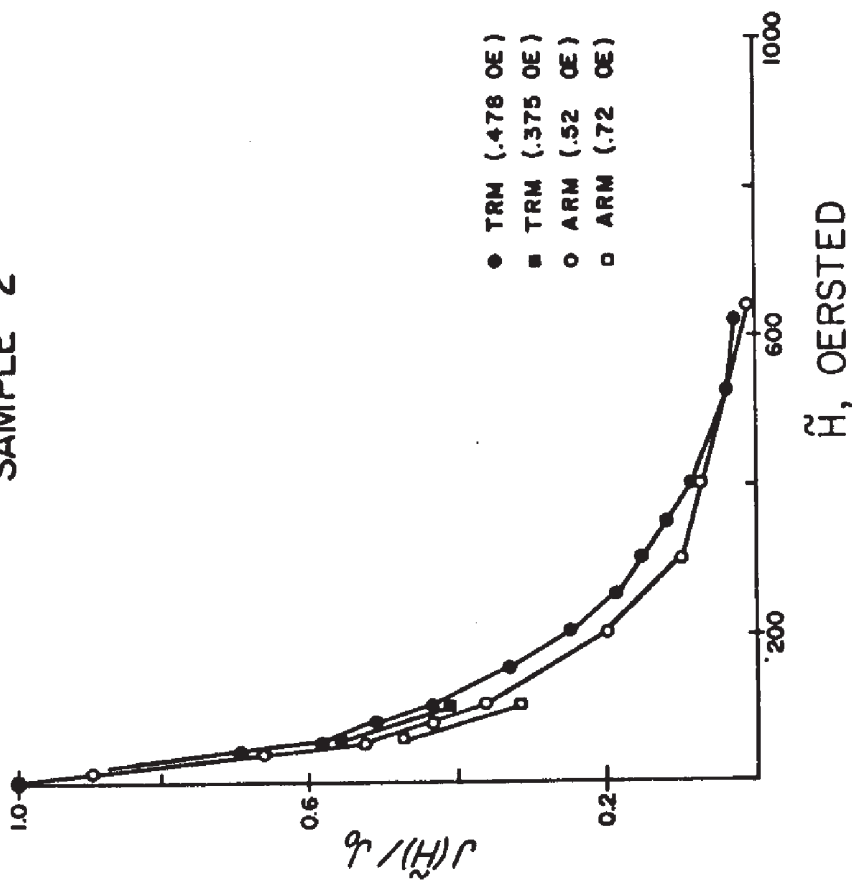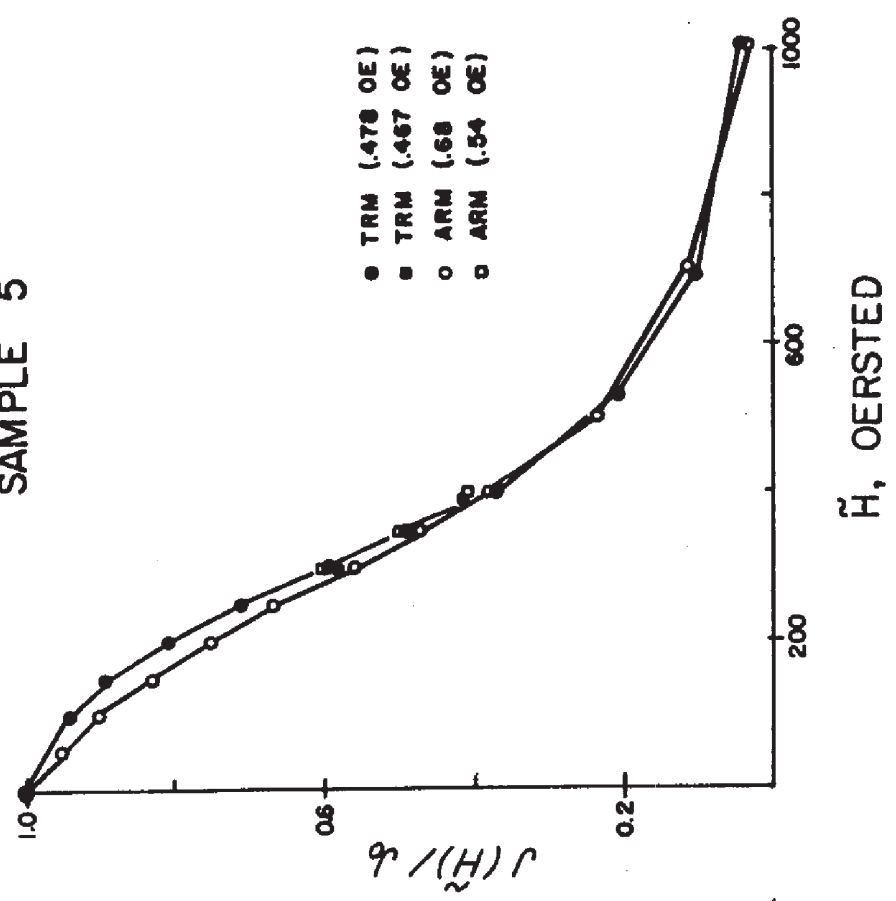
Figure 50

Alternating field demagnetization of ARM (open symbols) and TRM (solid symbols) for sample 7, containing synthetic, equidimensional,magnetite particles whose mean diameter is about .21 um. The squares represent independent demagnetization experiments to test the reproducibility of the curves and to redetermine the MDF value. The shapes of the ARM and TRM demagnetization curves are similar, and the inducing fields are indicated on the figure.

SAMPLE 7

TRM (.478 OE)
TRM (.467 OE)
ARM (.65 OE)
ARM (.74 OE)

$J(\tilde{H}) / J_o$

$\tilde{H}$, OERSTED

SAMPLE 6

TRM (.478 OE)
TRM (.467 OE)
ARM (.68 OE)
ARM (.54 OE)

$J(\tilde{H}) / J_o$

$\tilde{H}$, OERSTED

Figure 52

Alternating field demagnetization of ARM (open symbols) and TRM (solid symbols) for sample 9, containing synthetic, equidimensional, magnetite particles whose mean diameter is about .12 μm. The squares represent independent demagnetization experiments to test the reproducibility of the curve and to redetermine the MDF value. The shapes of the ARM and TRM demagnetization curves are similar. The inducing fields are indicated on the figure.
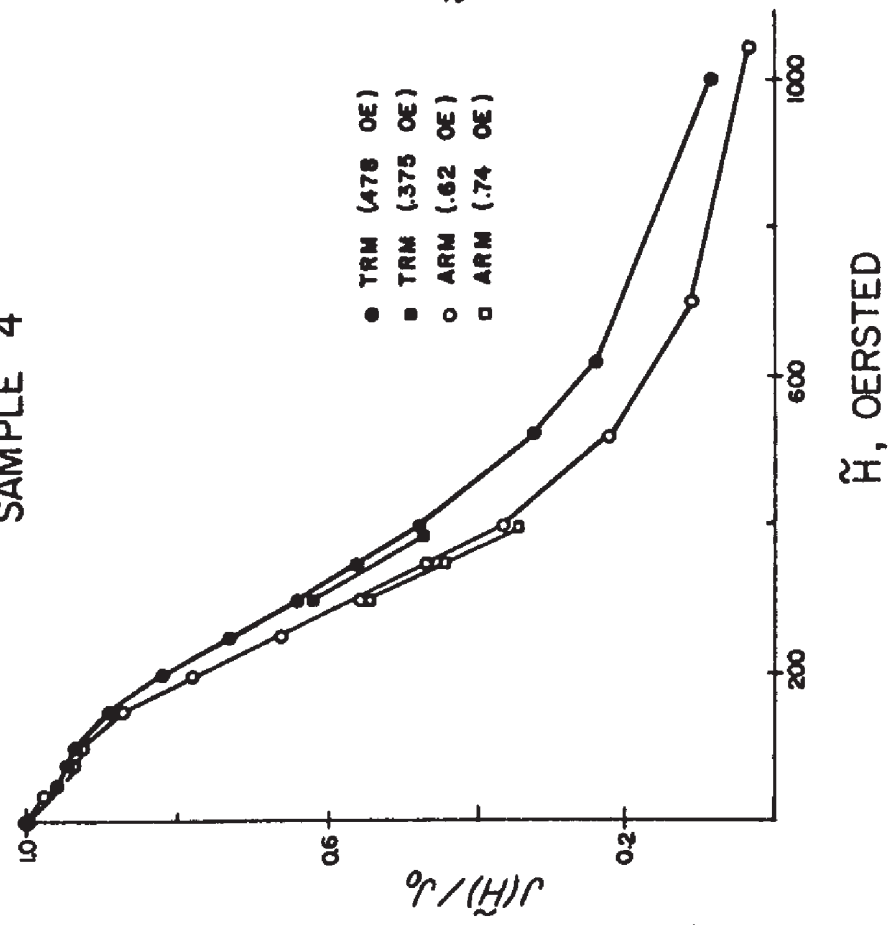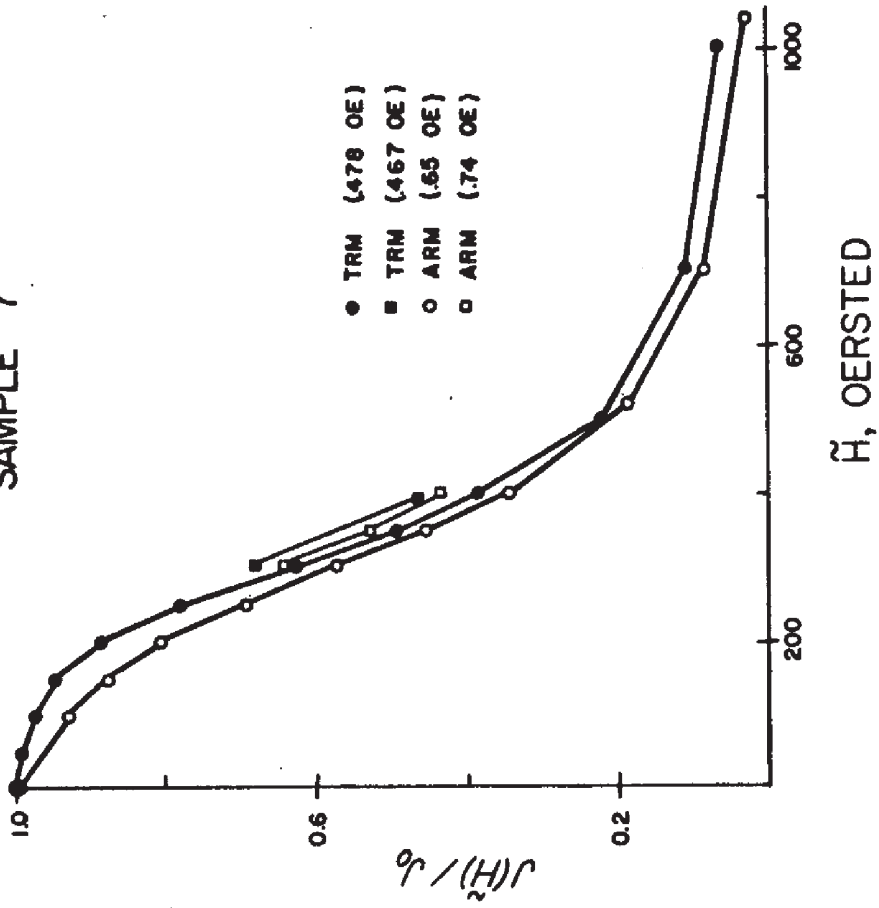
Figure 51

Alternating field demagnetization of ARM (open symbols) and TRM (solid symbols) for sample 8, containing synthetic, equidimensional,magnetite particles whose mean diameter is about .12 μm. The squares represent independent demagnetization experiments to test the reproducibility of the curve and to redetermine the MDF value. The shapes of the ARM and TRM demagnetization curves are very similar. The inducing fields are indicated on the figure.

SAMPLE 9

TRM (.478 OE)
TRM (.375 OE)
ARM (.68 OE)
ARM (.41 OE)

$J(\tilde{H})/J_0$

$\tilde{H}$, OERSTED

SAMPLE 8

TRM (.478 OE)
TRM (.375 OE)
ARM (.63 OE)
ARM (.40 OE)

$J(\tilde{H})/J_0$

$\tilde{H}$, OERSTED

Figure 54

Alternating field demagnetization of ARM (open symbols) and TRM (solid symbols) for sample 11, containing synthetic, highly acicular, magnetite particles whose axial ratio is of the order of 8:1. The squares represent independent demagnetization experiments to test the reproducibility of the curves and to redetermine the MDF value. The shapes of the ARM and TRM demagnetization curves are similar, but the ARM is consistently more stable. The inducing fields are indicated on the figure.

Figure 53

Alternating field demagnetization of ARM (open symbols) and TRM (solid symbols) for sample 10, containing magnetite particles of unknown shapes and sizes. The squares represent independent demagnetization experiments to test the re-producibility of the curves and to redetermine the MDF value. The shapes of the ARM and TRM demagnetization curves are similar, and the inducing fields are indicated on the figure.
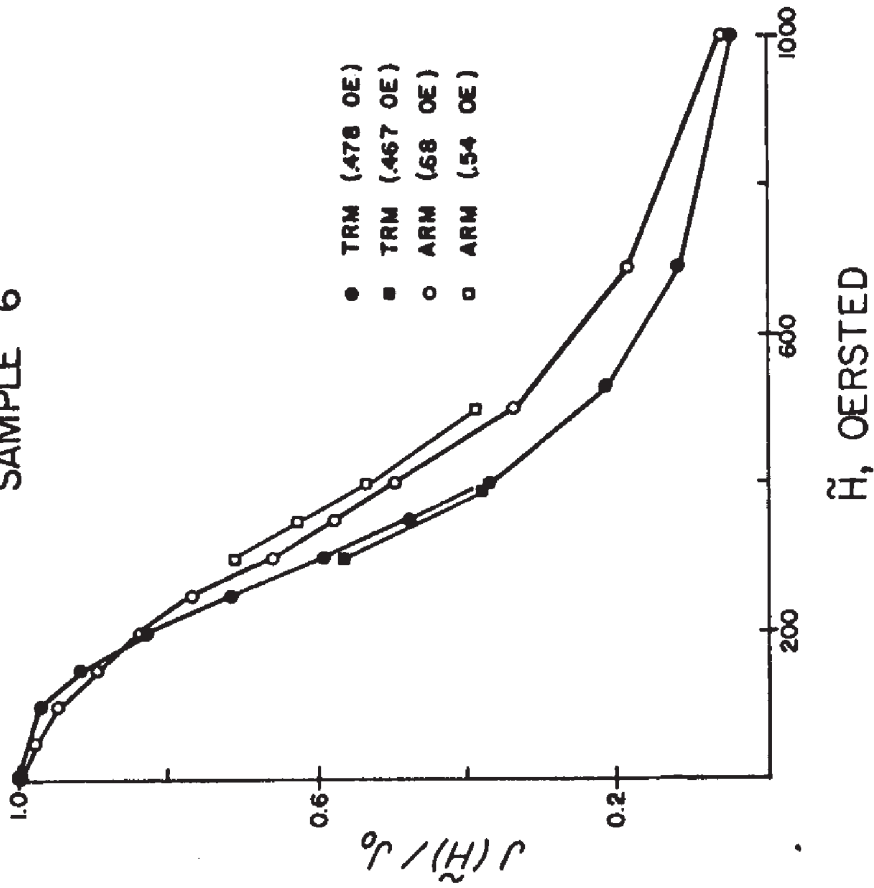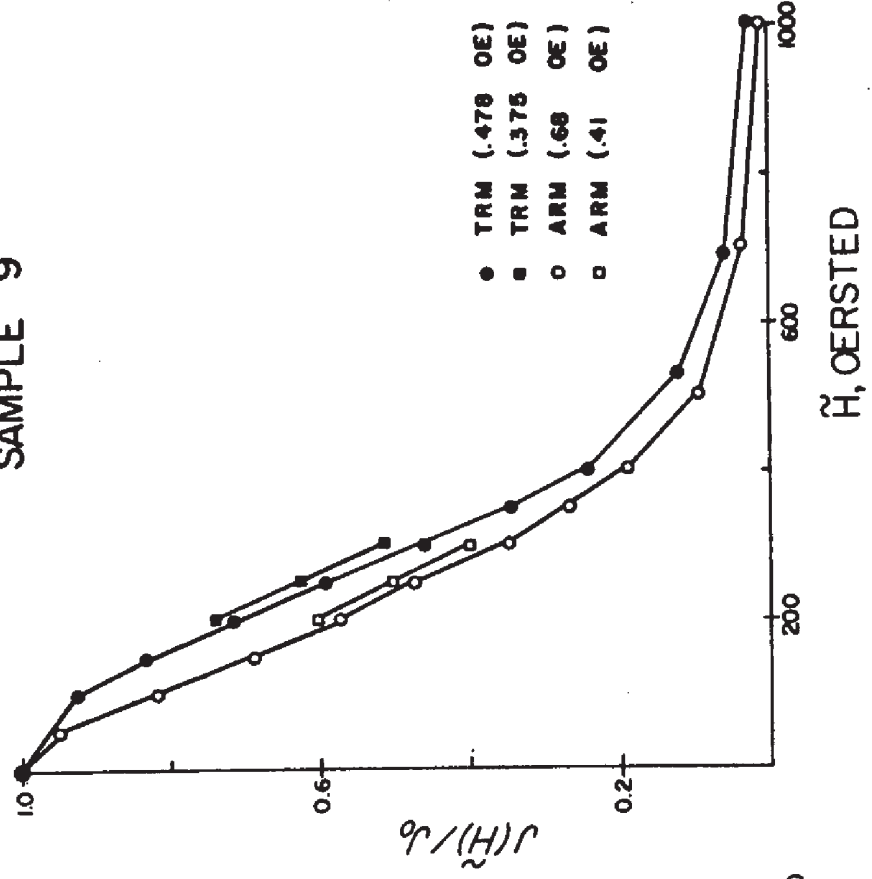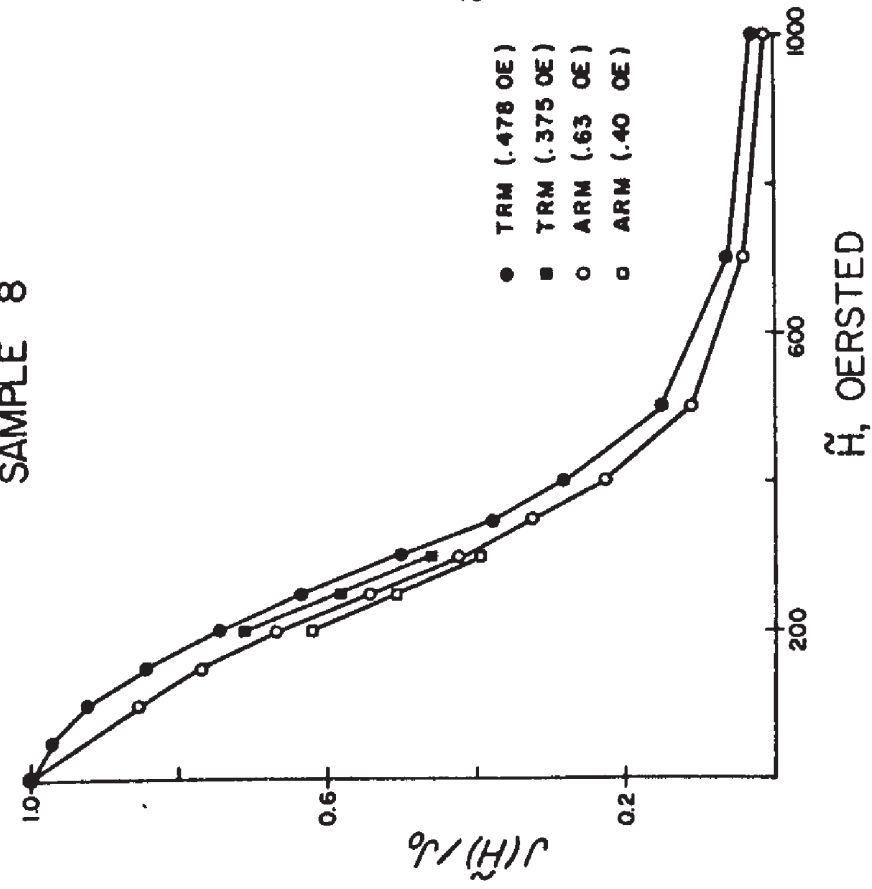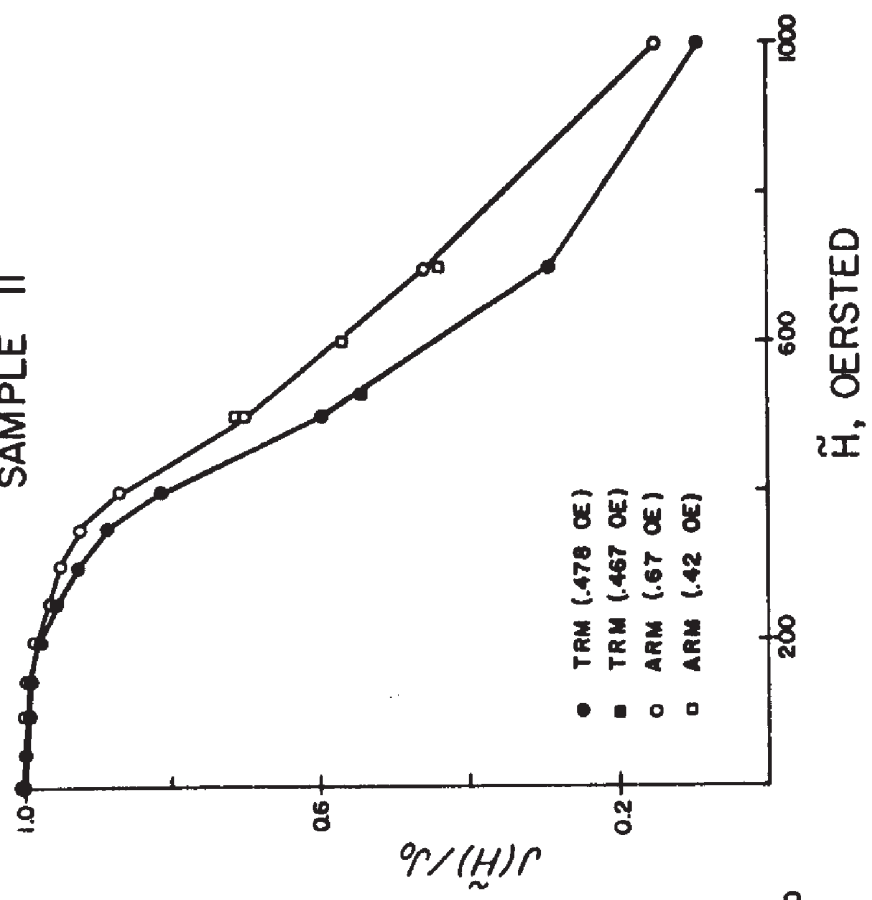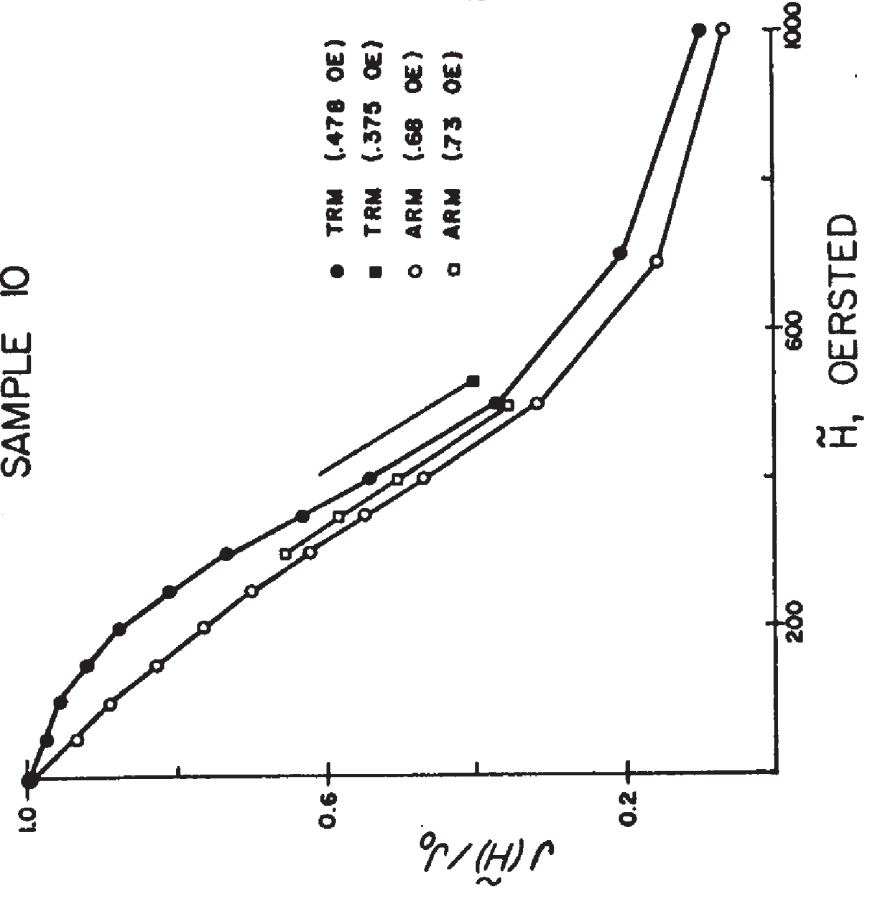
SAMPLE 10

SAMPLE II

within the experimental errors and therefore are not significant. For
four samples the ARM is more stable than the TRM. For the large crystals,
samples 0 and 1, the ARM is consistently more stable than the TRM. The ARM
curve of sample 11, which contains the acicular particles, diverges from
the TRM spectrum above 300 oe and remains decidedly more stable beyond
that point. This is consistent with the observations of Dunlop and West
(1969) who report that for single domain grains, a 1 oe ARM is slightly
more resistant to alternating fields than a 1 oe TRM. The ARM of sample 6
is 'softer' than the TRM for low alternating fields, but the curves inter-
sect at about 190 oe, and the ARM is 'harder' for all higher alternating
fields. The behavior of sample 6 is in sharp contrast with that of sample
7 whose TRM is consistently 'harder' than its ARM. This behavior contrast
is somewhat surprising because samples 6 and 7 contain the same magnetite
particles and the samples were prepared identically. The only apparent
difference between the two samples is that sample 7 contains about 10 times
as much magnetite as does sample 6. (See table 5, column 3.) It is quite
possible, therefore, that the observed differences are due to differences
in the magnetic interactions in the two specimens.

In comparison with samples 6 and 7, samples 8 and 9 are samples con-
taining the same species of magnetite powder -- though different from the
powder in samples 6 and 7. Samples 8 and 9 were prepared identically from
the same mixture and their magnetite concentration is very similar. (See
table 5, column 3.). Comparison of the samples' ARM curves and, separately,
their TRM curves and comparison of the relative behavior of each sample's
ARM and TRM show to the satisfaction of one's expectations and sense of
order that samples 8 and 9 are much more similar than any other pair, except

possibly samples 0 and 1.

Since the shapes of the demagnetization curves of all the samples are similar, and with one exception (that of sample 6) the surves do not intersect, it is convenient to use the median demagnetizing field, $\tilde{H}_{\frac{1}{2}}$ -- that alternating field for which the magnetization drops to half its original value -- to describe and compare the samples' stabilities against alternating fields. To test how reliably $\tilde{H}_{\frac{1}{2}}$ can be reproduced for each sample, a limited version of the demagnetization experiments was repeated, using the original data as a guide (circles in figure 1). Alternating field values were chosen to bracket $J(\tilde{H})/J_0 = 1/2$ to best estimate $\tilde{H}_{\frac{1}{2}}$. The second sequence of demagnetization experiments (represented by squares in figures 43 to 54) followed the first and was separated from it by the entire sequence of the partial-TRM experiments discussed in Chapter 7 and by one complete set of 'Thellier' experiments. Although some of the demagnetization curves and some of the values for $\tilde{H}_{\frac{1}{2}}$ shifted considerably between the two sequences of demagnetization experiments, the relationship between the respective ARM and TRM spectra did not. The values for $\tilde{H}_{\frac{1}{2}}$ are presented in table 8, column 3. The uncertainties associated with each value are estimated from the uncertainties in reproducing particular alternating fields and from uncertainties associated with plotting the curves and estimating $\tilde{H}_{\frac{1}{2}}$. In figures 43-54, the values of the fields inducing the various remanences are given, and at first one might suspect that the differences in the demagnetization spectra and $\tilde{H}_{\frac{1}{2}}$ values are due to variations in the inducing fields. A careful inspection, however, shows that this is not the case. Rather, it seems that the variations in $\tilde{H}_{\frac{1}{2}}$ are real changes in the coercivity

Figure 55

A plot of the median-demagnetizing-fields (oersted, linear scale) versus characteristic particle diameter (μm, logarithmic scale) for ARM (triangles) and TRM (circles) for magnetite-bearing samples. The median-demagnetizing-fields (MDF) for both ARM and TRM generally follow the same pattern.

The uncertainty bars associated with the mean particle diameters are related whenever possible, to the standard deviations of the particle diameters obtained from electron microscope photographers. The one exception is sample 10, which is labeled 'unknown' in the figure, for which there are no direct observations of the magnetic particles. The uncertainty bars associated with the MDFs represent deviations from the mean of independent determinations. From right to left along the abscissa the data correspond to samples 0, 1, 2, 3, 4, 5, 6 and 7, 8, 9, 10, and 11.
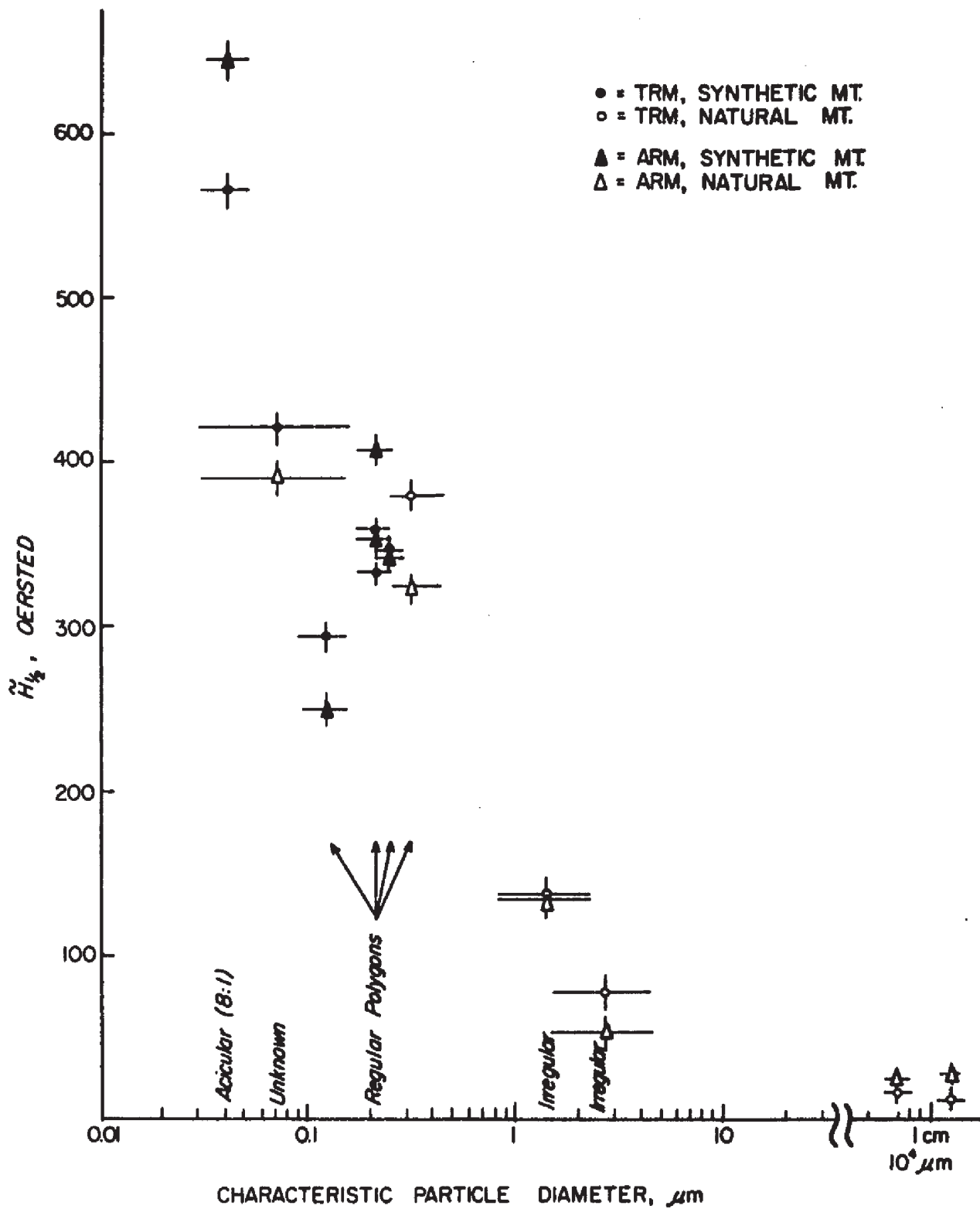
spectra of the samples, caused by multiple heatings. The consistent decrease in $\tilde{H}_{\frac{1}{2}}$ for both ARM and TRM of samples 2, 3, and 4 may be due to annealing effects at elevated temperatures. The data for redetermining $\tilde{H}_{\frac{1}{2}}$ is omitted for some of the samples in figures 43-54 to avoid unnecessary clutter and confusion. In figure 55 the last determinations of $\tilde{H}_{\frac{1}{2}}$ are plotted as a function of the magnetite grain sizes, as determined in chapter 2. The only sample whose magnetite sizes and shapes are not known is sample 10.

B. SPONTANEOUS DECAY

To investigate how ARM compares with TRM in acquiring viscous remanences, VRM, and to use it as another method for comparing the relative stabilities of ARM and TRM, the samples were subjected to total-ARM in a direct field of 0.65±.05 oe and then placed in null field for approximately 24 hours, at which time the remaining remanence was measured. A second spontaneous decay experiment was performed on a total-ARM where the direct field was 0.42±.05 ae. In the limited range of fields used in these experiments, there appears to be no field dependence of the spontaneous dcay of the magnetization of total-ARM. The mean of ARM remaining after spontaneous decay of about 24 hours, $J_{ARM}(h = 0, t = 24 \text{ hours})/J_{ARM}$, is listed for each sample in table 8, column 5 alongside similar spontaneous decay data for TRM reproduced from table 5, column 7. The uncertainties along the mean spontaneous decay values are merely deviations of the particular data from the means.

For samples 0, 1, 2, and 3 the ARM is significantly more resistant to spontaneous decay than the TRM. The TRM of samples 8 and 9 is significantly more resistant to spontaneous decay than the ARM. For the remaining

samples, samples 4, 5, 6, 7, 10, and 11, there is no significant difference between ARM and TRM. The values for the spontaneous decay, appearing in table 8.1, are also plotted in figure 56 whose ordinate gives the magnetization normalized to its initial value, and the abscissa is a logarithmic scale of the mean particle diameters, identical to that of figure 55.

C. LOW TEMPERATURE CYCLES

The decay of a sample's magnetization when it is subjected to temperature cycles below the magnetocrystalline anisotropy transition temperature is a measure of the relative fraction of the remanence that is controlled by the magnetocrystalline anisotrophy energy, through its effect on the coercivity and on domain-wall formation. The low temperature behavior was discussed at some length in chapter 4 in relation to TRM, and it was observed there that the decay of the magnetization after low temperature cycles followed more closely than any other stability criterion the samples' grain size pattern. The samples were given a total-ARM in a direct field of 0.65±.05 oe and stored in null field for approximately 24 hours to determine the magnitude of the spontaneous decay. After the remanence was measured the samples were immersed in liquid nitrogen in zero magnetic field for sufficient time (∿45 minutes) to equilibrate with the liquid nitrogen. The samples were then removed from the liquid nitrogen and allowed to reach room temperature -- the samples at all times remaining in null magnetic field. The remanence was then measured. The magnetization after the low temperature cycle is normalized with respect to the magnetization value obtained after the storage test. The samples were subjected to three consecutive low temperature treatments and the data is presented in table 8, column 4, alongside the equivalent TRM data

Figure 56

The circles represent the fraction of the ARM (open circles) and TRM (closed circles) remaining after spontaneous decay in zero field for approximately 24 hours of the magnetite-bearing samples. Each datum represents a mean value obtained from two independent determinations for each of the samples. (The deviations from the mean are listed in table 8 column 5.) It is seen that both ARM and TRM behave similarly under spontaneous decay.

The triangles represent the fraction of the ARM (open triangles) and TRM (closed triangles) remaining after the third cycle in zero field to below magnetite's isotropic temperature. Again, both ARM and TRM display similar behavior.

The abscissa is identical to that of figure 55, both feature data for the same ensemble of samples. Thus the 'characteristic particle diameters' of both figures are identical. The uncertainty bars have been omitted from figure 56 to avoid unnessory clutter.

NULL FIELD (24 HOURS)

- • = TRM RELAXATION
- ○ = ARM RELAXATION

CYCLES BELOW THE MAGNETOCRYSTALLINE
ANISOTROPY TRANSITION TEMPERATURE

- ▼ = TRM DECAY
- △ = ARM DECAY

J, NORMALIZED

CHARACTERISTIC PARTICLE DIAMETER, μm

TABLE 8

COMPARISON OF TRM AND ARM PROPERTIES IN MAGNETITE

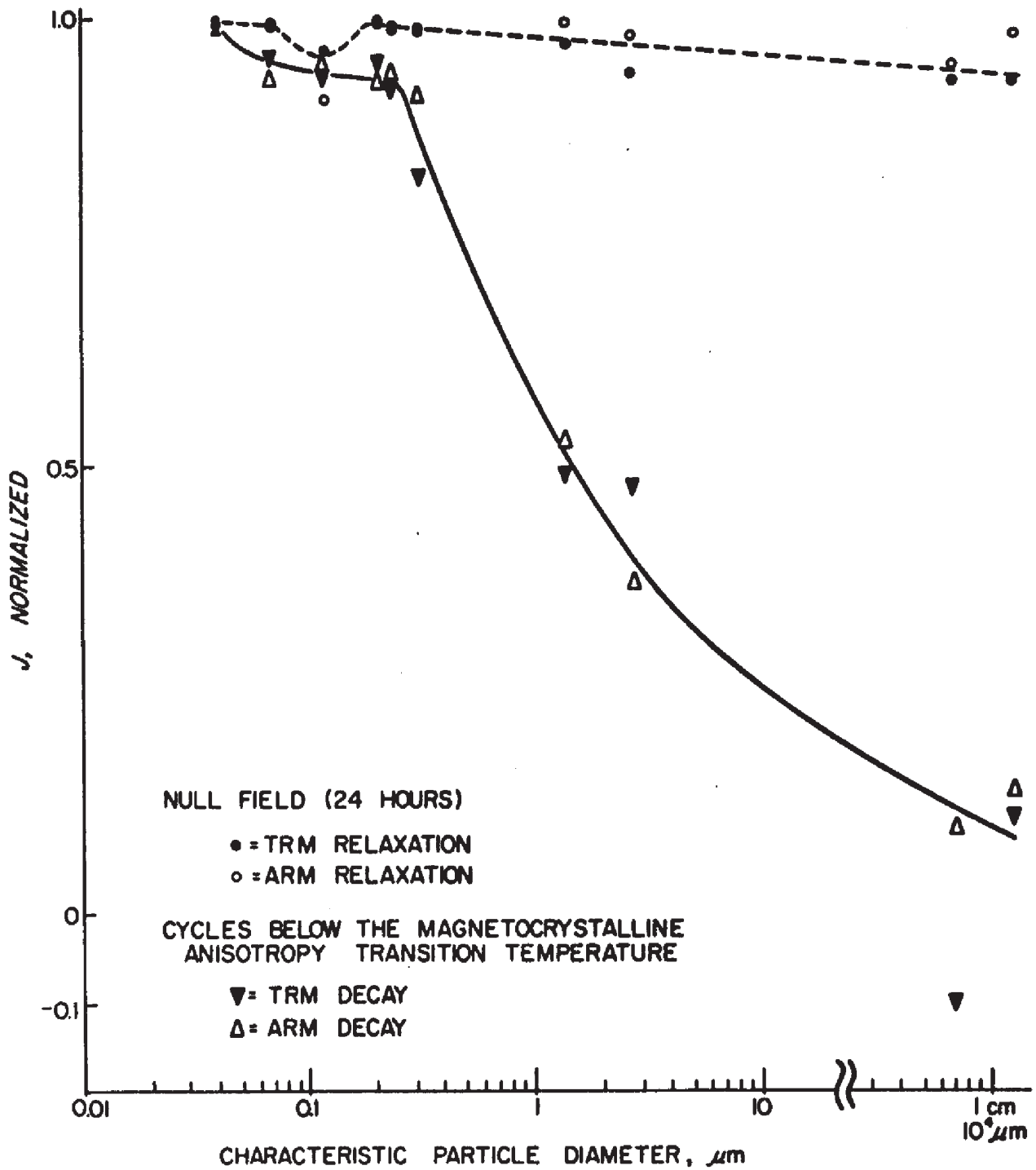| Sample Number	Description of Magnetite Particles	$\tilde{H}_{1/2}$ (Oersted)		Low Temperature Cycles Normalized		Spontaneous Decay t = 24 hours Normalized		χ_{ARM}/χ_{TRM}
		TRM	ARM	TRM	ARM	TRM	ARM	
0	Natural Crystal Euhedral 6.379 gm	12±3	27±3 27±3	.136 .110 .106	-.052 .116 .136	.926±.013	.975±.005	2.0±.4
1	Chip of Natural Crystal 3.569 gm	17±3	24±3 25±3	-.091 -.092 -.101	.144 .082 .092	.924±.012	.944±.012	1.5±.3
2	Natur., Irreg. $\langle d \rangle$=2.7 μm d_{max}=150 μm	82±5 74±5	58±5 49±5	.590 .465 .476	.413 .386 .370	.938±.002	.980±.004	.64±.06
3	Natur., Irreg. $\langle d \rangle$=1.5 μm d_{max}=50 μm	147±10 129±10	144±10 126±10	.593 .521 .497	.561 .537 .524	.970±.005	.995±.005	.45±.04
4	Natur. Regular $\langle d \rangle$=.31 μm d_{max} = 2 μm	388±10 373±10	330±10 315±10	.936 .889 .822	.929 .916 .913	.990±.002	.985±.004	.44±.04

TABLE 8
(cont'd)

COMPARISON OF TRM AND ARM PROPERTIES IN MAGNETITE

Sample Number	Description of Magnetite Particles	$\tilde{H}_{1/2}$ (Oersted) TRM	$\tilde{H}_{1/2}$ (Oersted) ARM	Low Temperature Cycles Normalized TRM	Low Temperature Cycles Normalized ARM	Spontaneous Decay t = 24 hours Normalized TRM	Spontaneous Decay t = 24 hours Normalized ARM	χ_{ARM}/χ_{TRM}
5	Synthetic, Cubes→Spheres $<d>=.24$ μm $d_{max} = .9$ μm	347±10 347±10	337±10 350±10	.945 .935 .929	.980 .942 .932	.992±.002	.990±.001	.188±.010
6	Synthetic, Cubes→Spheres $<d>= .21$ μm $d_{max} = .5$ μm	337±10 331±10	387±10 416±10 423±10	.976 .951 .945	.964 .964 .961	.995±.004	1.000±.000	.164±.008
7	Synthetic, Cubes→spheres $<d>= .21$ μm $d_{max} = .5$ μm	346±10 375±10	333±10 363±10 366±10	.965 .961 .955	.920 .914 .905	.998±.002	.998±.002	.108±.005
8	Synthetic, Cubes spheres $<d>= .12$ μm $d_{max} = .3$ μm	300±10 284±10	268±10 254±10 264±10	.990 .971 .965	.978 .974 .951	.967±.002	.926±.010	.50±.03

TABLE 8
(cont'd)

COMPARISON OF TRM AND ARM PROPERTIES IN MAGNETITE

Sample Number	Description of Magnetite Particles	$\tilde{H}_{1/2}$ (Oersted)		Low Temperature Cycles Normalized		Spontaneous Decay t = 24 hours Normalized		χ_{ARM}/χ_{TRM}
		TRM	ARM	TRM	ARM	TRM	ARM	
9	Synthetic Cubes spheres $<d> = .12\ \mu m$ $d_{max} = .3\ \mu m$	285±10 306±10	237±10 251±10 232±10	.986 .910 .907	.980 .976 .956	.958±.002	.895±.010	.49±.03
10	Magnetite Unknown Size and Shape	421±20	382±20 401±20	.982 .974 .960	.945 .934 .934	.994±.012	.993±.007	.312±.015
11	Synth. Acicular Axial Ratio 8:1 .35 μm x .04 μm	565±25	672±25 656±25	1.003 .995 .994	.995 .995 .988	.998±.002	1.000±.002	.238±.012

reproduced from table 5, colum 6. This data is plotted with the spontaneous decay data in figure 56. By and large, ARM and TRM seem to behave similarly under low temperature treatment. It should be noted that for the almost identical samples 8 and 9, the TRM of sample 8 is more stable than the ARM under low temperature treatment, while the opposite is true for sample 9. Similar behavior is noted with the similar samples 6 and 7, where for sample 7, the TRM is more resistant than the ARM to cycles to liquid nitrogen temperature, whereas for sample 6 the ARM is more resistant than the TRM. These examples suggest that small differences (a few percent) in the low temperature behavior may not be significant and that the important observation is to note the similarity of the behavior of ARM and TRM subject to cycles below magnetite's isotropic temperature.

9.4 CONCLUSIONS

It is interesting to note that whereas samples 8 and 9 rank very low in their stabilities against alternating fields and spontaneous decay, they rank high in their stability against low temperature cycles. This observation is consistent with the interpretation that these samples have a substantial fraction of their magnetite particles in the size range near the super-paramagnetic -- single domain boundary, having low relaxation times. In addition, their volumes are relatively small such that their ratio of surface area to volume is relatively large. Therfore surface stresses and surface anisotropy play a relatively more important role in determing the intrinsic coercivity and in controlling the remanent magnetization, while the magnetocrystalline anisotropy energy, which is volume dependent, becomes relativley less important.

The fact that ARM and TRM in the same samples and induced by similar fields behave very similarly in low temperature cycles strongly suggests that magnetocrystalline anisotropy plays a similar role in controlling the remanence in both ARM and TRM in magnetites of different origins and of a variety of grain sizes and shapes. In addition, the similarity of ARM and TRM stability against alternating field demagnetization and their similar spontaneous decay characteristics suggest an intrinsic similarity between ARM and TRM in magnetites are probably held in similar magnetic regions and their stabilities (relaxation times) are controlled similarly by the same magnetic anisotropies.

It appears, therfore, than an ARM model for TRM may be a useful first approximation in magnetites as far as most stability characteristics are concerned. Thus ARM can be used instead of TRM in most stability tests in rock magnetic and paleomagnetic studies with the exception of cases where extreme precision and resolution are required.

An additional experiment that might be useful in comparing and understanding the relationships between ARM and TRM would be to compare their respective blocking temperature curves for the same samples and similar remanence-inducing fields. Rimbert (1959) showed that for the magnetite powders that she used, ARM had a very narrow range of blocking temperatures just below the Curie point. To satisfy our natural urge to speculate, we venture to predict that the ARM blocking temperature curves will compare to the TRM blocking temperature spectra in a similar way as the ARM and TRM A. F. demagnetization curves are related.

THE EFFECT OF MAGNETIC INTERACTIONS ON THE

ACQUISITION AND STABILITY OF ARM AND TRM

10.1 SUMMARY

Experiments on the acquisition of ARM and TRM show that the low field

susceptibility ratio, $X_{ARM}/X_{TRM} < 1$ for fine patricles $(.1 \leqslant X_{ARM}/X_{TRM} \leqslant .6)$,

but for the large crystals of magnetite $X_{ARM}/X_{TRM} > 1$ (1.5 and 2.0 respec-

tively). It is argued that these differences in the susceptibility ratios

are caused by different interaction fields in the different samples due

largely to differences in the grain-self-demagnetizing factors and to

differences in the sample-self-demagnetizing factors.

Analysis of the various stability parameters of ARM and TRM in terms

of magnetic interactions, with particular emphasis on two samples contain-

ing different concentrations of the same magnetite powder, shows that in

our samples, where the magnetite concentration is always below 5% by

weight, there is no experimentally discernable effect on the various stability

parameters that can be unambiguously attributed to magnetic interactions.

10.2 A DISCOURSE ON THE ORIGIN AND EFFECTS OF MAGNETIC INTERACTION

In the introduction it was pointed out that despite the spectacular

success of Néel's single domain theory to qualitatively explain the main

features of TRM, more quantitative statements are extremely difficult to

make because of the need for precise knowledge of the particles' grain

size distribution and the grains' blocking temperatures, spontaneous

magnetization and microscopic coercivities. Dunlop (1968) pointed out

that TRM and ARM magnetization do not obey equation 15, derived by Néel,

but seem to have initial susceptibilities much lower than those predicted.
This is especially true for ARM for which simple theories, neglecting
thermal relaxation, predict an infinite initial susceptibility for non-
interacting single domain grains. ARM's finite susceptibilities have
been attributed to interactions among the magnetic grains (for example,
Eldridge, 1961; Wohlfarth, 1964; Waring, 1967; Kneller, 1968).

Experimentally it is clear that ARM has a finite susceptibility; yet,
it is not certain that TRM and ARM susceptibility values should be cal-
culated using equation 15, where it is assumed that the particles are
of uniaxial magnetic anisotropy and all the easy axes of magnetization
are parallel to the external field. Bean and Livingston (1959) showed
that for particles of uniaxial anisotropy whose easy axes are isotropi-
cally distributed with random or cubic orientation, the magnetization
will obey the Langevin function with an initial susceptibility, X, pro-
portional to $vJ_{SP}h/3kT$, 1/3 of the value obtained from equation 15. Bean
and Livingston also show that particles with cubic anisotropy will be
magnetized according to the Langevin relation. So, in view of their
work, it seems that for most samples used in paleomagnetism and rock
magnetism, the initial magnetization slopes should be of the order of
1/3 the value predicted by equation 15.

In their extensive experimental study to test Néel's single-domain
theory, Dunlop and West (1969) have shown that the discrepancy between
theory and experiments can usually be reduced and sometimes eliminated
by considering inter-particle interactions and by introducing appropriate
interaction fields. Recently, Banerjee and Mellema (1974) studied the
ARM properties of samples containing different concentrations (1, 5, and

10 percent by volume) of single domain CrO_2 powder, and they demonstrated the importance of magnetic interactions in the acquisition of ARM. In their experiments the effects of interactions manifest themselves in lower ARM susceptibilities and lower ARM stabilities against alternating fields for samples with progressively higher concentrations of magnetic powder.

Jaep (1971), applying thermodynamic considerations to an assembly of single domain particles, developed equations analogous to Néels', in which particle interactions are incorporated, and thus resulting in lower susceptibilities. Jaep's development of the ARM equation makes use of the kinetic equation and thermal fluctuations, leading to finite ARM susceptibility. Thus Jaep's contribution goes a considerable distance to bridge the gap between the experimental facts and our theoretical understanding of ARM. Although the importance of magnetic interactions has been recognized for many years, the problem of explicitly calculating the interaction field on a particle due to its neighbors has been an intractable many-body problem, which depends on the nature and geometry of the interacting particles, the external field and the sample's state of magnetization. Usually the interaction parameter is mentioned and included in the equations, but its value is adjusted to fit the experimental results.

There are at least three distinct ways in which interaction fields may arise; these fields, in addition to the externally applied field, act on each magnetic grain.

a. Each grain sees a field due to its near neighbors. This field depends on the neighbors' geometry and the manner in which they surround

the grain in question, on the neighbors' state of magnetization, and on the magnetic field in so far as it affects these factors.

b. Each grain is also subjected to its own self-demagnetizing field which depends on the grain's shape, its state of magnetization, $J_{SP}(T)$, and the orientation of the magnetization vector within the grain. When dealing with a completely specified assembly of single domain grains of simple shapes, the problem of calculating the grain's self-demagnetizing field is, in principle, relatively straight forward. For multidomain particles the problem is extremely complex as one has to deal with domain walls, with more than one magnetization vector, and with alteration of the domain configuration with variations in the effective field acting on the grain. On the other hand, domain configuration is established to minimize the grain's magnetostatic energy, and thus reduce the grain's self-demagnetization. As a rule of thumb, therefore, as the grain size increases and domain structure is more easily accomodated, the condition of flux closure is more closely approximated, thus substantially diminishing the self-demagnetization effects.

c. In addition, each grain is affected by the sample's demagnetizing field which, for a homogeneously magnetized sample, is determined by the sample's shape and magnetization vector.

The total interaction field is a composite of these effects. If the sample's net magnetization is parallel to the external field and is along the axes of the samples, the interaction fields caused by b. and c. above are antiparallel to the external field, when averaged over all of the sample's magnetic particles. The net direction of the interaction field cause by neighboring particles in a. above is more difficult to

ascertain.

With the exception of samples 0 and 1, all the samples are nearly identical cylinders 22 mm high and 22 mm in diameter so the relative magnitude of the sample-demagnetizing field can be obtained from the sample magnetization. Listed in order of decreasing magnitude of the sample-demagnetizing field, our samples are: 7, 11, 5, 1, 3, 0, 6, 8, 9, 4, 2, 10. (See table 5, column 3.).

To estimate the grains' self-demagnetizing fields, both the grain shapes and their magnetic configuration must be known. Using the mean grain sizes and shapes determined in chapter 2, and using J_{RS}/J_S as a measure of the grains' mean J_{SP} we estimate the mean grain self-demagnetizing field for each species of magnetite powder. We assume that the magnetite grains of sample 10 are sperical, and, since we have no measurement of J_{RS}/J_S for its magnetic particles, we use the fact that there is usually a direct correlation between stability with respect to A. F. demagnetization and values of J_{RS}/J_S. We therefore assume that J_{RS}/J_S value of the magnetite powder in sample 10 is second only to the acicular powder of sample 11. In decreasing order of their estimated mean grain self-demagnetizing field, the samples are: 10, 6, 7, 5, 8, 9, 11, 4, 3, 2, 1, 0. The particles of sample 11 have relatively low grain self-demagnetizing factors along their long axes, which are also their easy directions of magnetization. It is expected that samples 0 and 1 give rise to relatively low self-demagnetizing fields: Due to their large size and the relative 'softness' of their magnetization, their domain structure is more successful in establishing flux closure within the crystal thus minimizing the magnetostatic self-energy. Although calcu-

lation of interaction fields arising from the interactions of different remanence-carrying regions of the same magnetic crystal, such as the interaction between two domain walls or between a domain and a domain wall or between two domains, is beyond the scope of this study, the energy associated with such configurations must be inherently lower than those that they are designed to minimize. Indeed, it is likely that a particular domain configuration is established to minimize the various interaction fields within a particular crystal.

The interaction fields due to neighboring grains is difficult to estimate. It is expected that the 'neighbor effect' is relatively low for samples 0 and 1 which are isolated, neighborless crystals. Similarly, it is expected that this effect is low for sample 10, in which the magnetite powder is very dilute and evenly dispersed, as was discussed in chapter 3. On the other hand, it is not certain, for example, that sample 6 has a significantly lower interaction field due to the neighbor effect than sample 7, although sample 7 has an order of magnitude more magnetite powder. It was pointed out in chapter 3 that magnetite powders tend to agglomerate, and it is not certain to what extent these clusters are reduced upon dilution. The interaction field on a particular grain due to its neighbors probably is primarily a 'nearest neighbor' phenomenon; the field due to neighbors further removed decreases with distance as the as the dipole field according to $1/r^3$ law and its effect is partly screened out by neighbors closer to the grain of interest. The magnetite grains in samples 6 and 7 have a mean diameter of about .21 μm. This means that a typical grain totally surrounded by one layer of other typical grains has a cluster diameter of about .65 μm. Although the powders are carefully

mixed during sample preparation it is not expected that clusters on the order of 10 μm or less are disturbed. Therefore, it is our opinion that differences in the interaction fields of samples 6 and 7 are primarily due to differences in the sample-demagnetizing field.

Alternatively, the interaction fields due to neighboring grains can be viewed as follows: consider an isolated grain whose flux closure is less than complete, the net magnetic flux through any closed surface containing the entire magnetic particle (or totally excluding it) is zero. If this grain is now surrounded by similar grains whose magnetization vectors are, in one case, perfectly aligned or, in a second case, random, the stray field of the grain in question might be of any orientation with respect to the magnetization vectors that surround it, and its net contribution to the interaction fields of the surrounding grains will be statistically zero. It can be similarly argued that the net interaction field on a magnetic grain due to its neighbors is also statistically zero. (The complexity of the neighborhood interaction fields is substantially compounded as some of the magnetization vectors reverse during demagnetization).

Our study of the comparative behavior of ARM and TRM in the same magnetite-bearing samples may provide information regarding the comparative role of magnetic interactions in ARM and TRM. Since most theoretical work on magnetic interactions is restricted to homogeneously magnetized, single domain grains, our experiments may provide information and furnish constraints on the relative role of interaction for magnetite grains ranging from single domain to multidomain crystals, and for samples of varying

concentrations of magnetite powder.

10.3 THE EFFECT OF MAGNETIC INTERACTIONS ON THE ACQUISITION OF ARM AND TRM

In figure 57, we illustrate the low field acquisition of ARM and TRM for the various samples. The alternating fields for the ARM had peak values sufficient to saturate the samples for the particular biasing fields. The one exception, sample 11, was within 5 percent of saturation at the maximum alternating field of 2,000 oe. The ARM curves containing the larger magnetite grains, samples 0 through 5, are rather linear up to the maximum biasing field of 1.8 oe, whereas for the samples containing the smaller magnetite grains, samples 8 through 11, significant deviation from linearity toward saturation is observed at 1.8 oe. It is assumed that TRM is acquired linearly up to, at least, 0.5 oe, and this assumption has been supported whenever a third magnetization point was used. (The origin is an actual datum for each sample obtained by total thermal demagnetization). The ratio of the initial susceptibilities, X_{ARM}/X_{TRM} is listed in table 8, column 6. It is seen that the susceptibility ratio is substantially below unity ($.1 \leqslant X_{ARM}/X_{TRM} \leqslant .6$) for all samples containing fine particles; however, for the large crystals of magnetite, $X_{ARM}/X_{TRM} > 1$ (2.0 and 1.5, respectively).

(The above observations may help determine whether lightning remanence is an IRM or an ARM in rocks whose remanence resides in fine grained magnetite. For an observed lightning strike, if the lightning remanence is greater than a laboratory-induced TRM, where it is assumed that the sample's magnetic character is unaffected by heating, then the lightning remanence is most probably a strong field IRM. If the lightning remanence is less than the TRM, the question of ARM versus IRM remains unresolved,

Figure 57

Figure 57 a-f. Acquisition of ARM (open circles) and TRM
(closed circles) for samples 0 through 5 in small inducing fields,
h_{ex} < 2 oe. ARM was induced in alternating fields sufficient to
saturate the ARM for the particular biasing field.

(1000 oe $\leqslant \tilde{H} \leqslant$ 1500 oe).

SAMPLE 0

SAMPLE 1

SAMPLE 2

SAMPLE 3
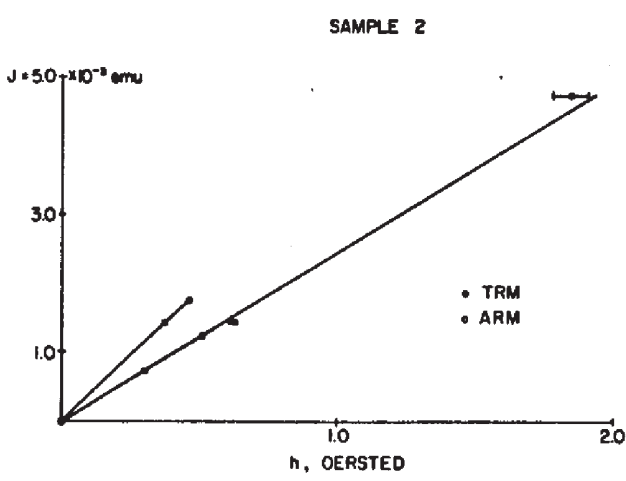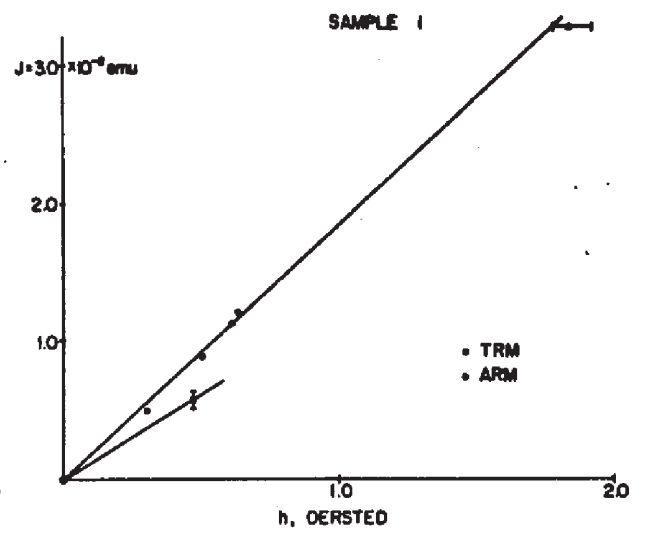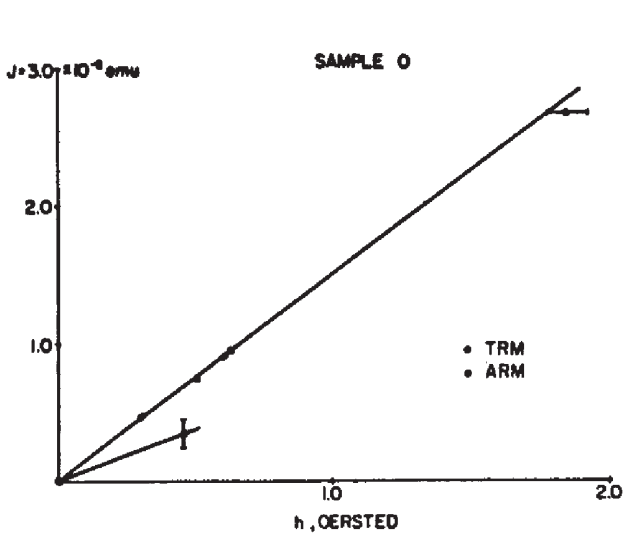
SAMPLE 4

SAMPLE 5

Figure 57

Figure 57 g-1. Acquisition of ARM (open circles) and TRM (closed circles) for samples 6 through 11 in small inducing fields, $h_{ex} < 2$ oe. ARM was induced in alternating fields sufficient to saturate the AR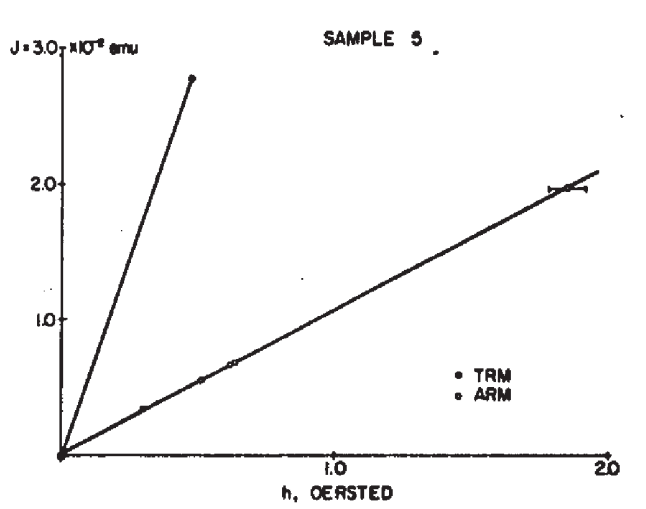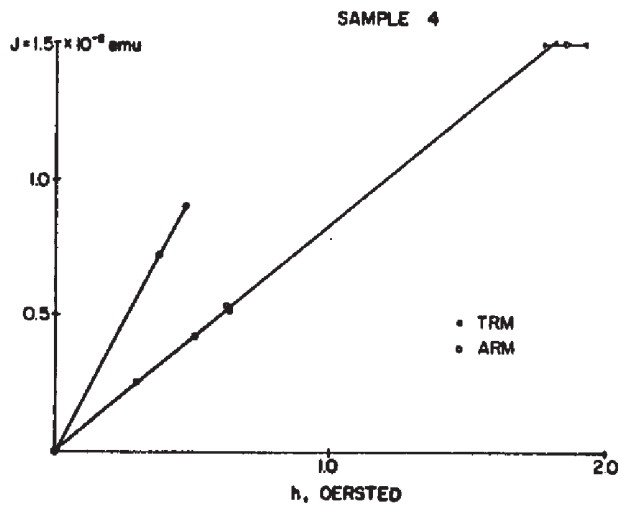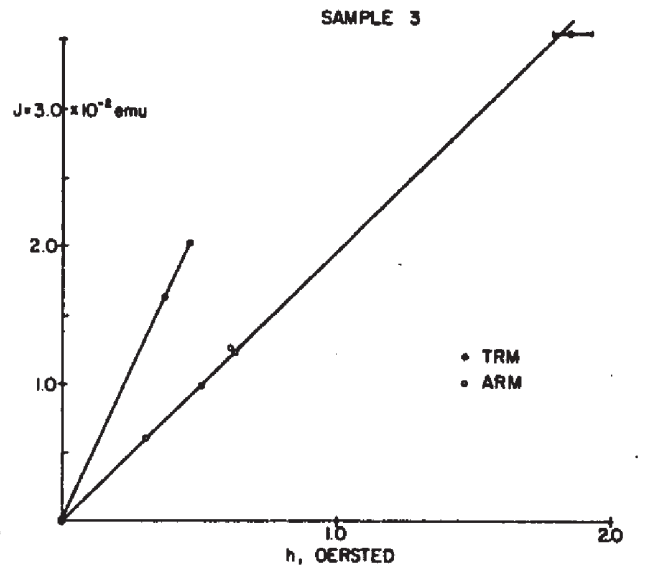M for the particular biasing field. ($\tilde{H} = 2000$ oe). The one exception was sample 11, which was within 5% of saturation at $\tilde{H} = 2000$ oe).

SAMPLE 6

J =15 × 10⁻⁸ emu

J =15 × 10⁻⁸ emu

SAMPLE 7

SAMPLE 8

J =2.0 × 10⁻⁸ emu

SAMPLE 9

SAMPLE 10
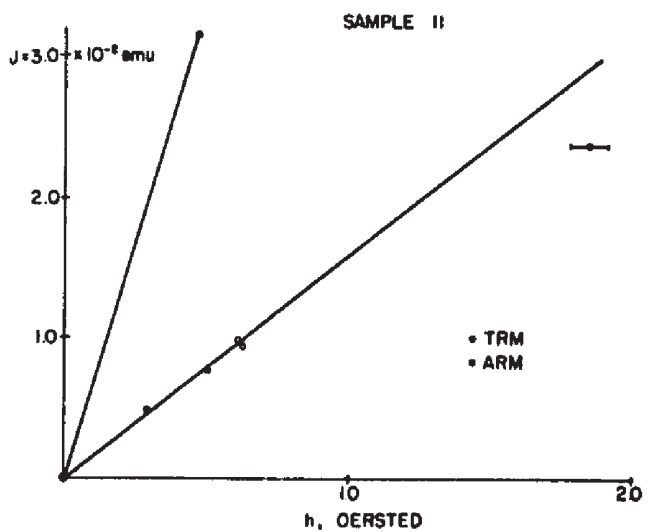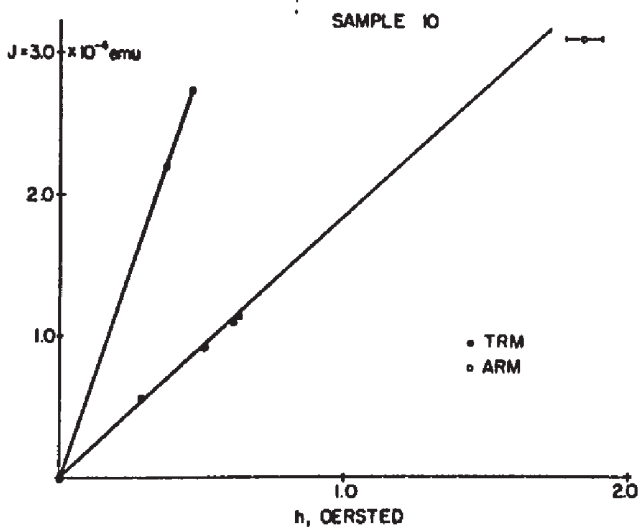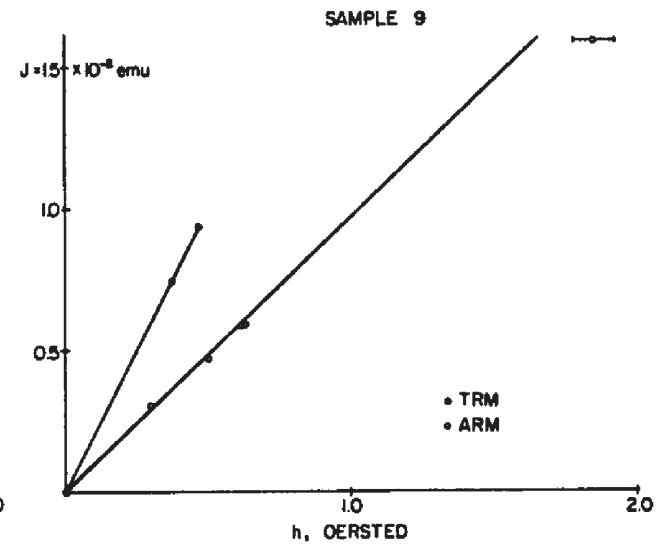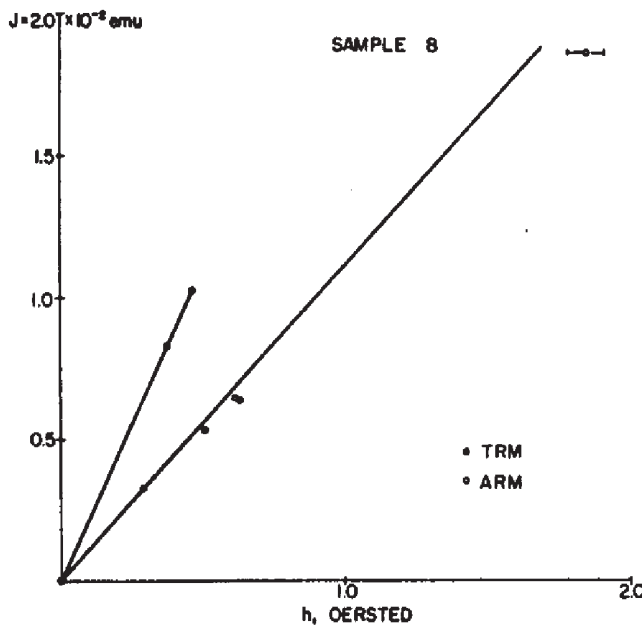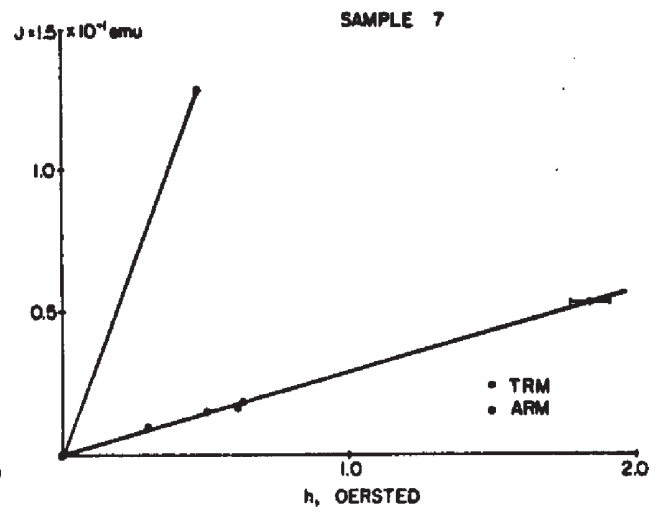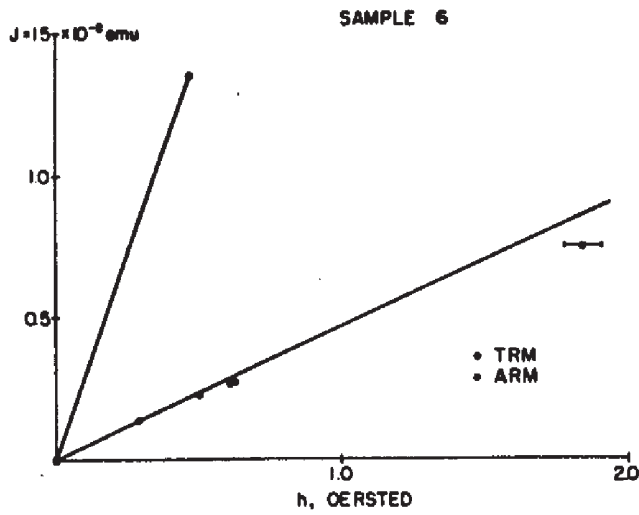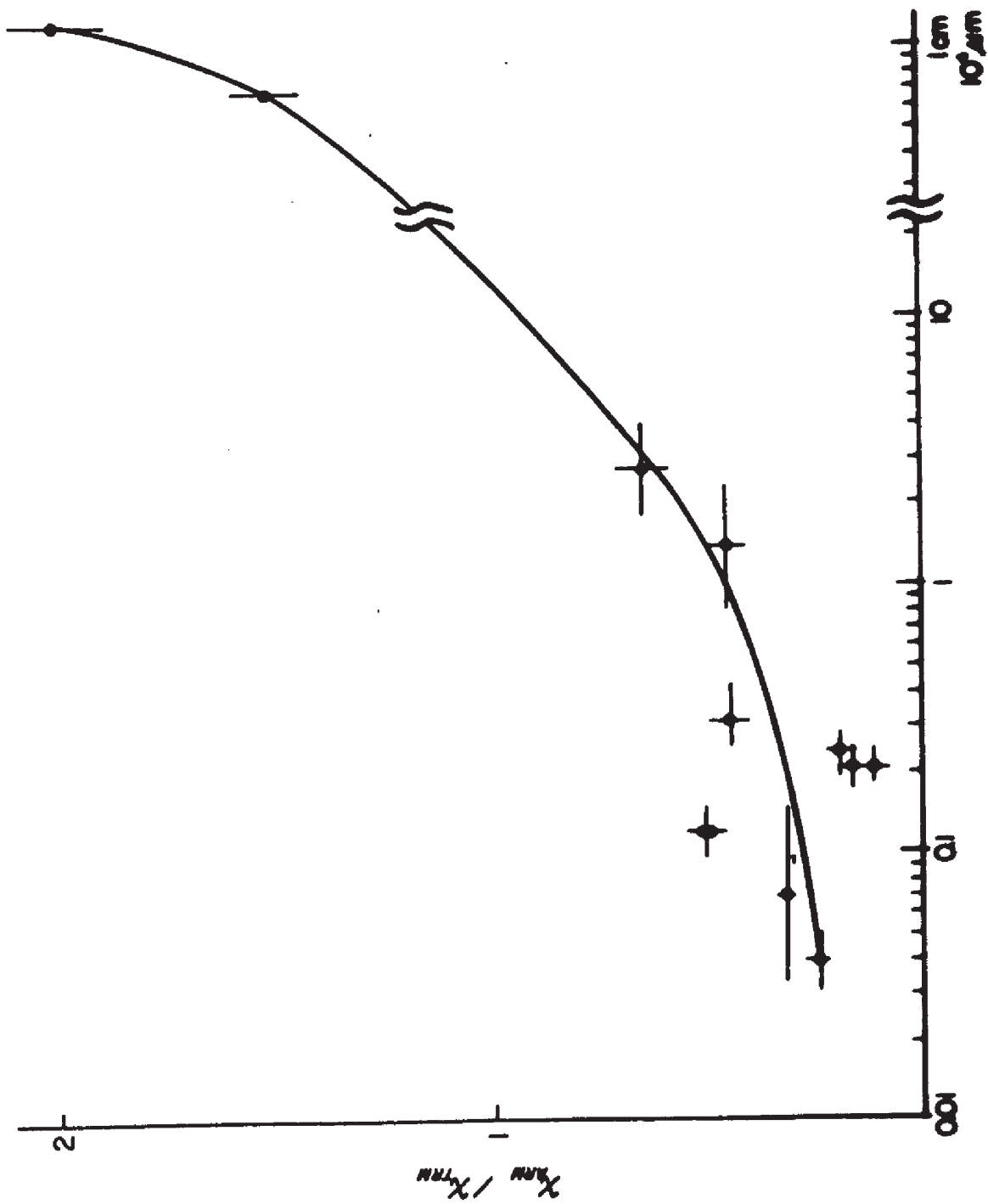
SAMPLE 11

CHARACTERISTIC PARTICLE DIAMETER, μm

Figure 58

Susceptibility ratios, X_{ARM}/X_{TRM}, versus particle size for the magnetite-bearing samples, 0 through 11. The abscissa is identical with that of figure 55. The uncertainty bars associated with the susceptibility ratios are deviations from the mean obtained from at least two independent measurements.

Note that the susceptibility ratios are substantially below unity for small particle sizes, but they are well above unity for the large magnetite crystals.
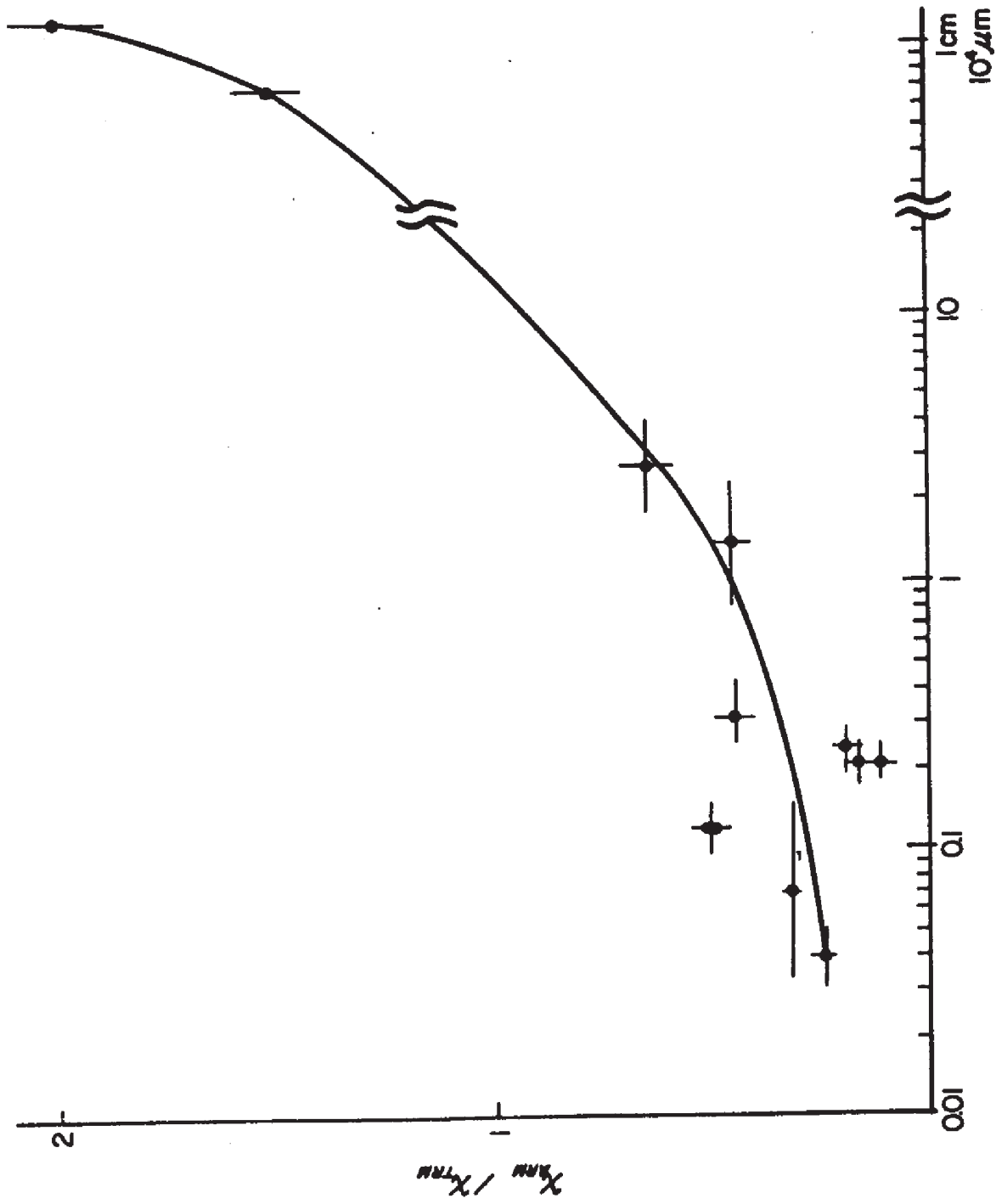
CHARACTERISTIC PARTICLE DIAMETER, μm

because the particular sample used may not have recorded the maximum value of the lightning remanence. Hopefully, however, the remanent directions can be resolved to help solve the problem as suggested earlier in chapter 9).

Dunlop and West (1969) measured the ARM to TRM ratio of four single domain samples whose remanence was acquired in a 1 oe biasing field. Their values are all substantially below unity. One value particularly relevant to our work is the ratio for a sample containing (less than 1% by volume) acicular magnetite. The ARM to TRM ratio for this sample was 0.182. Banerjee and Mellema (1974) report ARM to TRM initial suscepti- bility ratios for their single CrO_2 samples. The samples, diluted to 1, 5, and 10 percent volume concentrations, had initial susceptibility ratios of 0.199, 0.189, and 0.194, respectively. Dunlop and West (1969) and Banerjee and Mellema (1974) explain their observations in terms of inter- actions between the magnetic particles. In the following paragraphs we would like to extend previous work and concepts to explain some of our results. We would like, if possible, to understand the causes for the drastic difference between the susceptibility ratio of the large crystals and the submicron particles of magnetite. We would also like to deter- mine which types of interaction field are important in remanence acquisition.

For the region where TRM acquisition is linearly dependent on the field, the magnetization of single domain grains can be written as:

26.
$$J_{TRM}(T) = NvJ_{SP}(T)\eta \left[\frac{vJ_{SP}(T_B)}{kT_B} h_{eff}(T_B) \right]$$

This equation is similar to equation 15. $\eta = 1$ if equation 26 is the

linear approximation of the hyperbolic tangent of equation 14, and $\eta = 1/3$ if equation 26 is the linear approximation of the Langevin function. The external field, $\vec{h}_{ex}$, is modified by the interaction field to give:

27. $$\vec{h}_{eff}(T_B) = \vec{h}_{ex} + \vec{h}_{int}(T_B)$$

In our experiments the samples are cylindrical (except the two single crystals, samples 0 and 1) and the external field and the induced remanence are always along the axis of the cylinder, such that the sample self-demagnetizing field (in our experiments) is antiparallel to these quantities. For a large number of grains, isotropically distributed and whose easy axes are random, the net interaction field due to the grain self-demagnetizing factors is also antiparallel to the remanence and consequently to $\vec{h}_{ex}$. (This is not strictly true for each grain, because the self-demagnetizing factor is a tensor so that the interaction field is not, in general, anti-parallel to the magnetization vector). In addition, it was argued earlier that the interaction fields due to neighboring grains may be statistically zero. We therefore conclude that the total interaction field, $\vec{h}_{int}$, is antiparallel to $\vec{h}_{ex}$. Equation 27 can them be rewritten.

28. $$h_{eff}(T_B) = h_{ex} - h_{int}(T_B)$$

Equation 28 is further supported by the observation that the experimental susceptibilities are always lower than those predicted by theories neglecting magnetic interactions. Furthermore, the remanence in our experiments

is always parallel to $\vec{h}_{ex}$.

We assume that ARM acquisition is in principle similar to TRM acquisition and, therefore, governed by a similar equation, which in the region where ARM is linear with the biasing field, obeys the equation

29. $$\vec{J}_{ARM}(T) = NvJ_{SP}(T)\eta \left[\frac{vJ_{SP}(T)}{kT} \vec{h}_{eff}(T) \right]$$

where all the quantities are as in equation 26. If $T = T_R$, then equations 26, 28, and 29 yield:

30. $$\frac{X_{ARM}}{X_{TRM}} = \left[\frac{J_{SP}(T_R)/J_{SP}(T_B)}{T_R/T_B} \right] \left[\frac{h_{ex} - h_{int}(T_R)}{h_{ex} - h_{int}(T_B)} \right]$$

since $J_{SP}(T_R)/J_{SP}(T_B) > 1$

and $T_R/T_B < 1$

(Typically, $J_S(T_R)/J_S(T_B)$ is between 2. and 5. and T_R/T_B is between .35 and .46 for magnetites.)

31. $$\frac{X_{ARM}}{X_{TRM}} = A_o \left[\frac{h_{ex} - h_{int}(T_R)}{h_{ex} - h_{int}(T_B)} \right]$$

where A_o can vary from about 4 to 14. Setting $A_o = 10$, $h_{ex} = .5$ oe, and $h_{int}(T_B) = 0$, then to obtain $X_{ARM}/X_{TRM} = .2$, $h_{int}(T_R) \approx .49$ oe. If $A_o = 1$, $h_{ex} = .50$ oe, and $h_{int}(T_B) = 0$, then $h_{int}(T_R) = .4$ oe would yield $X_{ARM}/X_{TRM} \approx .2$. Although the requirements on h_{int} to yield the observed

susceptibility ratio seem unrealistically high, a spherical single domain grain whose spontaneous magnetization is 50 gauss (for magnetite $J_S(T_R)$ = 480 gauss) will have an associated grain self-demagnetizing field of $4/3\pi(50) \approx 200$ oe. On the other hand, a spherical sample whose remanence is 0.01 gauss has an associated sample-demagnetizing-field of $4/3\pi(.01) \approx .04$ oe. These extreme values provide broad and subjective brackets for $h_{int}(T_R)$. Undoubtedly the details of equation 30 are only approximate and may possibly be in error. However, if the assumption that the observed low values of X_{ARM}/X_{TRM} are due to magnetic interactions is correct, then equation 30 points out: 1) that for ARM $h_{int}(T_R)$ is substantial with respect to h_{ex}, and 2) that $h_{int}(T_B)$ is much less than $h_{int}(T_R)$. We shall assume that equations 26, 29, and 30 are as telling for multidomain as for single domain grains, and that differences between magnetic particles are accounted for by difference in $J_{SP}(T)$ -- the spontaneous magnetization.

The interaction fields are unique for each sample and have to be analyzed separately. Sample 10 is of particular interest. It has the lowest sample-demagnetizing field of all samples studied, being less than 1% of that sample 11. (See table 5, column 3.) Also, of all the prepared samples, sample 10 alone should be free of magnetite-powder agglomeration and its magnetic grains should be the most uniformly dispersed. (See discussion in chapter 3.) Therefore the interaction field due to neighbors should be lower for sample 10 than for samples 5, 6, 7, 8, 9, and 11. Still, sample 10 has a low value for its susceptibility ratio: X_{ARM}/X_{TRM} = .31 ± .01. This suggests that the grain self-demagnetizing

effect is dominant in suppressing the ARM. Samples 5, 6, 7, and 11 have greater sample self-demagnetizing fields and enhanced interaction due to neighbors, depressing X_{ARM}/X_{TRM} even further. Samples 6 and 7 are identical with the exception that sample 7 has an order of magnitude more magnetite powder than sample 6, the primary effect of which is to increase $\vec{J}$ and the sample self-demagnetizing field. The difference in X_{ARM}/X_{TRM} values for samples 6 and 7, which are .164 and .108, respectively, may be telling us about the order of magnitude of the sample self-demagnetizing effect on the remanence acquisition curves. Although sample 11 has a relatively high sample self-demagnetizing field, its magnetite particles have relatively low grain self-demagnetizing fields because of their needle shapes, which might explain the reason that its susceptibility ratio is higher than those of samples 6 and 7. It is not understood for what reason X_{ARM}/X_{TRM} of samples 8 and 9 is so much greater than that of samples 6 and 7.

As the grain size increases, and domain structure appears, the grain self-demagnetizing fields are reduced. Improved flux retention within the grains also reduces the interaction fields due to neighbors. X_{ARM}/X_{TRM} increases as h_{int} decreases. For sample 0 and 1, h_{int} is greatly reduced, and X_{ARM}/X_{TRM} is largely determined by $A_o > 1$.

In conclusion, if low values of X_{ARM}/X_{TRM} are caused by magnetic interactions, then grain self-demagnetizing fields are probably significant in suppressing ARM. Diminshing values of h_{int} are in the right direction to explain the fact that for submicron magnetite grains $X_{ARM}/X_{TRM} < 1$, while for large crystals, $X_{ARM}/X_{TRM} > 1$.

An experiment that might be instructive to further understand the role of interactions in ARM and TRM would be to obtain ARM susceptibilities at elevated temperatures. Ideally, samples with well-defined blocking temperatures should be used (for example, samples 11, 6, 7, 5, and 10 in our study). ARM should be given at elevated temperatures which are below the blocking points of most of the particles (up to 400°C for the samples mentioned). After inducing the ARM, the samples should be cooled in zero field to T_R. After correcting for the fraction of the grains unblocked at the elevated temperature and for the variation in J_{SP}, $X_{ARM}(T)/X_{TRM}$ is computed. If magnetic interactions are indeed responsible for the observed values of X_{ARM}/X_{TRM} and if our discussion above is on the right track, we would expect that

$$\lim_{T \to T_B} [X_{ARM}(T)/X_{TRM}] \to 1$$

10.4 EFFECTS OF MAGNETIC INTERACTION ON THE STABILITY OF ARM AND TRM

Comparisons of ARM and TRM stabilities for various samples with respect to several stability criteria have shown their remarkable similarity. Attention has been paid to similar samples (samples 0 and 1 and samples 8 and 9), and experiments have been repeated to determine the reproducibility of the data and the dispersion in the properties of distinct but similar samples. This has been done to gain a better appreciation for the significance of similarities and differences in the data.

Of the data presented thus far, only that of samples 6 and 7 can be used for a comparative study of the role of the concentration of magnetic

material in determining magnetic interactions in ARM and TRM. These samples contain the same species of magnetite powder and were similarly prepared; however, sample 7 contains about an order of magnitude more magnetite than sample 6. Samples 6 and 7 contain .19±.01 and 1.4±.1 weight percent of magnetite, respectively, and the average 0.5 oe TRM of samples 6 and 7 is .73x10^{-3} and 7.7x10^{-3} emu/gm, respectively, which are representative values for the magnetization of extrusive igneous rocks. In addition, the samples' stability parameters (see tables 5 and 8) are typical of rocks from which reliable paleomagnetic information has been obtained. Therefore, a comparative study of the magnetic properties of samples 6 and 7 may provide information about the importance of particle interactions for paleomagnetism in typical volcanic rocks.

Comparison of the ARM data for samples 6 and 7 in table 8 shows no significant difference in their behavior after low temperature cycles or in their spontaneous decay (see table 8, columns 4 and 5). The ARM of sample 6, however, is more resistant to alternating fields than that of sample 7. The demagnetization spectra are similar and are reproduced in figures 49 and 50. The determination of $\tilde{H}_{\frac{1}{2}}$ was repeated three times. Each of the last two determinations for the two samples was performed essentially simultaneously, so that although the absolute value of $\tilde{H}_{\frac{1}{2}}$ may be in slight error, the differences are very reliable. It is seen that the gap, $\Delta\tilde{H}_{\frac{1}{2}}$, for the two samples is consistent for the three determinations. The trend of our ARM results is the same as that observed by Banerjee and Mellema (1974), although their experiments were performed with acicular CrO_2 powder and the ARM was induced by a 200 oe biasing field superimposed on

a peak alternating field of 1,000 oe.

These results are also in general agreement with theoretical models predicting a decrease in the coercity with increasing concentration of magnetic particles. For an assemblage of single domain grains, Néel (1947) obtained an expression for the coercivity which is a linearly decreasing function of the grains' packing parameter.

32. $$H_C(\rho) = H_C(o)[1 - \rho]$$

ρ is the packing parameter, which varies from zero for an infinitely dilute mixture to unity. $H_C(0)$ is the coercive force for $\rho = 0$. (Equation 32 cannot be telling the entire story because in reality H_C ($\rho = 1$) > 0.) The magnetite particle concentrations of samples 6 and 7 are so low ($\simeq 19\%$ and 1.4% by weight) that equation 32 predicts that their coercivities should differ by no more than 1.5%. Certainly, the 15% difference in the ARM $\tilde{H}_{\frac{1}{2}}$ values of samples 6 and 7 is much too great to be explained by equation 32.

As with the ARM, the TRM behavior of samples 6 and 7 is not significantly different for low temperature cycles and for its pattern of spontaneous decay. (See table 8, columns 4 and 5.) In addition, the TRM blocking temperature spectra for the two samples are compared to assess whether they might be affected by different interaction fields. The spectra are very similar. The mean blocking temperature, $<T_B>$, of sample 6 is $507^{\circ} \pm 10^{\circ}C$ and that of sample 7 is $506^{\circ} \pm 10^{\circ}C$. The uncertainty of $\pm 10^{\circ}C$ is related to an absolute temperature determination. The closeness of the mean blocking temperatures for the two samples is considerably less

uncertain than $\pm 10^{\circ}C$, since it was observed in three separate thermal demagnetization experiments, in which the two samples occupied adjacent positions in the oven during simultaneous heatings.

In contrast to the ARM trend, the TRM of sample 6 is less resistant to alternating field demagnetization than the TRM of sample 7. (See table 8, column 3.) The observed difference, $\Delta \tilde{H}_{\frac{1}{2}}$, after the first experiment is of questionable significance, but the results of the second determination (which was performed essentially simultaneously for the two samples) indicate a yet broader gap, leaving little question as to its reality. This surprising result is not yet understood. If interactions play a significant role in TRM stability against alternating fields, we would expect the same stability as observed for the ARM (unless a totally different interaction mechanism is active near the TRM blocking temperature from the mechanism at room temperature). If magnetic interactions play a negligible role, the two samples should behave similarly.

With the exception of the A. F. demagnetization characteristics, our experiments show no significant difference in stability parameters of samples 6 and 7. The trend of the TRM A. F. demagnetization stability is opposite to the trend expected from equation 32. Although the ARM A. F. demagnetization stability does follow the trend of equation 32, equation 32 predicts that the differences in the coercivities of samples 6 and 7 should be much less than the differences actually observed in the $H_{\frac{1}{2}}$ values. It is therefore quite possible that the differences in the ARM and TRM A. F. demagnetization stabilities are not at all related to magnetic interactions.

Equation 32 was developed for an assembly of single domain grains, and it was verified by Morrish and Yu (1955) who showed that the bulk coercivity, H_c, (the reverse magnetic field for which the sample magnetization is zero) decreases linearly with increasing compaction for single domain (highly acicular) grains. They also showed that for cubic grains 1 μm in size, H_c decreases only slightly upon compaction, and for larger irregularly shaped grains, H_c is invariant under compaction. They argue that the latter grains behave as they do because they are multidomain with much improved flux retention within the grains such that compaction has a substantially reduced effect on altering the sample's magnetostatic energy configuration. The magnetite powder in samples 6 and 7 consists of regular polygons (hexagons and octagons mostly) whose mean diameter is .21 μm and whose volume is less than 1% of Morrish and Yu's 1 μm particles. No grains greater than 0.5 μm in diameter were observed in the electron microscope pictures, such that the ocercivity-compaction dependence of our magnetite would most probably be intermediate between the acicular, single domain particles and the 1 μm cubic magnetite powder. (See Morrish and Yu, 1955, figure 7.) H_c measurements of both the undiluted magnetite powder and of the mixture of which sample 7 was prepared yielded identical results: H_c = 105±3 oe.

10.5 CONCLUSIONS AND APPLICATION OF ARM TO ARM TO PALEOINTENSITY DETERMINATION

From our experiments on the stabilities of samples containing different concentrations of the same magnetite powder it seems that the stabilities are not measureably affected by the concentration of their magnetic particles (which lead to different sample self-demagnetizing fields and, possibly, to different interaction fields due to neighbors) as long as the concentration is less than about 1.5% by weight. It is impossible, of course, to

generalize from a few experiments with two samples to all paleomagnetic samples, although it was pointed out earlier that the remanences and the stabilities of samples 6 and 7 are typical of igneous rocks. It is quite probable that the magnetic minerals in rocks are more evenly distributed than the magnetites in our samples, thus further reducing the interaction fields due to neighbors. Clearly, more experiments are required to better understand the effects of magnetic interactions on the stabilites of ARM and TRM. However, the preliminary conclusion that emerges from our experiments is that magnetic interactions, in so far as they are determined by the concentration of the magnetic particles, seem to have at most a minor effect on the relative stabilities of TRM and ARM of samples whose magnetic properties are similar to those of many rock specimens. Similar experiments as reported here should be pursued first for several concentrations of clearly single domain (possibly acicular) particles, for which interaction effects should be the most readily recognized. The results should be carefully evaluated before deciding on whether or not to investigate further a greater variety of particles.

On the other hand, it was shown that the ratio of the initial susceptibilities, X_{ARM}/X_{TRM} varies widely depending upon the shapes and sizes and concentrations of the particular magnetite particles in a manner consistent with the trend of interaction fields. It was shown that for fine particles, $<d> < 3$ μm, $X_{ARM}/X_{TRM} < 1$ ($.1 < X_{ARM}/X_{TRM} < .6$), and for large crystals $X_{ARM}/X_{TRM} > 1$ (2.0 and 1.5, respectively). It appears, therefore, that, before a successful ARM technique for paleointensity determinations is successfully implemented, an independent determination of X_{ARM}/X_{TRM} is

required. Because X_{ARM}/X_{TRM} is dependent on the sizes and shapes and on the concentration of the magnetic particles and because of the difficulty in obtaining realistic grain size distributions in real rocks, it seems that in order to obtain X_{ARM}/X_{TRM} at least one heating to above T_c would be required, thus nullifying the chief attraction of an ARM paleointensity method. Although we have shown that the A. F. demagnetization curves of ARM and TRM in the sames samples are usually very similar (figures 43 to 54, chapter 9), the differences are sometimes substantial (for example, sample 11, figure 54), and the differences between the ARM and TRM demagnetization curves are sometimes of opposite sense. (Compare figures 53 and 54 for samples 10 and 11.) Thus any ARM method for paleointensity determination should also require A. F. demagnetization of the total laboratory TRM, which was obtained for the X_{ARM}/X_{TRM} determination. It should be repeated with emphasis that such a single heating above T_c does away with self-consistency checks which are such an integral part of the 'Thellier method', and all chemical and physical changes that occur during the first heating would go undetected. It appears to this writer that at this time the extra labor of the 'Thelleir method' is still required to obtain more reliable paleointensity results.

REFERENCES

Banerjee, S.K. and J.P. Mellema, A New Method for the Determination of
Paleointensity from the A.R.M. Properties of Rocks, Earth Planet.
Sci. Lett., 23, 177-184, 1974.

Bean, C.P., and J.D. Livingston, Superparamagnetism, J. Appl. Phys.,
30, 120S-129S, 1959.

Bickford, L.R., J. Pappis, and J.L. Stull, Magnetostriction and Permeability
of Magnetite and Cobalt-susbstituted Magnetite, Phys. Rev., 99,
1210-1214, 1955.

Bickford, L.R., J.M. Brownlow, and R.F. Penoyer, Magnetocrystalline
Anisotrophy in Colbalt Substituted Magnetite Single Crystals, Proc.
Inst. Eng., London, Pt B: 104, 238-244, 1956.

Bonhommet, N., Discovery of a New Event in the Brunhes Period at Laschamp,
France, in Paleogeophysics , S.K. Runcorn, Ed., 159-163, Academic
Press, 1970.

Bonhommet, N., and J. Zähringer, Paleomagnetic and Potassium Argon Age
Determinations of the Laschamp Geomagnetic Polarity Event, Earth
Planet, Sci. Lett, 6, 43-46, 1969.

Brown, W.F., Relaxation Behavior of Fine Magnetic Particles, J. Appl. Phys.
Suppl., 30, 130S-132S, 1959.

Chevallier, R., Propriétes magnétiques de l'oxyde ferrique rhomboédrique
($Fe_2O_3\alpha$), Phys, Rad., 12, 172-188, 1951.

Chevallier, R., and S. Mathieu, Propriétés magnétiques des poudres
d'hématites: Influence des dimensions des grains, Ann. Phys., Paris,
18, 258-288, 1943.

Chikazumi, S., _Physics of Magnetism_ , 554 pp, John Wiley, New York, 1964.

Coe, R.S., Paleointensities of the Earth's Magnetic Field Determined From Tertiary and Quaternary Rocks, _J. Geophys. Res._, 72, 3247-3262, 1967a.

Coe, R.S., The Determination of Paleointensities of the Earth's Magnetic Field with Special Emphasis on Mechanisms which could cause Nonideal behavior in Thelliers' Method, _J. Geomag. Geoelct._, 19, 157-179, 1967b.

Coe, R.S., Effects of Shape Anisotrophy Paleointensity Determinations, _EOS Trans. AGU_, 54, 1072, 1973.

Coe, R.S., and C.S. Gromme, A Comparison of Three Methods of Determing Geomagnetic Paleointensities, _J. Geomag. Geoelct._, 24, 415-435, 1973.

Daniel, E.D., and I. Levine, Experimental and Theoretical Investigation of the Magnetic Properties of Iron Oxide Recording Tape, _J. Acoust. Soc. Am._, 32, 1-15, 1960.

Dunlop, D.J., Monodomain Theory: Experimental Verification, _Science_, 162, 256-258, 1968.

Dunlop, D.J., Hysteretic Properties of Synthetic and Natural Monodomain Grains, _Phil. Mag._, 19, 329-338, 1969.

Dunlop, D.J., Magnetite: Behavior Near the Single-domain Threshold, _Science_, 176, 41-43, 1972.

Dunlop, D.J., Thermoremanent Magnetization in Submicroscopic Magnetite, _J. Geophys. Res._, 78, 7602-7613, 1973.

Dunlop, D.J., and G.F. West, An Experimental Evaluation of Single Domain Theories, _Revs. Geophys,_, 7, 709-757, 1969.

Eldridge, D.F., Quantitative Determination of the Interaction Fields in Aggregates of Single-domain Particles, J. Appl. Phys., 32, 247S-249S, 1961.

Elmore, W.C., Ferromagnetic Colloid for Studying Magnetic Structures, Phys. Rev., 54, 309-310, 1938.

Evans, M.E., Single-domain Particles and TRM in Rocks, Comments Earth Sci. Geophys., 2, 139-148, 1972.

Evans, M.E., and M.W. McElhinny, The Paleomagnetism of the Modipe Gabbro, J. Geophys. Res., 71, 6053-6063, 1966.

Evans, M.E., and M.L. Wayman, An Investigation of Small Magnetic Particles by Means of Electron Microscopy, Earth Planet. Sci. Lett., 9, 365-370, 1970.

Everitt, C.W.F., Thermoremanent Magnetization, I, Experiments on Single Domain Grains, Phil. Mag., 6, 713-726, 1961.

Everitt, C.W.F., Thermoremanent Magnetization, I, Experiments on Multi-domain Grains, Phil. Mag., 7, 583-597, 1962.

Everitt, C.W.F., Thermoremanent Magnetization, III, Theory of Multi-domain Grains, Phil. Mag., 7, 599-616, 1962.

Fletcher, E.J., Ph.D. Thesis, Univeristy of Newcastle Upon Tyne, 1971,

Fuller, M.D., Geophysical Aspects of Paleomagnetism, CRC Critical Reviews in Solid State Sciences, 137-219, July, 1970.

Gallagher, K.J., W. Feitknecht, and U.Mannweiler, Mechanism of Oxidation of Magnetite to γFe_2O_3, Nature, 217, 1181-1121, 1968.

Hargraves, R.B., and W.M. Young, Source of Stable Remanent Magnetism in Lambertville Diabase, Am. J. Sci., 267, 1161-1177, 1969.

Jaep, W.F., Anhysteretic Magnetization of an Assembly of Single-domain Particles, J. Appl. Phys. 40, 1297-1298, 1969.

Jaep, W.F., Role of Interactions in Magnetic Tapes, J. Appl. Phys., 42, 2790-2794, 1971.

Johnson, H.P., and R.T. Merrill, Magnetic and Mineralogical Changes Associated with Low-temperature Oxidation of Magnetite, J. Geophys. Res., 77, 334-341, 1972.

Johnson, H.P., and R.T. Merrill, Low Temperature Oxidation of Titano-magnetite and the Implication for Paleomagnetism, J. Geophys. Res., 78, 4938-4949, 1973.

Klapel, G.D., and P.N. Shive, High-temperature Magnetostriction of Magnetite, J. Geophys. Res., 79, 2629-2633, 1974.

Kneller, E., Magnetic-interaction Effects in Fine-particle Assemblies and in Thin Films, J. Appl. Phys., 39, 945-955, 1968.

Kobayashi, K., M.F. Campbell, and J.B. Moorhead, Size Dependence of Low-temperature Change in Remanent Magnetization of Fe_3O_4, 1965 Ann. Proc. Rep. Rock Magn. Res. Group Japan, 33-50, 1965.

Kobayashi, K., and M.D. Fuller, Stable Remanence and Stable and Memory of Multi-domain Materials with Special Reference to Magnetite, Phil. Mag., 18, 601-624, 1968.

Kono, M. and T. Nagata, Intensity of the Earth's Magnetic Field in Geologic Time, I. Late Pliocene in the Southwestern U.S.A., J. Geomag. Geoelect., 20, 211-220, 1968.

Lliboutry, L., _Ann. Physique_, 6,731, 1951.

Lowrie, W., and M. Fuller, Effect of Annealing on Coercive Force and Remanent Magnetizations in Magnetite, _J. Geophysc. Res._, 74, 2698-2710, 1969.

Lowrie, W., and M. Fuller, On the Alternating Field Demagnetization Characteristics of Multidomain Thermoremanent Magnetization Magnetite, _J. Geophys. Res._, 76, 6339-6349, 1971.

Maurain, G., Étude et Comparaison des procédés de réduction de l'hystérésis, _J. Phys. et Radium_, 3, 417-434, 1904.

Merrill, R.T., Low-temperature Treatments of Magnetite and Magnetite-Bearing, _J. Geophys. Res._, 75, 3343-3349, 1970.

Morrish, A.H., _The Physical Principles of Magnetism_ , 680pp., John Wiley, New York, 1965.

Morrish, A.H., and S.P. Yu, Dependence of the Coercive Force on the Density of Some Iron Oxide Powders, _J. Appl. Phys._, 26, 1049-1055, 1955.

Morrish, A.H., and L.A.K. Watt, Effect of Interaction Between Magnetic Particles on the Critical Single-domain Size, _Phys. Rev._, 105, 1476-1478, 1957.

Morrish, A.H., and L.A.K. Watt, Coercive Force of Iron Oxide Micropowders at Low Temperatures, _J. Appl. Phys._, 29, 1029-1033, 1958.

Nagata, T., The Natural Remanent Magnetization of Volcanic Rocks and Its Relation to Geomagnetic Phenomena, _Bull. Earthq. Res. Inst._, 21, 1-196, 1943.

Nagata, T., _Rock Magnetism_ , 350pp, Maruzen Co., Tokyo, 1961.

Nagata, T., Y. Arai, and K. Momose, Secular Variation of the Geomagnetic Total Force During the Last 5000 Years, J. Geophys. Res., 68, 5277-5281, 1963.

Néel, L., Cahiers Phys., 12, 2, 1942.

Néel, L., Cahiers Phys., 13, 18, 1943.

Néel, L., Théorie de l'effet du champ démagnetisant sur l'aimantation anhysteretique, Cahiers Phys. 17, 47-50. 1943.

Néel, L., Théorie du traînage magnétique des ferromagnétiques en grains fins avec applications aux terres cuites, Ann. Geophys., 5, 99-136, 1949.

Néel, L., Some Theoretical Aspects of Rock Magnetism, Advan. Phys., 4, 191-242, 1955.

Néel, L., R. Forrer, N. Janet, and R. Baffie, Aimantation anhysteretique et champ démagnetisant, Cahiers Phys., 17, 51-56, 1943.

Ozima, M. and M. Ozima, Origin of Thermoremanent Magnetization, J. Geophys. Res., 70, 1363-1369, 1965.

Parry, L.G., Magnetic Properties of Dispersed Magnetite Powders, Phil. Mag., 11, 302-312, 1965.

Patton, B.J., and J.L. Fitch, Anhysteretic Remanent Magnetization in Small Steady Fields, J. Geophys. Res., 67, 307-311, 1962.

Preisach, F., Über Die Magnetische Nachwirkung, Z. Phys., 94, 277-302, 1935.

Rathenau, G.W., Saturation and Magnetization of Hexagonal Iron Oxide Compounds, Revs. Modern Phys., 25, 297-301, 1953.

Rimbert, F., Contribution à l'étude de l'action de champs alternatifs sur les aimantations rémanentes des roches, applications l'géophysiques, Rev. Inst. Fr. Petrole, 14, 17-54, 123-155, 1959.

Roquet, J., Sur les rémanences des oxydes fer et leur intérêt en géo-

    magnétisme, Ann. Géophys, 10, 226-247, 282-325, 1954.

Shimizu, Y., Magnetic Viscosity of Magnetite, J. Geomag. Geoelec., 11,

    125-138, 1960.

Shive, P.N., The Effect of Internal Stress on the Thermoremanence of

    Nickel, J. Geophys. Res., 74, 3781-3788. 1969.

Shive, P.N., Dislocation Control of Magnetization, J. Geomag. Geoelec.,

    21, 519-529, 1969.

Soffel, H., The Single Domain-Multidomain Transition in Natural Inter-

    mediate Titanomagnetites, Zeit. Geophys., 37, 451-470, 1971.

Smith, P.J., The Intensity of the Ancient Geomagnetic Field: A Review

    and Analysis, Geophys. J.R. Astr. Soc., 12, 321-362, 1967.

Stacey, F.D., Thermoremanent Magnetization (TRM) of Multidomain Grains

    in Igneous Rocks, Phil. Mag., 3, 1391-1401, 1958.

Stacey, F.D., A Domain Theory of Magnetic Grains in Rocks, Phil. Mag.,

    4, 594-605, 1959.

Stacey, F.D., The Physical Theory of Rock Magnetism, Advan. Phys., 12,

    45-133, 1963.

Stacey, F.D., and S.K. Banerjee, The Physical Principles of Rock

    Magnetism , Elsevier, Amsterdam, 195 pp, 1974.

Schmidt, V.A., A Multidomain Model of Thermoremanence, Earth Planet. Sci.

    Lett., 20, 440-446 ,1973.

Syono, Y., Magnetiocrystalline Anistropy and Magnetostriction of Fe_3O_4-

    Fe_2TiO_4-Series with Special Application to Rock Magnetism, Jap.

    J. Geophys., 4, 71-143, 1965.

Syono, Y. and Y. Ishikawa, Magnetocrystalline Anisotropy of xFe_2TiO_4 $(1-x)Fe_3O_4$, _J. Geomag. Geoelec._, 18, 1230-1231, 1963a.

Syono, Y. and Y. Ishikawa, Magnetostriction Constants of xFe_2TiO_4 $(1-x)Fe_3O_4$, _J. Geomag. Geoelec._, 18, 1231-1232, 1963b.

Thellier, E., Sur l'amantation des terres cuiter et ses applications géophysiques, _Ann. Inst. Phys. Globe, Paris_, 16, 157-302, 1938.

Thellier, E. and F. Rimbert, Sur l'analyse d'aimantations fossiles par action de champs magnétiques alternatifs, _C.R. Acad. Sci._, _Paris_, 239, 1399-1401, 1954.

Thellier, E. and O. Thellier, Sur l'intensité du champ magnétique terrestre dans le passé historique et géologique, _Ann. Geophys._, 15, 285-376, 1959.

Verhoogen, J., The Origin of Thermoremanence Magnetization, _J. Geophys. Res._, 64, 2441-2449, 1959.

Waring, R.K., Magnetic Interactions in Assemblies of Single-domain Particles. The Effect of Aggregation, _J. Appl. Phys._, 33, 1005-1006, 1967.

Watkins, N.D. and S.E. Haggerty, Primary Oxidation Variation and Petrogenesis in a Single Lava, _Contr. Mineral. Petrol._, 15, 251-271, 1967.

Whitney, J., H.P. Johnson, S. Levi, and B.W. Evans, Investigations of Some Magnetic and Mineralogical Properties of the Laschamp and Olby Flows, France., _Quat. Res. 1_, 511-521, 1971.

Wohlfarth, E.P., A Review of the Problem of - Particle Interactions with Special Reference to Magnetic Recording, _J. Appl. Phys._, 35, 783-790, 1964.

Wohlfarth, E.P., Relations Between Different Modes of Acquisition of the Remanent Magnetization of Ferromagnetic Particles, *J. Appl. Phys.*, 29, 595-596, 1958.

Woodward, J.G. and E. Della Torre, Particle Interaction in Magnetic Recording Tapes, *J. Appl. Phys.* 31, 56-62, 1960.

APPENDIX A

CONVERSION OF SOME MAGNETIC QUANTITIES FROM

C.G.S. TO S.I. SYSTEM OF UNITS

In this dissertation the C.G.S. system of units has been used exclusively. In view of the recent recommendation by IAGA that the S.I. units be used in geomagnetism, we present below a limited conversion table so that the data in this dissertation can be easily converted to S.I. units. Most of what follows was taken almost directly from a copy of Resolution 3 of the IAGA Kyoto General Assembly held in September, 1973 in Kyoto, Japan.

(1) Values of the geomagnetic "field" should be expressed in terms of magnetic induction, B. S.I. unit = 1 Tesla.

1 Tesla = 1 Weber/meter^2 = 10^4 Gauss (= 10^4 Oersted)

1 Gamma = 10^{-9} Tesla = 10^{-9} Weber/meter^2 = 10^{-5} Gauss (= 10^{-5} Oersted)

(2) Values of "intensity of magnetization" should be expressed in terms of magnetization J.

S.I. unit = Ampere/meter.

1 Ampere/meter = 10^{-3} cmu/cc = 10^{-3} Gauss

(3) Values of the 'magnetic intensity', H, are defined by the equations: S.I. $\vec{H} = \vec{B}/\mu o - \vec{M}$

C.G.S. $\vec{H} = \vec{B} - 4\pi\vec{M}$

S.I. unit = ampere/meter

1 ampere/meter = $4\pi \times 10^{-3}$ Oersted (= $4\pi \times 10^{-3}$ Gauss)

(4) Values of the susceptibility, X, are to be expressed as the ratio between the magnetization, J, and the magnetic field intensity, H.

$$X_{S.I.} = 4\pi X_{e.m.u.}$$

APPENDIX B

EXPERIMENTAL PROCEDURES AND MEASURING TECHNIQUES

1. ALTERNATING FIELD (A. F.) DEMAGNETIZATION PROCEDURE.

The A. F. demagnetization unit used to obtain all the demagnetization curves that appear in this dissertation was constructed especially for the hot A. F. demagnetization experiments. The coil was designed to fit around a non-magnetic (non-inductively-wound) oven, placed in the center of a set of three pairs of orthogonal, 8 foot square Helmholtz coils, which with the aid of a self-correcting feed-back system, was designed to null the earth's field. It is conservatively estimated, as a result of many checks with a test fluxgate, that within the actual space of the experiment the field was nulled to better than 50 γ. The coil was capable of sustaining peak alternating fields of up to 1,000 oe. Because only uniaxial demagnetization was possible, it is important to note that the remanences in the prepared, cylindrical samples were always induced along the axes of the cylinders, and in the natural crystals the remanences were always along one of the [111] easy axes, and the axes along which the remanences were induced were always aligned parallel to the axis of the demagnetizing coil.

The alternating fields are produced by an inductrol unit which utilizes a variable transformer whose ferromagnetic core has hysteresis properties. Even if the input signal is perfectly sinusoidal, the hysteretic properties of the transformer-core will cause a phase delay of the fundamental harmonic and the appearance of the third harmonic

component. The relative magnitude of the third harmonic to the funda-
mental depends on the core's hysteresis properties and on the applied
field (Chikazumi, 1964, p. 397). These distortions in the wave form
of the alternating fields are translated into an ARM component that is
sometimes superposed on the uniaxial demagnetization curve. The alter-
nating field at which the ARM component has a noticeable effect on the
demagnetization curve depends on the ratio of the intensity of the
secondary ARM to primary magnetization and on the stability of the
sample. The greater the primary remanence ARM ratio, the lesser is
the relative effect of the ARM on the normalized demagnetization curves.
The greater the sample stability, the larger is the alternating field
required to induce the ARM. (If samples are tumbled in a truly random
fashion in the alternating field and if the alternating field decreases
very slowly compared to the tumbling rate, the ARM can be totally suppressed.
If the tumbling is not completely random, the ARM will appear but only at
much higher fields than in uniaxial demagnetization.)

In the A. F. demagnetization of our samples, the ARM effect is
present and sometimes noticeable. In most of the demagnetization
curves the ARM effect is unimportant until less than 20% to 25% of
the remanence remains. The lower the stability of the remanence of a
sample, the lower will be the alternating field for which the ARM
effect becomes significant. Usually the ARM sense was maintained for
each sample throughout the various demagnetization experiments so that
accurate comparisons could be made. The one time when the ARM sense

was reversed (by reversing the connecting leads), it is essentially

obvious from the demagnetization curves; see chapter 6.3.

In later A. F. demagnetization experiments (chapters 4,9, and

10) the ARM effect was cancelled by demagnetizing twice at each

alternating field value. The sample's remanence is placed parallel

and antiparallel to the ARM sense in the consecutive runs, and the

demagnetized remanences are averaged for each alternating field value,

cancelling the ARM component.

2. HEATING CHARACTERISTICS OF THE NON-MAGNETIC OVEN.

The cylindrically shaped oven was non-inductively wound so that

the heating current will generate no magnetic field within the oven

chamber. A brass sample holder having four levels was constructed.

Three of our samples could be placed on each level, such that the

sample holder could accommodate a maximum of 12 sample of size compar-

able to ours. Samples from adjacent levels were separated by a mini-

mum of 1/8" which is the thickness of the brass disc forming the sample

holder. Samples within a particular level were often rubbing shoulders.

Many heating experiments were done varying the number and the positions

of the samples on the sample holder. In addition, numerous experiments

were run where the sample number and position was fixed, but the orienta-

tions of the samples' magnetization vectors were reoriented, in other-

wise identical experiments, to produce maximum changes on neighboring

samples. At no time did we observe effects that could be attributed

to neighboring samples!

The sample holder is place inside a vycor tube whose outside

diameter is 64 mm; the tube is evacuated by a mechanical vacuum pump
and flushed with nitrogen gas before the temperature is increased.

To measure the actual temperature at the various sample positions,
we embedded a thermocouple in a sample-size cylindrical slug prepared
of the matrix material of which our samples are prepared. Our results
are summarized in table 9.

Table 9

Temperature Calibration of the Non-magnetic Oven

T_{DIAL} \ LAYER #	#1	#2	#3	#4
300°	301°	306°	304°	287°
400°	397°	405°	399°	380°
450°	446°	452°	447°	426°
500°	493°	501°	493°	468°
550°	538°	550°	540°	513°

The separation of the thermocouple in two adjacent layers is approxi-
mately 26 mm so that temperature gradients can be estimated for our
experimental configuration. It is seen that the temperature gradients
are a strong function of the temperature. In addition, the gradients
are very large in layers 4 and 1 and relatively small in layers 2 and 3.
At 550°C the gradient in layer 4 are in excess of 10°C/cm, whereas in
layer 2 they are of the order 4°C/cm.

Despite the sometimes high temperature gradients in the oven, the temperature at each point on the sample holder is reproducible to within a few $^\circ$C, probably better than±5°C. This is so primarily because of the automatic temperature controlling device whose thermocouple is fixed in the oven and the high degree of reproducibility of the sample holder position, which is within ± 1 mm. It should be noted that both oven and sample holder are cylindrically symmetric.

The only adverse effects of the temperature gradients occur and are clearly illustrated in chapter 8, when the Thellier and Thellier version of the Thellier method is executed. There the sample is rotated 180° about an axis parallel to the cylindrical faces between two heatings to the same temperature. The gradients cause the step-like appearance of the data, which is maximum for layers 4 and 1 and minimum for layers 2 and 3. As long as the position and orientation of the sample is maintained between runs the temperature gradients are more an esthetic disappointment than damaging.

3. MEASUREMENT OF BULK MAGNETIC PROPERTIES.

Hystersis parameters, H_C, H_{CR}, J_S, J_{RS}, Curie point, T_C, measurements, high-field magnetization versus temperature, J - T, measurements, and determinations of the temperature dependence of the hysteresis parameters were made on a Princeton Applied Research (P.A.R.) Vibrating Sample Magnetometer (VSM), capable of temperatures up to 700°C and fields as high as 8 koe. The samples are small, usually weighing less than 100 mg, and very weakly magnetic samples can not be studied.

4. REMANENCE MEASUREMENTS.

Remanence measurements, TRM, ARM, and IRM were made on a Schonstedt Slow Spinner Magnetometer, which has a maximum sensitivity of 10^{-7} emu, full scale, which is a good two orders of magnitude more sensitive than the least intense remanence studied in this dissertation.

Biography of Shaul Levi

Shaul Levi was born on May 10, 1942 in Haifa, Israel, to

Heinz Otto and Eleonore H. Levi. He graduated from G. Washington

High School in San Francisco, California in 1960, received a B. A.

in Physics from the University of San Francisco in 1964, and his

M.A. in physics in 1966 from the Unviersity of California, Davis.